Spectroscopic characterizations of Ferrogallic Inks and related pigments with interest in Cultural Heritage

UNIVERZITA PAVLA JOZEFA ŠAFÁRIKA V KOŠICIACH · 1959 ·

UAM Universidad Autónoma de Madrid

CSIC Consejo Superior de Investigaciones Científicas

Alba Espina García

Pavol Jozef Šafárik University in Košice
Faculty of Science
Department of Biophysics

Universidad Autónoma de Madrid
Facultad de Ciencias Químicas
Departamento de Química Aplicada

Instituto de Estructura de la Materia
Consejo Superior de Investigaciones Científicas

Doctoral Thesis

Spectroscopic characterizations of Ferrogallic Inks and related pigments with interest in Cultural Heritage

Alba Espina García

Madrid, 2022

Pavol Jozef Šafárik University in Košice
Faculty of Science
Department of Biophysics

Universidad Autónoma de Madrid
Facultad de Ciencias Químicas
Departamento de Química Aplicada

Instituto de Estructura de la Materia
Consejo Superior de Investigaciones Científicas

Doctoral Thesis

Spectroscopic characterizations of Ferrogallic Inks and related pigments with interest in Cultural Heritage

Alba Espina García
PhD candidate

Supervisors:

Dr. Zuzana Jurašeková
Dr. Santiago Sánchez Cortés

Madrid, 2022

Me gustaría basar estos agradecimientos en una analogía entre el viaje de Dorothy en el Mago de Oz y la aventura de doctorarse. Por ello iré introduciendo a los personajes del libro y a la vez que explicaré su relación de semejanza con las personas físicas.

Los primeros personajes que aparecen en la historia son el **Espantapájaros** y **Toto,** estos personajes siempre acompañan a Dorothy en su aventura desde el maizal hasta Kansas o en mi caso desde el principio hasta al final, gracias **Mamá, Papá** y **Siria**; mi familia.

El segundo personaje que aparece es el **hombre de Hojalata**, para mi un personaje bondadoso y amigable, que cuida de no lastimar a nadie. Se trata de las **amistades** que me bien quieren y que han aparecido a lo largo de este camino tanto dentro como fuera del laboratorio y que sin ellas no hubiera habido aventura.

En Asturias: Quizás les fontes inspiradores que m'impulsaron a empecipiar esti proyectu Guillermo Varela Carbajal y Ángela Fernández Iglesias, a día de güei puedo dicir bien arguyosa Dr. en les sos respectives areas.

En Eslovaquia: Carlos Calero Veloso, Diana Gomes, Bea Diniz Ferreira y Bruno Pereira a día de hoy pondría mi vida en sus manos, todos ellos Médicos Internacionales y parte de mi familia no sanguínea.
Con especial cariño y con muchas ganas de volver a verlas menciono a Martina Petrenčáková, Eva Dušeková y Nikol pero no me olvido de ninguno de mis compañeros del Departamento de biofísica en Košice. Quienes con frases hechas y muy ingeniosas me han ayudado a sobrevivir en el país, una de mis preferidas es "Čo sa stalo? Kuriatko sa pokakalo.", después de "Dvakrát pivo, prosím".

En Madrid: Giulia Vanucci, como piezas que encajan de un puzle, química interesada en el arte y yo restauradora interesada en la ciencia, compartimos sueños, techo y hasta algunas lagrimas dulces y saladas. Moisés Martín Garrido mi compañero de tupper, profesional en pasar datos de disquete a ordenador y viceversa, quien me explico cada día con ternura cada procedimiento en el laboratorio. Javier Manriva y Clochu, Zipi y Zape siempre de buen humor y dispuestos a tomar un Soplica. Bea, Esmeralda y Vera la mejor herencia que me pudo dejar Giulia en Madrid.

El tercer personaje que entra en escena es, **el León**, personaje en el que reside la esencia del coraje, valentía y fuerza. Para mi se trata de los investigadores inspiradores tanto por su trabajo como por sus valores **Dr. Sagrario Martínez Ramírez** y **Dr. Erik Sedlák** que siempre tendré como referentes.

Bruja Buena del Este, cuyo propósito principal es ayudar a Dorothy a encontrar al Mago de Oz para que pueda volver a casa además le da los zapatos de plata o herramientas necesarias para encontrar el camino, gracias por todo **Dr. Zuzana Jurašeková**.

El personaje que le da nombre al cuento, el **Mago de Oz**, hombrecillo experimentado, considerado un gran mago y científico además de supervisor de esta tesis **Dr. Santiago Sánchez Cortés**.

Ciudad esmeralda, la capital de Oz, que se encuentra al final del famoso camino de ladrillos amarillos como: **Dr. Daniel Jancura, Prof. Pavol Miškovský, Prof. José Vicente García Ramos** y **Dr. Rosa Menéndez** quienes ya lo han recorrido y nos muestran el camino a los demás.

Y por ultimo agradecer este **gran libro**, o marco en el que se ha desarrollado esta historia a las instituciones que lo han hecho posible, gracias a el **Instituto de Estructura de la Materia** (**CSIC**), **Universidad Autónoma** de Madrid y **Pavol Jozef Šafárik** University in Košice.

I would like to base these acknowledgements on an analogy between Dorothy's journey in the Wizard of Oz and the adventure of getting a PhD. Therefore, I will introduce the characters of the book and at the same time I will explain their relationship of resemblance to physical persons.

The first characters that appear in the story are the **Scarecrow** and **Toto**, these characters always accompany Dorothy in her adventure from the cornfield to Kansas or in my case from the beginning to the end, thanks **Mom**, **Dad** and **Siria**; my family.

The second character that appears is the **Tin Man**, for me a kind and friendly character, who is careful not to hurt anyone. These are **the friends** who love me well and who have appeared along the way both inside and outside the laboratory and without them there would have been no adventure.

In Asturias: Perhaps the inspirational sources that pushed me to start this project are Guillermo Varela Carbajal and Ángela Fernández Iglesias, today I can say, very proud that, they are Dr. in their respective areas.

In Slovakia: Carlos Calero Veloso, Diana Gomes, Bea Diniz Ferreira, Bruno Pereira today I would put my life in their hands, all of them International Doctors and part of my non-blood family.

With special affection and longing to see them again I mention Martina Petrencáková, Eva Dušeková and Nikol but I do not forget any of my colleagues from the biophysics department in Košice. They have helped me to survive in the country with very witty phrases, one of my favorites is "Čo sa stalo? Kuriatko sa pokakalo." after “Dvakrát pivo, prosím.“.

In Madrid: Giulia Vanucci, like pieces that fit of a puzzle, chemist interested in art and me a restorer interested in science, we share dreams, roof and even some sweet and salty tears. Moises Martín Garrido my tupper companion, professional in transferring data from diskette to computer and vice versa, who explained me every day with tenderness every procedure in the laboratory. Javier Manriva and Clochu, Zipi and Zape always in a good mood and ready to take a Soplica. Bea, Esmeralda and Vera, the best inheritance that Giulia could leave me in Madrid.

The third character that enters the scene is **the Lion**, a character in which lies the essence of courage, bravery and strength. For me it is about the inspiring researchers both for their work and for their values **Dr. Sagrario Martínez Ramírez** and Dr. **Erik Sedlák** that I will always have as referents.

Good Witch of the East, whose main purpose is to help Dorothy to find the Wizard of Oz so that she can return home and also gives her the silver shoes or tools necessary to find the way, thanks for everything **Dr. Zuzana Jurašeková.**

The character that gives his name to the story, the **Wizard of Oz**, an experienced little man, considered a great magician and scientist as well as supervisor of this thesis **Dr. Santiago Sánchez Cortés**.

Emerald City, the capital of Oz, which is at the end of the famous yellow brick road as: **Dr. Daniel Jancura, Prof. Pavol Miškovský, Prof. José Vicente García Ramos** and **Dr. Rosa Menéndez** who have already traveled it and show the way to others.

And finally, I would like to thank this great **book**, or framework in which this story has been developed, to the institutions that have made it possible, thanks to the Instituto de **Estructura de la Materia (CSIC), Universidad Autónoma** de Madrid and **Pavol Jozef Šafárik** University in Košice.

“La vida es como el Raman,
todo depende de donde pongas el foco.”

Alba Espina

Statutory Declaration

I do solemnly and sincerely declare that this Doctoral Thesis has been written by me under the guidance of my supervisors dr. Zuzana Jurašeková and dr. Santiago Sánchez Cortés, and with the use of the referenced literature.

Madrid, 31 October, 2022

Abstract

Iron gall ink (IGI) was the most widely used writing material until the early 20th century. They are probably the most broadly used writing and occasionally drawing tools throughout our history.

Its extensive use at the world level, has allowed the conservation and transmission of different recipes for its manufacture. Despite the immense diversity of recipes available from very different cultures and periods, all of them present a series of constant components in their composition. Recurrently, there can be find vegetable polyphenolic substances and mineral sulfates agglutinated by resins from trees in recipes.

The investigation of inks is crucial in many aspects. In particular, it is of a great importance in the study of historical **manuscripts** with many applications in **cultural heritage**. However, to analyze such complex systems, it is important both to develop an appropriate analytical method as well as to identify and characterize their individual components. That is why the purpose of our research project is to perform a structural analysis of IGIs, especially of the complex formation of **gallic acid** and other polyphenols with a similar structure, such as **pyrogallol, syringic acid, tannic acid**, with iron and copper ions.

In this doctoral thesis, we mainly present results obtained by using different optical spectroscopy techniques (UV-vis absorption, IR, **Raman** and **SERS**) to study the reaction mechanisms of **polyphenolic compounds** and their **iron** and **copper complexes**. The structure of the actual colorant in IGIs is still a matter of controversy, therefore, this work could represent an important and interesting contribution to the description and understanding of the IGIs chemical structure and composition.

In the final part of this thesis, Raman spectroscopy was applied and optimized for the ***in-situ*** and **non-destructive** analysis of historical manuscripts. An analysis of the aging process undergone by the manuscripts was done on the basis of the vibrational marker bands deduced from the study of the previous molecular models and the SERS results.

Keywords: **Iron gall inks (IGIs), cultural heritage, manuscripts, polyphenolic compounds (pyrogallol, syringic acid, gallic acid, tannic acid), iron complexes, copper complexes, *in-situ*, non-destructive**, **Raman spectroscopy, SERS, fluorescence, FTIR**

Resumen

Las **tintas ferrogálicas**, también conocidas internacionalmente como iron gall inks (IGIs), han sido el material de escritura más ampliamente empleado hasta principios del siglo XX. Probablemente sean las herramientas de escritura y ocasionalmente de dibujo más utilizadas a lo largo de nuestra historia.

Su extensa utilización a nivel mundial, ha permitido la conservación y transmisión de diferentes recetas para su fabricación. Pese a la inmensa diversidad de recetas disponibles provenientes de culturas y periodos muy diferentes, todas ellas presentan una serie de componentes constantes en su composición. Recurrentemente podemos encontrar en las recetas sustancias polifenólicas vegetales y sulfatos minerales aglutinados por resinas procedentes de árboles.

La investigación de las tintas es importante en muchos aspectos. Sobre todo, en el estudio de **manuscritos** históricos con múltiples aplicaciones en el **patrimonio cultural**. Sin embargo, para analizar sistemas tan complejos como las tintas son, es decisivo por un lado desarrollar un método analítico apropiado así como, por otro lado, hacer una identificación y caracterización de sus componentes individuales. Es por ello, que el propósito de la investigación de esta tesis es estudiar la formación de complejos del **ácido gálico** y otros polifenoles de estructura similar, como el **pirogalol, ácido siríngico** y **ácido tánico**, con iones de hierro y cobre.

En esta tesis doctoral, presentamos y discutimos los datos obtenidos mediante diferentes técnicas de espectroscopía óptica (absorpción UV-vis, IR, **Raman** y **SERS**) y estudiamos los mechanismos de reacción de dichos **compuestos polifenólicos** y sus correspondientes **complejos de hierro** o **cobre**. La estructura del colorante real de dichas tintas sigue siendo un motivo de controversia, por lo que este trabajo podría contribuir en el entendimiento de la composición y estructura química de las IGIs.

En la parte final de esta tesis se aplicó la espectroscopia Raman y se optimizó para el análisis ***in-situ*** y **no destructivo** de manuscritos históricos. Se realizó un análisis del proceso de envejecimiento sufrido por los manuscritos sobre la base de las bandas marcadoras vibracionales deducidas del estudio de los modelos moleculares anteriores y los resultados del SERS.

Palabras clave: **Tintas ferrogálicas, patrimonio cultural, manuscritos, compuestos polifenólicos (pirogalol, ácido siríngico, ácido gálico, ácido tánico), complejos de hierro, complejos de cobre, *in-situ*, no destructivo, espectroscopía Raman, SERS, fluorescencia, FTIR**

Abstrakt

Železogalové atramenty, tiež medzinárodne známe ako iron gall inks (IGIs), boli pravdepodobne najdôležitejšie a najčastejšie používané historické písacie a kresliace prostriedky, predovšetkým do začiatku 20. storočia.

Rozsiahle a celosvetové použitie čiernych atramentov umožnilo nielen zachovanie, ale aj ďalšie odovzdávanie a prispôsobovanie receptúr na ich výrobu, v závislosti od regiónu, kultúry, ako aj historického obdobia. Aj napriek tomu, že sa takto zachovalo mnoho a veľmi rozmanitých historických receptov na ich prípravu, všetky obsahujú rovnaké farbotvorné zložky: rastlinné polyfenoly (kyselinu galovú z tanínov) a vitrioly (sírany určitých kovov, najmä síranu železnatého), navzájom spojené a stabilizované v roztoku arabskou gumou.

Štúdium atramentov je významné v mnohých ohľadoch. Obzvlášť dôležitá je analýza historických dokumentov a **rukopisov** poskytujúca významné informácie ohľadne študovaných objektov a ich postavenia v **kultúrnom dedičstve**. Analyzovať takéto komplexné systémy znamená v prvom rade vedieť detekovať, identifikovať a charakterizovať ich jednotlivé zložky. Významným je aj vývoj vhodných analytických metód. Aj preto sme za jeden z hlavných cieľov nášho výskumu zvolili štúdium tvorby komplexov **kyseliny galovej** a štruktúrne jej podobných modelových **polyfenolových** zlúčenín (**pyrogalol, kyselina syringová, kyselina taninová**) s iónmi železa a medi.

V predkladanej dizertačnej práci prezentujeme a diskutujeme najmä výsledky štúdia mechanizmov tvorby a kinetiky daných **komplexov**, pričom na štúdium využívame rôzne techniky optickej spektroskopie (UV-vis absorpciu, IR, **Ramanovu** a **SERS spektroskopiu**). Keďže štruktúra samotného farbiva železogalového atramentu je ešte stále predmetom kontroverzie, očakávame, že aj výsledky tejto práce budú predstavovať dôležitý a zaujímavý príspevok k popisu a pochopeniu chemickej štruktúry a zloženia IGIs.

V záverečnej časti tejto dizertačnej práce sa prezentujú výsledky významné pre stanovenie vhodných postupov **nedeštruktívnej** a ***in-situ*** Ramanovej a SERS detekcie IGIs v historických rukopisoch. Vykonali sme tiež analýzu procesu starnutia, ktorému boli dané dokumenty vystavené a realizovali sme ju na základe vyhodnotenia konkrétnych vibračných pásov, tzv. spektrálnych markerov, ktoré vyplynuli z nášho predchádzajúceho štúdia molekulárnych modelov IGIs a príslušných SERS meraní.

Kľúčové slová: **Železogalové atramenty, kultúrne dedičstvo, rukopisy, polyfenoly (pyrogalol, kyselina syringová, kyselina gallová, kyselina taninová), komplexy železa, komplexy medi, *in-situ*, nedeštruktívny, Ramanova spektroskopia, SERS, modelové vzorky, umelecké diela**

TABLE OF CONTENT

LIST OF FIGURES

LIST OF TABLES

ABBREVIATIONS

AgC: citrate-reduced silver colloid

AgH: hydroxylamine-reduced silver colloid

AgNS: star-shaped Ag colloid

AuC: citrate-reduced gold colloid

C: charcoal activated

CT: charge transfer

CU (Cu): copper

DFT: density functional theory

ED: electronic delocalization

EM: electromagnetic (mechanism)

FE (Fe): iron

FT-Raman: Fourier-transform Raman (spectroscopy)

FWHM: full width at half maximum

GA: gallic acid

GACU (GA-Cu): complex of gallic acid and copper(II) sulfate pentahydrate

GAFE (GA-Fe): complex of gallic acid and iron(II) sulfate heptahydrate

HOMO: highest occupied molecular orbital

IGI(s): iron gall ink(s)

IR: Infrared (spectroscopy)

LMCT: ligand-to-metal charge-transfer bands

LSP(R): localized surface plasmon resonance

LUMO: lowest unoccupied molecular orbital

MAN: Museo Arqueológico Nacional (The National Archaeological Museum)

NPs: nanoparticles

NSs: nanostars

PL: photoluminescence

PY: pyrogallol

PYCU (PY-Cu): complex of pyrogallol and copper(II) sulfate pentahydrate

PYFE (PY-Fe): complex of pyrogallol and iron(II) sulfate heptahydrate

RAMAN (RS): Raman spectroscopy

SA: syringic acid

SACU (SA-Cu): complex of syringic acid and copper(II) sulfate pentahydrate

SAFE (SA-Fe): complex of syringic acid and iron(II) sulfate heptahydrate

SEM: scanning electron microscopy

SERS: Surface-enhanced Raman spectroscopy

STP: standard temperature and pressure

TA: tannic acid

TACU (TA-Cu): complex of tannic acid and copper(II) sulfate pentahydrate

TAFE (TA-Fe): complex of tannic acid and iron(II) sulfate heptahydrate

UV-vis: ultraviolet–visible (spectroscopy)

XANES: X-ray absorption near edge structure spectroscopy

XRD: difracción de rayos X

1. INTRODUCTION/INTRODUCCIÓN

1.1 Las tintas ferrogálicas

i) Introducción y recorrido histórico de las tintas ferrogálicas

Las tintas ferrogálicas (IGIs; *de inglés*: **I**ron **G**all **I**nks) llegaron a ser conocidas coloquialmente como "La Tinta Eterna" por ser más estables, y con mejores propiedades de saturación y luminosidad que las de base de carbón.

Debido a su gran versatilidad, fácil elaboración y múltiples usos que van desde cartas y documentos cotidianos, como los bosquejos de las libretas de los estudiantes, hasta manuscritos iluminados medievales, las IGIs fueron los materiales de escritura y ocasionalmente también de dibujo más ampliamente utilizados desde la Antigüedad. Aunque la escritura no fue su único uso documentado a lo largo de la historia. Este tipo de tinta fue empleada ya desde el siglo tercero de la era Cristiana en Egipto, tal como aparece en algunos papiros egipcios, fundamentalmente en el papiro de Leiden X, encontrado en la antigua ciudad de Tebas, que se conservan en la Universidad del mismo nombre en los Países Bajos [1]. Pero sin duda, su época dorada fue la Edad Media, y su uso se extendió hasta bien entrada la edad moderna [2], [3].

Es por ello, que estas tintas negras registran una parte muy significativa de nuestro patrimonio cultural durante diferentes períodos históricos, y que a día de hoy, encontramos numerosos ejemplos de su uso exhibidos en archivos y museos de diferentes partes del mundo. Algunos de estos ejemplos están representados en la **Figure 1**.

Figure 1. *Algunos ejemplos del uso de las tintas ferrogálicas utilizadas a lo largo de la historia humana: (a) los cuadernos de Leonardo da Vinci (1452-1519); (b) los bocetos de Rembrandt (1606-1669); (c) el dibujo preparatorio de V. van Gogh para el cuadro Wheat Field (1888); (d) las composiciones musicales de J. S. Bach (1685-1750); (e) las partituras originales de L. van Beethoven (1770-1827); y (f) el primer borrador de Abraham Lincoln de la Proclamación de emancipación (1863).*

Sin embargo, la utilización de tintas ferrogálicas comenzó a declinar en el siglo XX, viéndose desplazadas progresivamente por medios de escritura más modernos, basados en tintes sintéticos y colorantes resistentes a la oxidación [4]–[7]. En la mayoría de los casos, ha sido este último proceso de oxidación el que ha causado un mayor daño en los manuscritos y obras de arte que integran este tipo de tintas debido principalmente a la acidificación que este proceso lleva consigo. La **Figure 2** muestra los deterioros corrosivos producidos por la oxidación del hierro y acidificación producidos en la tinta ferrogálica.

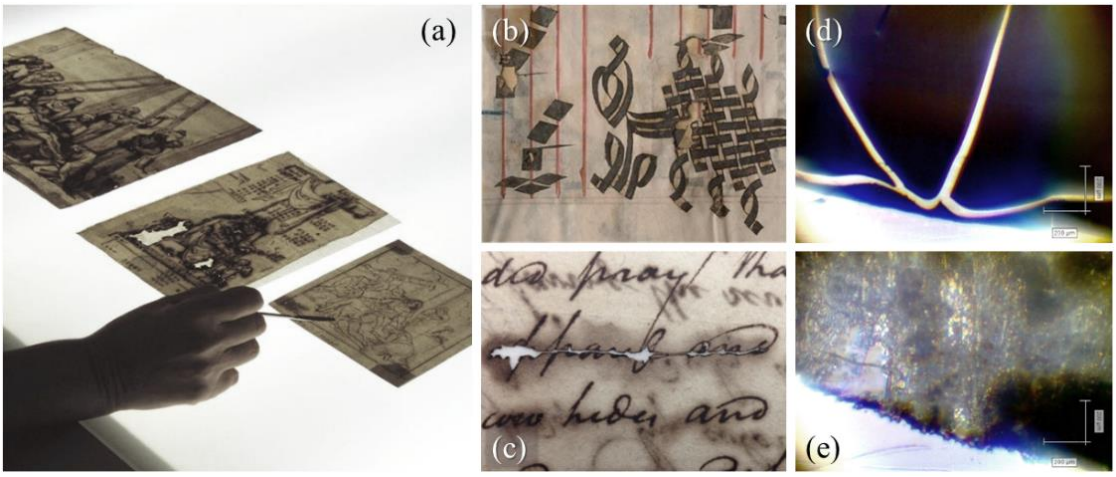

Figure 2. *Algunos ejemplos de posibles deterioros observados a causa de la tinta ferrogálica: (a) muestras de papel artesanal con la tinta ferrogálica apoyados sobre una mesa de luz cual facilita la observación de deterioros tales como perdidas de soporte, presencia de hongos, etc., así como la aplicación del proceso de su detención; (b) fotografía de una página del libro del coro manuscrito en pergamino con la pérdida de soporte por la oxidación de la tinta; (c) fotografía del soporte celulósico mostrando la pérdida de soporte y migración de la tinta; y fotografías de microscopía óptica de la tinta tánica (complejos del ácido tánico con sulfato de hierro(II)) preparada en nuestro laboratorio, usando las sigientes proporciones de ácido tánico y hierro, respectivamente: 1:10 (mayor presencia de hierro) (d) , 10:1 (mayor presencia de tánico) (e), y depositada sobre el papel.*

Los análisis científicos realizados sobre pigmentos, tintas o en general cualquier material empleado en la creación de obras de arte, resulta la mejor herramienta de la que disponemos para comprender su origen, procedencia, valor histórico o edad. También arrojan información muy valiosa sobre los mecanismos de degradación que intervienen en el bien de interés cultural, permitiéndonos conocerlos e identificarlos así como aplicar las condiciones adecuadas de su depósito y conservación.

El estudio científico de documentos, manuscritos o fotografías históricas implica el análisis de sus componentes intrínsecos, como pueden ser: los soportes (celulósicos,

los proteicos, los albuminados...), los aglutinantes, los aceites, los disolventes, los aditivos o los colorantes que se encuentren presentes en las obras. Estas investigaciones suelen ser muy complejas debido a que los bienes culturales están compuestos por múltiples materiales y capas.

Generalmente, hoy día, para llevar a cabo cualquier proyecto de investigación se requiere un enfoque interdisciplinar. Específicamente, en el caso del Patrimonio Cultural, este camino comienza con los conservadores y restauradores, es decir, los responsables de evidenciar la existencia de cualquier anomalía, que deberá de ser corroborada y contrastada por el método científico llevado a cabo colaborando con otros expertos del campo de química y/o física, etc. De tal manera, su estudio estará basado en diversas técnicas analíticas, que permitirán resolver los problemas y desafíos planteados durante la investigación.

ii) Degradación de las tintas ferrogálicas

Las obras de arte sobre papel a menudo cambian en apariencia, debido a la acción de diferentes factores endógenos y exógenos. Es bien conocido que factores externos, como la temperatura, la humedad relativa, la luz y/o los contaminantes del aire, están relacionados con la estabilidad química de cualquier material orgánico. Y por tanto, en un entorno adecuado o en condiciones estándar (STP), la velocidad de las reacciones de degradación, como la degradación oxidativa o hidrológica, disminuyen. Mientras que las condiciones de almacenamiento o manipulación inadecuadas contribuyen significativamente a cambios perjudiciales y a menudo hasta irreversibles para los materiales celulósicos [8], [9]. De igual manera, se debe de tener en cuenta otros efectos degradantes, como las catástrofes naturales (inundaciones o fuegos en archivos históricos) o el vandalismo (garabatos atemporales, subrayadores fosforitos, pegatinas, etc.), que también pueden ser una causa de su daño y pérdida de este tipo de obras.

Probablemente la consecuencia más negativa que se manifiesta en los documentos es la corrosión de la escritura, que se traduce en una degradación progresiva e incluso destrucción completa de los documentos [10]. Como se muestra en la **Figure 2**, la presencia y naturaleza de las sales de hierro (uno de los componentes fundamentales de esta tinta) es el principal factor de degradación del soporte celulósico. Es decir,

la oxidación de las sales metálicas implica una degradación del soporte, acompañada de efectos adversos generalmente asociados a la migración de las sales metálicas. En la **Figure 2**c se puede apreciar dicho efecto que visualmente se percibe como una aureola de baja intensidad cromática alrededor de la grafía. Otras consecuencias, más agresivas, causadas por la oxidación dada, se pueden ver en la **Figure 2**a (documento central), b o c en su caso más extremo. Como se observa, se trata de unas roturas del soporte, tanto celulósico (**Figure 2**a y c) como proteico (**Figure 2**b). En otros casos, la tinta no se ha preparado en proporciones equilibradas y por eso existe una distribución de alta concentración local de metales, como es el caso de la **Figure 2**d, dando lugar a una tinta quebradiza y seca con tendencia a agrietarse y desprenderse de la superficie con el roce. En contraposición, la **Figure 2**e presenta una tinta con baja concentración de sales metálicas cual es fácilmente detectable mediante microscopia óptica.

En general, la degradación del soporte histórico por las IGIs es un proceso sinérgico tanto de hidrólisis ácida causada por la naturaleza del propio soporte como por los ingredientes ácidos de tinta que produce oxidación catalizada por iones de hierro y/o cobre libres [11], [12]. Además, se debe de tener en cuenta la amplia variedad de recetas e ingredientes de diversa naturaleza presentes en la manufactura de IGI, así como las posibles impurezas de los materiales de origen histórico empleadas en su elaboración. La investigación de este material de escritura y dibujo se enfrenta a un sistema difícilmente reproducible que hace estos estudios de corrosión bastante bien complicados.

Es por ello que cada día más y más instituciones apuestan por el método científico como diagnosis, combinando con la actividad del Conservador-Restaurador. Esta sinergia tiene como objetivo final preservar la integridad física de la obra de arte el mayor tiempo posible.

iii) Composición de las tintas ferrogálicas

La extensa utilización a nivel mundial de las IGIs, ha permitido la conservación y transmisión de diferentes recetas de fabricación de estas tintas. Existe una inmensa diversidad de recetas disponibles provenientes de culturas y periodos muy diferentes, pero todas ellas presentan una serie de componentes constantes en su composición. En estas recetas tradicionales se pueden encontrar de manera recurrente sustancias

polifenólicas vegetales y sulfatos minerales aglutinados por resinas procedentes de árboles, vinculados en un medio líquido. La **Figure 3** muestra los principales componentes de las IGIs.

De todos modos, las recetas variaron a lo largo de la historia según la región, la cultura y/o tendencias históricas en las que IGIs fueron creadas y utilizadas. Así mismo, el análisis realizado sobre diferentes documentos y manuscritos históricos puede revelar información sobre sus componentes, ayudarnos a comprender los procesos de degradación ocurridos sobre los materiales de soporte o incluso, con la ayuda de los registros históricos, podría obtenerse también información sobre los períodos en los que fueron creados.

Figure 3. *Imágenes representativas de las fuentes naturales más comunes – de componentes principales - de la preparación de tinta ferrogálica: (a) agallas de los robles en el árbol (fuente natural del ácido tánico); (b) sulfatos minerales, generalmente de hierro, con impurezas de cobre, zinc o plomo; (c) goma arábiga precedente de la Acacia; (d) materia orgánica y microorganismos en agua estancada.*

La **Figure 3**a muestra la fuente natural más común de taninos hidrolizables, que son derivados del ácido gálico y actúan como agentes quelantes para unir iones metálicos, especialmente iones de hierro. El ácido gálico es capaz de crear complejos coloreados también con las partículas de cobre o incluso con otros metales de transición [11]. Los sulfatos ferrosos o vitriolos, denominados así en las recetas antiguas, representados en la **Figure 3**b, se obtienen de diferentes minas mediante diversas técnicas de extracción. Por tanto, la tinta ferrogálica puede también contener otro tipo de sulfatos, i.e. de cobre, manganeso, zinc, y/o alúmina. No es de extrañar, que en algunas recetas se mencione el sulfato de cobre como un componente principal para la fabricación de las IGIs [10].

En la **Figure 3**c está representada la goma arábiga, compuesto de color amarillo dorado que se extrae de la resina de ciertas variedades de *Acacia*. La goma arábiga

es soluble en agua y en la suspensión de la tinta tiene una función del emulsionante de las partículas de pigmento insolubles. Por lo tanto, cambia la viscosidad de la tinta y evita su sedimentación. Además, actúa como aglutinante de la tinta con la superficie del papel, mejora su adhesión y brillo y disminuye su penetración y esparcimiento por el papel. Se demostró que la goma arábiga también aumenta la tasa de formación de complejos, así como su estabilidad [13], [14].

Finalmente, la fase liquida de la IGI empleada en la dispersión de los materiales sólidos fue, según consta en la mayoría de las recetas, medio acuoso (agua de lluvia, agua estancada de lagos o charcos, etc.; **Figure 3**d). En otras ocasiones, sin embargo, se empleó vino, cerveza o vinagre. Cabe destacar que la adición del alcohol evita que la tinta se congele y reduce la tensión superficial del solvente, lo que permitió una adsorción más rápida de la tinta en el soporte del papel.

En los siguientes párrafos, se definen en más detalle cada componente principal de la tinta ferrogálica, así como algunos de los aditivos más comúnmente empleados. Este análisis se basa en los estudios previos de Gemma María Contreras Zamorano, recopilados en su tesis doctoral del departamento de Historia del Arte de la Universidad de Valencia [15].

■ Taninos

Debido a su alto contenido en taninos, las agallas han sido aprovechadas desde la Antigüedad con fines tintóreos, farmacéuticos y para la escritura. Generalmente, esta fuente de taninos se ha obtenido principalmente de las agallas de los robles, siendo las históricamente más famosas, las de Alepo (Siria) [15]. Presentan una forma esférica y regular con numerosas protuberancias. Las más valoradas fueron las de la tonalidad azul o verdosa y sin orificios, así que en numerosas ocasiones se recurría al fraude tapando los agujeros de salida de las larvas con cera. No se ha de confundir las agallas de los robles con el fruto del roble que es la bellota. Las agallas son estructuras de tipo tumoral inducidas por insectos, bacterias, hongos, etc., siendo la respuesta vegetal defensiva a la presencia de un parasito y/o infección.

Los taninos son polímeros complejos de metabolitos secundarios de plantas superiores, especialmente de la familia de *Leguminosae*, *Rosaceae*, *Polygonaceae*, *Fagaceae*, *Rhyzophoraceae*, *Myrtaceae* y *Melastomaceae* [16]. Las fuentes de taninos se pueden clasificar en varias categorías:

- Taninos condensables: comunes en las maderas de las plantas leñosas.
- Taninos hidrolizables: más pequeños y formados por ácidos fenólicos.
- Florotaninos: proceden de varias especies de algas.

Entre las características más peculiares de los taninos cabe destacar que son solubles en agua y poseen una estructura polifenólica. Aparte de eso, los taninos son sustancias reductoras sensibles a la oxidación en un medio ácido y precipitan después de su reacción con numerosos reactivos, entre ellos metales pesados como el hierro, el plomo, el cobre y el zinc. Los ácidos tánicos interaccionan con los sulfatos metálicos propiciando una coloración negra de gran intensidad que, en principio, representa el origen fundamental de la tinta ferrogálica [15].

Algunas de las investigaciones previas sobre el compuesto de ácido tánico, que forma parte de la tinta IGI, se ve recogido en los textos de Guibourt [17]. Este farmacéutico francés investigó ya en el año 1845 un gran número de productos naturales, entre ellos los óxidos, sulfuros, y otros compuestos del mercurio, el arsénico, así como sus compuestos correspondientes. Posteriormente, en el 1940, Ainsworth Mitchell, químico y científico forense británico, realizó un estudio microscópico y químico de la escritura a mano [18]. En sus estudios concluye que las agallas presentan un 65% de taninos en ellas, entre otros componentes como el ácido gálico, el ácido elágico o el ácido luteogálico, además de una pequeña proporción de azúcar, potasio y sales de calcio. Por otro lado, en los estudios realizados en 2015, por Zamorano, mediante microscopio electrónico de barrido (SEM-EDX), se advierte una importante presencia de potasio en la composición de las agallas. Además, sus estudios cromatográficos concluyen la presencia de ácido gálico de forma más intensa, así como de ácido elágico.

■ Sulfatos minerales

El sulfato de hierro es imprescindible para la elaboración de las tintas ferrogálicas. Sin embargo, Kroustallis en su diccionario de materiales y técnicas artísticas [19] escribe que generalmente en las tintas aparecen, a modo de impureza del hierro, también otros metales (en un porcentaje en torno a 15-20%), como el cobre o zinc. Es decir, son los residuos de metales pesados, como es también el plomo, procedentes de las calderas en cuales se purificaba el hierro. Además, en numerosas ocasiones aparecen también sodio y potasio asociado a la naturaleza de las minas de procedencia.

No resulta fácil identificar la naturaleza exacta de los sulfatos metálicos en las fuentes escritas debido a que existe una enorme confusión en su nomenclatura. Se utilizaban las denominaciones vitriolo, aceche y caparrosa, indistintamente y sin un criterio evidente respecto a su naturaleza. En la península ibérica al sulfato de cobre se le suele conocer cómo la caparrosa y así aparece recogido en las recetas del Libro de Oficios de Guadalupe así como en las recetas proporcionadas por Oscal Lillo conservadas en la Biblioteca de la Universidad de Salamanca. Por otro lado, el sulfato de cobre era identificado bajo la palabra aceche (az-zaj; de procedencia árabe) que aparece tanto en las recetas magrebíes, valencianas o cordobesas [15].

■ Gomas

Se trata de resinas procedentes de árboles tales como ciruelos, perales, cerezos, almendros, etc. La goma más empleada es la conocida como goma arábiga, extraída de la *Acacia* y es la de mayor calidad. Se emplea como aglutinante y aporta lustre a la tinta, además de elevar el grado de viscosidad y homogenizar la tinta misma.

Aunque su uso era generalizado, no siempre se cita o se recomienda en las recetas. Algunos estudios del arte de escribir consideran su uso incluso innecesario, especialmente en tintas destinadas a la escritura de los niños o cuando se trataba de su empleo fuera de los meses de verano [13], [19].

■ Solventes

El solvente por excelencia recomendado para la elaboración de las IGIs ha sido el agua de lluvia, cisterna o pozo. Es decir, agua sedimentaria, poco calcárea y llena de materia orgánica.

Aparte de eso, el vino blanco también ganó su popularidad como diluyente, especialmente durante el siglo XVI y principalmente en la zona de la Corona de Aragón. No ha estado presente en recetas musulmanas debido a que se trata de una bebida prohibida y por lo tanto de difícil acceso en Dar-el-Islam. En la práctica, se empleó el vino blanco, al vino tinto se hace referencia solo en contadas ocasiones.

El alcohol etílico o etanol facilita la extracción de los taninos, disminuye el tiempo de secado y protege a la tinta de las infecciones de microorganismos y hongos. Sin embargo, con el tiempo el etanol se convierte en ácido acético y vuelve la tinta más ácida propiciando su deterioro.

De manera puntual se pueden encontrar también recetas que emplean cerveza como un solvente. Generalmente es el caso de las recetas con orígenes en el norte de Europa.

Finalmente, el uso de otros solventes como el aguardiente, el vinagre, e incluso las claras de huevo que conferían a la tinta un aspecto brillante y mejor adhesividad, era raro, pero no excepcional.

■ Aditivos

Como aditivo se puede generalmente considerar todo aquel material que se puede encontrar mencionado en cualquier libro de técnicas artísticas tradicionales. En su mayoría se trata de materia de origen vegetal, como cortezas de frutos, raíces, flores, savias. Pero también los hay de origen animal, como hiel de carnero, clara de huevo, junto con diversos minerales y productos más elaborados como destilados alcohólicos y cerveza.

■ Preservante

El vinagre ha sido un recurso muy utilizado como un conservante e incluso ha llegado a utilizarse en sustitución del vino blanco como solvente para aclarar la tinta o espesarla en lugar de la orina, que también se empleaba a veces en la preparación de las IGIs. Al igual que la piedra de alumbre, mineral compuesto de sulfato aluminio y potasio presentaba propiedades antibacterianas y astringentes. Finalmente, algunos destilados y licores de alta graduación aparecen también entre los aditivos preservantes, por su acción antiséptica debida a su alto contenido de alcohol.

■ Colorante

El colorante más comúnmente empleado ha sido el mirto o arrayán cual al adicionar las hojas hervidas al preparado le aporta el color, así como el olor. Para intensificar o virar el color se empleaba también agua de carbón de pin picado o marfil quemado. En otras ocasiones se usaba la flor de amapola seca debido a que representa una fuente rica en taninos y además confiere un tinte rojizo a la tinta. Por otro lado, el palo morado y el palo de la India contribuyen a virar el color de la tinta aún a un tono más cobrizo.

Para obtener una tinta más azulada se usaron pigmentos de origen mineral y orgánico como, por ejemplo, el lapislázuli, que por su escasez y alto valor de mercado se sustituyó a finales del siglo XIX por el azul de Prusia o por el índigo conocido también como añil.

iv) Recetas representativas históricas e internacionales de preparación de IGIs

Se presentan en este apartado tres recetas internacionales, que han sido traducidas primero al inglés y posteriormente a muchos otros idiomas, y que pertenecen a y así representan diferentes cronologías y localizaciones. Con esta selección de recetas se pretende denotar los principales ingredientes utilizados, los protocolos de fabricación más comunes, así como la evolución en las recetas y sus variaciones. En todos los casos, la causa de la coloración de la tinta es la unión de la fuente de taninos y vitriolos o, en otras palabras, una reacción de ácido tánico con iones metálicos de hierro.

La primera receta presentada en la **Figure 4** proviene de Francia y pertenece al siglo XIV. Se encuentra recogida en "Le Ménagier de Paris" [20] y su correspondiente traducción al inglés se puede encontrar en "The Good Wife's Guide" del año 2009 [21].

Literamente se describe de la siguiente manera: "*To make 3 quarts of ink, take 2 ounces each of galls and gum arabic, and 3 ounces of copperas. Break the galls and soak them for 3 days, then boil in three half gallons of rainwater or water from a still pond. And when they have boiled long enough so that nearly half the water has boiled off (that is, there is only about 3 quarts left) take off the fire, and add the copperas and gum, and stir until cool. Store in a cold, clamp place. Note that after 3 weeks, it will spoil*."

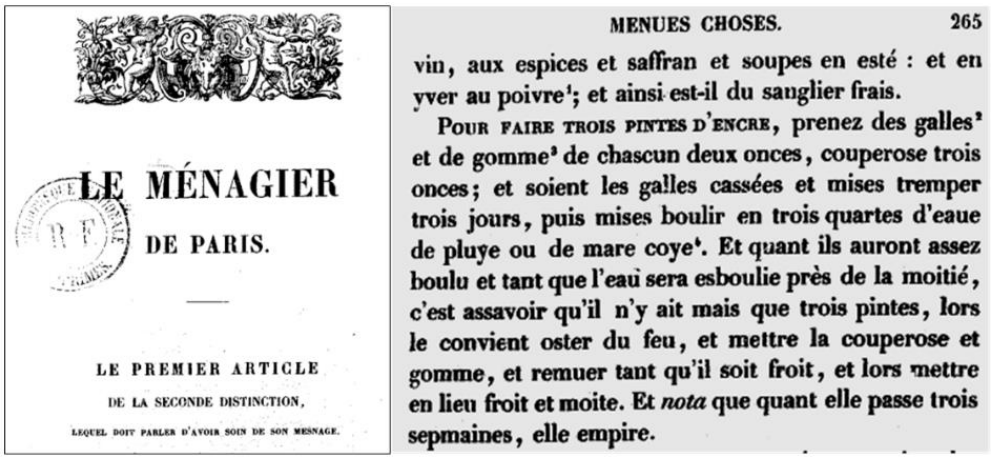

LE MÉNAGIER
DE PARIS.

LE PREMIER ARTICLE
DE LA SECONDE DISTINCTION,
LEQUEL DOIT PARLER D'AVOIR SOIN DE SON MESNAGE.

MENUES CHOSES. 265

vin, aux espices et saffran et soupes en esté : et en yver au poivre[1]; et ainsi est-il du sanglier frais.

POUR FAIRE TROIS PINTES D'ENCRE, prenez des galles[2] et de gomme[3] de chascun deux onces, couperose trois onces; et soient les galles cassées et mises tremper trois jours, puis mises boulir en trois quartes d'eaue de pluye ou de mare coye[4]. Et quant ils auront assez boulu et tant que l'eau sera esboulie près de la moitié, c'est assavoir qu'il n'y ait mais que trois pintes, lors le convient oster du feu, et mettre la couperose et gomme, et remuer tant qu'il soit froit, et lors mettre en lieu froit et moite. Et *nota* que quant elle passe trois sepmaines, elle empire.

Figure 4. *Imagen de la portada del libro "Le Ménagier de Paris" (tomo segundo, París, 1846) y de su corespondiente página (página 265) con la receta del tratado de moralidad y economía doméstica compuesta por un burgués parisino.*

La **Figure 5** muestra una receta elaborada en Italia a principios del siglo XV que se puede encontrar en el libro "Segreti per Colori" [22]. La receta original se refiere a la fabricación de una tinta para escribir mediante el uso de productos e ingredientes locales, como es, por ejemplo, un vino blanco fuerte.

Su traducción al inglés dice lo siguiente: "*4 oz. of galls well crushed, one handful of dried rinds of pomegranates, one handful of fresh bark of mountain ash scraped with a knife, and one handful of fresh bark of roots of walnut trees, and 2 ½ oz. of gum Arabic; mix the whole together with wine, and let the mixture remain for 6 to 8 days in the sun, stirring it well 4 or 6 times every day. Then add 2 ½ oz. of Roman vitriol, and mix it frequently, and let it remain so for several days; then put it over the fire to boil for the space of one miserere, let it cool, and then strain it and leave it for 2 days in the sun. If you then put in it a little roche alum it will make it much brighter, and it will be good and perfect writing ink.*

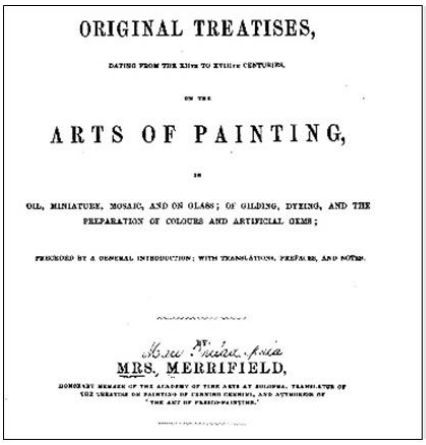
ORIGINAL TREATISES,

DATING FROM THE XIIth TO XVIIIth CENTURIES,

ON THE

ARTS OF PAINTING,

IN

OIL, MINIATURE, MOSAIC, AND ON GLASS; OF GILDING, DYEING, AND THE PREPARATION OF COLOURS AND ARTIFICIAL GEMS;

PRECEDED BY A GENERAL INTRODUCTION; WITH TRANSLATIONS, PREFACES, AND NOTES.

MRS. MERRIFIELD,

HONORARY MEMBER OF THE ACADEMY OF FINE ARTS AT BOLOGNA, TRANSLATOR OF THE TREATISE ON PAINTING OF CENNINO CENNINI, AND AUTHORESS OF "THE ART OF FRESCO-PAINTING."

374. ***A fare inchostro bono et da scrivare.***—Tolli uno bocale de vino bianco grande et bono et once 4 de galla amachata bene et una manciata de scorze de mele granate seche et una manciata de scorze de ornello fresco rase con lo cortello et una manciata de scorze de raiche de noce fresche poi tollj once 2 et ½ de goniarabico et mistica omne cosa insiemj cum lo sopradicto vino et fa stare per 6 o 8 di al sole et omne di lo mista 4 o 6 volte molto bene poi ce pone doi once et ½ de vitriolo romano et mistalo spesso et stia cosci per alcunj di et poi el pone al foco a bullire per spatio duno miserere et lassalo fredare et poi lo cola et metilo doi dj al sole et se ce mectj poi uno poco dalumj de rocho farallo piu lustro assa et vira perfecta et bona intinta da scrivare.

Figure 5. *Imagen de la portada del libro "Arts of Paintings" (traducido por Mary Philadelphia, 1849) y de su corespondiente página (página 590) con la receta de tratados originales, que datan de los siglos de XII al XVIII sobre las artes de la pintura, en óleo, miniatura, mosaico y vidrio; de dorado, teñido y preparación de colores y gemas artificiales.*

La tercera receta seleccionada y mostrada en la **Figure 6** se data a finales del siglo XVII y proviene de la Biblioteca de la Universidad de Yale [23]. En esta receta está escrito: "*To make excellent ink: Raine water 3 gallons, of white wine vinegar a quart, gaules two pounds, gum arabeck one pound, pomegranate pills one quarter of a pound, all these bruised but not beat too small, copporus two ounces, this will be ready the sooner, if it stands near by the fire, or in the sun.*"

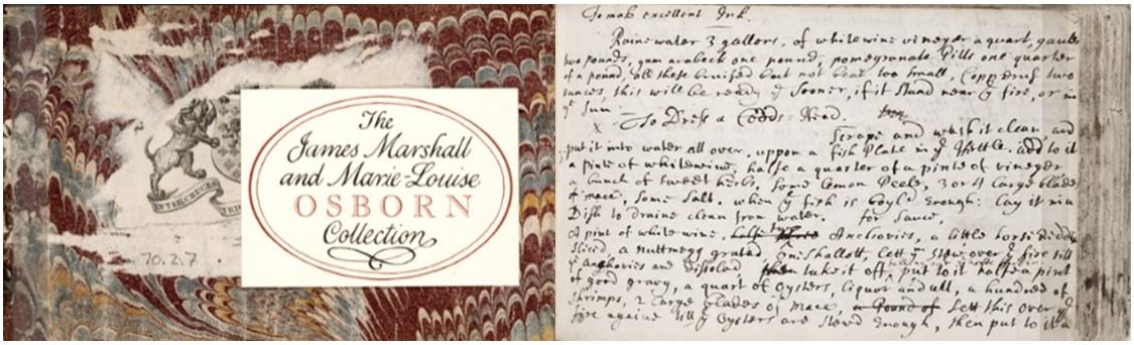

Figure 6. *Imagen de la portada del libro común que forma parte de la colección James Marshall y Marie-Louise Osborn de la Biblioteca de libros raros y manuscritos de Beinecke, Universidad de Yale y de su corespondiente página con la receta procedente de Osborn.*

v) Clasificación de diferentes tipos de tintas negras

En esta tesis hablamos de la tinta ferrogálica, un tipo de tinta negra. Sin embargo, a lo largo de la historia se han empleado diferentes tintas negras que se pueden clasificar en cuatro grandes grupos: 1) tintas a base de carbón, 2) tintas metalogálicas o más conocidas en la literatura como ferrogálicas, 3) tintas mixtas y 4) tintas incompletas. A continuación se presenta una tabla (**Table 1**) que recoge la información resumida de cada tipo de tinta negra, la forma de su preparación así como sus propiedades más características [24]. Cabe destacar, respecto a sus propiedades, que las tintas de carbono son menos reactivas químicamente que las tintas metalogálicas, pero más inestables frente al tiempo.

Table 1. Información recopilada de "Les Encres noiresau Moyen Age" respecto a la clasificación de las tintas negras propuesta por Monique Zerdoun Bat-Yehouda. El código de colores empleado es una simple representación de cada tipo de tinta.

Clasificación y Fórmula	Preparación	Propiedades
CARBÓN o ***noir de fumeé*** ■+□	Pigmento negro a base de productos calcinados de diversas sustancias procedentes de hollín (de madera, resinas, aceites); está mezclado con un ligante (como gomas, miel, gelatina, claras de huevo, colas animales o aceites).	No está sujeto a reducción u oxidación debido a la inercia química del carbono. Sin embargo, la mezcla de ligante-carbón no penetra muy bien en las fibras del soporte, por lo que la erosión suele ser suficiente para hacer desaparecer la tinta.
METALOGÁLICA o ***ferrogálica*** ■+■+□	Preparada a partir de extractos de plantas que aportan taninos - la sustancia activa se extrae por maceración de las plantas. Si al líquido obtenido se le añade una sal metálica, como sulfato de cobre o hierro, se forma un complejo negro. Para aumentar la viscosidad del medio se añade un aglutinante, generalmente goma arábiga.	Apenas se conoce la reacción química de la tinta del complejo ferrogálico. Las tintas metalogálicas son a menudo tintas corrosivas que hacen que el soporte sea más ácido y quebradizo.
MIXTA ■+■+□ ■+■+□ ■+■+■+□	Tintas de carbón a las que el preparador ha añadido extractos acuosos de sustancias tánicas o sales metálicas. También son tintas metalogálicas en las que se ha incorporado humo negro.	El negro de lámpara agregado a una tinta de agalla metálica acentúa la intensidad del color.
INCOMPLETA ■+■ ■+□ ■+□	Aparte de los elementos negros que caracterizan la naturaleza de una tinta, los fabricantes agregan también aditivos.	El negro de lámpara agregado a una tinta de agalla metálica acentúa la intensidad del color.
Leyenda: ■ Humo negro de productos calcinados □ Ligante ■ Extractos de taninos ■ Sal metálica		

1.2 Teoría del color: las causas del color

No todas las personas tienen el mismo sentido de los colores. Comprender y definir qué es el color en sí presenta un tema sumamente interesante para muchas áreas científicas diferentes, pero especialmente para la química, la física y la psicología. El color es percibido por nuestros sentidos, por lo que la percepción del color puede variar mucho cuando lo define una persona u otra. Sin embargo, en este trabajo intentamos ceñirnos a la definición del color desde un punto de vista físico. Y para ello me basaré en la frase publicada en el año 2010 por Kurt Nassau en la revista *Scientific American*: *"The Causes of Color are diverse, but they all stem from the same root: It is the electrons in matter, through their varied responses to different wavelengths of light, that make the world a many-colored place."* [25].

El color de una molécula se debe a diferentes fenómenos. Entre ellos la absorción de radiación es el más común, el cual consiste en una transición del electrón del nivel más bajo a uno más alto. Como se muestra en la **Figure 7**a, cuando una molécula absorbe la luz visible o ultravioleta, un electrón se promociona a un orbital de mayor energía. La longitud de onda (λ) de la luz absorbida depende de la diferencia de energía entre el estado excitado y el fundamental de la molécula. Por lo tanto, la promoción de los electrones a niveles superiores de energía induce la retirada de la luz cuya energía se emplea para llevar a cabo esa transición, quedando en el medio la luz complementaria que da lugar al color observado.

En consecuencia, cuanto mayor diferencia de energía exista entre los niveles energéticos iniciales y finales, mayor será la frecuencia de la luz absorbida o, lo que es lo mismo, menor será la longitud de onda de esa luz absorbida. Para la observación de un color, la energía que se pone en juego en la transición electrónica entre niveles energéticos debe de ser tal que la longitud de onda se encuentre comprendida en el intervalo 400-700 nm, que es el intervalo correspondiente a la luz visible [26], representado por sus longitudes de onda específicas en la **Figure 7**b.

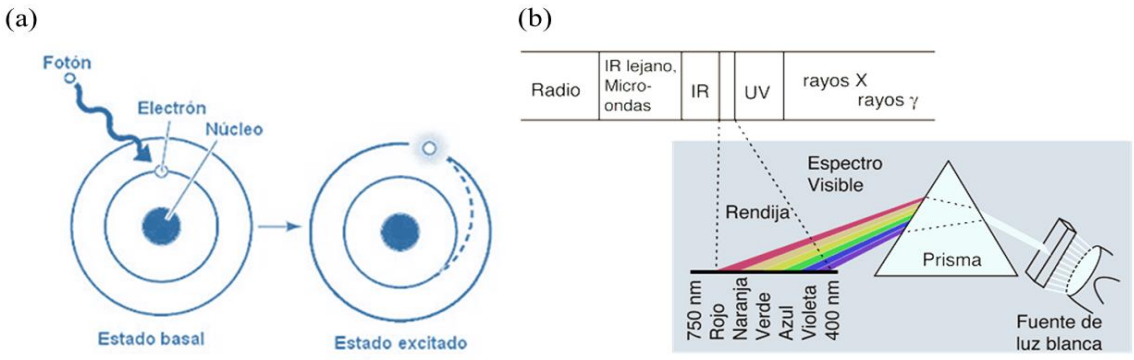

Figure 7. *Imágenes esquemáticas de (a) la excitación de electrones de una materia por la luz (radiación electromagnética), y (b) la dispersión de la luz blanca por un prisma dando lugar a una separación de ella misma en sus correspondientes colores espectrales.*

Las transiciones que dan lugar al color en las moléculas implican a los electrones de valencia **Figure 7**a. En general podemos clasificar los colorantes en orgánicos e inorgánicos. En las moléculas orgánicas existen unos grupos cromóforos que son más propensos a generar color. Estos grupos cromóforos están presentes en más de 8000 pigmentos, colorantes y/o tintes [26].

Los colorantes manifiestan un color porque absorben la luz en el rango del espectro visible y esto es así porque poseen grupos cromóforos o grupos portadores de color. En muchos casos la estructura de estos colorantes presenta enlaces tipo π o un sistema conjugado de enlaces π, es decir, una estructura de enlaces dobles y simples alternos. Esta conjugación da lugar a una resonancia electrónica que proporciona estabilidad a los compuestos orgánicos que la poseen [27]. La **Table 2** muestra algunos ejemplos de las moléculas con dobles y triples enlaces carbono-carbono, sistemas aromáticos, grupo carbonilo, imino (C=N), diazo (N=N), nitro o con enlaces del tipo C-Y, donde Y es un átomo con pares libres, que representan unos grupos cromóforos excelentes.

Table 2. Resumen de los principales grupos aportadores de color en la química orgánica: columna de la izquierda representa los grupos cromóforos y la columna de la derecha los auxocromos.

GRUPOS CROMÓFOROS		GRUPOS AUXOCROMOS	
-N=N-	Azo	-OH	Hidróxilo
>C=S	Tiocarbonilo	$-NH_2$	Amino
	Nitro	-COOH	Carboxilo
-N=O	Nitroso	R-N<H	Amino mono sustituido
-C=C-	Etilénico	R-N<R	Amino disustituido
>C=O	Carbinol	-CO-r	Ácido (r = radical de ácido graso)
-C=N- | H	Azometino	$-SO_3H$	Súlfonico
-S=S-	Disulfuro	-SR	Sulfuro
	Paraquinona	-	-
	Ortoquinona	-	-

Además, generalmente, la mayoría de los colorantes contienen también grupos auxocromos. Estos grupos frecuentemente están formados por átomos cargados positivamente, que intensifican la acción de otro grupo de átomos no saturados (sistema conjugado), de tal manera que su presencia hace que la sustancia química sea coloreada. Estos grupos se comportan como dadores de electrones, siendo responsables de la formación de sales débiles y fácilmente solubles. Los auxocromos son conocidos

también como ayudantes del color. Para que seamos más precisos, estos grupos no son responsables del color mismo, pero su presencia puede modificarlo. Además, pueden también influir la solubilidad de la molécula y por lo tanto tener un efecto modificador de su color. Algunos ejemplos típicos de dichos grupos son los grupos de metilo, halógenos, hidroxi, alcoxi, amino (**Table 2**).

En general, las moléculas aromáticas poseen una mayor tendencia para producir color debido a la existencia de enlaces π junto con los enlaces σ (**Figure 8**b y c). Los enlaces se establecen entre los orbitales híbridos sp^2 en el plano del anillo. El solapamiento de orbitales p perpendiculares al plano del anillo da lugar a enlaces π deslocalizados que podemos representar como una nube anular por encima y por debajo del plano formado por los átomos de C. Este solapamiento da lugar a la existencia de orbitales π enlazantes y antienlazantes en el anillo bencénico. Las transiciones entre orbitales enlazantes y antienlazantes suelen ser la fuente fundamental de color en este tipo de moléculas al implicar una radiación de energía comprendida en el intervalo visible-UV del espectro electromagnético.

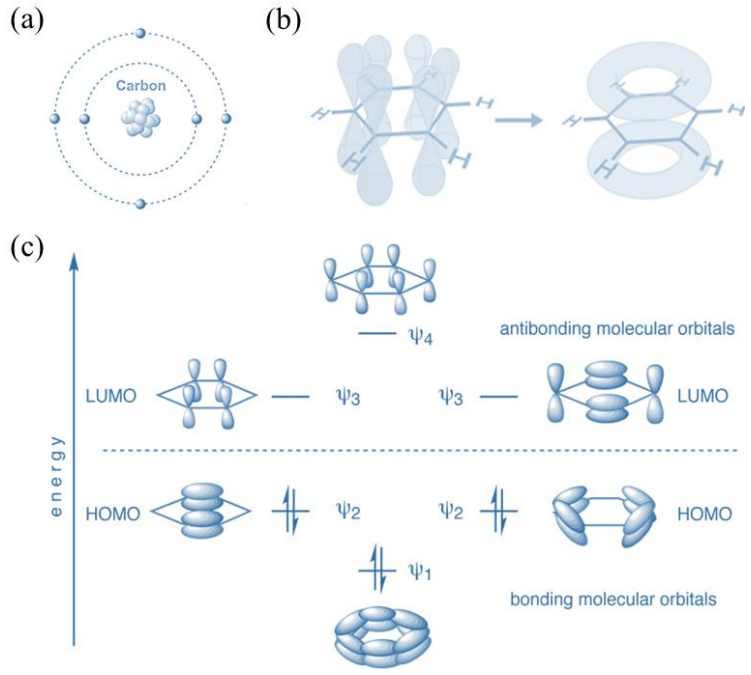

Figure 8. *Imágenes esquemáticas de (a) electrones de valencia en la molécula de carbono, la capa exterior de electrones contiene 4 electrones disponibles; (b) hibridación del orbital en los anillos de la molécula de benceno; (c) los orbitales moleculares π del benceno. La línea de puntos representa la energía de un orbital p, todos los orbitales por debajo de esta línea están enlazados, todos los que están por encima de esta línea están antienlazados. El benceno tiene seis electrones en su sistema π, por lo que todos los orbitales moleculares de enlace están ocupados. El término HOMO se refiera al orbital molecular ocupado de mayor energía), mientras que LUMO se refiere al orbital molecular desocupado de menor energía.*

Como caso especial de colorantes en el ámbito del Patrimonio, las tintas ferrogálicas, desde el punto de vista químico, son polifenoles que presentan gran número de grupos bencénicos aromáticos que suelen estar conjugadas con otros grupos químicos dando lugar a transiciones dentro de la zona UV-visible del espectro. Las transiciones energéticas entre orbitales π en estos polifenoles son demasiado energéticas para producir un efecto de color, ya que la energía que implican se encuentra dentro de la zona UV. Sin embargo, la interacción con metales de transición como el hierro y el cobre, induce la creación de nuevas transiciones electrónicas en los complejos formados que son de menor energía. Este desplazamiento en energía sí es suficiente para inducir color en estos compuestos y es el método empleado para inducir el color oscuro en tintas ferrogálicas.

Finalmente, se muestran en este trabajo también las causas del color clasificadas según Alex Byrne [28], cual describe 5 grandes tipos de sí mismas, que se luego subdividen en un total de 14 categorías (**Table 3**).

Table 3. Tabla extraída de clasificación de las "Causas del color" propuesta por Alex Byrne, en la cual se destacan las dos causas principales del color en las tintas de agallas de hierro [28].

Transiciones electrónicas en átomos e iones libres, transiciones vibratorias en moléculas.	Excitaciones electrónicas	Incandescencia, llamas, chispas, rayos, descargas de gas, algunos láseres.
	Vibraciones	Coloración azul-verdosa de agua pura o hielo.
Cristales	Transiciones-metal puros	Turquesa, la mayoría de los pigmentos, algunos láseres, algunos fósforos, algunos materiales fluorescentes.
	Transiciones-metal impurezas	Rubí, esmeralda, arenisca roja, algunos láseres.
	Irisacióno Centros de color (desequilibrios de cargas en una determinada zona)	Cuarzo ahumado, cristal de amatista del desierto.
Transiciones entre orbitales moleculares.	Transferencia de carga	Zafiroazul, magnetita.
	Enlaces conjugados	Tintes orgánicos, la mayoría de los colores de plantas y animales, lapislázuli, luciérnagas, láseres.
Transiciones entre materiales con bandas de energía.	Conductoresmetálicos	Cobre, plata, oro, hierro, latón.
	Semi conductores puros	Silicio, galena, cinabrio, diamante.
	Semiconductoresdopados	Diamante azul, diamante amarillo, diodos emisores de luz, láseres semiconductores, algunos fósforos.
Ópticageométrica y física	Refracciódispersiva	El arco iris, ópalo de fuego, aberración cromática.
	Scattering	Azul del cielo, rojo de los atardeceres, piedra lunar, zafiro estrella.
	Interferencia	Película de aceite en el agua, revestimientos de lentes, algunos colores de insectos.
	Rejilla de difracción	Ópalo, cristales líquidos, algunos colores de insectos.

Las celdas marcadas en color azul reflejan las que a priori serían las causas de color de las tintas ferrogálicas bajo estudio en esta Tesis. Estas categorías están seleccionadas por ser las más compatibles con la tinta ferrogálica según los elementos que la conforman.

1.3 Estructuras de las tintas ferrogálicas propuestas en la bibliografía

Hasta ahora hemos introducido las IGIs en el contexto de su origen, fabricación y composición. Sin embargo, es importante conocer y comprender también la química de las IGIs para poder identificarlas, evaluar su estado actual, así como conocer los posibles procesos químicos de degradación. Hasta la fecha han sido propuestas diferentes estructuras de los complejos entre los compuestos polifenólicos y hierro(III) que pueden ser encontradas en la literatura científica.

Varios estudios han intentado describir la estructura y composición del complejo de galato de hierro, la principal especie responsable del color de las IGIs. En la literatura existe poco consenso sobre la estructura química o composición de este complejo. Hasta ahora, solo algunas de las estructuras propuestas han sido también reconocidas como las estructuras de referencia.

Las estructuras más comúnmente aceptadas y citadas en la literatura científica son las de Wunderlich. Posteriormente, se propusieron las de Feller y Cheetham que eran similares a las de Wunderlich, aunque no fueron tan reconocidas. Finalmente, la estructura de Krekel fue otra de las configuraciones estructuralmente propuestas y generalmente aceptadas. A continuación se procede a describirlas con un poco más de detalle (**Figure 9**) [14], [29], [30]. En general, en todos estos trabajos de caracterización estructural se han empleado mayoritariamente técnicas de basadas en rayos X como la absorción de rayos X (XANES) y la espectroscopía Mösbauer.

■ Wunderlich

En el año 1990, Wunderlich demostró que la reacción entre el ácido gálico y Fe(III)Cl_3 da como resultado un material polimérico insoluble de coloración negro-azulado. Básicamente, era una estructura amorfa que contenía también unos cristales negros procedentes del polímero de coordinación de galato de Fe(III). Wunderlich concluyó, basándose en estudios realizados con XANES y espectroscopía Mösbauer, que la unión del complejo, tiene lugar principalmente a través de los grupos carboxílicos

y fenólicos, y que el complejo formado contiene hierro octaédrico coordinado con seis átomos de oxígeno y cuatro moléculas de ácido gálico, como se visualiza en la **Figure 9**a.

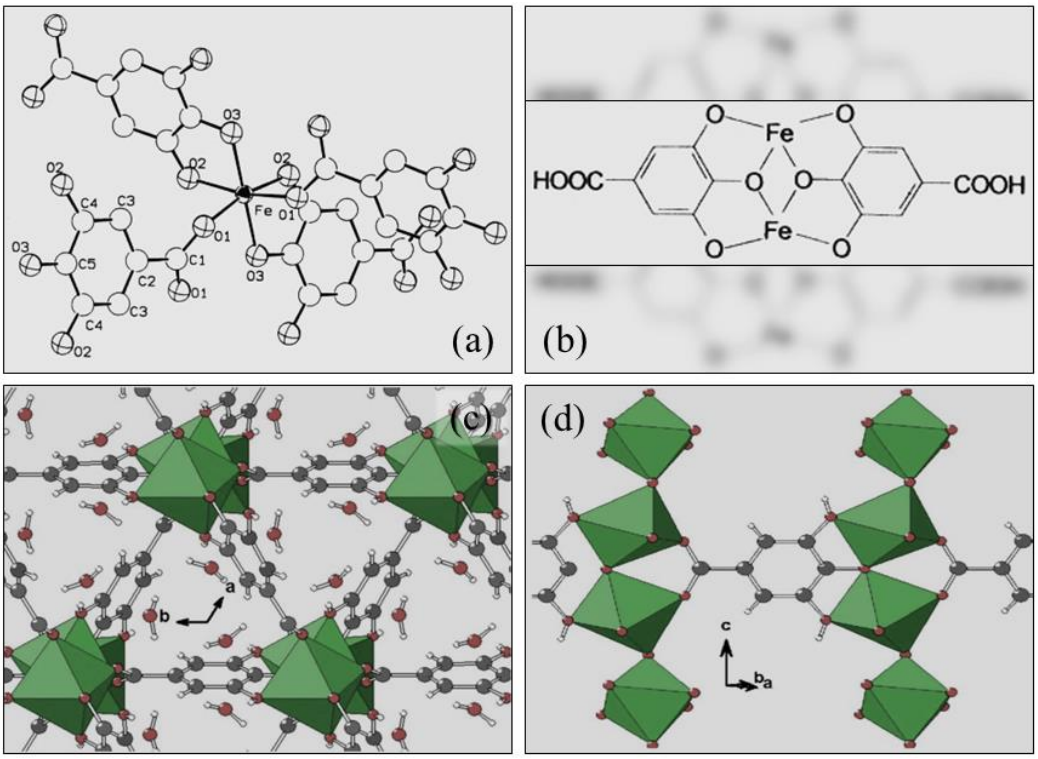

Figure 9. *Estructuras de los complejos de las IGIs propuestas por (a) Wunderlich; (b) Krekel; y (c, d) Feller y Cheetham. Los puntos rojos representan los átomos de oxígeno, los grises los de carbonos y los blancos representan los hidrógenos [30].*

■ Krekel

A continuación, en el año 1999, Krekel propuso un modelo alternativo basado en las interacciones molares proporcionales de sulfato de hierro(II) y ácido gálico basándose en técnicas como la espectrometría de masas, la espectroscopía infrarroja y la espetroscopía Mössbauer, propuso la estructura mostrada en la **Figure 9**b. Según su teoría, la oxidación inicial de Fe(II) ocurre dando lugar a un complejo tetraédrico de bis-galato de Fe(III). Posteriormente, este mismo autor sugirió el complejo sufre una descarboxilación adicional de los ligandos de galato produciendo así un complejo negro e insoluble de pirogalina octaédrico de Fe(III). Krekel asumió que la descarboxilación se debe a la acción catalítica de iones Fe(III) presentes en el sulfato ferroso como impurezas. Aunque hay sólo una ligera evidencia estructural o espectroscópica para apoyar estas propuestas, el complejo de pirogalina-octaédrico Fe(III) de Krekel fue ampliamente aceptado.

■ Feller y Cheetham

Finalmente, en el año 2006, Feller y Cheetham obtuvieron cristales de color negro-azulado, con morfología acicular o de varilla. Con el mismo complejo que Wunderlich, a proporciones molares iguales de cloruro de Fe(II) y ácido gálico, y utilizando métodos hidrotermales (**Figure 9**c y d).

Todas estas estructuras propuestas en la literatura, y en general ampliamente aceptadas, tienen un aspecto en común: lo que proponen es una interacción de taninos con los cationes de hierro u otros iones metálicos a través de los grupos –OH y –COOH formando los correspondientes quelatos [30]. En concreto, la complejación ocurre de tal manera que una unidad de ácido fenólico de los taninos se une a tres iones de hierro. Hay que destacar que incluso la forma más sencilla de las IGIs, compuesta exclusivamente por el ácido gálico y hierro, no resulta nada simple en términos de estructuras. Por lo tanto, la estructura de tal complejo es muy difícil de interpretar. Ponce et al. propusieron una estructura tridimensional para los complejos entre ácido gálico y Fe(III) parecida al modelo de Wunderlich basándose en difracción de rayos X (XRD) y espectroscopía Mössbauer. Estos autores emplearon también técnicas vibracionales (infrarrojo y Raman), pero los resultados con estas últimas técnicas no se correlacionaron en profundidad con las técnicas basadas en rayos X.

Todos estos estudios se han realizado con modelos experimentales controlando los parámetros y simplificando al máximo posible la reacción causante del color de las IGIs. Sin embargo, si dicho proceso se escala a circunstancias más próximas a la realidad, todos estos factores comienzan a complicarse. De tal manera que, por ejemplo, cuando hablamos de taninos vegetales no hablamos de un solo tipo de molécula (como cuando nos referimos al ácido gálico). Los taninos naturales están compuestos por diferentes sustancias con tendencias a polimerizaciones realmente complejas.

El efecto de la goma arábiga, componente empleado en la fabricación de las tintas para aportar viscosidad a la tinta, no ha sido tratado en profundidad en estos estudios anteriores. Por lo tanto, cada nuevo componente complica el estudio del sistema coloreado que da origen a la tinta. Todo cambio de las propiedades de la tinta como color, densidad, brillo, etc., supone también una modificación de su estructura interna debido a que este cambio viene producido por la agregación de un nuevo componente al sistema.

Las estructuras de IGIs discutidas por el momento, se tendrán en cuenta a la hora de la caracterización espectroscópica de los sistemas modelo de IGIs que se han tratado en esta Tesis.

1.4 Estado del arte

Hasta el momento, en la literatura disponible, se han utilizado diferentes análisis instrumentales, tanto los destructivos como no destructivos, para analizar las IGIs y así resolver y dilucidar la composición, estructura y causas de deterioro observado en las tintas. Varias son las técnicas comúnmente empleadas, en el estudio de las tintas, entre ellas: la espectroscopía de emisión de rayos X inducida por protones [4], [31]–[33], la microscopía electrónica de barrido con microanálisis de dispersión de rayos X [32], [34], la espectroscopía de fluorescencia de rayos X [35], [36], los microanálisis de sonda electrónica [37], la espectrometría de masas de plasma [36], [37], y la espectroscopía de absorción atómica [36]. Se debe de señalar que los análisis del estado de oxidación del hierro se realizan habitualmente mediante espectroscopía de Möessbauer [38], [39] y la microabsorción de rayos X [40]. Por otro lado, el análisis de los componentes moleculares de las tintas se ha realizado mediante cromatografía de gases combinada con espectrometría de masas [41] y la espectroscopía infrarroja por transformada de Fourier [32], [42]. Los métodos analíticos que se utilizan habitualmente para la detección de IGIs se basan en técnicas cromatográficas [43], [44]. Siendo estos muy sensibles y selectivos, pero también son destructivos para la muestra bajo análisis.

En las últimas décadas, la espectroscopía Raman ha demostrado ser una técnica no destructiva muy adecuada y eficaz, siendo aplicada en estudios de identificación sobre materiales muy diversos, desde pigmentos inorgánicos [45], [46] hasta biomateriales empleados en obras de arte [46], [47], así como en un gran número de materiales artísticos y arqueológicos [47], [48]. Se debe señalar que la espectroscopía Raman también está disponible en la actualidad como sistema portátil, lo que permite su desplazamiento y uso en bibliotecas, archivos y museos, es decir, para realizar los análisis *in-situ* [49].

De esta manera la espectroscopía Raman promete ser una excelente herramienta analítica también para la identificación de los materiales artísticos. Además, no es destructiva y el tamaño de muestra requerido es menor que en otras técnicas. Su eficacia para la detección sensible y selectiva, así como para la identificación

y caracterización de diferentes compuestos reside en el principio de interacción de la radiación electromagnética con la materia de tal manera que cada material absorbe una cantidad de energía discreta y bien definida y que sea al final selectivamente dispersada. En el caso de Raman, hablamos de una dispersión inelástica, que proporciona una información química y estructural muy específica, llamada también el "fingerprint" de la materia analizada, y eso nos permite identificarla. Para más detalles, consulte el párrafo 1.5 Introducción a la espectroscopía vibracional.

Existen suficientes evidencias referenciadas en la bibliografía que señalan la microespectroscopía Raman como técnica *in-situ* en el análisis de tintas ferrogálicas debido a que no es invasiva para el objeto estudiado. Hay que también destacar, que se trata de una técnica de análisis molecular, y como hemos mencionado ya antes, una técnica no destructiva, con alta selectividad y que, además, no requiere preparación previa (ninguna o mínima) de la muestra. Este último detalle resulta ser muy interesante teniendo en cuenta que el método más empleado hasta el momento ha sido y sigue siendo la cromatografía, la espectroscpía Mösbauer o las técnicas basadas en rayos X que son métodos destructivos que requieren de una preparación de muestra muy laboriosa y costosa.

A pesar de estos aspectos positivos, su uso ha sido bastante limitado, especialmente en lo que respecta a la detección e identificación de pigmentos y colorantes orgánicos naturales. Las razones son: *(i)* la intensa emisión de fluorescencia, característica especialmente de tintes naturales, que se solapa con la emisión Raman; *(ii)* la debilidad de la señal Raman en comparación con otras técnicas espectroscópicas ópticas como la luminiscencia o la absorción infrarroja; *(iii)* la escasa disponibilidad de material en los objetos artísticos bajo estudio, a menudo menor que el límite de detección de la técnica Raman, y por lo tanto la señal muy débil o hasta indetectable; *(iv)* la complejidad de la matriz que embebe la tinta, es decir el soporte.

Actualmente sabemos que la microspectroscopía Raman se ha aplicado con éxito también al análisis *in-situ* de pigmentos y algunas tintas de color contenidas en manuscritos iluminados [50]–[56]. Este estudio fue posible gracias al uso de la espectroscopía Raman por medio de una transformada de Fourier (FT-Raman) que emplea una fuente de excitación el láser de infrarrojo cercano, es decir, el láser que permite atenuar la fluorescencia característica de los colorantes (naturales).

La técnica de FT-Raman ya ha sido probada con éxito para investigar la tinta embebida en el soporte [4], [57].

No obstante, estos problemas podrían superarse también mediante espectroscopía Raman mejorada o mejor dicho intensificada por superficie (SERS, de inglés: **S**urface-**E**nhanced **R**aman **S**cattering or Spectroscopy). El SERS se ha convertido en un método prometedor para identificar tintes y pigmentos orgánicos que normalmente poseen una señal de alta fluorescencia [32]. Esta técnica se basa en la intensificación de la señal Raman mediada por metales plasmónicos nanoestructurados [58]. La aplicación de estas nanopartículas metálicas aumenta la sensibilidad de la técnica Raman, induciendo además una disminución de la emisión fluorescente lo que redunda también en la reducción considerable de la cantidad de muestra necesaria para realizar el análisis.

Las ventajas del SERS en el análisis de colorantes ya fueron puestas de manifiesto en algunos ejemplos ya reportados en la literatura como es el caso del Cristal Violeta [59] y la Rodamina 6G como molécula de prueba [60]. Para estos colorantes ha sido incluso posible la detección de una sola molécula. También se ha propuesto la utilización de microgotas de coloide de plata *in-situ*, un método descrito por Benedetti [61], que permite lograr una alta resolución espacial de las medidas. Nuestro grupo de investigación posee una vasta experiencia de estudios previos en la detección SERS de los compuestos polifenolicos. Concretamente, se ha estudiado con profusión la absorción química de los polifenoles sobre superficies de diferentes nanopartículas metálicas, especialmente las de plata [12], [62], [63].

Actualmente solo hay unos pocos estudios *in-situ* sobre análisis de la tinta depositada sobre el papel o pergamino históricos [34], [57], [64]. Sin embargo, en los últimos tiempos esta escasez de estudios se está revirtiendo debido al mayor acceso que se tiene en el uso de la técnica Raman para muchos laboratorios y museos. La disponibilidad de instrumentos Raman portátiles ha favorecido también esta tendencia aunque su uso aplicado a las IGIs sigue siendo un desafío [65]. Existe el problema adicional de que la interpretación de los datos es complicada debido a los cambios químicos que se producen como consecuencia de la interacción de átomos de hierro con polifenoles. Proceso éste que se complica aún más por la presencia de otras moléculas orgánicas en las tintas ferrogálicas clásicas. En este sentido, la asignación de las bandas Raman es un tema aún pendiente que no ha sido abordado en profundidad por ninguno de los grupos que ha aplicado la técnica Raman al estudio de este tipo de colorantes.

El uso de otras técnicas como la espectroscopía FTIR será providencial para ayudar en esta asignación [65], [66]. Asimismo, el análisis de modos vibracionales mediante métodos teóricos será también de gran ayuda en esta interpretación.

1.5 Introducción a la espectroscopía vibracional

La mayor parte de lo que sabemos sobre la estructura de los átomos y las moléculas procede del estudio de su interacción con la luz. Diferentes regiones del espectro electromagnético proporcionan diferentes tipos de información como resultado de tales interacciones. Por lo tanto, la espectroscopía es el estudio de la interacción entre la materia y la radiación electromagnética.

Cuando un fotón de un determinado valor energético llega a una estructura de la materia, tiene la probabilidad de ser reflejado, dispersado, absorbido o transmitido (**Figure 10**). La probabilidad de que alguno de estos fenómenos se produzca en el intercambio energético radiación/materia se conoce como sección eficaz y viene determinada por el valor energético del fotón incidente y de los estados energéticos discretos dentro de la estructura de la materia.

La espectroscopía vibracional tiene muchas aplicaciones porque prácticamente cualquier molécula con enlaces covalentes y en cualquier estado de la materia (gas, líquido, sólido, etc.) da origen a un espectro vibracional, y los espectros se pueden registrar también en condiciones extremas de temperatura o presión. Es decir, la espectroscopía vibracional ha sido empleada en el estudio de materiales de diversa naturaleza.

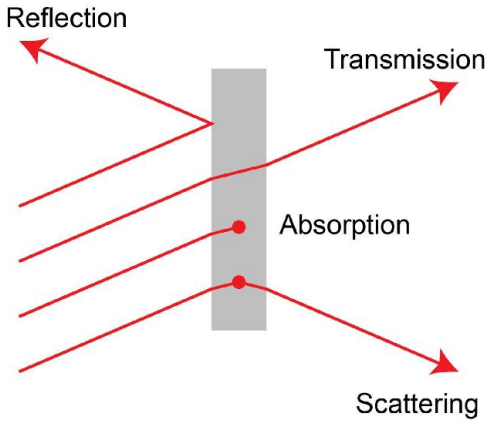

Figure 10. *Esquema de las distintas interacciones de la luz cuando ésta alcanza la superficie de un objeto.*

Cada molécula tiene un conjunto de estados vibracionales (y rotacionales) que son característicos de su estructura y de la naturaleza de los enlaces químicos que la forman. En concreto, una molécula de N átomos tiene 3N grados de libertad: 3 de translación, 3 de rotación (2 si molécula es lineal), y 3N-6 de vibración (3N-5 si es lineal). Los movimientos de vibración de una molécula se pueden descomponer en oscilaciones en las que los átomos se mueven en fase y que se llaman *modos normales de vibración*, cada uno de los cuales tiene una frecuencia característica. Por otro lado, los principales modos normales de vibración de las moléculas son combinación lineal de modos de vibración más simples, llamados *coordenadas internas*, tales como: *tensiones de enlace*, *deformaciones de ángulos de valencia y de ángulos diedros*, *deformaciones en y fuera del plano*, etc., que en muchos casos todavía pueden ser simétricas o asimétricas (**Figure 11**).

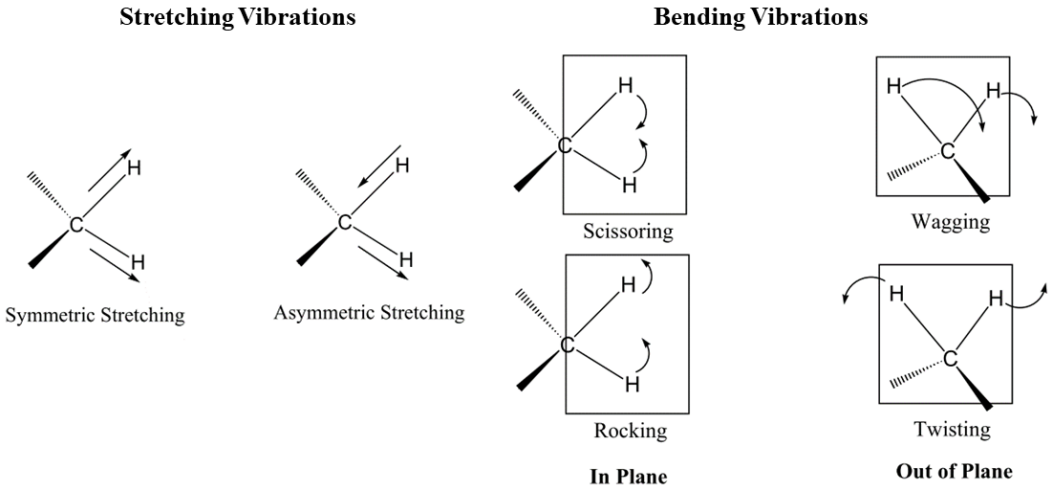

Figure 11. *Ejemplos de algunos tipos de vibraciones moleculares.*

En el caso de las moléculas poliatómicas, el movimiento exacto de los átomos y el modo de vibración depende de sus masas (μ) y de la fuerza con que se unen a las moléculas, es decir de la constante de fuerza de cada enlace (K). El cálculo exacto de las frecuencias vibratorias está determinado por la Ley de Hook:

$$\bar{\upsilon} = \frac{1}{2\pi c}\sqrt{K.\mu} \qquad \text{donde } \mu = \frac{m_1+m_2}{m_1.m_2} \qquad \text{(Eq. 1)}$$

De la Eq. 1 se puede deducir que la frecuencia es directamente proporcional a la constante de fuerza e inversamente proporcional a la masa reducida. La frecuencia exacta a la que ocurre una vibración dada está determinada por la fuerza de todos los enlaces involucrados y la masa de todos los átomos que la componen. Por eso,

la aparición de una banda a una frecuencia característica puede ser asignada a un determinado grupo de moléculas y puede ayudarnos a estimar la presencia de dicho grupo en la estructura del compuesto estudiado [67].

En resumen, la energía de la radiación incidente provoca transiciones en los niveles vibracionales y rotacionales de la molécula estudiada y permite su caracterización estructural debido a que estas vibraciones se pueden detectar y medir.

Debido a que la espectroscopía Raman junto con la espectroscopía SERS son las técnicas analíticas principales utilizadas en este proyecto de investigación, en la siguiente sección se presentarán los principios fundamentales, así como las características y aplicaciones de ellas mismas.

i) Espectroscopía Raman

Como ya se ha mencionado, la interacción de la luz con la materia puede provocar transiciones entre los niveles de energía de las moléculas que dan lugar a unos procesos de absorción o emisión (**Figure 12**).

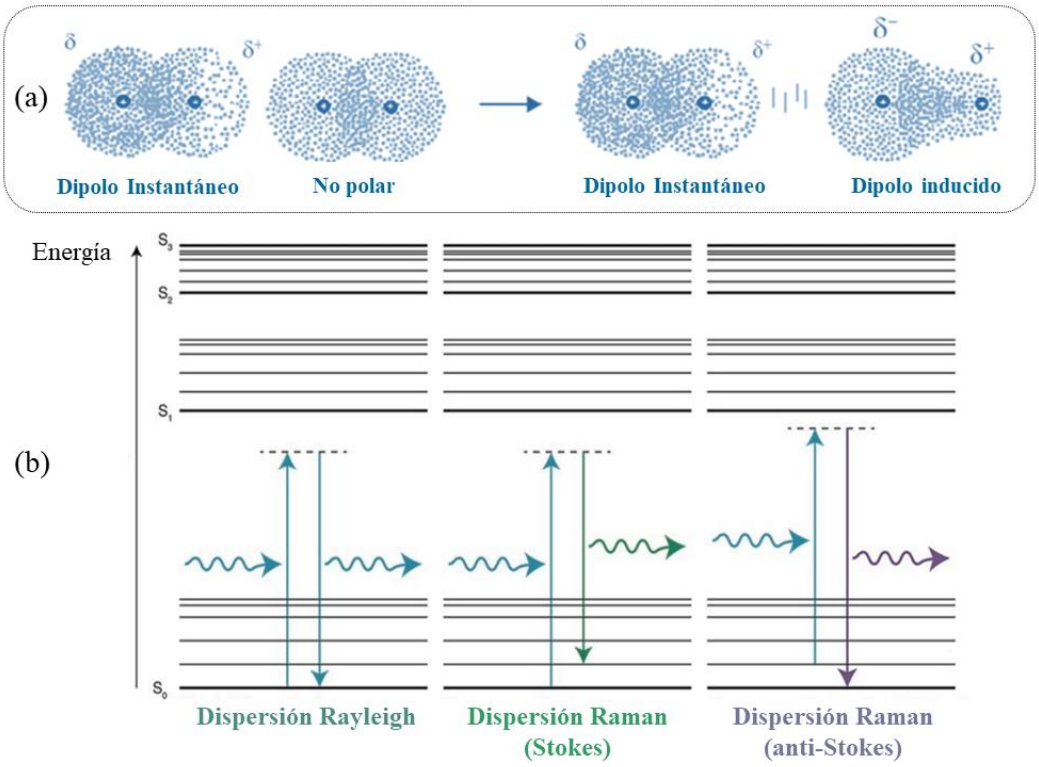

Figure 12. *(a) Esquema de momentos dipolares de una molécula diatómica. (b) Ilustración esquemática de las dispersiones Rayleigh (sin efecto Raman) y Raman (Stokes – la molécula absorbe energía; anti-Stokes – la molécula pierde energía).*

En concreto, cuando un rayo monocromático de un láser con cierta frecuencia interactúa con una molécula, la componente eléctrica del campo electromagnético de la luz ejerce una fuerza sobre todos los electrones de la molécula y tiende a moverlos de sus posiciones de equilibrio alrededor de los núcleos cargados positivamente. Este proceso induce un momento dipolar en la molécula que, en consecuencia, se convierte en un dipolo que vibra a la frecuencia del láser (**Figure 12**a). Como resultado, la molécula emite radiación denominada radiación dispersada. La mayor parte de la luz dispersa tiene la misma frecuencia que la luz incidente y se conoce como dispersión elástica o de Rayleigh que no proporciona información sobre la composición (**Figure 12**b). Solo una fracción muy pequeña de la luz dispersa, 1 fotón disperso de 10^6 incidentes, presenta ligeros cambios de frecuencia y es lo que conocemos como dispersión inelástica o Raman. Esta información es una propiedad característica de la naturaleza química y el estado físico de la muestra y su frecuencia es independiente de la luz incidente.

Es solo la dispersión Raman la que proporciona una gran cantidad de información específica sobre las estructuras moleculares y sus interacciones. La intensidad de la luz dispersada es proporcional a la polarizabilidad de la molécula que depende del tamaño, forma y orientación de la molécula y puede modificarse cuando cambia alguno de estos parámetros. Así, cada espectro depende de la estructura de la molécula, es la llamada *huella dactilar* o *DNI molecular*, y se puede utilizar para la identificación de compuestos químicos.

Si la energía del fotón laser coincide o está muy próxima a la de una transición electrónica permitida por el mecanismo de radiación de dipolo eléctrico, es decir está en condiciones de resonancia Raman, la molécula está excitada hasta un estado que generalmente coincide con el primer estado electrónico (singlete) excitado. En este caso, el espectro Raman se presenta muy intensificado.

La espectroscopía Raman (RS) proporciona información química y estructural de gran ayuda para comprender la naturaleza del material que se analiza. Los cambios en las señales Raman, como los que afectan a la altura, el ancho y la posición de las bandas Raman, permiten diferenciar los materiales mediante la comparación de sus espectros y así determinar la cantidad relativa de material o su cristalinidad. Además, la RS puede diferenciar estructuras químicas, incluso si contienen los mismos átomos en diferentes disposiciones estructurales.

Por otro lado, la RS es una técnica sin contacto y no destructiva para la muestra y, por lo general, no necesita preparación de la muestra. Otra característica que hace que esta técnica sea particularmente interesante es la sensibilidad a pequeños cambios en la estructura del material. Las bandas Raman resultan directamente de las vibraciones moleculares mientras que éstas son muy sensibles a los cambios en la química y la estructura, por lo que la RS puede detectar diferencias sutiles en el entorno molecular. Casi todos los materiales exhiben dispersión Raman. Los metales también dan lugar abandas características de la red que se denominan fonones, asociados a vibraciones generales de su estructura.

La dispersión Raman ocurre cuando la luz interactúa con las vibraciones moleculares. Esto es similar a la espectroscopía de absorción IR más conocida, pero se aplican reglas diferentes. Para que ocurra el efecto Raman, se requiere un cambio en la polarizabilidad molecular durante la vibración. En concreto, la condición para que se produzca radiación Raman es que la molécula sea anisotrópicamente polarizable; mientras, todas las moléculas lineales (incluyendo las diatómicas) son anisotrópicamente polarizables y, por tanto, presentan actividad Raman. En consecuencia, podemos decir que un enlace no polar es generalmente activo en Raman mientras que un enlace polar, en una molécula asimétrica tendrá poca o ninguna eficacia de dispersión Raman.

ii) Interpretación del espectro Raman

En un experimento Raman convencional, la información obtenida se caracteriza por el número de ondas, la anchura y la intensidad de las bandas, lo que permite en condiciones adecuadas llevar a cabo también un análisis cuantitativo (no solo cualitativo).

Cada banda del espectro Raman puede cambiar su frecuencia, se estrecha o se ensancha, o varía en intensidad. Estos cambios pueden revelar información sobre la muestra, variaciones en la cristalinidad y la cantidad de material. Las variaciones en los espectros con la posición en la muestra revelan cambios en la uniformidad (homogeneidad) del material. El espectro Raman de los cristales a menudo ve solo una banda Raman dominante (porque solo hay un entorno molecular del cristal).

Por lo tanto, un espectro Raman consta de una gama de características, cada una asociada con un modo de vibración. El espectro es exclusivo del material y permite

identificarlo. Sin embargo, la RS puede presentar también algunos desafíos: *(i)* la baja sección eficaz de la dispersión Raman y *(ii)* la fotoluminiscencia (PL) que con frecuencia se emite por la molécula o las impurezas que la acompañan lo que puede enmascarar la información Raman. Cuando una muestra se ilumina con un láser, suelen ocurrir ambos procesos, tanto la dispersión Raman como la PL.

Estos mecanismos aparecen porque las intensidades de las bandas de un espectro Raman dependen de la molécula en cuestión, de la polarizabilidad molecular y del tipo de láser utilizado para obtener el espectro, es decir, de la luz que se caracteriza por su frecuencia y por la intensidad del campo electromagnético que genera.

La PL comprende procesos de fluorescencia y fosforescencia y se origina a partir de un proceso de absorción/emisión entre diferentes niveles de energía electrónica en el material. La cantidad y el tipo de PL depende del material que se esté estudiando y de la longitud de onda del láser que se utilice. La interferencia de la fluorescencia, normalmente no deseada, se puede evitar eligiendo una longitud de onda de láser adecuada, láser de infrarrojo cercano (por ejemplo, 785 nm). También el material de vidrio, como cubetas de vidrio o portaobjetos de microscopio, puede enmascarar las señales Raman de las muestras, así que se recomienda utilizar preferentemente el cuarzo.

iii) Espectroscopía Raman *vs* IR

La diferencia principal entre las dos técnicas vibracionales reside en la naturaleza de las transiciones moleculares. Para que una transición sea activa en Raman, debe haber un cambio en la polarizabilidad de la molécula durante la vibración. Esto significa que la nube de electrones de la molécula debe sufrir un cambio de posición. Por otro lado, para una transición detectable por IR, la molécula debe sufrir un cambio de momento dipolar durante la vibración. Así, cuando una molécula es simétrica, no podemos observar ninguna línea de absorción IR, ya que la molécula no puede cambiar su momento dipolar. Se ha observado que las moléculas con un fuerte momento dipolar suelen ser difíciles de polarizar.

Por otro lado, la absorción IR es un proceso resonante y la dispersión de Raman no es, en principio, una interacción de resonancia. Sin embargo, las dos técnicas de espectroscopía Raman e infrarroja proporcionan información vibracional complementaria [68]. Además, el Raman también tiene interés para el estudio

de sustancias acuosas (por ejemplo, en medios biológicos), ya que el agua absorbe fuertemente en el IR, tapando otras bandas, pero este efecto no ocurre en el Raman, ya que el agua presenta una señal Raman débil.

El uso de una combinación de espectroscopías IR y Raman puede generar información valiosa. Mientras que la espectroscopía IR es sensible a cualquier grupo químico que presente un momento dipolar significativo (como es, por ejemplo, C-H y C=O, que se encuentran comúnmente en los grupos laterales de polímeros), la RS es más sensible a grupos altamente polarizables, como son los C-C y C=C, que se encuentran comúnmente en la cadena principal del polímero o en grupos aromáticos. Por lo tanto, cuando se usan conjuntamente, se puede obtener más información de la que está disponible con cualquiera de las técnicas individuales para la determinación completa de la estructura química y física del material estudiado, sobre todo en el caso concreto de los polímeros [69].

iv) Espectroscopía SERS

La espectroscopía SERS se basa en la mejora de la dispersión inelástica, hasta 10^6 veces, de ciertas moléculas adsorbidas sobre o en las proximidades de superficies metálicas nanoestructuradas. Los principios teóricos son los mismos que los de Raman, pero no lo son los espectros de vibraciones moleculares y electrónicos, así como hay que tener en cuenta también los espectros de emisión y absorción de radiación de nanopartículas (NPs) o nanoestructuras.

Se puede decir que el SERS es un efecto derivado de los efectos plasmónicos en ciertos metales. La plasmónica es una rama de la nanofotónica basada en el estudio de los procesos de interacción entre la radiación electromagnética (EM), la luz y los electrones de conducción en la superficie del metal. Estos procesos pueden interpretarse sobre la base de la existencia de plasmones, que son oscilaciones colectivas de los electrones libres de conducción presentes en un metal. Estos fenómenos tienen características relacionadas con el metal, su geometría y dimensiones, la longitud de onda de iluminación y el medio que lo rodea.

Podríamos visualizar el plasmón como una onda superficial rodando a través del mar de electrones de conducción en el metal. Así como la energía de las ondas de luz

se presenta en unidades cuantificadas como partículas llamadas fotones, así se transporta la energía y las llamamos plasmones.

Los metales macroscópicos, además de reflejar la luz, tienen una propiedad óptica menos conocida: bajo ciertas condiciones, la luz puede viajar a lo largo de las superficies metálicas sin alejarse de ellas. Esta es una propiedad muy peculiar, ya que en condiciones normales la luz viaja a través de las tres dimensiones del espacio y no puede ser confinada fácilmente. En realidad, esta luz superficial es una onda más complicada que la luz normal, ya que no consiste solo en un campo EM, sino que también involucra a los electrones libres presentes en los metales. Estos modos electromagnéticos que se producen en la superficie de metales se conocen como polaritones. En metales nanoestructurados dichos polaritones están localizados y generan altas intensificaciones del campo eléctrico en las superficies de los mismos [70].

La causa del extraordinario aumento de la dispersión Raman en presencia de nanoestructuras metálicas es todavía materia de discusión, aunque se reconocen dos modelos fundamentales, basados ambos en la necesidad de la existencia de una superficie rugosa para que el efecto tenga lugar: *(a)* el modelo electromagnético, y *(b)* el modelo químico o de transferencia de carga. Ambos se dan simultáneamente, aunque no existe un acuerdo definitivo acerca de la contribución de cada uno de ellos en el factor de intensificación total.

El modelo del *mecanismo electromagnético* (EM) se puede simplificar considerando la intensificación de la señal Raman cuando la radiación de una determinada frecuencia incide sobre la superficie de una nanoestructura metálica. La intensidad del campo electromagnético que incide sobre la molécula está compuesta por la intensidad del campo de la radiación láser a una frecuencia dada (E_0) y la misma frecuencia dispersada por el propio metal (E_S) tal como se indica en la **Figure 13**. Cuando la frecuencia de la radiación incidente coincide con la frecuencia de resonancia de los plasmones superficiales del metal entonces el campo disperso es mucho mayor.

Como se ha visto, los sustratos metálicos nanoestructurados tienen la capacidad de soportar plasmones superficiales. Cuando éstos son irradiados con una radiación de frecuencia apropiada, estos plasmones dan lugar en nanoestructuras al fenómeno conocido como localización de plasmones superficiales resonante (LSPR en inglés). En estas condiciones se produce una enorme intensificación de los campos

electromagnéticos incidentes y dispersos y decaen exponencialmente a medida que se alejan de la superficie (**Figure 13**).

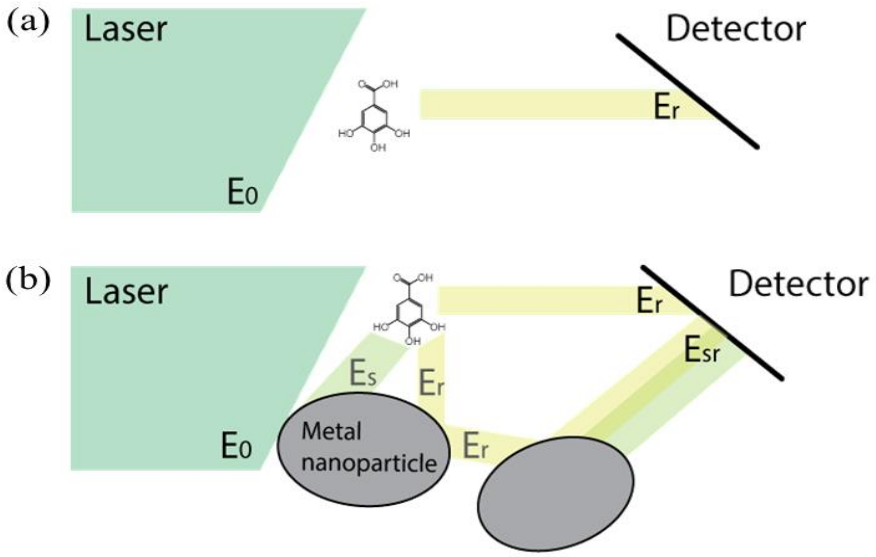

Figure 13. *Esquema del proceso de dispersión Raman en: (a) ausencia y (b) presencia de nanopartículas de metal esferoidal. (E_0 denota la radiación incidente; E_S corresponde a la radiación producida por las NPs; E_r es la emisión Raman de la molécula y E_{rs} es la radiación Raman intensificada por el efecto LSPR de NPs).*

La intensificación detectada depende del metal utilizado y de la morfología de su superficie, pero también de la molécula a estudiar y otras variables experimentales. No todas las bandas del espectro se intensifican uniformemente, esta intensificación relativa es muy variable incluso para una misma molécula dependiendo de las condiciones de registro. A diferencia del Raman convencional, la técnica SERS es capaz de reducir la intensidad de la fluorescencia.

Para ilustrar el fenómeno de la intensificación de campo eléctrico que se produce en nanoparticulas metálicas se suele emplear el modelo de nanoesferas metálicas. El momento dipolar inducido μ_{ind} en una nanopartícula plasmónica iluminada con una radiación es proporcional a la intensidad del campo electromagnético (E), siendo α la polarizabilidad de la nanopartícula:

$$\mu_{ind} = \alpha . E \qquad \text{(Eq. 2)}$$

Cuando la radiación empleada es de la misma frecuencia que la asociada a la energía de oscilación de los plasmones superficiales de la nanopartícula, cerca de la cual se encuentra la molécula, la luz puede excitar estos plasmones induciendo

una consiguiente intensificación del campo eléctrico, $\vec{E}$. La intensificación global del sistema se suele expresar como $g=|E_S/E_0|^2\times|E_r/E_0|^2$, ya que implica un efecto multiplicativo de la intensificación individual de tanto la radiación incidente (E_S) como la radiación dispersada Raman emitida por la molécula (E_r). Esta intensificación es del orden de 10^6, que es la intensificación que se aprecia en las señales Raman-SERS respecto a las medidas en los espectros Raman convencionales.

A medida que aumenta el tamaño de la nanoesfera, se observan tres cambios en los espectros de extinción asociados: *(1)* aumenta la sección eficaz de la dispersión, *(2)* la resonancia del plasmón se desplaza hacia longitudes de onda más altas, y *(3)* aumenta la anchura de banda a media altura (FWHM, de inglés: Full-Width at Half-Maximum).

Tal como se ha mencionado, cuando la partícula se irradia con la frecuencia adecuada, el campo electromagnético se amplifica con respecto al campo electromagnético incidente. Esta amplificación depende a su vez de las propiedades optoelectrónicas específicas de cada metal. El factor de amplificación (g) puede ser expresado también en función de la permitividad eléctrica del metal mediante la siguiente ecuación:

$$g = \frac{\varepsilon_{metal}-\varepsilon_{medium}}{\varepsilon_{metal}+2\varepsilon_{medium}} \qquad \text{(Eq. 3)}$$

De la Eq. 3 se puede deducir que se produce la resonancia de plasmón para aquellos metales que cumplen la condición: $\varepsilon_{metal} + 2\varepsilon_{medium} \approx 0$. Esta relación es el origen de la intensificación del campo por resonancia de plasmones superficiales localizados (LSPR). Sin embargo, como la permitividad eléctrica del metal viene expresada en función de una parte real y otra imaginaria: $\varepsilon_{Ag} = \varepsilon_{real} + i\varepsilon_{img}$, siendo la ε_{img} el término asociado a la amortiguación o *damping* debido a colisiones de los electrones con los iones del cristal o impurezas existentes en la estructura metálica, se tiene que éste debe de ser despreciable para que se produzca una intensificación efectiva.

Las moléculas que están directamente en contacto o en las inmediaciones de las superficies de nanopartículas metálicas en donde se ha hecho incidir una radiación que excita los plasmones del metal en esas nanopartículas generan una amplificación de la señal Raman proveniente de la molécula. Asimismo, el mecanismo EM predice una dependencia de la intensificación de la señal Raman que depende estrechamente

de la distancia al metal. Generalmente, la amplificación es sólo efectiva para distancias comprendidas entre 1 y 10 nm de distancia entre la molécula y la superficie nanoestructurada.

Otro aspecto interesante del mecanismo EM es el carácter fuertemente polarizado del campo existente sobre la superficie. Los cálculos teóricos predicen una componente perpendicular de campo más intensa que la paralela a la superficie. Por lo tanto, los modos vibracionales que se desarrollan en dirección perpendicular a la superficie se verán más intensificados que los paralelos, lo que constituye una auténtica regla de selección de vibraciones moleculares, muy útil para la deducción de la orientación molecular sobre el metal.

El *mecanismo de transferencia de carga* (CT) ocurre solo en aquellas moléculas que forman un complejo con el metal. Es un mecanismo de corto alcance que afecta solamente a las moléculas de la primera capa de adsorción directamente ligadas al metal, o adsorbatos, que modifica la polarizabilidad molecular favoreciendo la emisión Raman. Básicamente se basa en un mecanismo de intensificación por resonancia en el nuevo complejo molécula/metal dando lugar a una señal Raman amplificada. Normalmente, la transferencia de carga es del metal a la molécula, cuanto más fuerte esté la molécula unida al metal, mayor será la mezcla entre los orbitales y esto favorecerá la CT. Según la fuerza de interacción existen diferentes modos de interacción de las moléculas con el metal:

- *Fisisorción*: la interacción entre el adsorbato y el metal es débil, por lo que la modificación de la polarizabilidad del adsorbato es pequeña dando como resultado un espectro SERS bastante similar al Raman, pero en ciertas ocasiones puede inducir una orientación fija de la molécula dando como resultado diferentes intensificaciones de los modos vibratorios en función de su simetría.
- *Quimisorción*: la alteración de la nube electrónica del adsorbato es significativa produciendo la formación de un complejo superficial entre una molécula y el metal, en el que se originan nuevas transiciones electrónicas distintas a las del propio metal o de la propia molécula. Este fenómeno afecta fundamentalmente a la primera monocapa de adsorción.

v) Nanoestructuras y coloides metálicos

A nivel de los nanomateriales, las leyes de la física atómica pueden cambiar algunas de las propiedades de los materiales, ya que su tamaño extremadamente pequeño está en la misma escala que el tamaño crítico de algunos fenómenos físicos. Así, algunas de las propiedades de la superficie, como los niveles de energía, la estructura electrónica y la reactividad pueden ser muy diferentes respecto a los metales macromoleculares, dando lugar a un material con nuevas propiedades.

Las nanopartículas metálicas en suspensiones coloidales (coloides metálicos) se caracterizan por una alta relación área superficial/volumen, lo que les otorga propiedades únicas que son muy diferentes de las propiedades clásicas del mismo material [71]. El metal que produce SERS más intenso es con diferencia la plata y en menor medida el cobre, el oro y los metales alcalinos, aunque se ha podido realizar SERS con todo tipo de metales.

Las nanopartículas metálicas presentan una interfase compleja dotada con cargas positivas debido a un defecto de electrones en la superficie de los átomos, los cuales pasan al medio lo que afecta la distribución de iones cerca de la región interfacial (**Figure 14**).

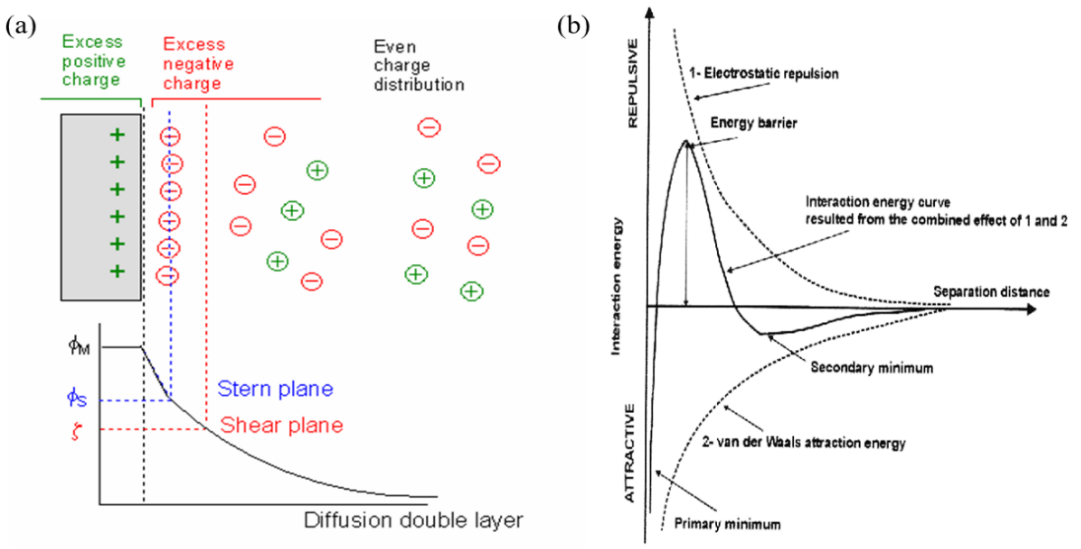

Figure 14. *(a) Arriba: Distribución de iones negativos sobre la superficie positiva de las nanopartículas metálicas donde se muestra la formación de una doble capa electrica en la superficie Stern. Abajo: Representación del potencial eléctrico en función de la distancia a la superficie donde se identifican varios potenciales característicos: el potencial ϕ_m correspondiente a los iones fuertemente adsorbidos sobre el metal en la primera capa; el potencial ϕ_s correspondiente a la segunda capa de adsorción de iones negativos dotados de una mayor movilidad en la capa Stern; y el potencial zeta ζ correspondiente al plano que separa la zona de mayor movilidad del medio líquido de la zona más rigida que rodea la NP. (b) Representación de las energías de atracción van der Waals y repulsión electrostática y energía global del sistema en función de la distancia interpartícula.*

La carga positiva de las nanopartículas es neutralizada con cargas negativas procedentes del medio (iones metálicos provenientes de electrolitos de la disolución) dando lugar a la formación de una doble capa eléctrica en la capa de Stern (**Figure 14**a). Esta configuración da lugar a la existencia de una carga residual negativa que asegura la estabilidad de las nanopartículas en suspensión por repulsiones electrostáticas. Esta carga residual proporciona un potencial eléctrico en la superficie llamado potencial zeta (ζ). Sin embargo, cuando las NPs están suficientemente cercanas, entonces actúan unas fuerzas de atracción de naturaleza van der Waals (**Figure 14**). La combinación de fuerzas atractivas de corto alcance y las repulsivas de largo alcance da lugar a la distribución de energías mostrada en la **Figure 14** .Esta distribución muestra un máximo correspondiente a la barrera de potencial que las NPs deben superar para acercarse y agregarse. Esta barrera de potencial depende del potencial ζ, que puede modificarse por adición de sales y moléculas neutras que puedan ser adsorbidas sobre el metal, desplazando iones ya adsorbidos, induciendo la agregación de las NPs.

Finalmente, cabe señalar que los soportes SERS se obtienen por diferentes métodos: ciclos de oxidación-reducción galvánica, condensación sobre soportes de metales evaporados, deposición por irradiación con láseres pulsados, reducción química de sales metálicas de Ag, Au o Cu, ablación láser de metales macroscópicos, etc. Estos últimos métodos químicos dan lugar a NPs en suspensión coloidal.

Lo que realmente caracteriza a las suspensiones coloidales es el tamaño de partícula que está entre 10 nm y 1 μm. Las partículas coloidales en suspensión tienen el problema de su alta inestabilidad, es decir, tienden a precipitarse con el tiempo. Al preparar coloides, se debe prestar especial atención a su estabilización por diferentes métodos.

Los coloides tienen propiedades ópticas derivadas del tamaño de las partículas en suspensión, como la propiedad de dispersar la luz incidente por reflexiones y refracciones sucesivas en un efecto conocido como efecto Tyndall. Las NPs metálicas pueden considerarse como un estado intermedio entre un átomo simple y un material compacto.

Un aspecto interesante de la técnica SERS es que el agua produce una señal Raman muy débil, lo que permite el registro rutinario de moléculas solubles en ella sin interferencia de disolvente. Debido a que los coloides de plata preparados por reducción química presentan una relativa inestabilidad con el tiempo, éstos suelen

utilizarse inmediatamente después de su preparación y como máximo hasta 3 semanas después de la preparación. En la literatura se han reportado diferentes métodos para la obtención de coloides de plata y de oro, en esta tesis se han utilizado diferentes métodos: *a)* obtención de NPs esféricas a partir de una solución acuosa de nitrato de plata ($AgNO_3$) usando citrato trisódico como reductor [67], [72]; *b)* obtención de NPs esféricas a partir de una solución acuosa de $AgNO_3$ usando hidroxilamina como reductor [73]; *c)* obtención de NPs con forma de estrella usando una solución acuosa de $AgNO_3$ y dos ciclos de reducción con hidroxilamina seguida de citrato [74]; y *d)* obtención de NPs esféricas de oro a partir de una solución acuosa de ácido tetracloro aúrico ($HAuCl_4$) usando citrato trisódico como reductor [75].

2. OBJECTIVES OF THE THESIS

The principal goal of this dissertation thesis is to understand and define a correlation between the structure of the selected phenolic compounds and the chemical reactions and processes characteristic of iron gall inks (IGIs) analysed by spectroscopic techniques. In particular, we are looking for specific reactions points in the structure of the phenolic molecules which possess special reactivity towards the metal ions (especially with iron), and, in consequence, it is possible to define them as structural and spectral markers for sensitive and selective detection, identification and characterization of polyphenols, and thus, for IGIs.

Since we have experimented a significant lack of the scientific papers concerning the systematic study and spectroscopic characterization, especially by means of Raman and SERS spectroscopy, of gallic acid and other structurally similar phenolic compounds and their complexation with different transition metal ions, we also plan to perform basic research dedicated to their vibrational characterization.

Therefore, the specific objectives of the current work are proposed as follows:

- To carry out the spectroscopic study of the selected polyphenolic compounds (pyrogallol (PY), gallic acid (GA), tannic acid (TA) and syringic acid (SA)) by means of UV-visible absorption, IR and Raman spectroscopies. To perform DFT calculations and assign the recorded vibrational modes.

- To prepare and carry out spectroscopic study of the complexes formed by the interaction of the selected polyphenolic compounds and iron(II) and copper(II) ions by means of UV-visible absorption, IR and Raman spectroscopies. To perform DFT calculations and interpret the recorded spectral changes and define specific spectral markers.

- To carry out studies of the effect of several factors such as solvent, base (support), metal, pH, time (ageing) on the formation of IGIs.

- To register SERS spectra of IGIs and to optimize the SERS experiments.

- To perform *in-situ* SERS analysis of IGIs in selected real historical manuscripts and documents in order to establish a correlation between the studied effects (pH, time, metal, binder) and the aging effect observed in historical manuscripts.

3. MATERIALS AND METHODS

3.1 Chemicals

Polyphenolic substances and metal salts used for IGIs preparation: Pyrogallol (1,2,3-Trihydroxybenzene, at purity of ≥98%, CAS Number: 87-66-1; hereinafter called PY), syringic acid (3,5-Dimethoxy-4-hydroxybenzoic acid, ≥95%, CAS Number: 530-57-4; hereinafter called SA), gallic acid (3,4,5-Trihydroxybenzoic acid; 97.5-102.5% titration, CAS Number: 149-91-7; hereinafter called GA), tannic acid (the purity of this macromolecule is unknown, CAS Number: 1401-55-4; hereinafter called TA), iron(II) sulfate heptahydrate ($FeSO_4.7H_2O$, ≥87%, CAS Number: 7782-63-0; hereinafter called Fe or FE) and copper(II) sulfate pentahydrate ($CuSO_4.5H_2O$, ≥98%, CAS Number: 7758-99-8; hereinafter called Cu or CU), were purchased from Sigma-Aldrich® and used as such for the spectral measurements.

In the majority of cases, stock solutions of polyphenols in water were prepared at a concentration of 10^{-2} M and stored in the dark to protect them from light. For the same reason, to minimize the possible photodegradation of phenol molecules, the examined solutions were protected from light during out-of-measurement times. The stock solutions were further adequately diluted for the required final concentration.

Gum Arabic from acacia tree (CAS Number: 9000-01-5), branched polysaccharide, whose molecular purity is unknown was also purchased from Sigma-Aldrich® and used as such for the spectral measurements.

Silver nitrate, trisodium citrate dihydrate, hydroxylamine hydrochloride and other reagents were of analytical grade and purchased from Sigma-Aldrich® and Fluka. Nitric acid (65%, Merck®) and sodium hydroxide (≥98%, Sigma-Aldrich®) aqueous solutions were used to adjust the pH. All solutions were freshly prepared with Milli-Q water (obtained with a Millipore Sigma Milli-Q® Integral 3 water purification system) before experiments and used immediately.

3.2 Preparation of complexes and sampling

i) Preparation of metal complexes

Four different phenolic compounds (pyrogallol (PY), syringic acid (SA), gallic acid (GA) and tannic acid (TA); and their reaction with selected reagents, in particular, with different metal ions (iron(II) and copper(II)), were studied here. The phenolic compounds and their reagents have been chosen on the base of the commonly known composition of

the IGIs, as described at the 1.1.iii) section (Composición de las tintas ferrogálicas), whereas the information found in traditional historical recipes were taken into account.

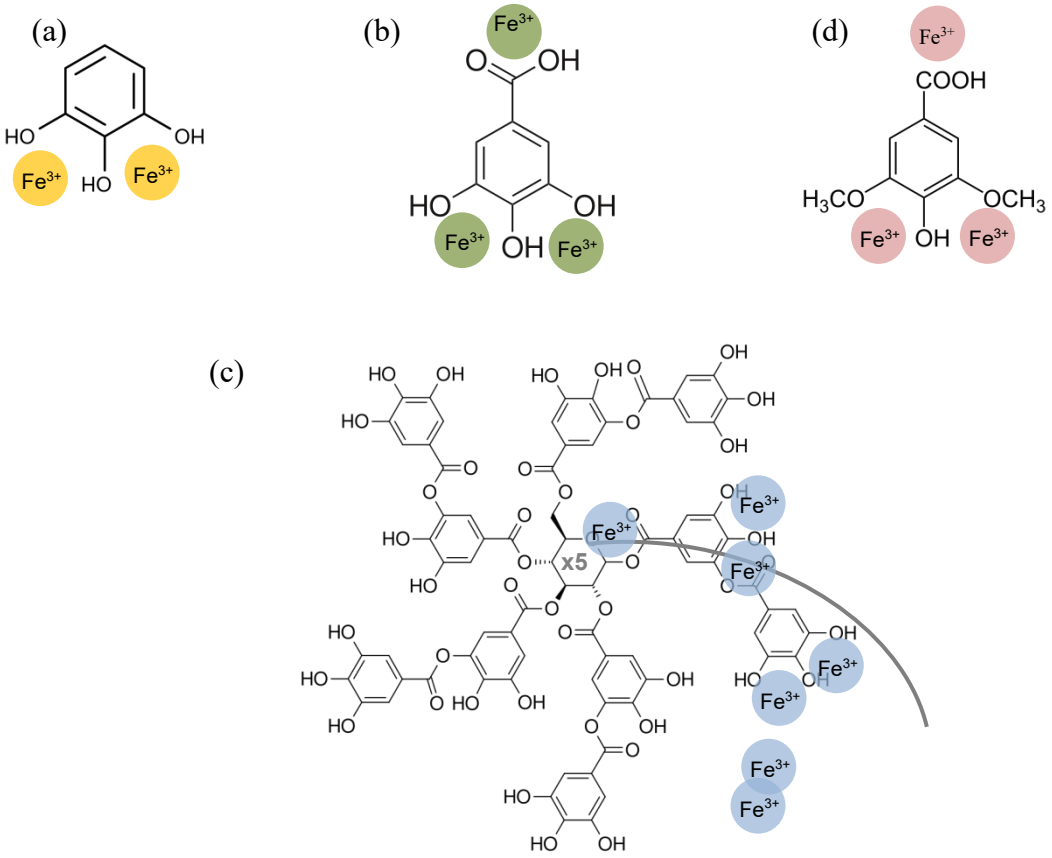

Figure 15. *Representative diagram of molecular structure of the studied polyphenolic molecules: (a) pyrogallol (PY); (b) gallic acid (GA); (c) tannic acid (TA); and (d) syringic acid (SA) with the marked so-called possible reaction points having potential to interact with metal ions and giving rise to the formation of the corresponding iron-polyphenol complexes. It is worthy to note that the molecular structure of gallic acid and pyrogallol can be found in the structure of the tannic acid molecule.*

In particular, the above molecular models were chosen in order to study the interaction of iron with chemical structures that are actually present in oak gallnuts, the most employed material to fabricate IGIs (**Figure 15**). In this way, the molecules of GA and TA are the principal components of IGIs, as described in the literature [15]. On the other hand, PY and SA were employed as models to study the interaction of iron with similar structures to the GA one, and, more precisely, to evaluate the importance of the presence of both the carboxylic and the –OH groups in the benzene ring. Although TA is only present in a limited species of plants, it can serve to mimic all the different tannic structures present in oak gallnuts.

Liquid samples

Figure 15 shows the possible binding points between the used polyphenols and metals. Regarding this, different molar ratios between polyphenols and metals were considered to better understand the interaction mechanism at different concentrations.

For this purpose, stock solutions of molecules were prepared at $2x10^{-2}$ M, except for TA where the $2x10^{-3}$ M stock solution was used. Thus, $2x10^{-2}$ M PY and $4x10^{-2}$ M iron sulfate water solution were used to prepare the corresponding complex at the molar ratio 1:2 (PY-Fe; hereinafter called PYFE). In the case of SA and GA, we have prepared complexes with the molar ratio 1:3 (SA-Fe (SAFE) or GA-Fe (GAFE)). Finally, the molar ratio of the TA-Fe (hereinafter called TAFE) was 1:30 resulting from mixing TA aqueous solution at $2x10^{-3}$ M concentration with the aliquot of the $6x10^{-2}$ M iron sulfate water solution. The same protocol was applied for the preparation of polyphenols-copper complexes (complexes hereinafter called PYCU, SACU, GACU and TACU). **Figure 16** shows all the above-mentioned solutions, prepared in a wide range of pH, from 3 to 12. In addition **Figure 17** presents their appearance when deposited and dried on a cellulosic support.

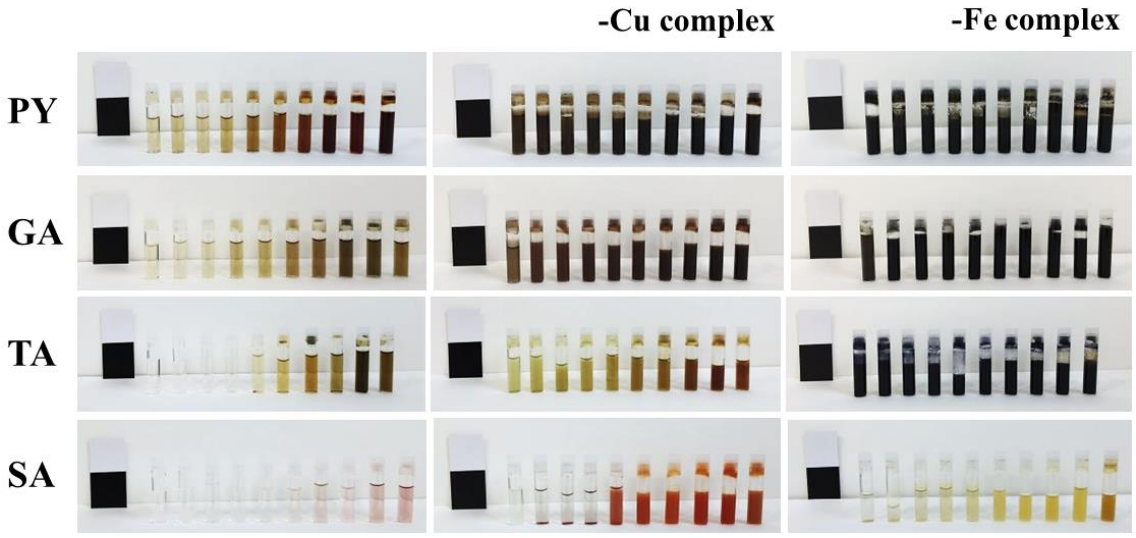

Figure 16. *Photograph of 10^{-2} M solutions of individual phenolic compounds (left) and when complexed with copper (center) and iron (right). Samples were prepared at different pHs, from 3 (left) to 12 (right).*

The pH of the complexes applied on paper was measured by dropping 500 µL of the complex solution on the paper surface. This drop was maintained during 90 seconds

on the paper. Then, the drop was removed from the paper and its pH was measured.

The experiment at different TA-Fe concentration ratios was carried out by preparing solutions of TA and $FeSO_4$ at the concentration 10^{-2} M in water and mixing different volumes of these solutions to reach the following TA-Fe ratios (v/v): 10:1, 3:1, 1:1, 1:3, and 1:10.

Solid samples

A drop (~ 30 µL) of the previously prepared inks solutions was deposited on glass microscopy slide or filter paper (**Figure 17** and **Figure 18**) and left to dry at room temperature until the total water evaporation, at least for 24 hours. Afterwards, the resulted inks layers were scratched (**Figure 18**) and the corresponding ink flakes were analyzed without any other treatment.

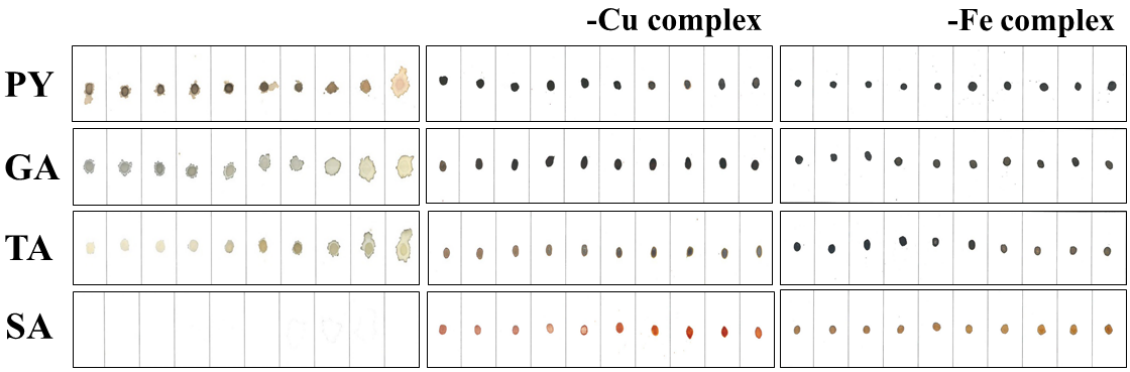

Figure 17. *Photograph of 10^{-2} M solutions of individual phenolic compounds (left) and when complexed with copper (center) and iron (right) deposited on paper. Samples were prepared at different pHs, from 3 (left) to 12 (right).*

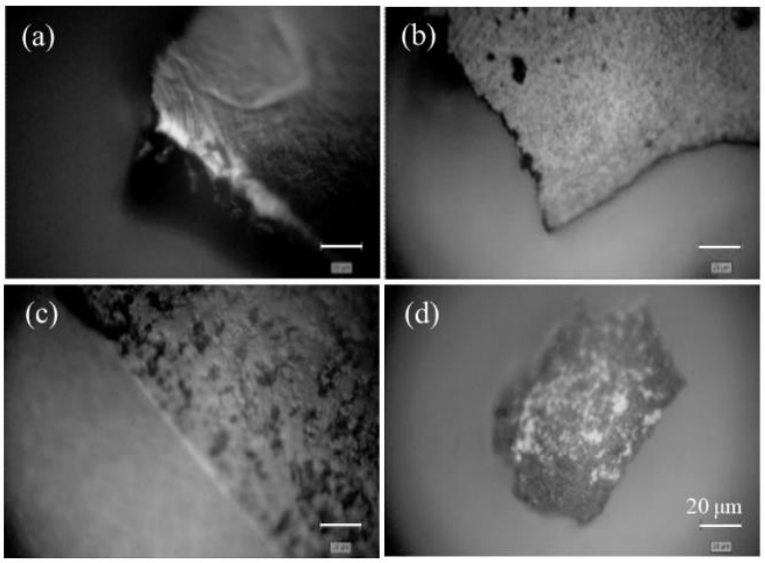

Figure 18. *Microscopic images of solid IGI samples taken under 50x-long distance objective. From left to right and above to below: (a) PYFE at pH 10, (b) GAFE at pH 3, (c) TAFE at pH 6, and (d) SAFE at pH 6.*

ii) Preparation of samples for FTIR spectroscopy

IR spectra were measured on the KBr pellets of the IGIs prepared by mixing the corresponding solid sample and KBr at 1:30 ratio in weight. Besides, gum Arabic samples have also been prepared by adding 50% in weight of gum to the iron-polyphenol complexes. Pellets were prepared using a 16 mm-diameter stainless steel matrix and press machine operating with load configuration at 10,000 kg pressure applying it during 5 or 10 minutes (in vacuum). The resulting samples (**Figure 19**) were dried at room temperature.

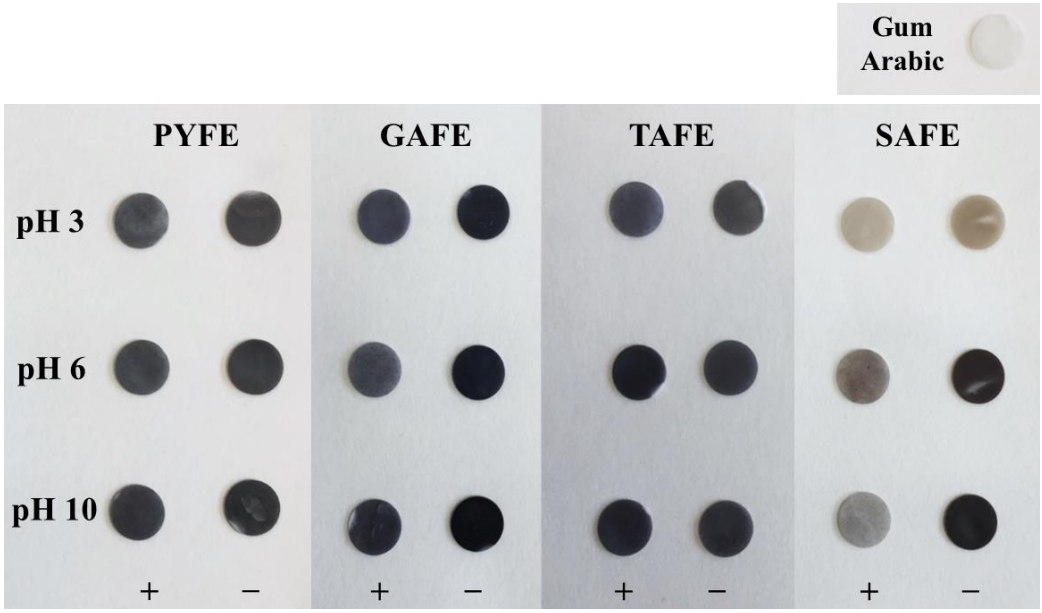

Figure 19. *Images of the infrared pellet samples of polyphenol-iron complexes prepared with (+) and without (-) gum Arabic at pH 3, pH 6 and pH 10.*

iii) Preparation of inks based on historical recipes

Different IGIs were also prepared following the procedures found in the literature [76]. The different composition in weight percent of the prepared inks is displayed in **Figure 20.**

For instance, the IGI4 ink was prepared as follows: 4,1 g of TA was dissolved in 20 mL of Milli-Q water. Then, 0,12 g of $FeSO_4$ was added and water was refilled to obtain 50 mL of solution. Afterwards, 33,5 mL of an aqueous solution of gum Arabic (gum) was also added. Concentration of aqueous solution of gum was 78,5 $g.L^{-1}$.

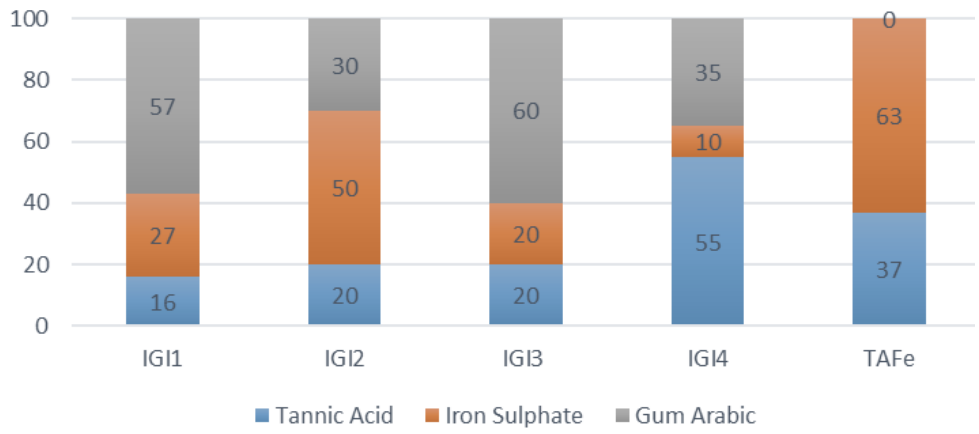

Figure 20. *Composition in percent weight of different TA-based inks prepared according to different recipes reported in the literature and used in the study.*

3.3 Preparation and characterization of metal nanoparticles

We have previously defined that plasmons correspond to the collective electron oscillations in metal NPs. Therefore, they are sensitive to changes occurred regarding the NPs' morphology (shapes), aggregation state as well as presence or absence of a specific medium which defines the NPs' interface. Therefore, different preparation protocols were selected in order to change the morphology (spherical *vs* nanostar shapes and different sizes) of the metal nanoparticles and the chemical properties of the surface. Silver nanoparticles (Ag NPs) are the most commonly and frequently used SERS substrates due to their high resonance of the surface plasmon in the visible-infrared range, high sensitivity and stability, as well as an easy manufacture. There are several ways of Ag NPs production, the most common ones are the chemical reduction and/or laser ablation since they represent simple and effective methods. In the present thesis we have selected chemical reduction methods because they rendered the more stable results. Gold colloids were also fabricated in order to be compared with Ag.

Ag colloidal suspensions of NPs were prepared by the chemical reduction of an aqueous solution of silver nitrate ($AgNO_3$) using two different reduction agents: trisodium citrate dihydrate and hydroxylamine hydrochloride. The aqueous solutions were prepared by using Milli-Q water.

- Citrate-reduced silver colloid (AgC, **Figure 21**) was prepared according to a modified Lee-Meisel method [77]. In concrete, 10^{-3} M $AgNO_3$ (aq) solution was prepared by dissolving a total of 8,5 mg of $AgNO_3$ in 50 mL of Milli-Q water.

Then, a total of 1 mL of a 1 % (w/v) trisodium citrate aqueous solution was added to 50 mL of a boiling silver nitrate solution. The mixture was kept boiling under reflux for one hour. The obtained colloid showed a turbid greyish aspect with an extinction maximum at ~ 420 nm (**Figure 21**) and a final pH of ~ 6-7. Despite being highly sensitive, when using this type of NPs in SERS measurements, it is common to observe Raman bands arising from citrate or other coating agents that can negatively interfere with the identification of the studied molecules [62], [78], [79].

- Hydroxylamine-reduced silver colloid (AgH, **Figure 21**) was obtained by the method described by Leopold and Lendl [77]. Briefly, solutions of silver nitrate (10^{-2} M) and hydroxylamine hydrochloride ($1{,}6x10^{-3}$ M) were prepared in Milli-Q water. Then, 10 mL of a silver nitrate solution was added dropwise to 90 mL of hydroxylamine hydrochloride solution adjusted to pH ~ 9 under vigorous stirring at room temperature. The resulting colloid showed a dark gray coloration with spherical Ag NPs of 35 nm average diameters and plasmon extinction band at ~ 405 nm (**Figure 21**) [80]. Because of the reduction, the final pH decreased up to 6-7.

The obtained colloid shows a similar sensitivity as the AgC colloid. However, AgH colloidal NPs can be used immediately after their preparation and the advantage that no anomalous Raman bands of the residual ions are visible here. By modifying the order and speed of stirring of the two main reagents, the size and dispersion of the resulting colloids can be controlled.

- Citrate-reduced gold colloid (AuC, **Figure 21**) was prepared according to a modified Sutherland-Winefordner method [81]. 1 mL of citrate solution (1% w/w) was added to 50 mL of a boiling solution of $HAuCl_4$ at concentration 0,01 % w/w keeping the mixture boiling during 5 min. The resulting spherical nanoparticles rendered a plasmon resonance maximum at 520 nm and showed a rather homogeneous distribution of sizes (15 nm of average diameter).
- Star-shaped silver colloid (AgNS, **Figure 21**). These nanoparticles were prepared by using the method reported by Garcia-Leis *et al.* [77]. According to this, 500 µL of $6x10^{-2}$ M neutral hydroxylamine were mixed with 500 µL of NaOH (0,05 M).

Later, 9 mL of 10^{-3} M $AgNO_3$ were droped to the first solution under agitation. The solution became brown. After 5 min, 100 µL of an aqueous solution of trisodium citrate (1 % w/w) was added to the mixture. The resulting solution was shaken for 15 min. The resulting NPs showed a predominant star-shaped morphology with diameters oscillating between 100 and 300 nm. These NPs were demonstrated to be more efficient in the intensification of the electric field in comparison to the spherical NPs [77]. This is due to the existence of areas with a great curvature in the tips of NSs highly increases the electromagnetic field by the lightening effect making unnecessary the aggregation of the nanoparticles as in the case of the spherical NPs. However, in the case under study, regarding the studied polyphenols and their metal complexes, both the Au NPs and Ag NSs were not so efficient as AgC or AgH colloids, therefore, we have used them just for the basic characterization.

The pH value, UV-vis extinction and Raman spectra of such colloids were always checked before their employment. The AgC and AgH colloids demonstrated to have similar morphological and chemical characteristics usually observed in such SERS substrates [66], [73], [82].

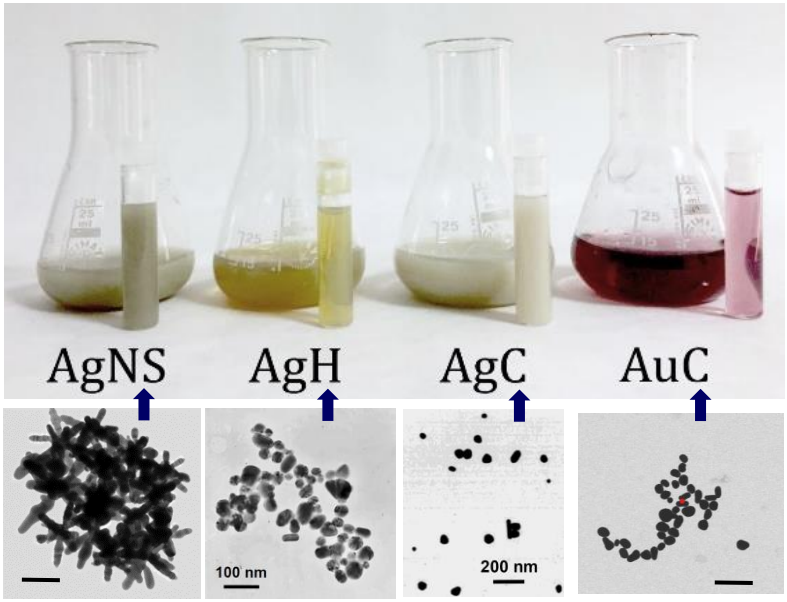

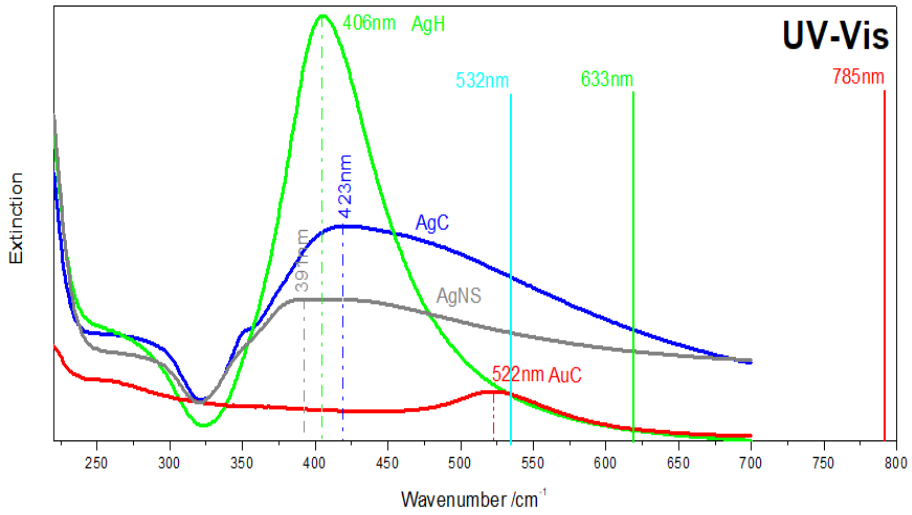

Figure 21. *Top (in the previous page): Visual appearance of the metal colloids prepared in this thesis. Medium (in the previous page): TEM images obtained from the NPs contained in these colloidal suspensions. Bottom: UV-vis extinction spectra of the colloids.*

i) Preparation of samples for SERS

As mentioned above, chemical synthesis of SERS-active nanoparticles is commonly done by reducing metal ions in a solution, using reducing agents such as citrate, sodium borohydride or hydroxylamine hydrochloride whereas all Ag^+ ions are assumed to be reduced to atomic silver. Besides, capping agents which bind to the surface of the nanoparticles thereby preventing aggregation by either repulsive or steric forces are also commonly used. In addition, as in our case, a potassium nitrate (KNO_3) as a charge neutralizer and to aggregate the colloid can be used, making the particles larger in size and apparently changed in their shape [83], [84].

SERS measurements were carried out mostly on silver colloids. Since the addition of the polyphenol molecule did not induce any significant aggregation of the colloid, the activation of the colloid before adding the polyphenols was needed in the case of the spherical NPs. This activation consisted of a partial aggregation of the colloidal particles and, to accomplish this, an aliquot (usually 50 µL) of 0,5 M potassium nitrate was added to 1 mL of the colloid. The final concentration of the polyphenols in colloidal suspensions were 10^{-5} M (if not stated otherwise).

3.4 Historical Manuscripts

Different documents, manuscripts and letters were collected by the doctorand over the years in Slovakia and Spain. She visited the local flea markets as well as made exchanges or bought directly different documents and/or fragments found in different institutions or private collections. **Table 4** shows a summary of the acquired and analysed artefacts. We have focused to collect pieces which come from both Slovakia and Spain (country where they were collected), and which can be dated to different centuries, from the year 1703 to 1930. The objects were analyzed in the laboratory of Raman spectroscopy at the Dpt. of biophysics, Faculty of Science, UPJŠ in Košice, by using the Renishaw InVia Raman microspectrometer. Besides the Raman spectra, we have also revised the pH of the studied documents by using an innovative drop method of the pH-measurement.

Our group have also established a collaboration with different Spanish institutions which possess collections/deposits of manuscripts and documents containing IGIs. In particular, we regularly visited the MAN (Museo Arqueológico Nacional) in Madrid (Spain) and the analysed artefacts are summarized in **Table 5.** We studied sealed document called "Mensaje a Castelar 1899"* *in-situ* by means of the Delta Nu portable Raman spectrometer. (*Don Emilio Castelar y Ripoll was a Spanish republican politician, and a president of the First Spanish Republic.)

In each case, the analysis of the work *in-situ* is made difficult by the support that contains it, cellulose for this type of manuscript. The ink penetrates through the paper fiber and this makes it difficult to analyze. This support increases the Raman fluorescence, hindering a clear and defined spectrum.

To obtain an *in-situ* Raman spectrum, the most important thing is to correctly tune the focus point on the surface. For this, it is recommended to use a silicon plate, which has an intense band at 520 cm^{-1}, when this is at its maximum intensity we will have for sure the point of focus.

It is also recommended to look for microscopically ink crystals formed on the surface to obtain an optimal Raman signal. However, in some situations, on these points the signal is so strong that the equipment saturates. Then, at this point is possible to vary the power/exposure time or move the focus to a less saturated point of ink.

Table 4. Summary of the photos and microscopy images (50x-objective) of the art works (documents, manuscripts, etc.) analyzed by the Renishaw InVia Raman spectrometer.

Sample	S001	S002	S003
Year	1855	1855	-
Description	Official documents from different archives of Kežmarok (Slovakia).	Official documents from different archives of Kežmarok (Slovakia).	Fragments of documents of unknown origin and time.
Image	 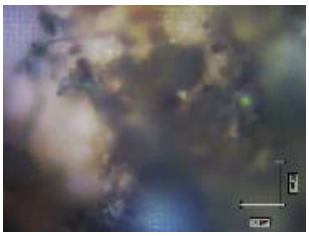	 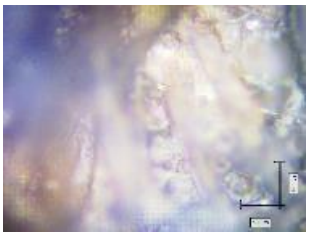	 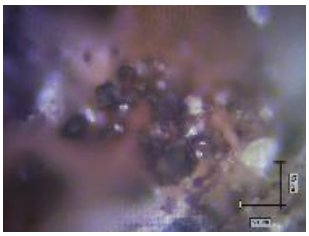

Sample	S004	S005	S006
Year	-	1856	1855
Description	Fragments of documents of unknown origin and time.	Official documents from different archives of Kežmarok (Slovakia).	Official documents from different archives of Kežmarok (Slovakia).
Image			

	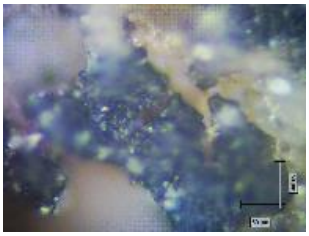		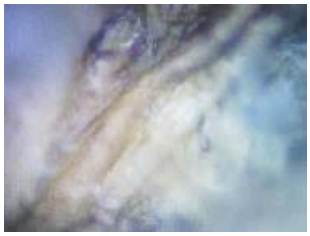

Sample	S007	S008	S009
Year	1858	1854	1930
Description	Official documents from different archives of Kežmarok (Slovakia).	Official documents from different archives of Kežmarok (Slovakia).	Written correspondence between Spanish emigrants in Cuba.
Image	 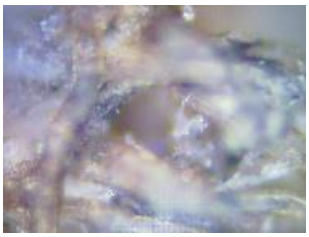	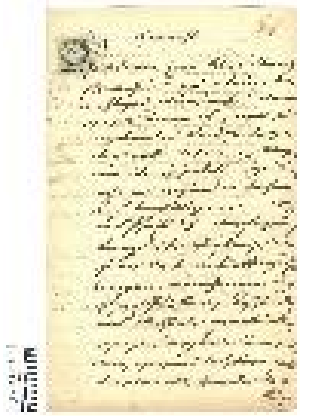 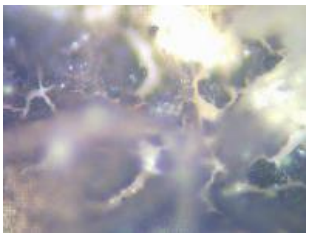	 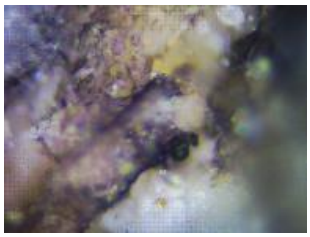

Sample	S010	S011	S012
Year	1930	~ 1930	1835
Description	Written correspondence between Spanish emigrants in Cuba.	Written correspondence between Spanish emigrants in Cuba.	Supplier and infrastructure maintenance invoice commissioned by hospital in Oviedo (Spain).
Image			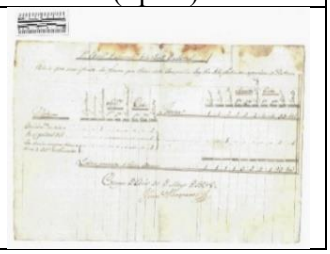

	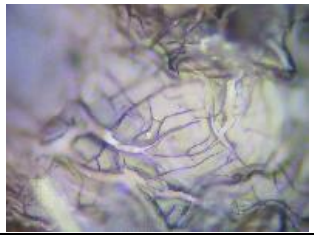	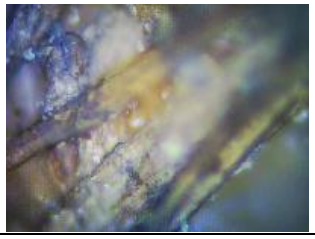	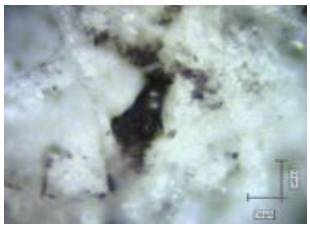

Sample	S013	S014	S015
Year	1905	1775	1703
Description	Music sheet issued from the company "Andres Vidal y Llimona Barcelona" (Spain).	The last sheet belonging to Breviarium Romanum scrawled in time with ink.	Courtesy sheet belonging to missal scrawled in time with ink.
Image	 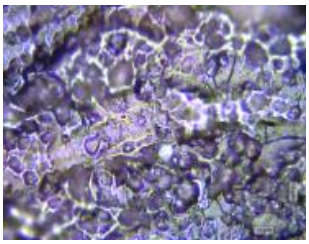	 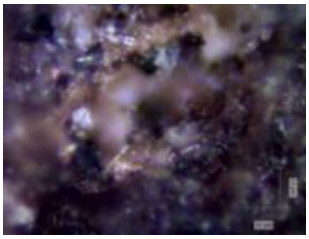	 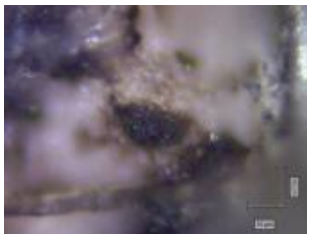

Table 5. Table corresponding to the signatures found in "Mensaje a Castelar 1899" analyzed in this thesis. They are sorted by province, counted and an estimation of signatures written by different inks is also given.

"Mensaje a Casterlar 1899"								
Province	Number of manuscript folds and the number sign in each						Total	≠
	1º	2 º	3 º	4 º	5 º	6 º		
Lugo	65	51	34	31	65		264	33
León	83	130	118	96	38	91	556	40
Pontevedra	15	48					93	9
Ourense	12	49	156	124			341	19
Coruña	74	198	123	53			448	43
Palencia	70						70	10
Soria	71						71	17
Guadalajara	45						45	7

3.5 Measurement of the pH on historical manuscripts

The pH of manuscripts was measured by using the drop method which is increasingly used in the field of cultural heritage, especially in the case of pictorial surface analysis. For instance, its use is divulged by institutions such as the Getty Museum through Chris Stavroudis and his Youtube channel "Getty Conservation Institute" [85]. In addition, it is also discussed in scientific publications dedicated to contemporary paintings and prepared by the Department of Conservation and Restoration of Cultural Heritage, Faculty of Fine Arts, Polytechnic University of Valencia [86].

It is a very innovative method since the pH of liquids has been commonly measured, but not that of solids. The proposed method allows measuring in a certain way the ionic charge of a solid using a drop of water or a gel deposited on its surface and used as a vehicle, thus, assessing the pH of the studied solid. It is supposed, that the water drop, when applied to the manuscript's surface, is going to reach an equilibrium with the ink of the manuscript what results in a possibility to estimate indirectly a pH.

The measurement protocol was determined as follows: firstly, the measurement time was decided to be one minute to avoid a significant loss of the drop volume. At the same time, the minimum volume of the drop needed to carry out an accurate experiment was defined by the instrument and the corresponding technical parameters. It means, a generous drop of Milli-Q water of about 500 µL was deposited on the manuscript's surface and left to rest for one minute. Further, it was essential to collect as much as possible of the residual volume of the drop, put it in an appropriate container and measure its pH. The Hanna HI 2221pH/ORPM pH meter was employed to accomplish it.

3.6 Instrumentation

i) UV-vis spectrophotometer

UV-vis absorption/extinction spectra were obtained by using a Shimadzu UV-VIS/NIR 3600 double-beam spectrophotometer (Shimadzu Corp., Kyoto, Japan) equipped with a PMT for light detection in the UV-visible range, and detector for the near infrared (NIR). Samples were placed in quartz cells of 1 cm-optical path, after dilution to 30% in Milli-Q water (v/v) and spectra were recorded in the 250-1000 nm range with the 0,5 or 1 nm-step.

ii) Infrared spectrometer

FTIR spectra of pure polyphenols in powder were registered directly by the ATR method at room temperature in the region 2000-520 cm^{-1}, on the FTIR spectrometer (ABB, model FTLA2000-100) using Nicolet 8700 IR Microscope. The spectra resolution was set to 4 cm^{-1} and the final spectra are the results of 128 scans. Further, FTIR spectra of iron complexes in KBr pellets were registered by absorption/transmission measurements in a FTIR Bruker IFS66 spectrometer, performing 1000 scans and using the Globar source and the DTGS detector.

iii) Fourier-Transform Raman spectrophotometer

FT-Raman spectra were obtained by using a Bruker MultiRAM spectrometer (model RFS 100/S) equipped with Nd-YAG excitation source at 1064 nm and high purity Ge detector cooled by liquid nitrogen. Spectra were acquired with the 4 cm^{-1}-resolution, in the spectral range 4000-100 cm^{-1} and a 180º geometry was employed. The output laser power was set to 200 mW, and the laser power at the sample was 20 mW. The Raman spectra displayed in this work were the results of averaging 500-1000 accumulations.

iv) Dispersive Raman spectrophometer

Raman spectra were recorded by using a micro-Raman inVia Renishaw spectrometer (Wotton-under-Edge, Gloucestershire, UK), equipped with an electrically cooled CCD camera, and a Leica DM 2500 microscope. The laser excitations at 785 nm (diode laser), 532 nm (Nd-YAG laser with doubler of frequency), 442 nm and 325 nm (He-Cd) laser were employed as excitation sources. The measurements were performed using different notch filters as well as different diffraction gratings in function of the used laser excitation in order to optimize the measurements and to increase the final spectral resolution. The Raman signal was collected over the range 100-2000 cm^{-1} (or 4000 cm^{-1}), under macro conditions using glass vials and working with a spectral resolution of 1 cm^{-1}. The laser power at the sample was up to 2 mW. The signal was firstly calibrated by using the 520 cm^{-1} line of a Si wafer and a 20x objective.

v) Portable Raman instrument

The *in-situ* measurements of manuscripts corresponding to the Castelar's letters of the MAN museum were recorded by using the Raman Inspector DeltaNu portable instrument. This instrument was coupled to a NuScope microscope in order to register small areas on the manuscript. The laser excitation was at 785 nm with a laser spot of 0,01-1 mm on the sample. The spectral resolution was 8 cm^{-1}.

vi) Data management

All the recorded data were processed using the software programs OriginLab and Microsoft Excel.

vii) DFT calculations

In the present study, Raman spectroscopy was mainly used to carry out the analysis of different iron and copper complexes of the selected polyphenols (TA, GA, PY and SA) to find a correlation between Raman spectra and the IGI colorant structure. In order to elucidate the structure of the IGIs and to perform a detailed assignment of the vibrational modes of polyphenols and their complexes (something that was missed in previous applications of Raman to IGIs), an optimization of the geometry of GA and two different iron complexes, GA-Fe and GA-Fe_2, was performed (**Figure 22**). This optimization was followed by theoretical calculations of the normal vibrational modes which was carried out by Density Functional Theory (DFT) methods. Since the overall structure of TA is very complex, the theoretical study was performed on GA, its basic structural unit. It is also worth noting that DFT calculations were performed for the first time on the gallic acid complex with iron in the present thesis.

In the first case (GA-Fe complex; **Figure 22**b), the metal interacts with the COOH group of GA, and in the second one (GA-Fe_2 complex; **Figure 22**a), two Fe ions interact with the OH groups of GA molecules. The Raman spectra of the optimized structures were also calculated, in order to aid in the normal mode assignment of the GA, GA-Fe and GA-Fe_2 vibrations.

For the GA molecule and the GA-Fe and GA-Fe_2 complexes, the optimization of the ground state of the structures and the calculation of the theoretical Raman spectra were performed in vacuum conditions with DFT using the Gaussian 09 package [87], [88]. Calculations for GA were carried out considering the neutral and deionized (GA^-) singlet molecule, using a B3LYP hybrid exchange correlation functional in combination with 6-311+G* as a basis set. The calculations of Fe complexes were performed considering the Fe^{3+} ion resulting from the oxidation of the initial Fe^{2+} ion. Two different complexes were calculated considering the interaction of two Fe^{3+} ions with the ionized –OH groups (complex GAOH-2Fe), and the complexation of one Fe^{3+} ion with the carboxylate anion (GACOO-1Fe), following the models reported by Ponce *et al.* [89]. In addition, the state multiplicities were considered to be quintet and sextet for the complexes with two and one Fe ion, respectively. For simplicity, the coordination

water molecules, necessary to complete the octahedral geometry of the Fe^{3+} complexes, were not included in the analyzed structures. This approximation was previously used in the study of the Fe-catecholate complexes [90]. However, other authors included the water molecules in their DFT calculations [91].

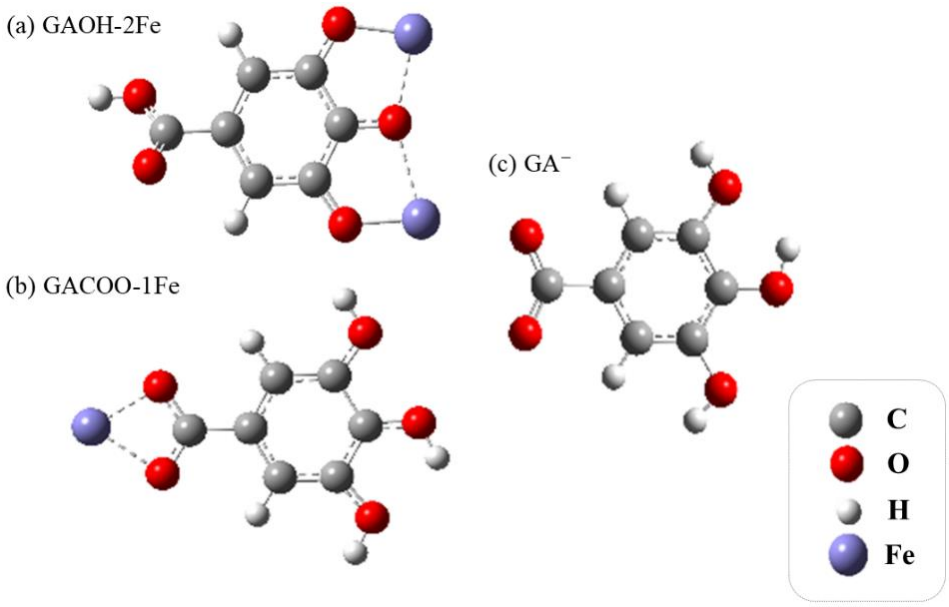

Figure 22. *Optimized structures of the Ga-Fe_2 or GAOH-2Fe complex (a), where two Fe atoms interact with the O atoms placed in positions 3,4,5; GA-Fe or GACOO-1Fe complex (b), where the Fe atom interacts with both O atoms in the carboxylate group, and the non-complexed GA^- (without interacting with any Fe atom) (c) employed for theoretical calculations of spectra.*

The mixed basis sets 6-311+G* + LANL2DZ (Los Alamos National Laboratory 2 double ζ) were used for the calculations of the Fe complexes. LANL2DZ is a widely used effective core potential (ECP)-type basis set, and it was used to model the metal atoms [92]. Both basis sets have been widely used along with DFT methods for studies of transition metals-containing systems. Thus, the Los Alamos effective core potential was employed on the transition metal, and the Pople-type basis set was used on all other atoms (C, H, and O).

Upon optimization of the molecular geometry, Raman spectra were obtained. No imaginary wavenumbers were observed in the calculated spectra. The GaussView 5.09 software was employed to view data and output images. Detailed assignments of the vibrational normal modes were based on the best fit comparison of the wavenumbers of calculated and experimental Raman bands. Scaling factors of 1.05 was applied in all cases.

4. RESULTS AND DISCUSSION

4.1 UV-visible absorption spectra

UV-vis spectroscopy is a very suitable technique for the study and quantification of phenolic compounds [79], [80], [81]. These colorless compounds do not show absorption features in the visible region of the electromagnetic spectrum. However, phenolic substances can strongly absorb UV light. Thereto, certain phenolic compounds can still lead to absorption features also in the visible range displaying a color. Pyrogallol, having three hydroxyl groups attached to the aromatic ring (**Figure 15**a), presents only a weak absorption maximum at 266 nm and a medium shouldering band at 222 nm (**Figure 23**).

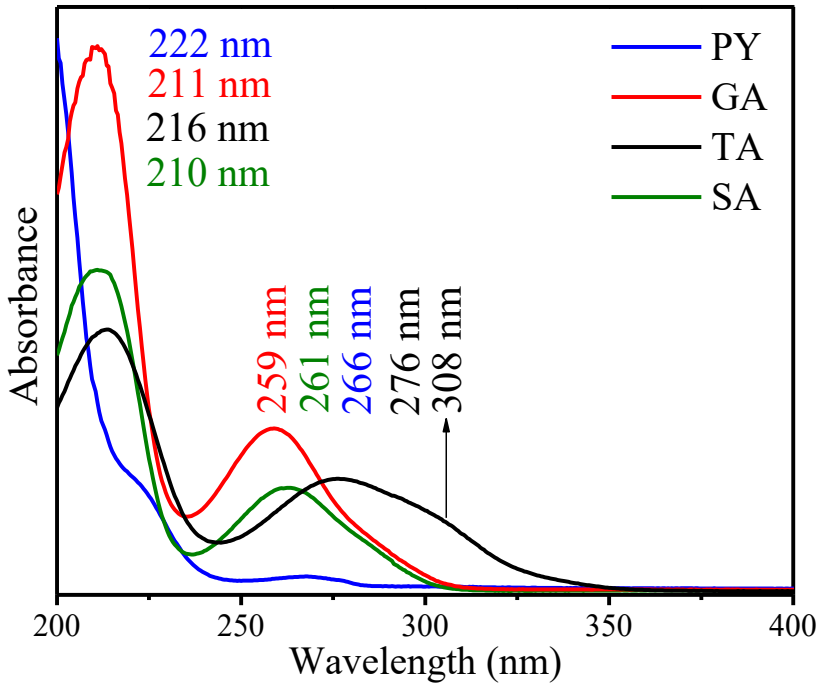

Figure 23. *UV-vis absorption spectra of 10^{-5} M aqueous solutions of the studied polyphenolic compounds, pyrogallol (PY), gallic acid (GA), tannic acid (TA) and syringic acid (SA), measured at pH 7.*

On the contrary, the UV-vis absorption spectrum of GA in an aqueous solution shows two characteristic phenol bands appearing at 211 and 259 nm, corresponding to the $1L_a$ and $1L_b$ bands, respectively, originating from $\pi \rightarrow \pi^*$ transitions [84][85]. In the case of SA, the latter can be observed as slightly red-shifted (to 261 nm) because of methyl substitution of the two of three phenolic hydroxyl groups, **Figure 15**d, i.e. because of the larger conjugated system. For tannins, despite the degree of polymerization of these polyphenolic structures, the absorption features remain the same with a predominant absorption band at around 276 nm. In particular, at neutral pH, the absorption spectrum

of **TA** aqueous solution exhibits peak at **216 nm** and a very broad band at **276 nm** with a shoulder at **308 nm** (**Figure 23**), due to the all possible configurations that are possible in its intrinsic molecular complexity, and assigned to its neutral form as was previously reported elsewhere [98]–[100].

i) Effect of the metal on the UV-visible spectra

A study of the UV-vis absorption of the studied polyphenol compounds and their iron and copper complexes was carried out at different pH ranging from 3 to 12 (**Figure 24** and **Figure 25**).

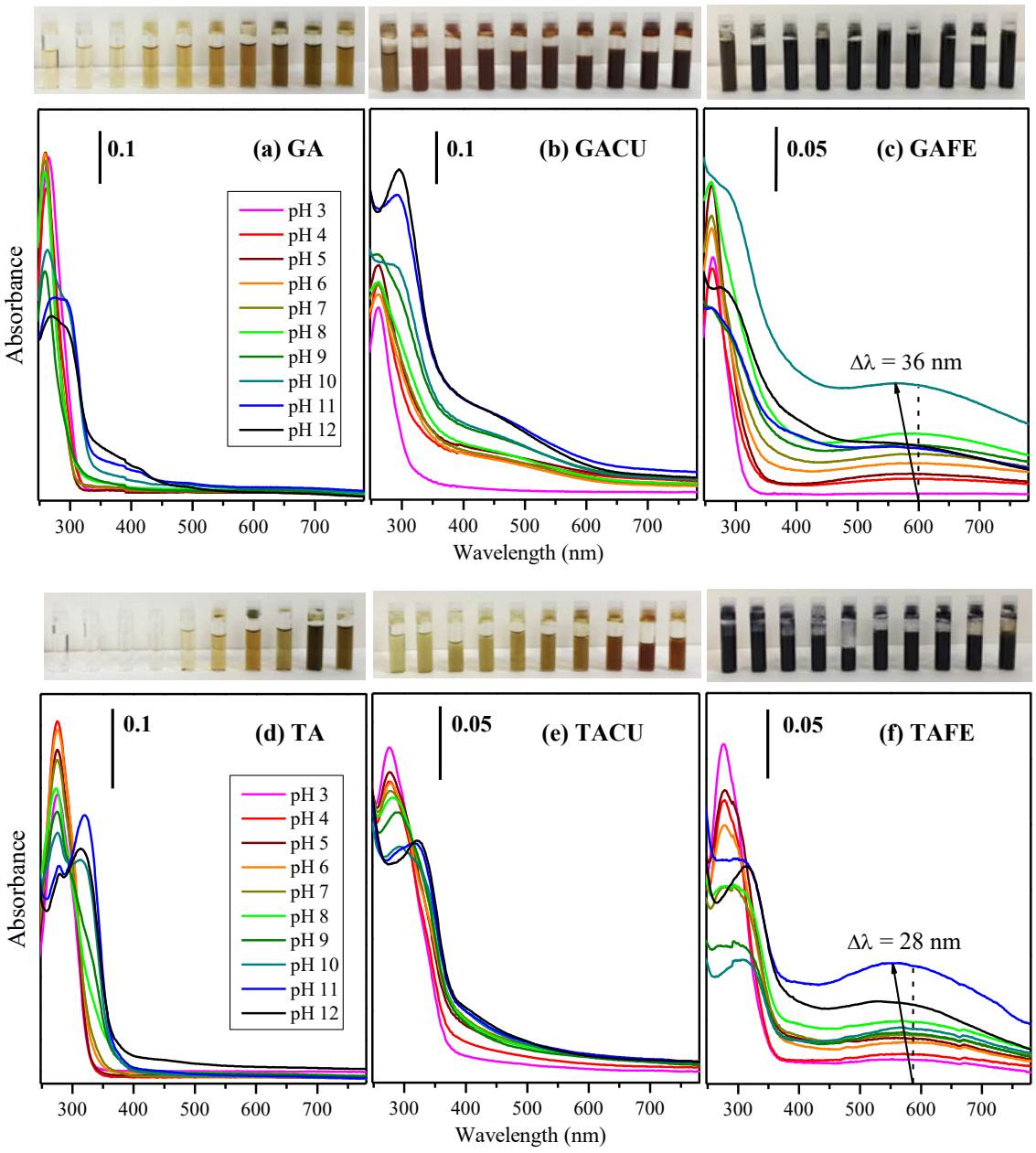

Figure 24. *(In the previous page) UV-vis absorption spectra of GA and TA (a,d), at concentration 6,6x10^{-5} M and the complex with Cu^{2+} (b,e) and Fe^{2+} (c,f) in aqueous solution at 1/3 (gallic acid/metal) molar ratio (6x10^{-5}/19.5x10^{-5} M/M) for GA-Fe complex and 1/30 (tannic acid/metal) molar ratio (6x10^{-5}/19.5x10^{-4} M/M) for TA-Fe complex. For the sake of simplicity, the absorbance intensity is indicated with an inner bar. The spectra were not offset and start from absorbance zero at the bottom. The upper pictures show the colors of the solutions/suspensions of molecules and their corresponding metal complexes obtained at pH ranging from 3 (left) to 12 (right).*

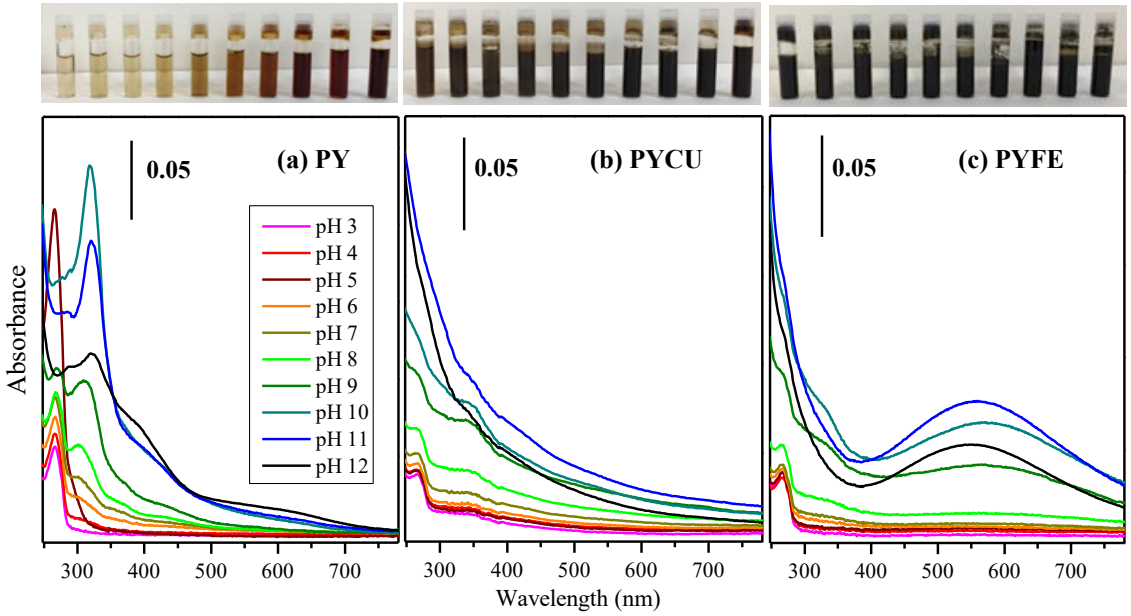

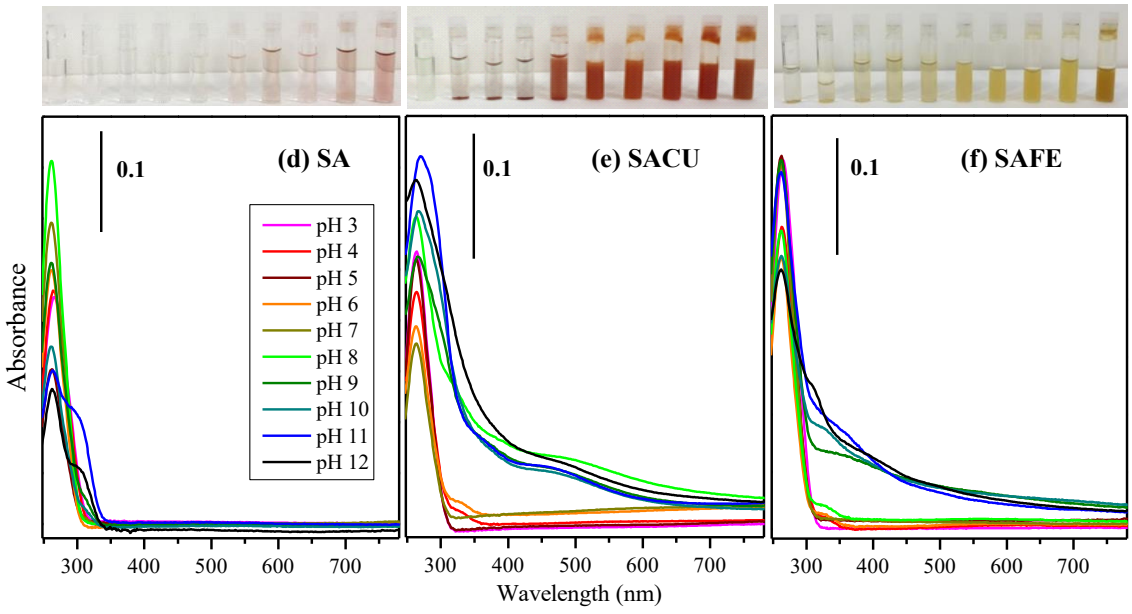

Figure 25. *UV-vis absorption spectra of PY and SA (a,d), at concentration 6,6x10^{-5} M and complexes with Cu^{2+} (b,e) and Fe^{2+} (c,f) in aqueous solution at 1/2 (phenol/metal) molar ratio for PY (6x10^{-5}/13.0x10^{-5} M/M) and 1/3 for SA (6x10^{-5}/19.5x10^{-5} M/M). For the sake of simplicity, the absorbance intensity is indicated with an inner bar. The spectra were not offset and start from absorbance zero at the bottom. The upper pictures show the colors of the solutions/suspensions of molecules and their corresponding metal complexes obtained at pH ranging from 3 (left) to 12 (right).*

The interaction of iron with all polyphenols studied in this work induced a strong change in color that can be characterized by UV-vis absorption. However, this also can be observed to the naked eye (see upper pictures in **Figure 25** for the individual molecules at different pHs ranging from 3 to 12). In addition, the increase of pH in non-complexed polyphenols also led to a darkening, which is weaker than that produced by the iron complexation. This fact can be attributed to the ionization of OH groups and a possible oxidation and polymerization of the smaller units leading to more complex structures [63], [79].

Figure 26 shows the UV-vis absorption spectra of GA (**Figure 26**a) and TA (**Figure 26**b) at selected pHs in order to observe more easily the effect of the different metals.

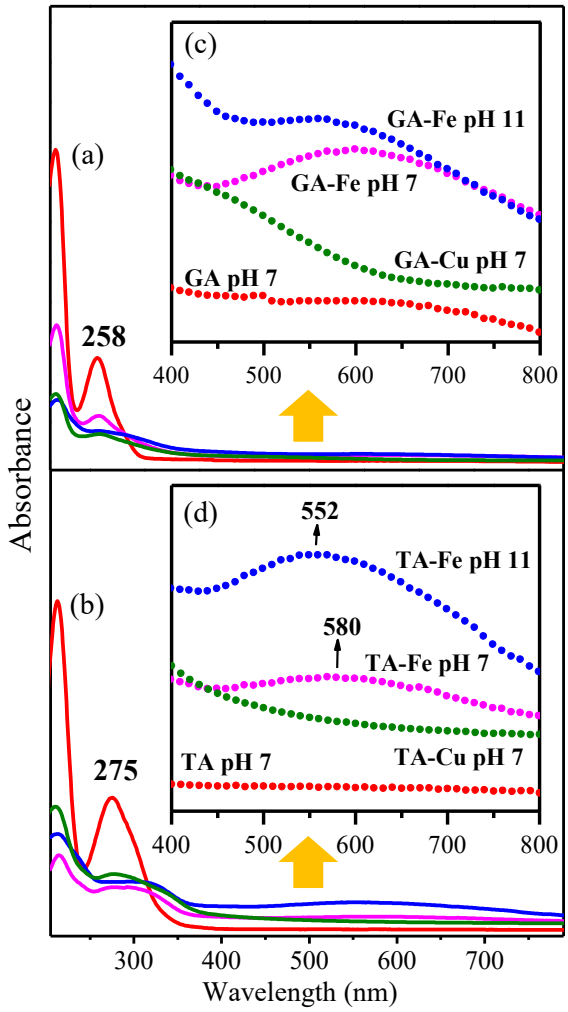

Figure 26. *UV-vis spectra of GA (a) and TA (b) without metal (red), with iron at pH 7 (purple) and pH 11 (blue), and with copper at pH 7 (green). Polyphenols were at concentration 6,6x10^{-5} M without metal and at 1/3 (gallic acid/metal) molar ratio (6x10^{-5}/19.5x10^{-5} M/M) for GA-metal complex and 1/30 (tannic acid/metal) molar ratio (6x10^{-5}/19.5x10^{-4} M/M) for TA-metal complex. The region corresponding to the new broad band appearing at longer wavelength due to the ligand-to-metal charge transfer (LMCT) is amplified for tannic acid (c) and gallic acid (d).*

As we have already discussed (**Figure 25**), the UV-vis absorption spectrum of GA (**Figure 26**a) shows two characteristic phenol bands appearing at 210 and ~ 260 nm [88] which are in the case of TA shifted to 213 and 275 nm due to the polymer structure of all the gallotannins and simpler galloyl glucoses included in this commercial sample (**Figure 26**b). The interaction with metal cations, Fe^{3+} and Cu^{2+}, induces a weakening of both $1L_a$ and $1L_b$ band intensities together with a redshift. This is more evident for the $1L_b$ band, which is shifted to 310 nm in the case of TA. In addition, a new broad absorption band appears at longer wavelengths, which in the case of Fe^{3+} leads to a maximum at 550−600 nm. This new feature is the responsible for the strong colour change observed in the interaction of Fe^{3+} with phenolic compounds. In particular, the new broad band appearing at longer wavelength is attributed to the ligand-to-metal charge transfer (LMCT) from the polyphenol to the Fe^{3+} center of the complex [101], [102]. It is interesting to note that the maximum of this new band undergoes a blue shift from 600 to 564 nm and from 580 to 552 nm upon increasing the pH to 11 in both GA and TA, respectively (**Figure 25**c and f). This shift is likely due to the polyphenol autoxidation at alkaline pH, giving rise to quinone structures (**Figure 27**) [103] as well as oligomerization of polyphenols promoted at alkaline pH [104], [88].

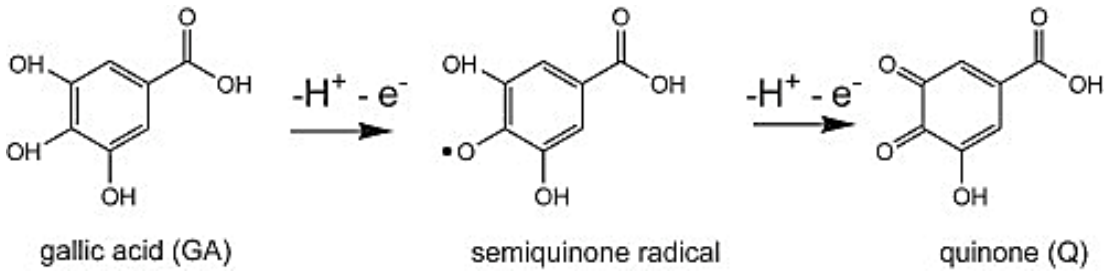

Figure 27. *The reaction mechanism of the oxidation of gallic acid. The quinones are a class of organic compounds derived from aromatic compounds such as benzene by conversion of an even number of –CH= groups into –C(=O)– groups with any necessary rearrangement of double bonds, resulting in a fully conjugated cyclic dione structure [105].*

However, a change in the interaction stoichiometry of the ligand with the Fe^{3+} after OH group ionization can also account for this shift [88]. The absorbance increase of this band as the pH rises (**Figure 28**) is likely connected to structural changes occurring in polyphenols (ionization, oxidation, and polymerization). These changes modify the complexing pattern of these molecules with metal ions.

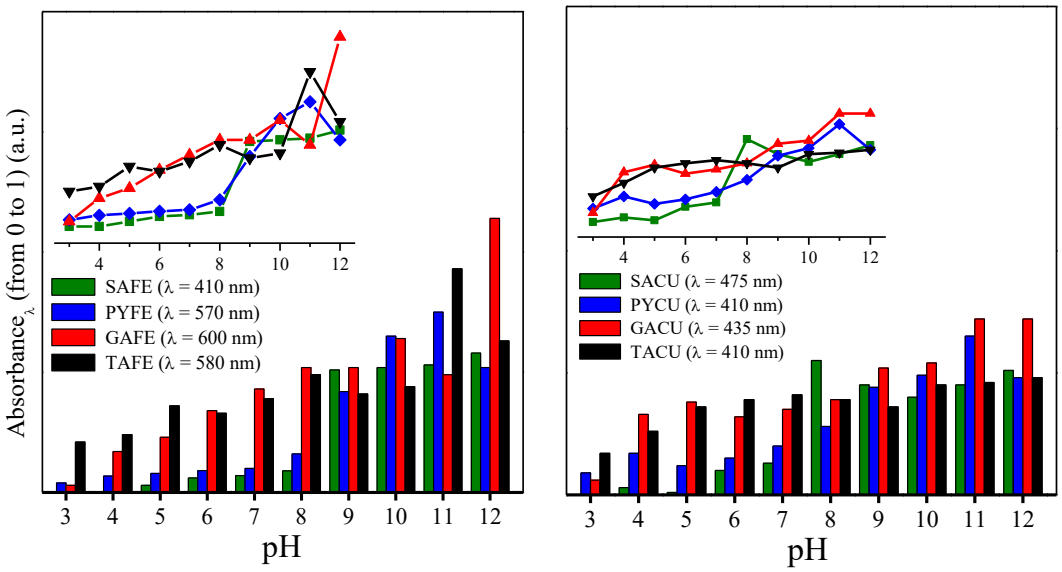

Figure 28. *Bar and line-symbol graphs show intensity changes of the absorbance bands associated with metal-ligand complex formation as a function of different pH for iron and copper; the polyphenol molecule concentration was 10^{-5} M.*

It is known that Fe^{3+} has a $3d^5$ electronic configuration (**Figure 29**), and that the application of a strong crystal field induces, in an octahedral symmetry, a splitting of the five orbitals into two groups e_g (dz^2 and dx^2y^2) and t_{2g} (dxy, dxz and dyz) (**Figure 30**) [102]. The energy difference between the two orbital groups lies between 20,000 and 18,000 cm^{-1} for most of the Fe^{3+} complexes with cathecolate and other polyphenols [106]. Usually, the LMCT band in the different iron-phenolic acid complexes are similar but quite different from the value calculated for $Fe(OH)_6^{3-}$ (ca. 770 nm). This difference can be explained by partly oxidized character for the ligand (semi-quinone) and the partly reduced character of iron in the excited state during the charge transfer [106]. For this reason, the ultraviolet absorption of iron-phenolic acid complexes is quite different from $Fe(OH)_6^{3-}$. This is an important fact that is related to the specific structure of polyphenols when complexed by metals, which in turn also depends on the number of ligands surrounding the metal sphere of coordination [88]. Also, this effect can serve to establish a correlation between the UV−vis absorption spectrum and the structure.

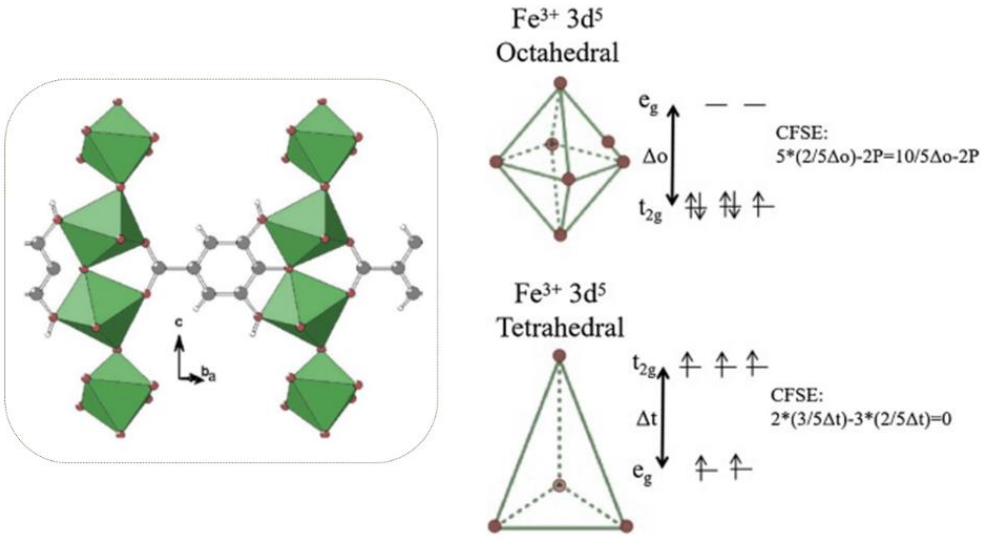

Figure 29. *Structure proposed by Russell Feller and Anthony Cheetham. The red points represent the oxygen atoms, the gray ones the carbons and the white depict the hydrogens, the green is octahedral-crystal structure of the Fe^{3+}. Schematic electronic configurations of Fe^{3+} Td and Fe^{3+}Oh. Δo and Δt are the octahedral and tetrahedral crystal field splittings in iron ions [89].*

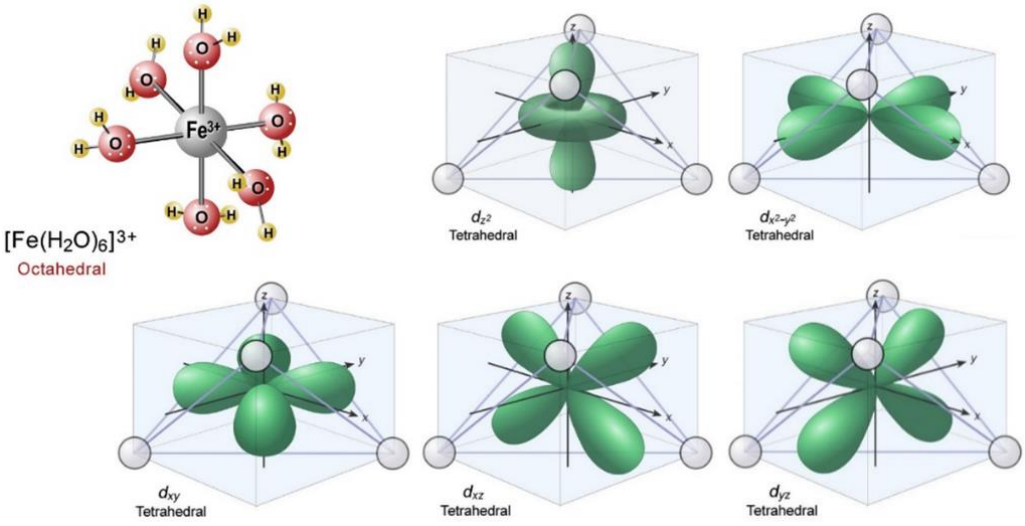

Figure 30. *Diagram shows the octahedral complex ion formed between Fe^{3+} ion and water and the groups eg (dz2 and dx2y2) and t2g (dxy, dxz and dyz), the 5d orbital in a tetrahedral crystal field [107].*

In the specific case of Cu^{2+}, the LMTC band is rather observed as a shoulder in the 400−500 nm region. This leads to a noticeable increase of the absorbance at 400−600 nm that can be seen in all polyphenols in the presence of the metal, which is summed to the autoxidation and polymerization of the polyphenols and more evident at high pH (**Figure 26**c and d; **Figure 26**b and e).

4.2 Vibrational spectra

i) Raman spectra

Raman spectroscopy (RS) allows us not only to identify and characterize the selected compounds but also to monitor, for example, deprotonation of the molecules, their interactions with metal ions as well as different structural changes that occurred during these processes. Since the four phenolic compounds analyzed here exhibit a certain fluorescence emission in the UV-vis region, firstly, we have registered the FT-Raman in their solid-state (**Figure 31**).

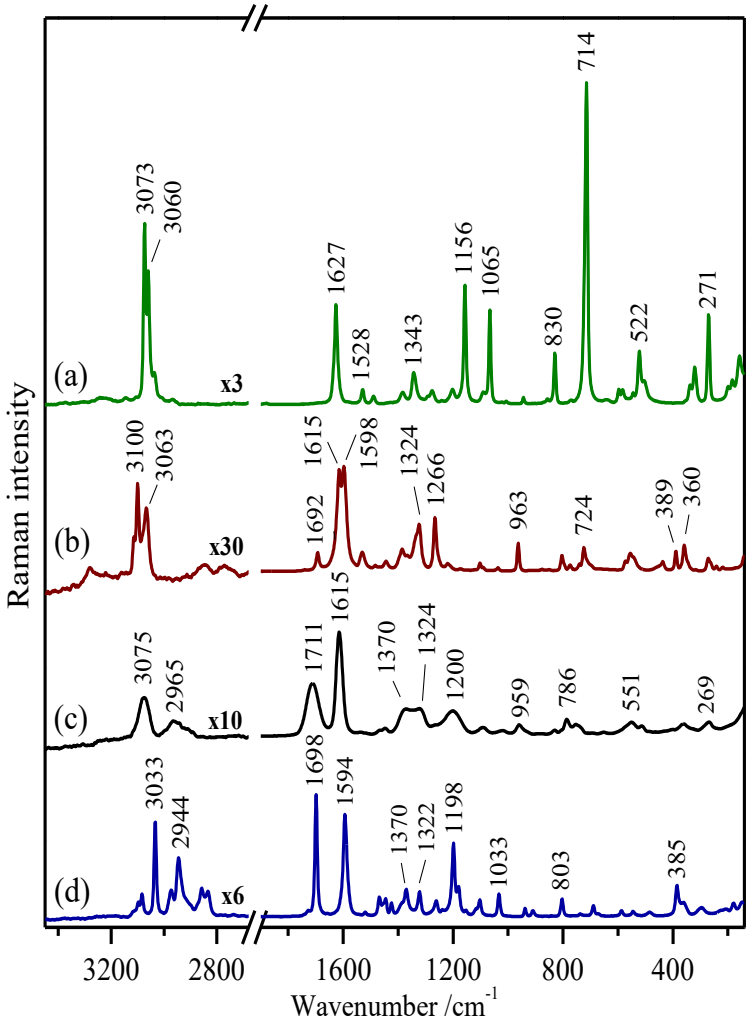

Figure 31. *FT-Raman spectra of the studied polyphenolic compounds in their solid state: (a) pyrogallol; (b) gallic acid; (c) tannic acid; and (d) syringic acid. Raman spectra were normalized to the bands at 1627-1594 cm^{-1}. Excitation line: 1064 nm.*

As expected, spectral differences can be observed, but at the same time, common spectral features can also be found in the recorded spectra. This allows us to compare

them, and consequently, to carry out an assignment of their vibrational modes. To do a complete and detailed vibrational assignment is not a simple task. In fact, no satisfactory assignment of bands was found in the literature although the Raman spectra of many phenolic compounds have been already published [11], [84], [93]-[99]. Furthermore, the comparison of the IR and Raman spectra also serves as an additional help for a more accurate assignment, since they are complementary due to the different selection rules applied in these techniques which give rise to the vibrational bands with different relative intensities. Thus, a vibrational assignment has been performed on the basis of the recorded vibrational spectra as well as results found in the literature for the studied molecules, their derivatives as well as other structurally related molecules [54], [76], [84], [97], [99]-[101]. The experimental IR and Raman frequencies for various modes of vibration are assigned and presented in **Table 6**.

In general, all polyphenols show a similar spectrum below 1000 cm^{-1} (in the 'fingerprint' region) owing to the similar skeletal structure; though, the exception is the PY Raman spectrum. In contrast, the spectral region from 2000 to 1000 cm^{-1} displays a higher diversity. This is not the case of the region corresponding to the C=O and C=C stretching vibrations (ν(C=O) and ν(C=C)) seen in the 1710-1530 cm^{-1} region, where some similarities are found between these molecules, with the exception of PY which has no ν(C=O) functional group. However, the main differences between them are found in the 1400-1000 cm^{-1} region where OH deformations (δ(O-H)) and ν(C-O) motions appear, and this is because of the different substitution and distribution of the functional groups (OH, OCH_3) in the studied molecules. Finally, the region from 4000 to 2800 cm^{-1} is characteristic of the stretching vibrational modes associated with the groups containing hydrogen (O-H, C-H), which is also variable according to the substitution pattern of the aromatic rings.

Raman spectrum of the PY molecule differs the most (comparing to the other three molecules) regarding especially the intensity of the observed bands (**Figure 31**a). Firstly, an intense Raman band at 3073 cm^{-1} assigned to the aromatic C-H stretching vibrations (ν(C-H)) is visible. GA and TA do not differ too much concerning the frequency of the ν(C-H) bands. In particular, the bands at 3100/3063 cm^{-1}, and 3075/2965 cm^{-1} can be seen in the Raman spectra of GA and TA, respectively (**Figure 31**b and c). Nevertheless, the Raman intensities of ν(C-H) bands are relatively weaker in these two polyphenols. Furthermore, as expected, the Raman spectrum of SA shows a higher

number of bands at this high-wavenumber edge of the spectrum due to the presence of two methyl groups which give rise to symmetric and asymmetric stretching modes of the O-CH_3 group observed at 2834 and 2857 cm^{-1}, and at 2944 and 2973 cm^{-1}, respectively. The stretching at 3033 cm^{-1} is the most intense ν(C-H) band among these polyphenols.

The bands attributed to ring C-C stretching appear in the region between 1400 and 1650 cm^{-1}. In the Raman spectrum of PY, the benzene C=C stretching *8a* mode appears at relatively high position: 1627 cm^{-1} (**Figure 31**a). In the case of GA, a doublet at 1615 and 1598 cm^{-1}, assigned to the phenyl stretching vibrations coupled with the δ(O-H) and CH in-plane bending modes, is visible (**Figure 31**b). It was seen that the observed doublet is characteristic of the GA crystals present in the monomer form [100]-[103]. Because of the concurrent presence of the band at 1692 cm^{-1} we can also suppose the presence of the dimeric form of the gallic acid. However, the monomer dominates the Raman spectrum of GA in its solid-state as deduced from the recorded FT-Raman spectrum.

The high position of the *8a* stretching vibration in PY (1627 cm^{-1}) as compared to the other polyphenols can be attributed to absence of the conjugation of the C=O bond with carbon double bonds of the phenyl ring than occurs in the other polyphenols. The ν(C=O) of the carboxylic group is in the Raman spectrum of GA visible at 1692 cm^{-1} as a very weak band. On the contrary, the band at 1698 cm^{-1} in the Raman spectrum of SA is the strongest ν(C=O) band of this series (**Figure 31**d). The high intensity of this band, as compared to the equivalent one in GA, points out that this molecule is not forming dimmers as in the case of GA.

TA displays a medium-intense and broad band at 1711 cm^{-1} assigned to the conjugated ν(C=O) vibration in the ester group (**Figure 31**c). The broadening of this band is due to the numerous carbonyl groups found in the structure of TA as well as existence of different intra- and inter-molecular hydrogen bonds. It can be also seen a second strong band at 1615 cm^{-1} in the Raman spectrum of TA which is assigned to the C=C stretching *8a* mode at a similar position than GA. In general, TA presents very broad spectral bands due to the different possible structures existing in the molecule.

In the next region, two intense bands at 1156 and 1065 cm^{-1} can be seen in the Raman spectrum of PY (**Figure 31**a). They are related to the C-H in-plane bending vibrations,

ring-deformation in-plane bending modes and C-O stretching vibrations [86], [100]. Finally, the fingerprint zone of the PY Raman spectrum is dominated by the intense band at 714 cm^{-1} which is attributed to the ring breathing mode [112].

The major differences between the three molecules (GA, SA and TA) can be found in the 1500-1000 cm^{-1} region, where the C-H and O-H bending modes as well as C-O stretching motions appear, because of the different functional groups found in the structure of these molecules. In addition, bands assigned to aromatic ν(C-C) and δ(C-C-H) also appear in this region; while the ν(C-O) modes mainly appear in the 1300-1200 cm^{-1} interval. SA shows a great deal of bands in this spectral region because of the presence of the C-H bending modes of the methyl groups, showing the most intense band at 1198 cm^{-1} assigned mainly to the ring δ(CH) vibrations (**Figure 31**d). GA displays two relatively intense bands at 1324 and 1266 cm^{-1} ascribed to ν(C-C), ν(C-O) and δ(C-OH) modes (**Figure 31**b). The spectrum of TA displays similar bands but showing a general broadening of the different vibrational modes (**Figure 31**c). This is also typical for complex molecular systems where numerous hydrogen bonding takes place [119].

Since TA polymer includes in its structure many GA units, it is interesting the comparison between the Raman spectra of both molecules in order to understand the effect of polymerization in GA, aiming at the discrimination between these two molecules in IGI inks. It is very well known the fact that TA can be degraded under certain conditions, like acidic pH or by the polymer oxidation [120]. Therefore, the finding of spectral markers associated with this degradation could be very helpful in the analysis of the manuscript chemical status. The main differences found between the Raman spectra of both molecules in their solid-state are related to a general broadening of bands, already commented, and the presence of three main bands in TA at 1711, 1370 and 1200 cm^{-1} (**Figure 31**c), attributed to the ester groups existing in TA. In addition, the presence of characteristic bands at 1692, 1530, 1266 and 724 cm^{-1} in GA Raman spectrum (**Figure 31**b) can be related to the carboxylic group in the non-polymerized molecule.

Table 6. Observed (IR and Raman; solid-state, λ_{exc} = 1064 nm) vibrational frequencies of the studied polyphenol molecules (pyrogallol, PY; gallic acid, GA; tannic acid, TA; and syringic acid, SA).

FTIR [a] / cm^{-1}				FT-Raman [a] / cm^{-1}				Vibrational assignment [b,c]
PY	**GA**	**TA**	**SA**	**PY**	**GA**	**TA**	**SA**	
				157 *w* 184 *vw* 198 *vw* 271 *w-m*	142 *w* 219 *vw* 242 *vw*	269 *w*	149 *wm, sh* 178 *wm* 207 *w* 221 *vw, sh* 296 *w*	δ(CCC)
				321 *w* 337 *w*	317 *vw*	331 *vw, sh*		γ(CO), γ(ring)
					360 *wm* 389 *wm*	360 *w*	362 *wm, sh* 385 *m*	δ(CO)
					437 *w* 454 *w, sh*		485 *w*	γ(OH), γ(ring)
540 *w*	532 *wm* **555 *s***			504 *w, sh* 522 *w* 545 *vw, sh*	547 *wm, sh* 554 *wm*	514 *w* 551 *w*	545 *w*	γ(ring)
582 *m*		586 *vw, br*	577 *ms*	583 *vw*	572 *w, sh*		587 *w*	γ(CO), γ(ring), *16a*
	635 *m* 648 *wm, sh*	650 *w, br*		597 *vw*		653 *vw*		γ(CO), ν(ring)
669 *m, sh* **700 *vs***	669 *m* 692 *m, br*	669 *w*	**669 *ms*** **687 *ms***		695 *vw, sh*	693 *vw*	672 *vw, sh* 689 *wm*	γ(OH)
715 *m*				714 *s*	**724 *w***			ν(ring breathing)
764 *s*	**731 *svs*** 766 *m*	**737 *m, sh*** **754 *ms***	737 *w* **768 *ms***		740 *vw, sh* 774 *w*	753 *wm* 786 *wm*	738 *vw*	γ(CH)+γ(OH)
827 *m* 860 *vw* 872 *w*	791 *w* 800 *w* 864 *s* 899 *m, br*	781 w, sh 831 *w, sh* 870 *m*	802 *w* 841 *vw* 864 *wm* 908 *wm*	830 *w* 857 *vw*	803 *w* 850 *vw* 877 *vw*	830 *w* 878 *vw*	803 *m* 844 *vw* 867 *vw* 909 *w*	γ(CH)
	959 *w*	957 *m, sh, br*	937 *w*	944 *vw*	963 *w-m*	959 *w*	938 *w*	ν(C-COOH)
999 *vs*	**1022 *vs***	**1014 *svs***	1040 *m*	1008 *vw*	1037 *vw*	1019 *vw*	1033 *wm*	δ(CH), ν(ring), *18a*
1065 *m*				1065 *m*				δ(CH)

	1097 *w*	1082 *ms*		1091 *w, sh*	1091 *w, sh*	1091 *w*		δ(CH), *9b*
1157 *s*			**1101 *vs***	1156 *m*	1102 *w*		1102 *wm* 1116 *w, sh* 1154 *w*	δ(CH), ν(CO)
1190 *vs*	1178 *svs* 1202 *svs*	**1178 *vs, br***	**1175 *s*** **1194 *s***	1202 *w*	1174 *vw*	**1200 *m***	1179 *s, sh* 1199 *s*	δ(CH), δ(OH)
1242 *s* 1283 *s*	1217 *svs* 1243 *m* 1261 *svs*		1244 *wm* 1265 *w*	1241 *vw* 1276 *w* 1293 *vw, sh*	1220 *w* **1266 *ms***	1260 *wm, sh*	1239 *w* 1266 *wm*	δ(CH), ν(ring), ν(CO)
1317 *s* 1329 *s, sh* 1350 *s, sh* 1385 *s, sh* 1398 *s, br*	1309 *s* 1383 *w*	1308 *svs*	1317 *m* 1367 *ms* 1383 *m, sh*	1343 *wm* 1384 *w*	1324 *ms* 1334 *ms, sh* 1368 *m*	1322 *m* **1370 *m***	1322 *m* 1370 *m* 1386 *w, sh*	δ(CH), δ(OH),δ(C-OH), ν(ring)
		1444 *m*	1418 *m*		1443 *w*	1447 *w*	1424 *w* 1445 *w*	ν(ring), δ(OH)
1481 *s*			1456 *m*	1490 *w*	1484 *vw*	1466 *vw, sh*	1469 *w*	ν(ring), δ(OH), *19a*
1518 *s*	1541 *m*	1533 *m, br*	1520 *m*	1528 *w*	**1530 *wm***	1536 *vw*	1521 *vw*	ν(ring), δ(C-OH), δ(CH), *19b*
1618 *s*	1608 *s*	1606 *s*	1595 *m, sh* 1616 *m*	1627 *m*	1598 *vs* 1615 *vs*	1615 *vs*	1594 *vs* 1658 *vw*	ν(ring), δ(OH), δ(CH), *8a*
	1672 *m, br*	**1699 *s, br***	1693 *ms*		**1692 *wm***		1698 *vs*	ν(C=O) in acid
						1711 *s*		ν(C=O) in ester

[a] ***vw***, *very weak;* ***w***, *weak;* ***wm***, *weak medium;* ***m***, *medium;* ***ms***, *medium strong;* ***s***, *strong;* ***svs***, *strong very strong;* ***vs***, *very strong;* ***sh***, *shoulder;* ***d***, *double*
[b] ***ν***, *stretching;* ***δ***, *in-plane bending/deformation;* ***γ***, *out-of-plane bending*
[c] *The assignments were done on the basis of references [49, 56, 58-62].*

ii) Infrared spectra

To complete the vibrational features of the studied molecules we have also recorded their FTIR spectra in the region from 2000 to 520 cm^{-1} (**Figure 32**). Since the molecules have no center of symmetry, most of their fundamental vibrations are active in both Raman and IR spectra whereas the FTIR spectra of all four molecules showing greater similarity than their Raman spectra. As expected, the IR spectra of phenolic compounds

show common spectral bands associated mainly with the aromatic six-membered rings and phenols moieties.

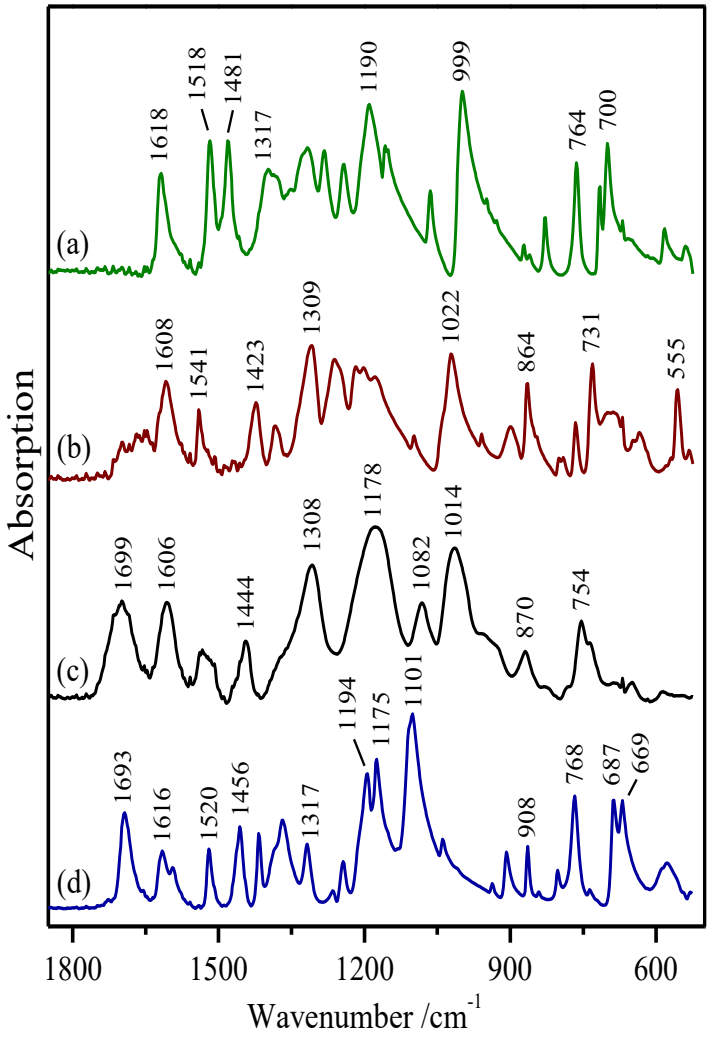

Figure 32. *ATR-FTIR spectra of the studied polyphenolic compounds in their solid state: (a) pyrogallol; (b) gallic acid; (c) tannic acid; and (d) syringic acid.*

The FTIR spectra of these molecules are dominated by strong broad bands in the 1200-1000 cm^{-1} attributed to ν(C-O), ν(C-C) and in-plane δ(C-H). In general, the vibrations containing the in-plane δ(C-H) vibration appears in the range of 1450-1000 cm^{-1}, while the vibrations including the out-of-plane δ(C-H) motions are stronger in the FTIR spectra and appear in the 1000-750 cm^{-1} range in aromatic compounds (**Table 6**). In addition, the O-H in-plane bending motions may couple with C-H bending vibrations and ring stretching vibrations leading to very broad bands appearing in the region 1420-1300 cm^{-1}. Besides, broad absorption bands appearing in the region

710-520 cm^{-1} are generally associated with the out-of-plane bending vibrations of the O-H group and it is characteristic for the spectra of alcohols and phenols [46], [53].

SA displays a characteristic series of very narrow medium intense bands at 1456-1317 cm^{-1} (**Figure 32**d) attributed mainly to in-plane deformations and associated with the presence of the methyl groups in its structure (**Figure 15**d). On the contrary, GA and TA FTIR spectra display intense absorption bands at 1309 and 1308 cm^{-1}, respectively (**Figure 32**b and c) which are related to the coupled vibrations of the ring ν(C-C) and the carbonyl ν(C=O), together with the contribution from δ(C-H) and δ(C-OH) vibrations [115].

In the FTIR spectra of TA and SA the band assigned to ν(C=O) vibrations is observed at 1699 and 1693 cm^{-1}, respectively (**Figure 32**c and d). In the case of GA, there is just a weak broad and not well-defined band in this spectral range due to the existence of dimers that partially quenches the activity of the ν(C=O) mode in –COOH dimer vibrations (**Figure 32**b). As expected, the PY does not possess this vibration (band in its spectrum; **Figure 32**a) due to the absence of the carboxyl group in its structure (**Figure 15**a).

While in the Raman spectra the ring stretching vibrations in polyphenols are very prominent and highly characteristic of the aromatic rings (these vibrations appear in the range of 1650-1200 cm^{-1}), in FTIR spectra these vibrations are less intense than those involving oxygen functional groups. For instance, the *8a* benzene ring vibration appears at 1618 cm^{-1} in PY (**Figure 32**a). However, PY shows two more intense and characteristic bands observed at 1518 and 1481 cm^{-1} attributed to δ(C-OH) coupled to ring stretching motions that correspond to the *19a* and *19b* ring vibrations [112]. GA shows the *8a* benzene ring band at 1608 cm^{-1} and a new band at 1541 cm^{-1} also corresponding to δ(C-OH) motions coupled to ring stretching vibrations (**Figure 32**b). In the TA FTIR spectrum, the *8a* benzene ring band is downshifted to 1606 cm^{-1} and an equivalent broad band centered at 1530 cm^{-1} appears (**Figure 32**c). In the case of the SA, the ring stretching appears at 1616 cm^{-1} with a shoulder at 1595 cm^{-1}, and, in addition, bands at 1520 and 1456 cm^{-1} attributable to δ(C-OH) and δ(CH_3) are also seen (**Figure 32**d).

As mentioned above, the ν(C-O) stretching vibrations also coupled with the adjacent ν(C-C) modes lead to strong band in the 1260-1000 cm^{-1} region. Since these bands occur

at different position depending on the structure of the analyzed compounds, they could be good spectral markers for the identification of each polyphenol. For instance, intense bands can be observed at 1190 cm^{-1} and 999 cm^{-1} in the PY FTIR spectrum; in the GA FTIR spectrum at 1022 cm^{-1}; the TA FTIR spectrum shows broad bands at 1178 cm^{-1} and 1014 cm^{-1}; and finally, a doublet at 1194/1175 cm^{-1} as well as a very strong band at 1101 cm^{-1} are seen in the FTIR spectrum of SA. The latter can be also assigned to the ether C-O-C bond existing in this molecule [79].

Furthermore, the analysis of the fingerprint zone, where out-of-plane bending vibrations of the O-H group mainly appear, reveals the existence of characteristic marker bands associated to each polyphenol. For instance, PY shows two intense bands at 764 and 700 cm^{-1}; in the GA spectrum two bands, at 731 and 555 cm^{-1}, are visible; TA with its complex structure gives rise to a broad and not so intense band at 754 cm^{-1} with a shoulder centered at 737 cm^{-1}; and finally, SA displays a series of very intense bands at 768 and 687/669 cm^{-1}.

iii) Vibrational spectra of polyphenol/metal complexes

Raman spectra

The Raman spectra of TA display bands at 1711 and 1613 cm^{-1} (**Figure 33**c and **Figure 33**a) attributed to the C=O stretching of the carboxylate and the *8a* stretching vibrational mode of the benzene ring, respectively (**Table 7**) [121]. These two bands undergo a strong decrease upon the interaction with iron. The band at 1711 cm^{-1} almost disappears as a consequence of the metal complexation, while the *8a* vibration of the benzene ring undergoes a strong decrease and a shift to 1580 cm^{-1} (**Figure 33**a and c). The latter also agrees with the suggested spectral ranges for vibrations of monosubstituted benzenes: for the "light" substituents the *8a* vibration can be found in the wavenumber range from 1620-1590 cm^{-1} whereas the "heavy" substituents shift the band to lower wavenumbers, within the 1615-1565 cm^{-1} region [122].

Definitely, the Raman spectrum of the Ta-Fe complex is dominated by three main bands appearing at 1477 (ν_1), 1344 (ν_2), and 603 (ν_3) cm^{-1}. In fact, these bands are the classic ones employed for a positive identification of iron gall inks in historic documents as described by Lee [4]. A similar metal effect was also observed in the case of the GA−Fe complex (**Figure 33**e and g) as well as for PY and SA (**Figure 34**). **Figure 35** and **Table 7** summarize the position of these marker bands in the cases of TA, GA,

PY, and SA. The big difference between free and the metal-complexed polyphenols suggest a deep restructuration of the polyphenol, which is also translated to their vibrational spectra.

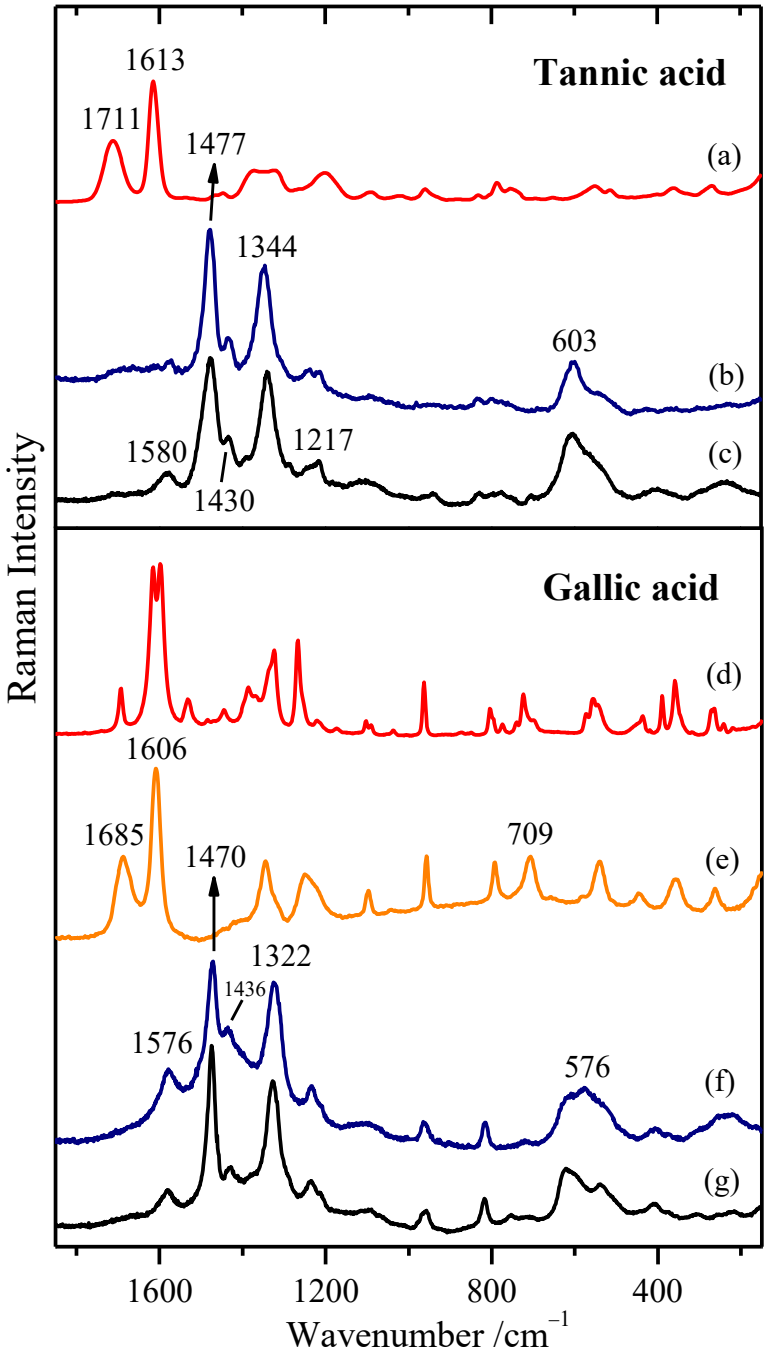

Figure 33. *Raman spectra of TA in the solid state (a), TA−Fe complex on paper (b) and in aqueous solution (2 ×10^{-3} /6 ×10^{-2} M/M) at pH 7 (c), GA in the solid state (d) and in aqueous solution (2 ×10^{-2} M) (e), and GA−Fe complex on paper (f) and in solution (2 ×10^{-2}/ 6 ×10^{-2} M/M) at pH 7 (g). The excitation line was at 1064 nm for the samples in the solid state (FT-Raman) and 785 nm for the solutions and complexes deposited on the paper.*

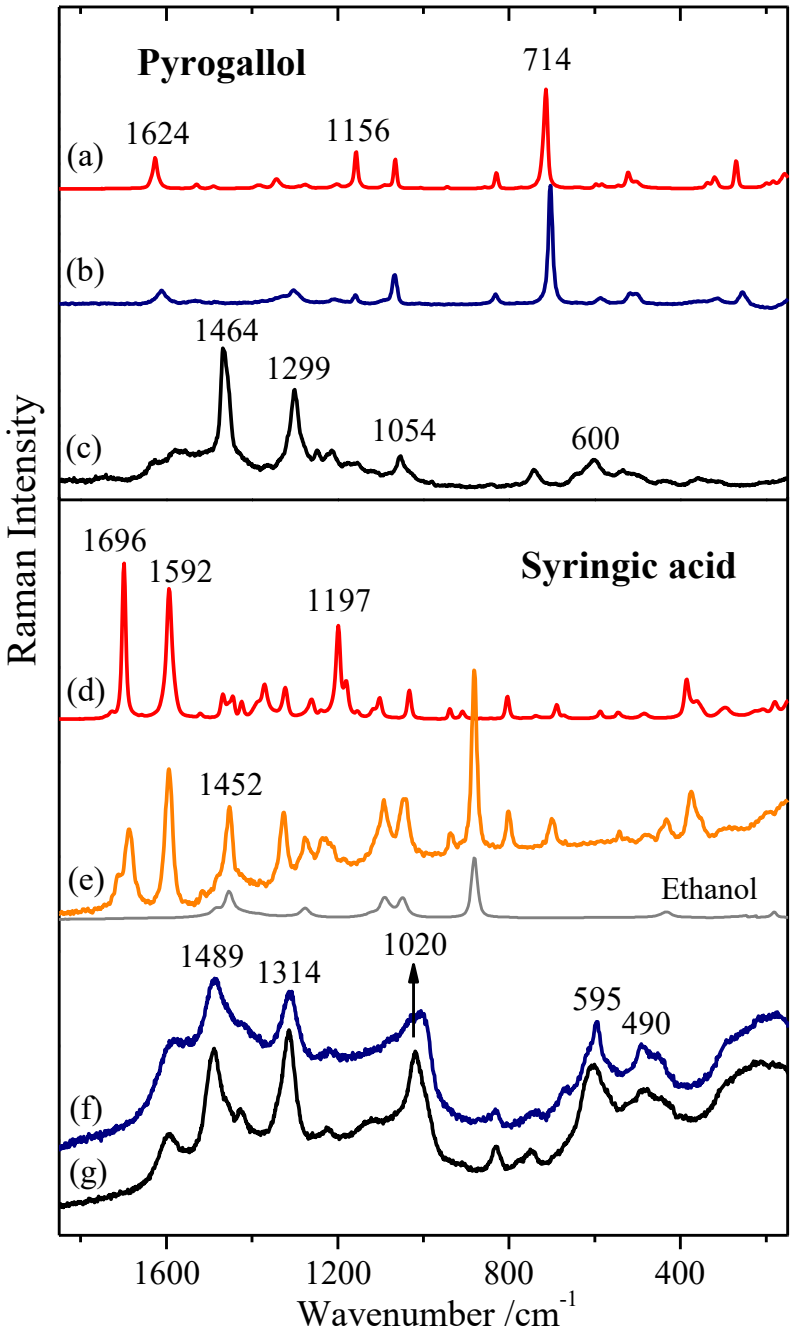

Figure 34. *Raman spectra of PY in solid state (a) and in aqueous solution (2 ×10⁻² M) at pH 7 (b) and PY−Fe complex on paper (c), SA in solid state (d) and in aqueous solution (2 ×10⁻²/6 × 10⁻² M/M) at pH 7 (e), and SA−Fe complex on paper (f) and in solution (2 ×10⁻²/6 ×10⁻² M/M) at pH 5 (g). The excitation line was at 1064 nm for the samples in the solid state (FT-Raman) and 785 nm for the solutions and complexes deposited on the paper.*

The new vibrational features observed in the Raman spectra correspond to the characteristic bands detected in many IGIs found in manuscripts, which have been traditionally employed to attribute black colours in paintings or inks in manuscripts [15], [31]–[39]. Even so, the assignment of these bands was not carried out in depth so far.

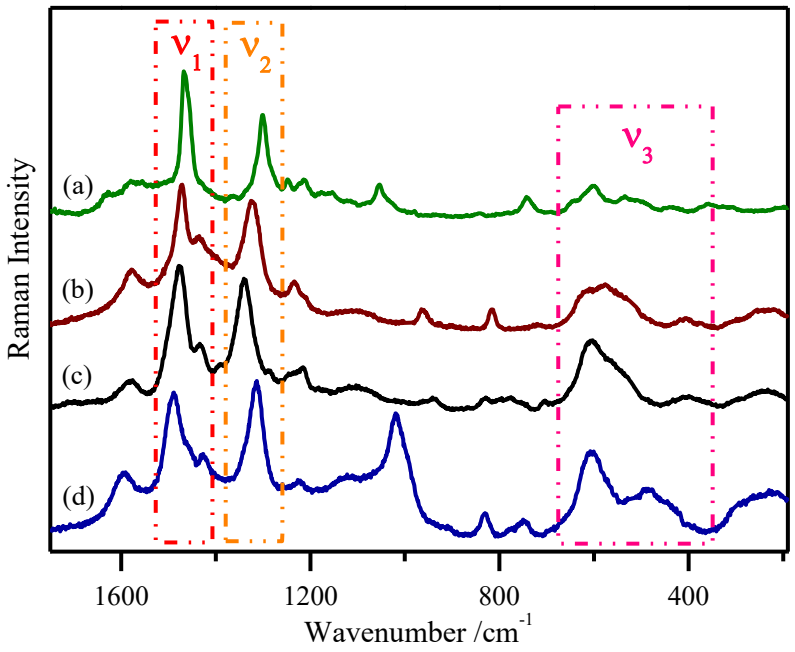

Figure 35. *Raman spectra of polyphenol-iron complexes in aqueous solution recorded at pH 7 (at pH 5 for the SA-Fe complex): PY-Fe ($2\times10^{-2}/6\times10^{-2}$ M/M) (a), GA-Fe ($2\times10^{-2}/6\times10^{-2}$ M/M) (b), TA-Fe ($2\times10^{-3}/6\times10^{-2}$ M/M) (c), and SA-Fe ($2\times10^{-2}/6\times10^{-2}$ M/M) (d). Spectra were background-subtracted and normalized to the intensity of the ν_1 band.*

Table 7. Positions of the marker polyphenol-iron complex bands (ν_1, ν_2 and ν_3) and differences between the position of the ν_1 and ν_2 bands deduced from the corresponding Raman spectra of the polyphenol-iron complexes recorded at pH 7 (at pH 5 for the SA-Fe complex). For comparison, the same characteristics are also given for the TA−Cu complex Raman spectra recorded at pH 5.

	ν_1 /cm^{-1}	ν_2 /cm^{-1}	ν_1-ν_2 /cm^{-1}	ν_3 /cm^{-1}
PY-Fe complex	1464	1299	165	600
GA-Fe complex	1470	1322	148	576
TA-Fe complex	1477	1344	133	603
SA-Fe complex	1489	1314	175	595 / 490
TA-Cu complex	1492	1319	173	270

In order to elucidate the assignment, we have measured the Raman spectra of TA−Fe complexes at different conditions: *(i)* in aqueous solution at different pHs and *(ii)* in the solid state (it will be discussed later). This analysis was performed to evaluate the influence of pH on the ink. In order to assist in the assignment of the TA−Fe and GA−Fe complexes' Raman spectra, DFT calculations of GA

and the GA−Fe complex were also carried out. The resulting theoretical spectra are compared to the experimental spectrum in **Figure 35**. As can be seen, similar spectral changes are deduced from the calculations between the GA−Fe complex (**Figure 36**b) and GA (**Figure 36**c).

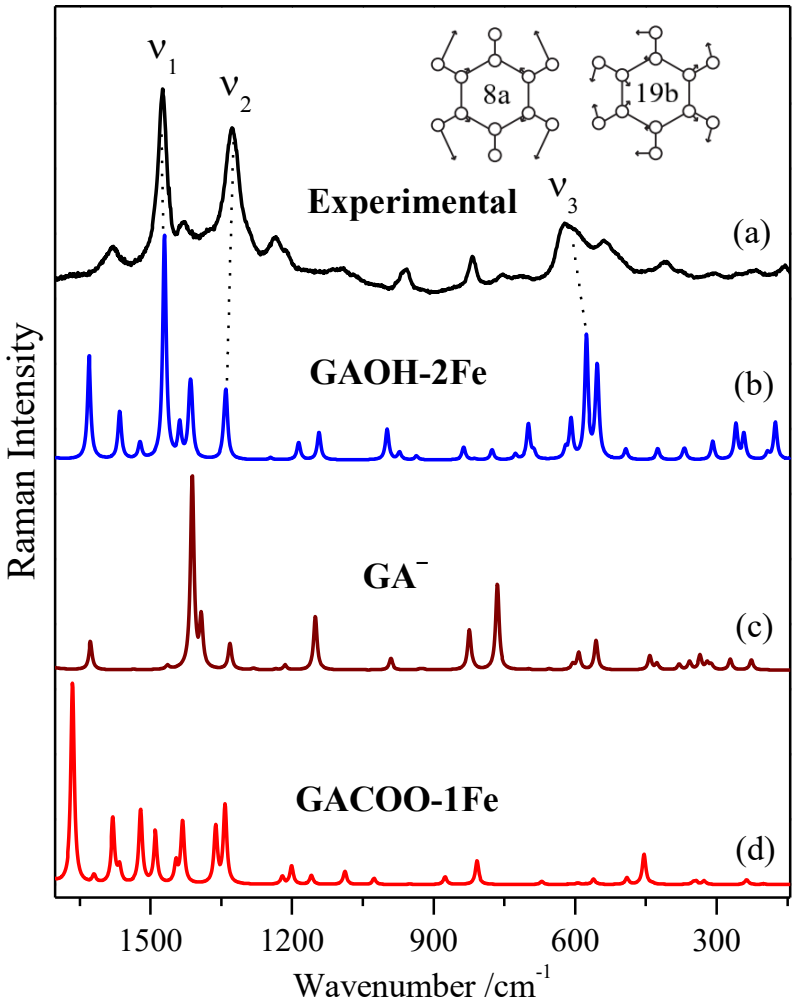

Figure 36. *Experimental Raman spectrum of GA−Fe in water (2 ×10⁻²/6 ×10⁻² M/M) at pH 7 exciting at 785 nm (a) and calculated Raman spectra of the GAOH−2Fe complex (b); GA⁻ (c) and GACOO−1Fe complex (d). The theoretical spectra were multiplied with a 1.05 correction factor. Schemes of the 8a and 19b benzene ring vibrational modes discussed in the text are included in the figure.*

The ν_1 band appears in the 1485−1465 cm^{-1} interval, depending its position on the structure of the phenol (**Figure 35** and **Table 7**). According to the performed calculations (**Figure 36**), this band can be attributed to the benzene *19b* vibration coupled to C−O stretching (ν(C−O)) and C−H bending (δ(C−H)). This agrees with the assignment reported by other authors in ortho-disubstituted benzene [123]–[125]. Therefore, this vibration has a large contribution from the stretching of carbons attached

to the oxygen atoms [124]. In general, this band is weak in the non-complexed phenol. However, the complexation gives rise to an intense enhancement because of the strong variation of polarizability that induces the coordination with iron.

In the case of PY, where three OH groups are disposed in an adjacent positions in the benzene structure (**Figure 15**a), the interaction of oxygen atoms with iron is presumably stronger leading to a ν_1 band downshifted to 1464 cm^{-1} (**Figure 34**b and c). When the benzene is substituted by more mesomeric (M+) groups, like carboxylic acids or esters, the wavenumber of the ν_1 band is shifted to higher values, reaching its maximum value at 1489 cm^{-1} in the specific case of the SA−Fe complex (**Figure 34**f and g). In this case, the interaction with iron is weaker due to the substitution of the OH by methoxy groups. Therefore, the position of this band is highly connected to the chemical structure of the polyphenol, and it could be used as sensitive marker to classify different inks fabricated from different polyphenolic plant sources.

The ν_2 band appears in the 1345−1295 cm^{-1} region and is attributed to ring stretching bands coupled to ν(C−O) and δ(C−H) [121]. This mode is also sensitive to the polyphenol structure, and an increase of the wavenumber value is observed in the direction TA > GA > SA > PY (**Figure 35** and **Table 7**). This band also exhibits sensitivity to the pH, but this is lower than that of the ν_1.

Other less intense bands of the TA−Fe complex appear at 1580, 1430, 1395, 1290, 1217 and 1100 cm^{-1} (**Figure 33**c). The relative intensity of these bands is variable among the phenolic compounds and could also help discriminate among the different molecules. Unfortunately, poor attention was devoted to all these bands in previous Raman analysis. The 1580 cm^{-1} band is attributed to the *8a* ring mode, which is strongly weakened upon the interaction with the metal. The 1430 cm^{-1} band and, presumably, the 1395 cm^{-1} one are associated to the $-COO^-$ symmetric vibrations. These normal modes are present in the TA Raman spectrum due to the existence of an ester while in GA or SA it is attributed to the carboxylate $-COO^-$. PY does not show such bands due to the absence of these groups in its structure. The weak doublet at 1299/1217 and the broad band at 1100 cm^{-1} (**Figure 34**c) can be assigned to ν(C−O) and δ(C−H) vibrations [125]. These bands can be very useful in the identification of phenolic compounds in inks due to the fact that they are related to the specific localization and substitution pattern in the ring of polyphenolic compounds.

The ν_3 band is attributed to the stretching modes of the new Fe−O bonds (ν(Fe−O)) resulting from the interaction of iron with oxygen in polyphenolic compounds [125], [126]. This band can appear in a very large range of wavenumbers from 650 to 400 cm^{-1}. In this region, several peaks can be distinguished that are related to the different interactions of the iron cation with the oxygen atoms in polyphenols. In fact, different ν(Fe−O) bands appearing at 650, 600−595, 560−550, and 400 cm^{-1} can be seen in the Raman spectra of TA and the other polyphenols. The position of the ν(Fe−O) bands can vary due to the different molecular environment of this bond. In amorphous IGI complexes, as it is the most common case, a non-completely coordinated Fe octahedral coordination sphere is expected, and thus, the octahedron is completed with water molecules in chelate (**Figure 37**a) and bichelate (**Figure 37**b) complexes [91], [124], [127]. In this case, there will be a coupling of the Fe−O stretching with the Fe−O−H bending vibrations. Conversely, in crystalline IGI complexes the iron octahedral coordination sphere is supposed to be completely filled with GA molecules (**Figure 37**c) that can interact with the metal through both the OH and carboxylate groups in a bridging structure [128]. Another element of variability is the fact that iron can be found under two different forms: Fe^{2+} and Fe^{3+}. This is due to the incomplete oxidation of the ferrous form of vitriol, stopped in part by the reducing character of the paper, since the position of the Fe−O stretching band is predicted to vary depending on the state of oxidation of iron [91]. Since ferrogallic ink recipes often imply a large excess of the ferrous sulfate, the reaction products of Fe^{2+} with cellulose may even be a major constituent of the ferric iron in manuscripts [66].

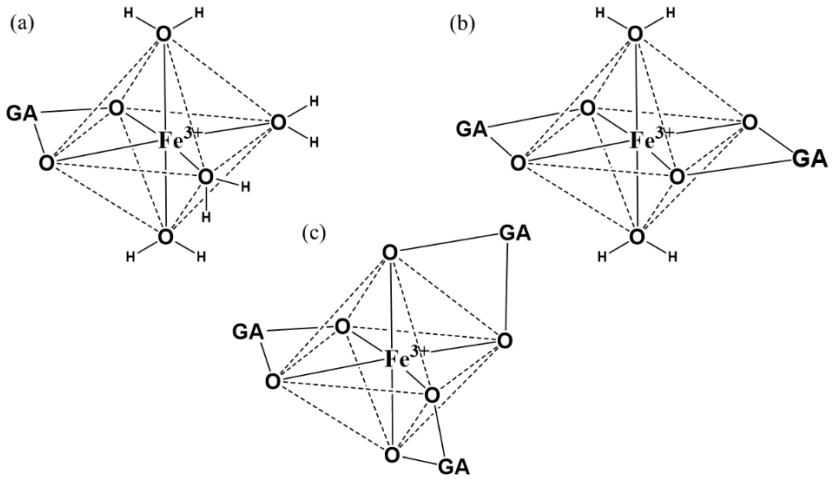

Figure 37. *Schemes of the different possibilities in the GA−Fe coordination complex at the level of the iron octahedral coordination sphere: (a) chelate, (b) bichelate, and (c) completely bridged complex.*

Because of this high variability, the exact structure of iron complexes in inks is still unknown. Ponce *et al.* reported a structure where three iron atoms interact with a single molecule of gallate at a 3:1 concentration ratio of Fe and GA [30]. According to this, two different types of Fe−O bonds could be associated with the complex: those linked to the −OH groups and those associated to the carboxylate. In addition, the complexes with −OH groups can be of different configurations: monodentate, bidentate, chelate or even bichelate. This means that a large amount of different Fe-O structures is possible in IGIs as has been reported by several authors [129]–[131]. **Figure 36** shows the theoretical Raman spectra resulting from the calculation of two different GA−Fe complexes: one having two Fe^{3+} ions interacting with the −OH groups (GAOH−2Fe complex; **Figure 22**a and **Figure 36**b) and another where one Fe^{3+} interacts with both O atoms in the carboxylate group in GA (GACOO-1Fe complex; **Figure 22**b and **Figure 36**d). As can be seen, the first one matches better the experimental GA−Fe spectrum (**Figure 36**a), and it is also very close to the experimental TA−Fe.

The normal mode calculation also predicts several vibrational modes corresponding to the symmetric and asymmetric Fe−O stretching in the GAOH−2Fe appearing between 550 and 650 cm^{-1} (**Figure 36**b). The lower component of the experimental TA−Fe and GA−Fe complexes (at 560 cm^{-1}) can be attributed to bichelate ring vibrational modes as in the case of catecholate−iron complexes (**Figure 37**b) [128], [90]. Conversely, the higher component (595−600 cm^{-1}) is assigned to Fe−O vibrations associated to chelate interactions where terminal −OH groups interact with the metal and the coordination sphere is completed with water molecules (**Figure 37**a) [132]. In the latter complexes, the ν(Fe−O) vibration is coupled to deformations of either Fe−O−H bonds and the benzene deformation rings at these lower wavenumbers [106]. Moreover, the 490 cm^{-1} band observed in the SA−Fe complex can be ascribed to the Fe−COO^- symmetric stretching band, which corresponds to the theoretical band at 452 cm^{-1} in the case of the GACOO−1Fe complex (**Figure 36**d). The last band is not seen in the GA−Fe complexes, so a preferential interaction of iron with the −OH groups is deduced for the amorphous complexes. Finally, the extreme bands at 650 and 400 cm^{-1} can be attributed to Fe−O stretching in bridging structures (**Figure 37**c) [90], which are more evident in more crystalline IGIs.

Therefore, the bands related to Fe−O bonds are very sensitive to the ink preparation protocol and, presumably, on the aging process after its fabrication. Thus, they could also serve to discriminate among different types of IGIs.

The difference between the position of the ν_1 and ν_2 bands is associated to the structure of polyphenols since these bands are related to the degree of electronic delocalization (ED) inside the aromatic system. In general, the smaller this difference, the higher the ED. At pH 7, this difference is 133, 148, and 165 cm^{-1} for the TA−Fe, GA−Fe, and PY−Fe complexes, respectively (**Figure 35** and **Table 7**). The delocalization is higher in TA due to the polymerization of several GA units. For SA, this difference rises to 175 cm^{-1}, which is also attributed to the lower ED of this molecule due to the presence of methoxy groups. These functional groups exert a positive mesomeric effect on the aromatic ring due to the withdrawal of electrons from the aromatic system.

The ν_1 band is also related to the electronic state of phenolic rings as it depends on the bond order inside the benzene ring of the phenol. Moreover, the intensity ratio between the two main bands (ν_1/ν_2) can be related to the structure of the ligand in the complex as this ratio depends on the ionization state (related to the −OH groups) of the molecule, and thus, it depends on the pH of the medium as it will be shown in the section 4.2.iv). In degradation processes resulting from the manuscript aging, this ratio was demonstrated to be very useful to deduce the time effect (results will be discussed later).

Copper complexes

The interaction of the ion Cu^{2+} with all the polyphenols was also investigated. **Figure 38** shows, as an example, the spectrum of the GA−Cu complex at pH 5 together with the corresponding GA−Fe spectrum.

In general, the resulting Raman spectra of the copper complexes are much weaker than the iron ones, as indicated by the stronger sulfate band. This is attributed to a lower Raman resonance effect of these complexes. UV−vis absorption spectra reveal the existence of LMCT band at ca. 500 nm (**Figure 38**a and b). The general increase of the absorbance in the visible region induces a darkening of the solution. However, the suspension adopted a reddish colour due to the blue shift of the absorbance maximum. The interaction with Cu^{2+} ions induces similar spectral changes on GA as observed for the GA-iron interaction.

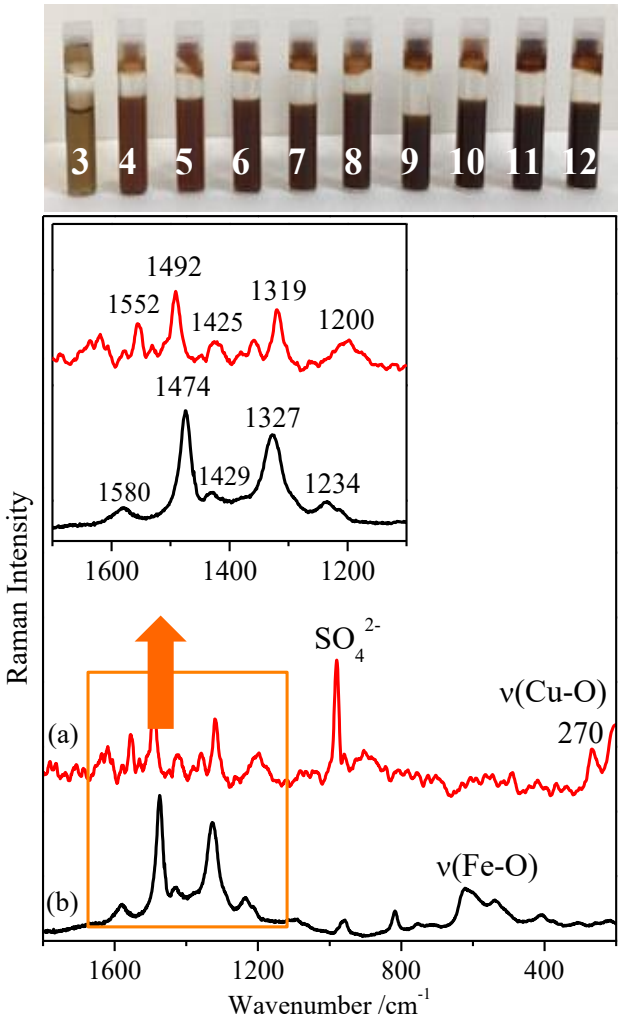

Figure 38. *Raman spectra of the TA−Cu complex (a) as compared to the TA−Fe complex (b) at concentration $2\times10^{-3}/6\times10^{-2}$ M/M. The inset plot displays in more detail the region corresponding to the vibrational modes ν_1 and ν_2. The upper picture shows the colors of the TA−Cu complexes obtained at pH ranging from 3 (left) to 12 (right).*

The most intense bands are observed at 1492 and 1319 cm^{-1}, corresponding to the ν_1 and ν_2 modes. The difference between these bands is 173 cm^{-1}, which is very similar to the difference observed for iron when interacting with SA (**Figure 34**). This fact indicates that the interaction with copper ions is weaker than that of iron, since the degree of electronic delocalization inside the aromatic system is also low. The ν_3 band corresponding to the Cu−O interaction may correspond to the band observed at 270 cm^{-1} since this is the most intense band also observed in CuO oxide [11].

FTIR spectra

The FTIR spectra of the GA and TA complexes with iron together with the FTIR spectra of non-complexes GA and TA are shown in **Figure 39**. The FTIR spectra of these molecules are dominated by strong broad bands at 1200−1000 cm^{-1} attributed to ν(C−O), ν(C−C), and in-plane δ(C−H) and δ(C−OH) motions [133][99]. In addition, intense absorption bands at 1309 and 1308 cm^{-1}, respectively (**Figure 39**a and c), which are related to the coupled vibrations of the ring ν(C−C) and the carbonyl ν(C=O), form together with the contribution from δ(C−H) and δ(C−OH) vibrations [76]. The band assigned to ν(C=O) vibrations are observed at 1693 and 1699 cm^{-1}, respectively.

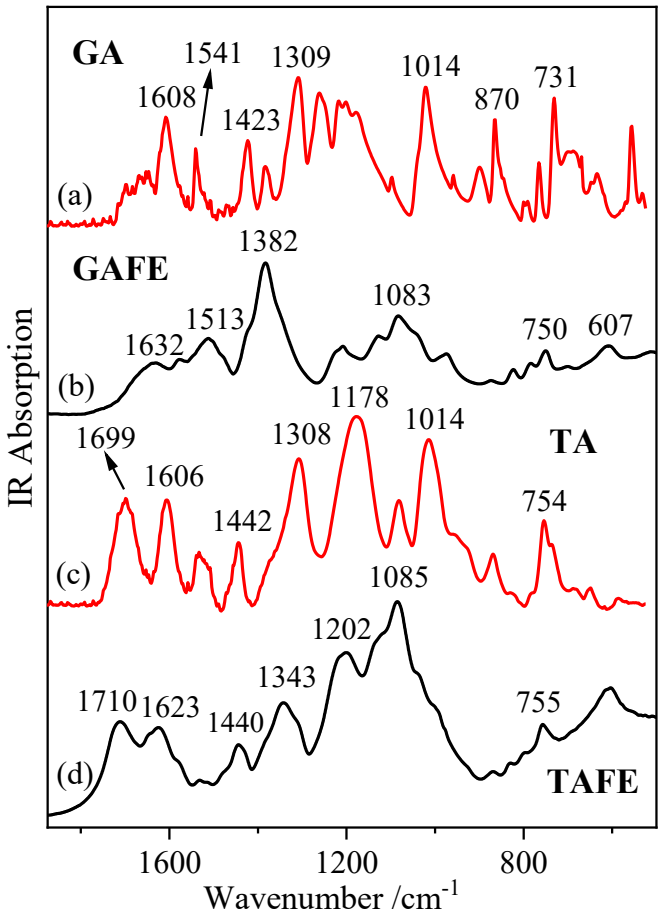

Figure 39. *FTIR spectra of: (a) GA (in ATR); (b) GA-Fe complex (in KBr); (c) TA (in ATR); and (d) TA-Fe complex (in KBr).*

While in the Raman spectra the ring stretching vibrations in polyphenols are very prominent and highly characteristic of the aromatic rings (these vibrations appear in the range of 1650−1200 cm^{-1}; **Figure 39**), in FTIR spectra, these vibrations are less intense than those involving oxygen functional groups. The GA spectrum shows the *δa*

benzene ring band at 1608 cm^{-1}, while that of TA shows that this band downshifted to 1606 cm^{-1} (**Figure 39**c). The complexation with iron induces strong changes in the 1300−1000 cm^{-1} region. In the GA spectrum, the strong bands at 1309 and 1014 cm^{-1} decrease, and a strong feature at 1083 cm^{-1} appears instead (**Figure 39**b). Since these bands have a large contribution from the ν(C−O), δ(C−OH), and ν(C−C) vibrations, an interaction of iron with the −OH groups of the phenolic group is deduced. The strong band appearing at 1382 cm^{-1} in the GA−Fe complex is attributed to the carboxylate group interacting with the metal in the complex.

Additionally, the interaction with OH groups induces intense changes in the out-of-plane bending vibrations of the O−H group (γ(OH)): the band at 870 cm^{-1} is weakened, and the 731 cm^{-1} band is shifted to 750 cm^{-1}. The new band observed at 607 cm^{-1} can be assigned to the ν(Fe−O) band of the GA−Fe and TA−Fe complexes. Similar results were observed in the FTIR spectrum of the TA−Fe complex (**Figure 39**d). The intense bands seen at 1308, 1178, and 1014 cm^{-1} in TA spectrum (**Figure 39**c) decrease in the case of the TA−Fe complex, and a strong band at 1085 cm^{-1} appears. Furthermore, the ν(Fe−O) band appears at 607 cm^{-1}. The bands at 1710, 1440, 1343, and 1202 cm^{-1} in the complex are associated with the ester group in TA [49], [129]. All these bands undergo a large shift upon complexation that suggests the interaction of iron with the ester groups.

iv) pH effect on the Raman spectra of polyphenol-iron complexes

The structure of the polyphenol is not a unique factor that can affect the position of bands in the Raman spectrum in IGIs. We have observed that some phenol bands can undergo a shift in these inks due to a possible structural degradation caused by light, pH, humidity, and other unknown effects that evolve with time. Therefore, firstly, we have focused on the effect of pH on the Raman spectra both in solution and in the solid ink deposited on paper. In the TA−Fe complex, a shift from 1478 to 1472 cm^{-1} is noted upon increasing the pH of the original TA solution from 3 to 12 (**Figure 40**c). In contrast, this band shifts from 1469 to 1482 cm^{-1} in the GA−Fe complex on paper. A similar trend is observed in solution (**Figure 40**b). The same can be observed for the PY−Fe complex, where this band shifts from 1452 to 1467 cm^{-1} in going from acidic to alkaline pH (**Figure 40**a). In contrast, a negligible sensitivity to the pH variation is observed in the case of the SA−Fe complex (**Figure 40**d).

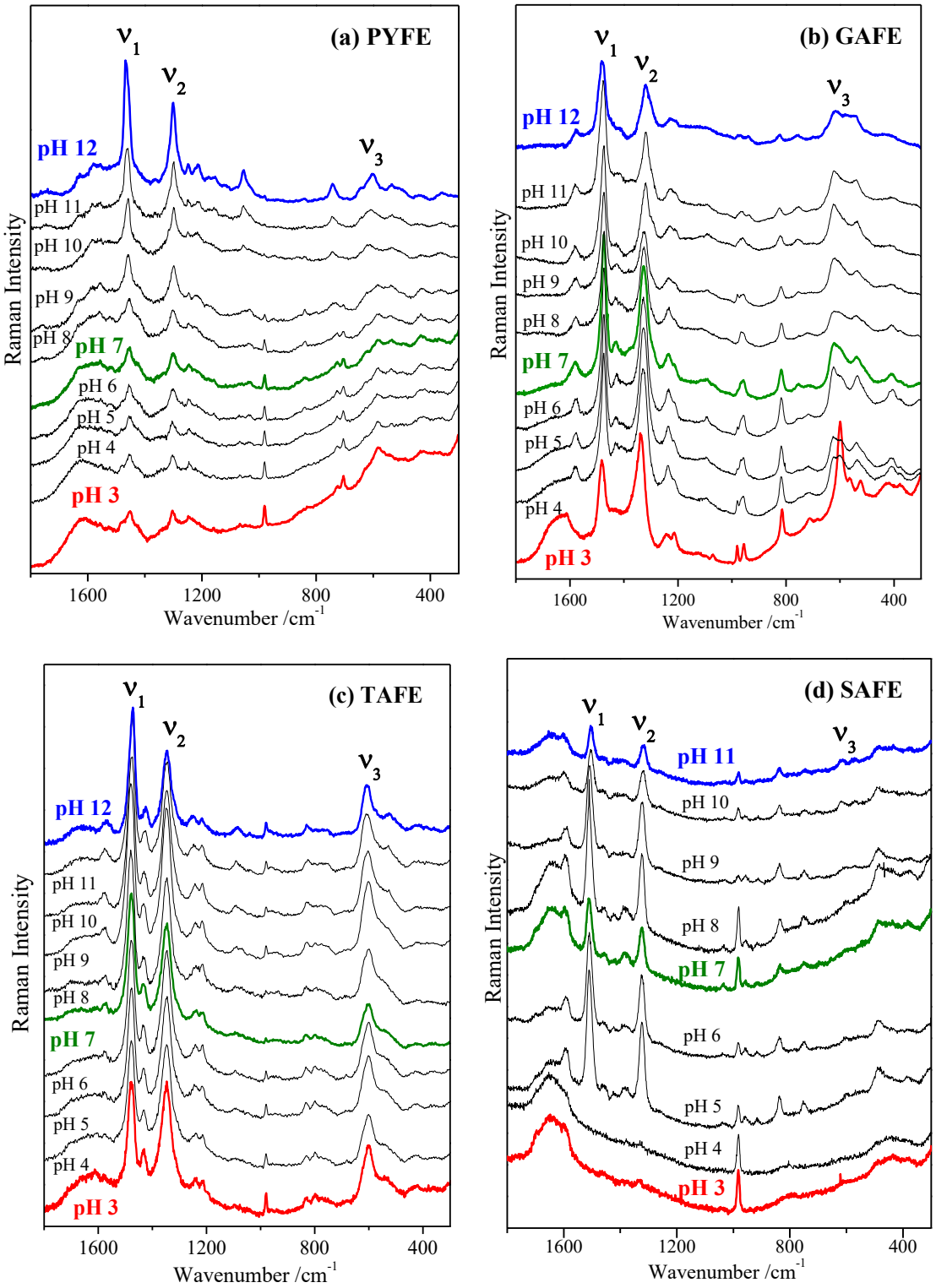

Figure 40. *Raman spectra of (a) PY-Fe complexes (PY:Fe = 1:2; [PY] = 6.6x10^{-5} M); (b) GA-Fe complexes (GA:Fe = 1:3; [GA] = 6.6x10^{-5} M); (c) TA-Fe complexes (TA:Fe = 1:30; [TA] = 6.6x10^{-5} M); and (d) SA-Fe complexes (SA:Fe = 1:3; [SA] = 6.6x10^{-5} M), recorded in suspension at different pH. Spectra were normalized to the intensity of the ν_1 band. Excitation line: 785 nm.*

In addition, pH and redox processes are linked in IGIs. The effect of iron on polyphenols cannot be only simplified in a mere change in the colour based on a darkening of the solution. The presence of Fe^{2+} can also induce a series of redox reactions related to the Fenton reaction due to the presence of molecular oxygen in the solution where the pH plays an important role [134], [135]. The Fe^{2+} ion undergoes autoxidation by the molecular oxygen, leading to the formation of Fe^{3+} [129]. This autoxidation is strongly pH-dependent, and it is almost hampered at pH below 7 [101], but the strong interaction of Fe^{3+} with polyphenols, in particular, gallic acid, accelerates the autoxidation [40], giving rise to the strong darkening of the solution.

On the other hand, the complexation with polyphenols induces the release of protons to the medium, thus inducing a pH decrease. Therefore, despite the pKa values being in the range of 7–9 for the most phenolic hydrogen, polyphenols are easily deprotonated at or below neutral pH in the presence of iron and form very stable complexes [60]. All these processes are fast and occur immediately after the addition of ferrous sulfate to the polyphenol solution (**Figure 41**).

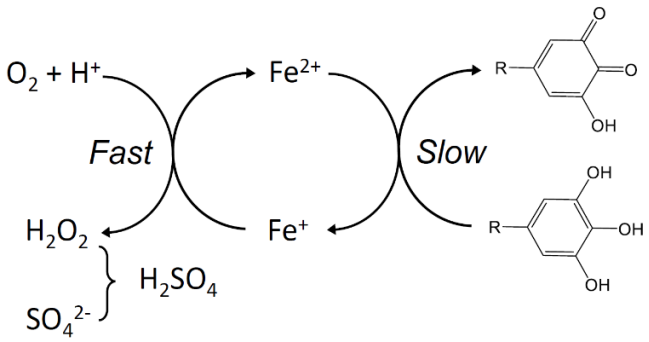

Figure 41. *Scheme of the redox reactions occurring in pyrogallol-type polyphenols.*

The oxidation of Fe^{2+} to Fe^{3+} upon binding to polyphenol ligands is facilitated by the higher stability of the interaction of Fe^{3+}, which is a harder Lewis acid than the ferrous ion, with the hard Lewis base oxygen ligands existing in polyphenols [30]. Afterward, slower redox processes can occur consisting of the oxidation of polyphenols, in particular pyrogallol-like ones [136], [137], giving rise to o-quinone structures and Fe^{2+}, and releasing H^+ ions with the time. These processes are considered responsible for the subsequent acidification of IGI inks and the degradation of paper in ancient manuscripts.

Because of all the above effects, one of the consequences of the redox processes occurring in IGIs is the pH decrease in the mixture. As can be seen in **Figure 42**a, the addition of Fe^{2+} to a TA solution prepared at pHs ranging from 3 to 12 leads to a reduction of pH of the mixture. The value of the pH is maintained at 3 until the pH of the TA solution is increased above 9. This is an effect related to the ionization of OH groups in polyphenols. The pH decrease is moderated when the ink is deposited on paper since it stays constant at 6.5 regardless of the pH of the TA solution. Only when the pH of the solution is above 9 it increases up to 7 in presence of the TA−Fe complex. This effect can be attributed to the buffering effect of the cellulose of the paper on the pH of the ink. A similar effect was observed when using other polyphenols and Cu^{2+} instead of iron. The addition of gum arabic, another important ingredient of IGI inks, to the tannic-iron complex, also induced an increased pH [13].

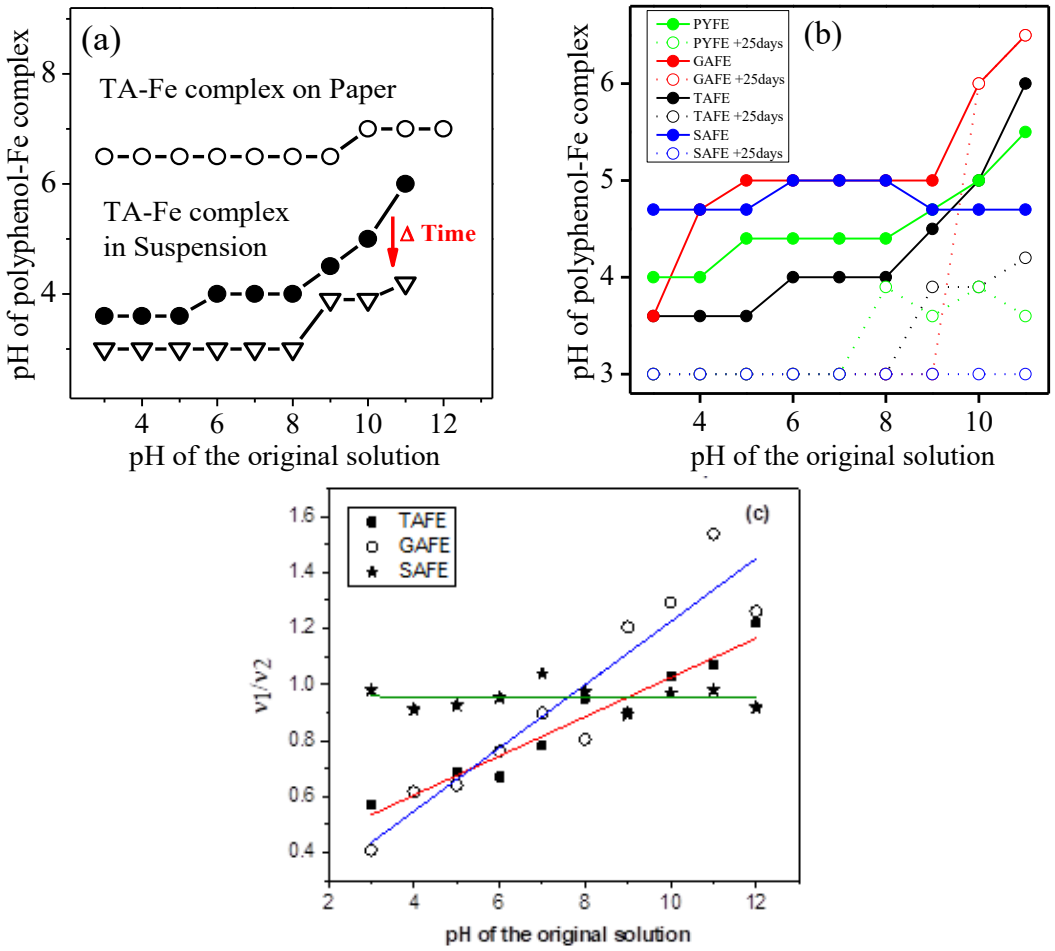

Figure 42. *(a) Variation of the pH in the TA−Fe complex at the following situations: in a just prepared aqueous suspension (black circles), the same aqueous suspension after 25 days (open triangles), and after drying on paper (open circles). (b) Variation of the pH measured for the different polyphenol/Fe complexes and effect of the time on this pH. (c) Variation of the v_1/v_2 ratio with the pH of the original solution for the TA−Fe (shaded squares), GA−Fe (open circles) and SA-Fe (stars) complexes.*

Figure 42b shows the effect of time on the pH of the different polyphenol/Fe complexes studied in this thesis. As can be seen, the time induces a further diminution of the pH value to a common value of 3,0 because of a combined effect of the oxidation of Fe(II) to Fe(III) and the progressive interaction of the latter ion with OH groups in polyphenols. The latter interaction induces a removal of H^+ ions from polyphenols.

The acidification of TA−Fe complexes seems to occur as well in the case of GA−Fe, PY−Fe, and SA−Fe complexes as deduced from the similar behaviour at different pHs. The effect of time with further acidification was also observed for the other polyphenols. This means that this is a general behaviour of these compounds.

Since the pH of the polyphenol solution is decreased after the complexation with iron, the *a posteriori effect* of pH after the formation of the complex was also analysed. **Figure 43** shows the Raman spectra of TA−Fe complexes at pHs ranging from 3 to 12. The resulting spectra show changes in the 1473/1340 cm^{-1} bands, which slightly shift to higher wavenumbers, while the (ν_1−ν_2) value decreases as the pH gets more alkaline. These changes can be attributed to the ionization of OH groups since the ν(C−O) and δ(C−OH) vibrations of these groups are involved in the ν_1 and ν_2 bands.

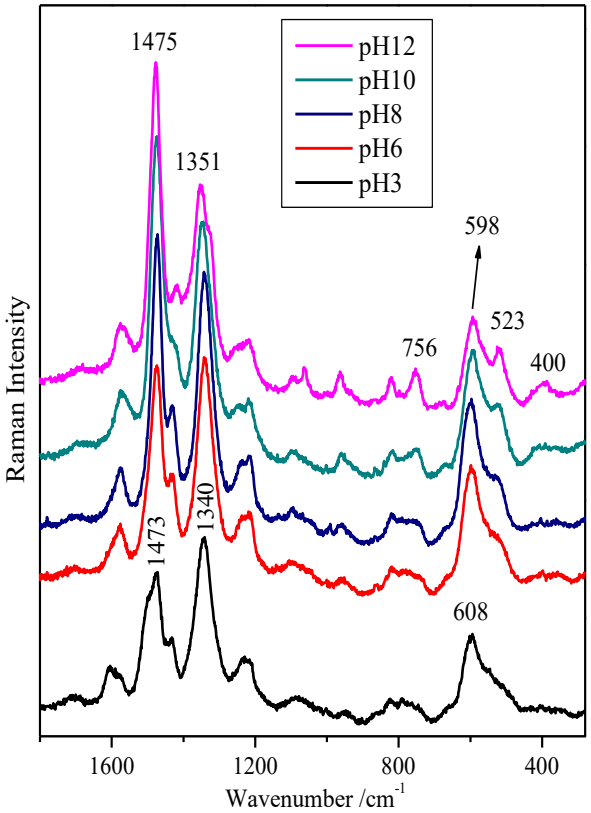

Figure 43. *Raman spectra of the TA−Fe complex measured at different pH regulated after the formation of the complex. Samples on the paper. Excitation at 785 nm.*

Figure 42c shows the variation of the v_1/v_2 ratio with the pH for the studied polyphenols where a clear increase of the v_1/v_2 ratio when increasing the pH is observed in the case of TAFE and GAFE complexes. In fact, at high pH, the ionization of phenol groups to phenolate induces a negative mesomeric effect (M-), which increases the bond order of the ring C=C bonds in the aromatic ring. This leads to an enhancement of the v_1 band intensity. On the contrary, the v_1/v_2 ratio does not undergo any variation for the SAFE complex. This is attributed to the different behaviour of the unique –OH present in SA molecule, which shows a lower acidity because of the presence of methyl groups.

The ionization of OH groups on increasing the pH highly affects the complexation pattern of polyphenols with iron. This is evident when analyzing the situation of the Fe–O bands. The main band observed at 608 cm^{-1} at pH 3 indicates that the interaction at acidic pH is taking place through terminal –OH groups in TA. Moreover, these Fe atoms might be also coordinated to water molecules forming TA–Fe–OH_2 adducts. However, the increase of other Fe–O stretching bands at 523 and 400 cm^{-1} at alkaline pH suggests the existence of other structures where the coordination sphere of iron is completely filled by phenolic groups, leading to the formation of TA–Fe–TA adducts [49], [62], [129]. The increase of the coordination number at alkaline pH values is attributed to the higher stability of the complexes of completely coordinated Fe atom after the ionization of polyphenols [130]. Moreover, a possible degradation of IGIs can be also induced at alkaline pH since similar bands are also observed in historical inks analyzed by Raman [25]. The degradation of inks could be related to the increase of redox processes occurring in the polyphenol–iron mixture that can lead to the oxidative browning of the ink with time. This colour change is produced by the slow oxidation of polyphenols to o-quinone structures. Moreover, the oligomerization of polyphenol units associated to the OH ionization and quinonization of the ring can also occur [62], [78].

Fluorescence quenching

One of the most interesting effects of the complexation of iron with polyphenols is the strong fluorescence quenching induced on the Raman emission spectra of these molecules. **Figure 44**a shows the emission spectrum of TA, which consists of both Raman and fluorescence signal, before and after complexation with iron. The spectrum of TA in aqueous solution shows a large fluorescence emission centered at 2000 cm^{-1}

(which corresponds to 724 nm since the excitation line was 633 nm in this case). This emission is enhanced at alkaline pH (red bars in **Figure 44**b). This is attributed to the absorbance increase undergone by TA in the red region at alkaline pH due to the formation of phenolate ions and the possible structural change of polyphenols at high pH.

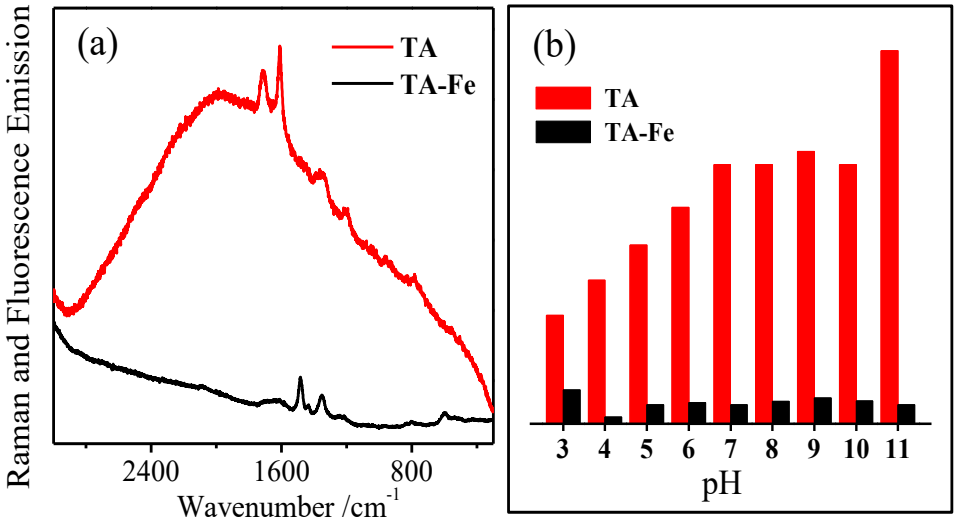

Figure 44. *(a) Emission (Raman and fluorescence) spectra of TA and the TA−Fe complex measured at pH 6 (excitation at 633 nm). (b) Variation of the fluorescence emission of the 2000 cm^{-1} band (724 nm) for TA alone and the TA−Fe complex at different pH (excitation at 633 nm).*

The complexation with iron leads to a significant quenching of the fluorescence emission band. This quenching is attributed to the LMCT from the polyphenol to the Fe^{3+} center of the complex. In addition, the fluorescence decrease is effective at all the studied pH, being higher as the pH increases (**Figure 44**b). This effect limits the analysis of IGIs by fluorescence imaging techniques and favors IGIs Raman analysis.

Similar trends were observed for all iron-complexes of the studied molecules except for SA (**Figure 45**a). Moreover, the situation is similar, but slightly different in the case of polyphenol-copper complexes. The fluorescence decrease is observed also here, however, it occurs mainly at higher pH values (**Figure 45**b).

As a general rule, and in the cases that concern us most, i.e. TAFE and GAFE complexes, the addition of iron decreases the fluorescence in solution and even more so in the solid state. PYFE has a similar effect to the previous ones as from pH 8 and SAFE shows hardly any change. In the case of the copper complex and TA (TACU), the fluorescence of this solution decreases, whereas in the case of the solid TACU,

the fluorescence increases at pH < 5. Solution of the GACU complex again decreases fluorescence, even more in solid. On the other hand, SACU shows an even higher fluorescence signal in solution and, finally, PYCU complex from pH 9 onwards decreases its fluorescence.

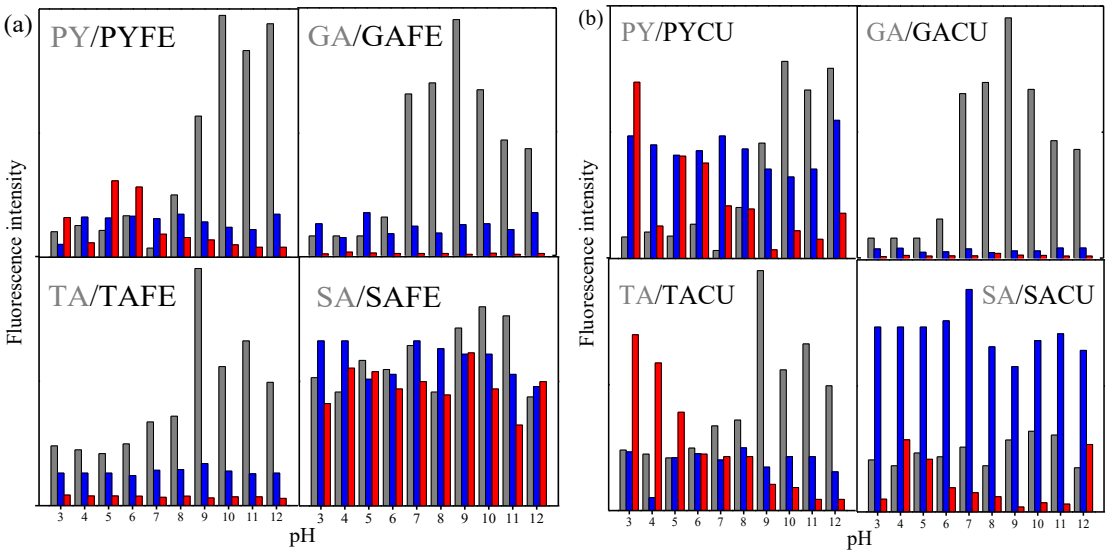

Figure 45. *Variation of the fluorescence emission of the 2000 cm^{-1} band (~ 724 nm) for polyphenol-Fe (a) and polyphenol-Cu (b) complexes (bars in blue) recorded in solution (bars in grey) and solid (bars in red) state at different pH (excitation at 633 nm).*

v) Effect of the Iron Concentration

Figure 46 shows the Raman spectra of TA−Fe complexes obtained after varying the relative concentrations of TA and $FeSO_4$ in aqueous solutions. This experiment was carried out in order to test the influence of the relative ligand-to-metal (TA:Fe) stoichiometry in the resulting complex. At relatively high TA concentrations (9×10^{-3} M in the 10:1 ratio complex, v/v) a clear effect of iron is already observed with the appearance of the ν_1 band at 1497 cm^{-1}, the ν_2 band at 1344 cm^{-1}, and the ν_3 band at 602 cm^{-1}.

At this high concentration, the number of bridged oligomers rises as demonstrated by the presence of Fe−O stretching bands at 550, 506, and 362 cm^{-1}. A progressive downshift of the ν_1 band from 1497 to 1472 cm^{-1} is observed upon increasing the iron concentration. In addition, the band at 606 cm^{-1} in the Fe−O stretching region dominates the spectrum at high metal concentration. This is observed from 1:1 to 1:10 complexes, 5×10^{-3} M/5×10^{-3} M and 10^{-3} M/9×10^{-3} M TA-Fe ratios. These changes are a consequence of the coordination restructuration of the TA−Fe complex at different

relative metal concentrations. Thus, a transition from bridged (TA−Fe−TA) to terminal (TA−Fe−water) structures takes place as the concentration of iron is increased [62], [78]. As the relative concentration of iron increases, a weakening of the *8a* mode of benzene, which is downshifted, and a strong enhancement of the *19b* mode at 1472 cm^{-1} are also observed. The iron concentration also has an important effect in the texture of the resulting sample. Inset images in **Figure 46** show the pictures of two dried complexes obtained at 1:10 and 10:1 ratios. The latter shows a rough grainy appearance, and the former displays a darker and flat look.

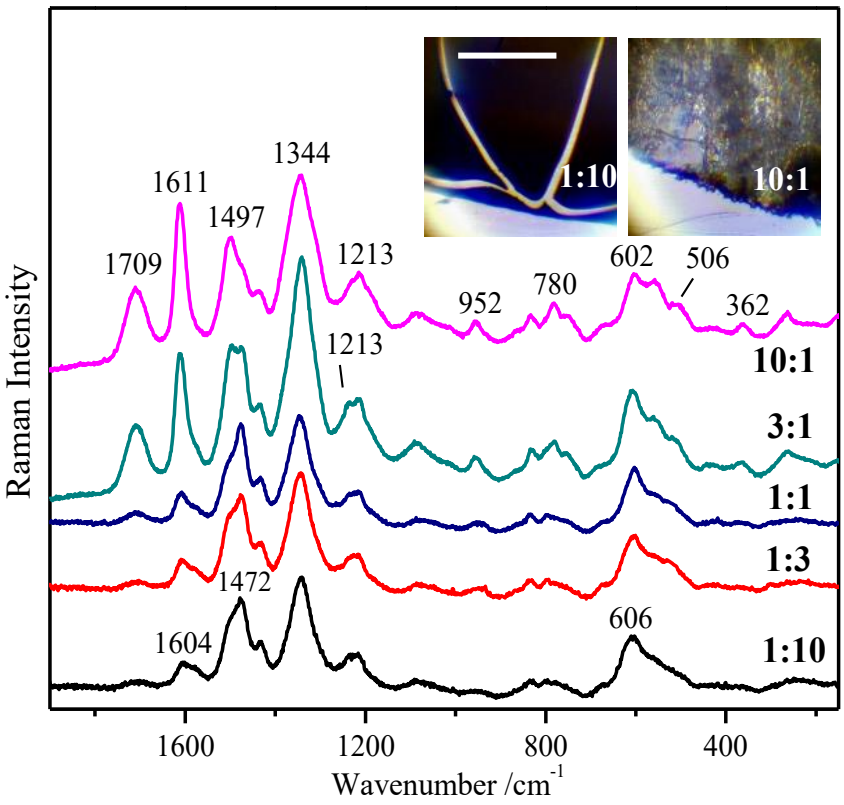

Figure 46. *Raman spectra of the TA−Fe complexes deposited on paper at different TA:Fe relative ratio as indicated on each spectrum, meaning that this ratio was used in the different added volumes of original 10^{-2} M concentrations of both TA and $FeSO_4$ in aqueous solution. Inset pictures correspond to the TA−Fe complexes prepared by using 1:10 and 10:1 ratios, respectively, and deposited on the paper.*

It can be seen that the 3:1 ratio presents an excess of tannins and the 1:1 ratio is in balance with iron. The changes observed in Raman correlate with those provides by the UV-vis absorption spectra for the same samples, indicating that the restructuration of the TAFE complexes with different stoichiometry is also projected to the color appearance.

Figure 47 shows the plot of the maximum absorbance bands registered as a function of the TA-Fe ratio as derived from the corresponding UV-vis data. The intensity of the 275 nm-absorption band decreases proportionally to the amount of iron present in the sample, except for the 1:30 ratio where a slight increase in comparison to the 1:10 ratio is observed. Since this band is a characteristic absorption feature of the polyphenol molecules, its decrease with iron concentration's increase points out on an effective interaction of the polyphenol molecule with the iron ions.

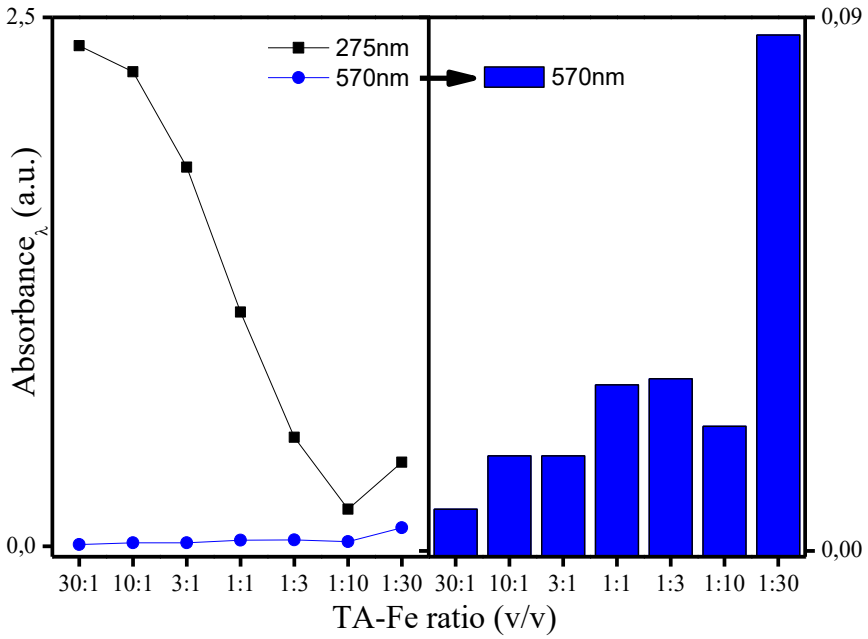

Figure 47. *Plot of the UV-vis absorption maxima (at 275 and 570 nm) measured in the TA-Fe complexes at different Fe^{2+} concentrations. The TA-concentration was maintained constant ([TA = 10^{-5} M) in order to test the effect of the ligand to metal (TA-Fe) stoichiometry in the resulting complex.*

In addition, at the visible spectral region, an increase of the absorption band at 570 nm is visible when increased concentration of the iron ions in the samples, whereas the 1:30 TA-Fe complex shows the highest intensity. The enhancement of the 570 nm maximum is due to the formation of iron coordination centers in the mixture.

vi) Effect of time

The composition of the ink can vary with ingredients, pH and time. **Figure 48** shows Raman spectra of the TA-Fe complexes in solution recorded at different times ranging from 1 hour to 8 days.

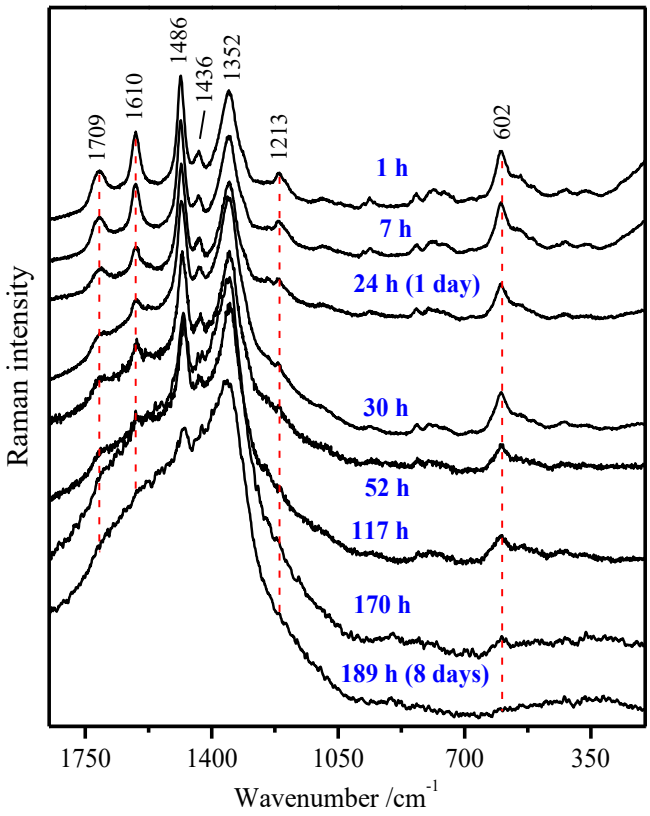

Figure 48. *Raman spectra of TA-Fe complexes in solution obtained at different times: from 1hour to 8 days after the complex preparation.*

At first look, the Raman spectra show a gradual decrease of the total intensity resolution which denotes a strong chemical changes, i.e. a degradation process takes place. In addition, the spectral profile also changed significantly with time losing resolution in comparison to the first spectrum. In particular, a series of intense bands, at 1709, 1610 and 1486 cm^{-1} which are respectively attributed to the stretching vibration of the ester C=O band, the benzene C=C stretching *8a* and *19b* modes, decrease in time until the first two bands totally disappear. The intense band related to different bending vibrations, at 1352 cm^{-1}, remains the same and the most pronounced one even after 8 days. Besides, the fluorescence background signal also increases in time. Finally, the loss of the complex structure can also be deduced from the decreased intensity/disappearing band at 602 cm^{-1} which is assigned to the ν(Fe−O) vibration of the TA−Fe complex.

vii) Effect of gum Arabic

Since gum Arabic is one of the principal ingredients of the IGIs, we have also studied its effect on the vibrational spectra of these inks in order to get some information about its influence on the overall structure of the actual colorant of IGIs, i.e. the polyphenol

complex with metals. Since this polysaccharide has a low Raman cross section we have studied the effect of the gum by FTIR spectroscopy.

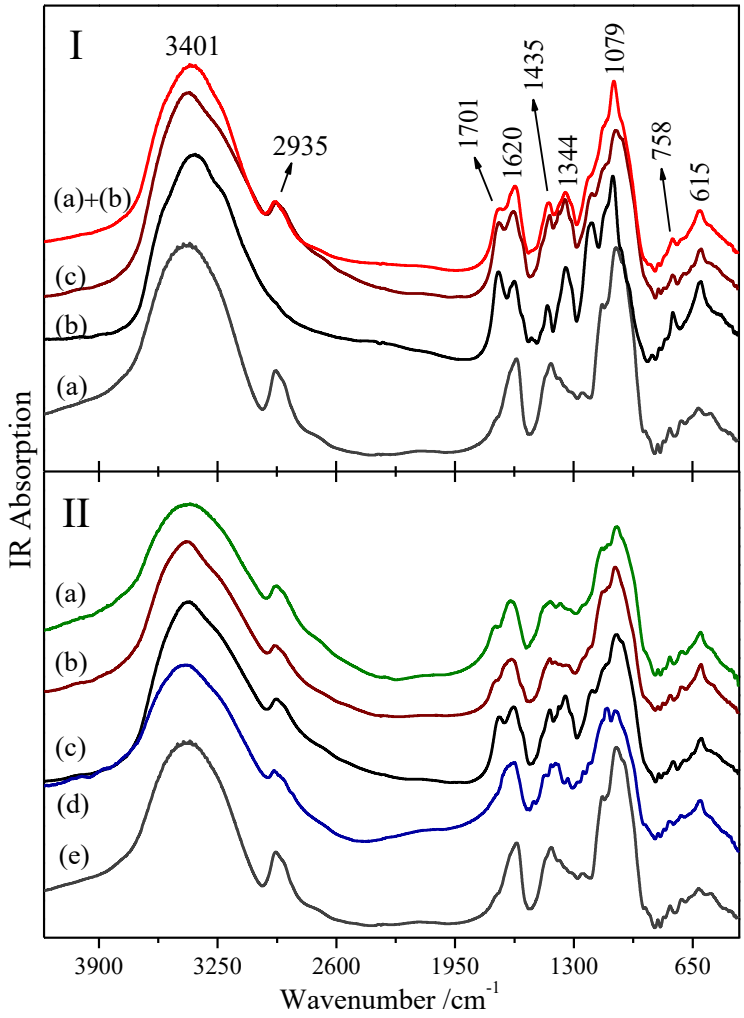

Figure 49. *IR absorption spectra of the polyphenol-Fe complexes in the presence of gum Arabic prepared as pellet samples at pH 6. (I) (a) Gum Arabic (gum), (b) TA-Fe complex, (c) TA-Fe-gum sample, (d) sum of the spectra (a) and (b). (II) (a) PY-Fe-gum sample, (b) GA-Fe-gum sample, (c) TA-Fe-gum sample, (d) SA-Fe-gum sample, and (e) Arabic gum (gum). All spectra were normalized to the –OH stretching vibration band at ~ 3400 cm^{-1}.*

Figure 49 Ib and c shows the FTIR spectra of TAFE complex in the absence and in the presence of the gum Arabic compared to the FTIR spectrum of the polysaccharide (**Figure 49**Ia). A significant participation of the gum can be deduced from the IR spectra of all studied polyphenols. Gum Arabic exhibits characteristic vibrational bands, at 3402 cm^{-1} and 2932 cm^{-1}, assigned to the stretching vibrations of the -OH and -CH_2/-CH_3 aliphatic groups, respectively. The absorption band at 1614 cm^{-1} is related to the symmetric stretching movements of the –COO^- functional

group. In addition, carboxylic acids show characteristic -OH in-plane bending band at 1423 cm^{-1} [138]. The bands observed between 1200 cm^{-1} and 800 cm^{-1} represent fingerprint zone of carbohydrates, i.e. C-O, C-C and C-O-C stretching, C-O-H and C-H bending modes of the polymer backbone [139]. Finally, the bands lying between 700 cm^{-1} and 400 cm^{-1} can be attributed to the skeletal mode vibrations of the pyranose ring. The presence of gum in the TAFE complex induce clear changes in the region corresponding to ν(C-O) motions, where it is observed a shift from 1082 to 1068 cm^{-1}. In addition, a new band is observed as a shoulder at ca. 1030 cm^{-1}. Other changes are the weakening of the 1208 cm^{-1} band of TAFE and the slight intensification of the *19b* mode at 1478 cm^{-1}. All these features point out the existence of H-bonds between gum Arabic and phenol groups in TA that could be the responsible for the stabilization of the mixture.

Figure 49II shows the FTIR spectra of all polyphenols in the presence of gum Arabic. The analysis of these spectra also reveals differences in the region corresponding to the *8a* and *19b* modes as well as the 1200-1000 cm^{-1} region corresponding to the ν(C-O) vibrations.

4.3 SERS spectra

Surface-enhanced Raman scattering (SERS), in general, can overcome the main disadvantages of Raman spectroscopy because of the fluorescence quenching of the analyte, as well as the high sensitivity provided by the giant intensification of the radiation intensity in the presence of the metal nanoparticle. As a Raman derived techniques, an additional advantage of SERS is that it affords a vibrational spectrum from the analysed molecule, which can be useful to determine its structure and possible chemical changes that occur on fading or other molecular degradation. Therefore, SERS is being developed as a promising microdestructive technique for characterizing natural organic pigments and dyes in works of art and cultural heritage materials. Moreover, Raman analysis of black inks can also be found in the literature [4], [64], [129], [140]–[142]. Nevertheless, to the best of our knowledge, up to now, there are no SERS studies of the IGIs; we have found just one paper dedicated to the application of TERS (Tip-Enhanced Raman Spectroscopy) for *in-situ* detection of indigo and IGIs on paper [143]. However, the SERS spectra reported in this paper could not correspond to the IGI ink but

to another component also present in the analysed manuscripts. In this thesis, we have also focused on the SERS analysis of IGIs. The SERS spectra of the polyphenols were previously measured in order to better attribute the SERS features of the iron complexes.

i) SERS spectra of polyphenols

The corresponding SERS spectra of the analyzed polyphenols (**Figure 50** and **Figure 51)** show significant changes in comparison with the Raman spectra of the polyphenols both in solid state (**Figure 31**) and in aqueous or ethanol solution (**Figure 33** and **Figure 34**). The Raman spectra of polyphenols in aqueous solution (in the case of SA in ethanol) are also shown in **Figure 50** and **Figure 51** for comparison with the corresponding SERS spectra. In solution, these polyphenols only show slight spectral differences in relation to the solid state attributable to the different molecular states with respect to the formation of intramolecular and intermolecular hydrogen bonds in the solid-state and the interaction with the solvent.

The SERS spectra were obtained by using AgC NPs. On the contrary, no SERS spectra could be obtained on AgH NPs except for the SA molecule (**Figure 50**d). However, the AgC colloid may show bands of the residual citrate ions used for preparing the colloid which can overlap the bands of the analyte. The higher activity of AgC NPs to render intense SERS spectra is related to the fact that the citrate residual species, still adsorbed onto the metal surface, and its oxidation products can better interact with the –OH groups of polyphenols through the establishment of H-bonds between –COOH in citrate and –OH groups in phenols [30].

In general, the SERS spectra are dominated by broad bands that may corroborate the formation of H-bonds between the adsorbed molecules and the organic molecules covering the NPs. Moreover, the big changes observed between the Raman spectra in solution and the SERS points out the occurrence of strong polyphenol structural modifications as a consequence of their interaction with the metal surface. Another reason that may contribute to the broadening of bands is the deep structural changes that these polyphenol molecules may undergo because a possible polymerization leading to more complex structures as we have also reported in previous works [30], [63], [121], [142]–[149].

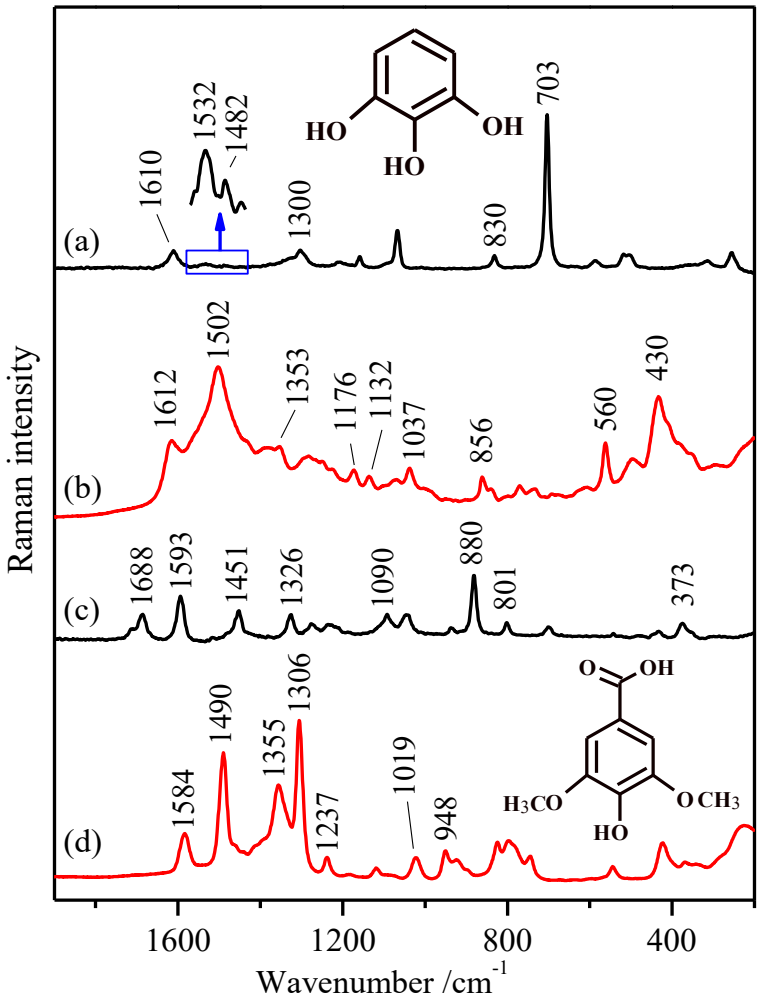

Figure 50. *(a) Raman spectrum of PY in aqueous solution (20 mg/mL); (b) SERS spectrum of PY (at concentration 10^{-5} M) in AgC NPs; (c) Raman spectrum of SA in ethanol solution (20 mg/mL) after subtracting the ethanol spectrum; and (d) SERS spectrum of SA (at concentration 10^{-5} M) in AgH NPs. Excitation line: 785 nm.*

At first look, the adsorption of the acidic polyphenols (GA and SA) on Ag nanoparticles induces the ionization of carboxylate groups that can be deduced from the weakening of bands at 1688 and 1687 cm^{-1}, for SA and GA, respectively, of the solution (**Figure 50**c and **Figure 51**a). In addition, a remarkable weakening of the *8a* mode is observed in all the cases. Another important feature in the SERS of all polyphenols is the intensification of a band in the 1505-1475 cm^{-1} region, attributed to the *19a* mode of the benzene ring [112], [113], [140], that seems to be enhanced regarding the same weak band in aqueous solution upon the interaction of these polyphenols with the metals surface (see expanded spectrum over the **Figure 50**a one in the 1450-1550 cm^{-1} region). This mode is more intense in the FTIR spectra,

due to the fact that the corresponding vibration implies a strong variation of the molecular dipolar moment, while the variation of polarizability is rather weak [7], [15], [151].

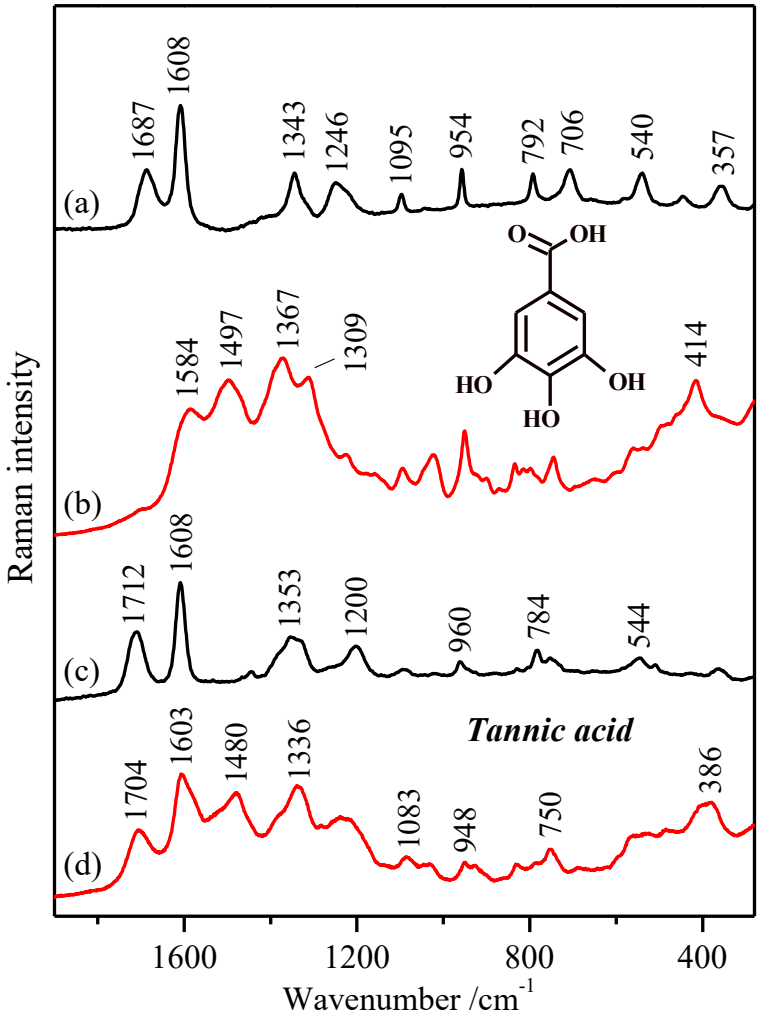

Figure 51. *(a) Raman spectrum of GA in aqueous solution (20 mg/mL); (b) SERS spectrum of GA (at concentration 10^{-5} M) in AgC NPs; (c) Raman spectrum of TA in aqueous solution (20 mg/mL); and (d) SERS spectrum of TA (at concentration 10^{-5} M) in AgC NPs. Excitation line: 785 nm.*

Therefore, the interaction with the metal in the surface seems to induce a structural change of the molecule in such a way that leads to an increase of the variation of polarizability associated with the *19a* mode. Furthermore, another general characteristic of SERS spectra is the enhancement of a new broad band which appears with a high intensity at 435-410 cm^{-1} region in the SERS spectra of PY, SA and GA (**Figure 50**b and d, and **Figure 51**b), while in TA it appears at slight lower wavenumbers (386 cm^{-1}) (**Figure 51**d).

It is worth noting the singularity of the SA SERS spectrum (**Figure 50**d) regarding the observation of sharp and intense bands unlike the SERS spectra of the other three molecules (GA, TA and PY). This result can be related to the presence of the methoxy groups in its structure. These groups may exert an influence on the natural tendency of polyphenols to polymerize, and for this reason sharper bands could be observed. The strong band observed at 1306 cm^{-1}, attributed to the ν(C-O) motion coupled to ring stretching, seems to be an evidence of the preservation of the original structure of this molecule and the absence of any polymerization.

In contrast, the SERS spectrum of PY (**Figure 50**b) displays strong changes regarding the aqueous solution with a new strong band at 1502 cm^{-1} together with the intensity decrease of the *8a* vibration at 1612 cm^{-1}. But the most important change in this molecule is the complete disappearance of the ring breathing band seen in the aqueous solution at 703 cm^{-1} (**Figure 50**a). Besides, new strong bands in the low wavenumber region, i.e. at 560 and 430 cm^{-1}, appeared likely associated to the deep structural changes undergone by this molecule upon adsorption on the surface.

The SERS spectrum of GA also displays a great deal of changes that indicates a deep structural change of this polyphenol on Ag NPs (**Figure 51**b). There are hints that points out a direct interaction of GA carboxylate groups with silver, specifically, the strong weakening of the 1687 cm^{-1} band in aqueous solution (**Figure 51**a), attributed to the carboxylic acid, and the enhancement of the band at 1367 cm^{-1} in the SERS (**Figure 51**b) attributed to the carboxylate group in the gallate ion.

In contrast to the other analyzed polyphenols, the SERS of TA (**Figure 51**d) is the one that displays a lower difference in comparison to the corresponding Raman spectrum (**Figure 51**c). The main difference is the new band at 1480 cm^{-1}, associated with the *19b* ring mode due to the interaction of phenol groups with metals, that is general for all the other polyphenols. The higher correspondence with the Raman in solution indicates that TA may undergo a lower structural transformation on the silver surface due to its higher size and the fact that it is an already polymerized polyphenol. Likewise, a high correspondence can be observed between the SERS of GA and TA (**Figure 51**b and d), being the main difference the existence of a medium band at 1704 cm^{-1} attributed to the ester ν(C-O) vibration, that seems to be absent in the SERS of GA. This similarity corroborates that GA undergoes a polymerization on the surface although it does not involve the formation of ester groups.

Concluding, the SERS spectra of the analyzed polyphenols show significant changes in comparison with the Raman spectra. This result indicates the occurrence of strong polyphenol structural modifications as a consequence of their interaction with the metal surface. Another effect observed in the SERS spectra is the broadening of bands derived from a possible polymerization of this molecules to more complex structures. The most important modifications observed in the SERS spectra of these compounds is the remarkable weakening of the *8a* ring vibration and the subsequent intensification of the *19a* and *19b* mode of the benzene ring. This latter mode is also more intense in the FTIR spectra, and its intensification in the SERS spectra could be related to an increase of the variation of polarizability associated with the *19a* and *19b* modes as a consequence of the structural change of the molecule induced by a strong interaction with the metal in Ag NPs.

Tannic acid is the polyphenol that displays a lower difference in comparison to the corresponding Raman spectrum, and this is attributed to a weaker interaction with the surface that implies a lower structural modification when adsorbed on the surface. In contrast, gallic acid undergoes deep structural changes on the Ag surface. The similarity of the SERS of gallic with that of the tannic acid suggests that the first may undergo a polymerization when adsorbed on the surface of silver.

ii) SERS spectra of Iron Gall Inks

In this thesis, the first SERS spectra of iron gall inks were obtained. No previous applications of plasmonic nanoparticles to analyze these kind of materials was reported up to now.

The analysis of IGI inks by SERS leads to a huge increase of the Raman scattering signal from the ink. This is an important effect that allows the analysis of tiny amounts of materials that can be detached from the manuscript. In SERS, there are two questions that must be addressed when analyzing some organic material: 1) the possibility of a structural change when the organic molecule interacts with the metal substrate employed for doing SERS; and 2) the limit of detection that the technique can provide in the analytical detection.

The first issue is a direct consequence of the SERS analysis. In fact, this technique is based on the approaching of the analyte to the interface. This converts the analytical

method in an adsorption associated method that depends on the specific solution to surface equilibrium stablished between the adsorbate and the metal surface. This process involves the solubilization of the molecule in the aqueous medium, as well as the subsequent diffusion of the analyte to the surface and the corresponding adsorption on this surface. There are many factors affecting the adsorption. Among them, the pH of the medium is obviously an important factor that may influence all these processes, both solubilization and adsorption. Therefore, this was an effect that was deeply studied in the case of the complexes of polyphenols with iron. The effect of time was also investigated in order to know if the iron complexes underwent some structural modification.

iii) SERS of different IGIs

The SERS spectra of the different IGIs prepared in this thesis, including the TAFE complex, are shown in **Figure 52**. The normal Raman spectra of the IGIs are shown in **Figure 53** for comparison. SERS spectra display similar spectral patterns in relation with the TAFE complex and IGI inks, although some differences can be observed between them. These differences are more evident in the Ag-O and Fe-O regions, which are enhanced in the SERS regarding the normal spectra, and this reflects a different interfacial behavior of the iron complexes between TA, Fe, citrate, chloride and the silver surface.

For instance, it is possible to observe a weakening of the shoulder at 620 cm^{-1} of the TAFE spectrum in the aqueous solution (**Figure 52**a) and the intensification of bands at 567, 530 and 425 cm^{-1} (**Figure 52**b-f). These changes are associated to a structural rearrangement of the iron sphere coordination when adsorbed on the silver surface. In fact, we observed the enhanced of bands related to bridged TA-Fe complexes, where the coordination sphere of the iron is interacting with different ligands. The predominant band in solution and on AgNPs is observed at 597 cm^{-1}, which is assigned to terminal complexes where the iron ion sphere is not completed and the unoccupied places are filled with water molecules [78], [80], [113]. In general, the intensification of the ν_3 band at 597 cm^{-1} in SERS is connected with different effects: a) approaching of the Fe-O bonds to the surface according to the SERS selection rules; b) a resonance effect mediated by the charge-transfer from the complex to the silver surface involving the specific part of the iron environment.

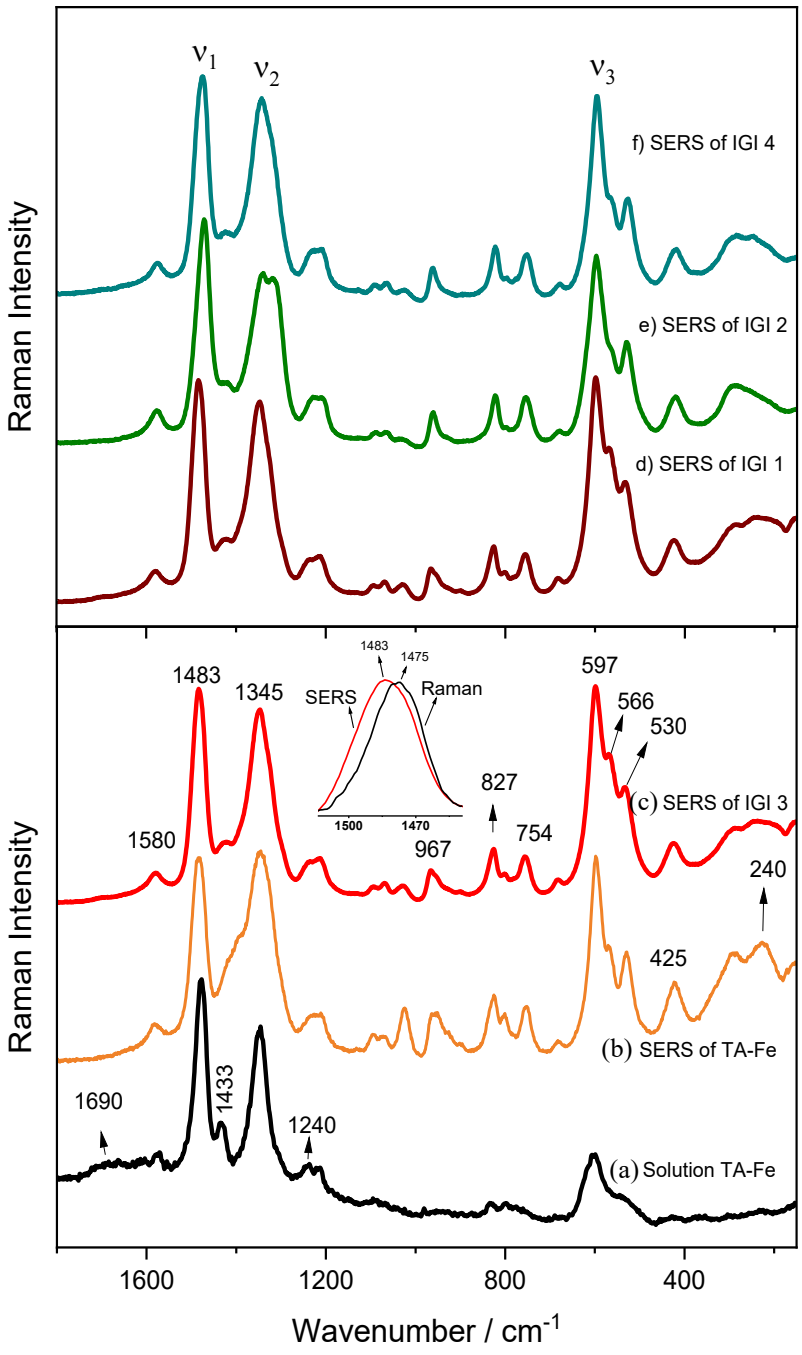

Figure 52. *Normal Raman spectrum of the TAFE complex in aqueous solution at concentration TA/Fe $10^{-2}/2x10^{-2}$ M/M (a). SERS spectra of TAFE complex ($10^{-5}/2x10^{-5}$ M/M) (b) and the inks IGI3, IGI1, IGI2 and IGI4 (c-f). Inset plot: comparison of the ν_3 band in the SERS and normal Raman of the TA-Fe complex.*

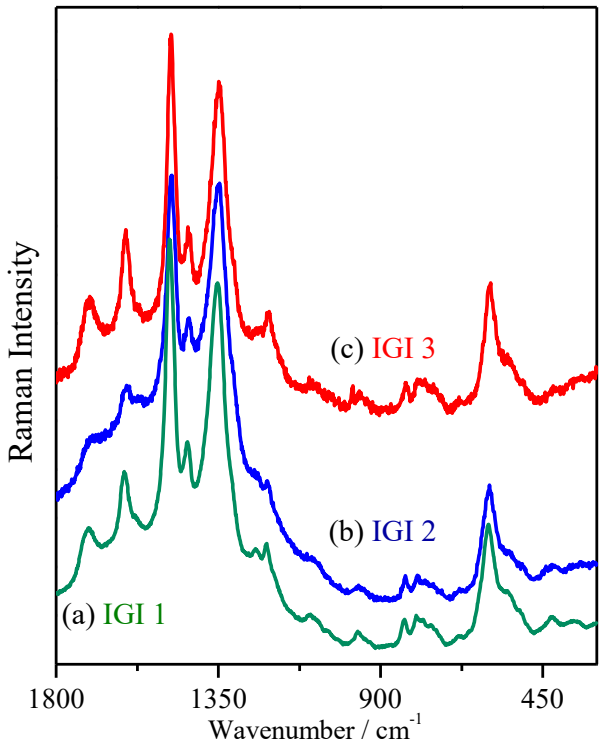

Figure 53. *Normal Raman spectra of the inks: (a) IGI1, (b) IGI2, and (c) IGI3.*

Another noteworthy change is the appearance of new bands falling in the Ag-O region corresponding to the adsorption of oxygenated species on the silver surface. These species can be citrate, the oxidation products of citrate [80], [152], and the different species integrating the TA sample [49]. The new bands appearing in the latter region are seen at 290 and 225 cm^{-1} [129].

In addition, it was also observed an enhancement of certain bands in the 1000-700 cm^{-1} region at 744, 827, 967 cm^{-1}. The latter bands may be assigned to ring vibration (ring breathing and trigonal vibrations) which undergo an intensification due to the resonant Raman effect induced by the presence of the silver surface. This resonance is related to the adsorption of the iron complex on the metal nanoparticle and is associated to charge-transfer processes existing between the complex at the level of the iron coordination center and Ag. The resonant effect is supported by the appearance of new bands at 1938 and 2076 cm^{-1} that are due to the sum of ($\nu_1+\nu_3$) and ($\nu_2+\nu_3$) modes (**Figure 55**), respectively. These combined modes are intensified under resonance conditions [124], [153].

These structural changes also affect the aromatic rings. In fact, the ν_1 band at 1477 cm^{-1} in the Raman spectrum of the solution undergoes a shift to 1483 cm^{-1}

in the SERS. This is indeed associated to structural rearrangements of the complex in the presence of the metal surface and the specific complexation established on the metal surface. The shift towards higher wavenumbers involve a weakening of the polyphenol interactions with iron, as deduced from previous experiments with different polyphenol/iron complexes. The weakening of the complex bonds on the presence of the Ag NPs is attributed to the adsorption of the TA complexes on the silver surface through the iron Fe^{3+} ion. This is related with the formation of a new iron-tannin complex on the surface mediated by the citrate ions adsorbed on the surface. The formation of these kind of complexes accounts for the formation of bridged complexes and the shift upwards of the ν_1 mode.

Finally, the weak bands observed in the normal Raman at 1240, 1433 and 1690 cm^{-1}, attributed to C-O and C=O stretching vibrations of the TA ester groups, undergo a clear weakening upon the presence of Ag NPs. This effect is a consequence of the further position of these groups regarding the silver surface and the short-range effect of the SERS effect [154], [72], [115].

Another effects that should be considered when TA-Fe complexes are adsorbed on the surface are the chemical processes that the TA ligands may undergo in the presence of the Ag surface. These effects are produced by the hypothetical catalytic effect that the silver surface can exert on polyphenolic molecules [12]. Among the possible chemical changes on the surface we can mention the hydrolysis, oxidation and iron complex rearrangement [135], [128], [155].

At first look it seems that only slight variations between each ink are seen. However, the main changes are observed in the Fe-O and the Ag-O regions. As mentioned above, the more striking effect of the adsorption of the ink complex on Ag NPs is the intensification of bands in the Fe-O, with the appearance of new bands and shoulders associated with the establishment of new iron bonds with the oxygenated species present on the interface. As can be seen, only small differences can be observed between the Raman of inks prepared with different recipes. The intensity of the bands at 1600 and 1700 cm^{-1}, related to free ligands in TA, is lower in the IGI2. This is attributed to the high iron/TA ratio that leads to a higher complexation degree.

Additionally, between the different IGI samples, we have noted slight differences that mainly affect the Fe-O and Ag-O regions. In some cases, it is evident the existence

of stronger bands at 530 and 425 cm^{-1}, and the corresponding Ag-O bands observed below 300 cm^{-1} (samples IGI2, IG4 and TA-Fe). We hypothesize that the 530/425 cm^{-1} pair of bands is related to stretching vibrations derived from carboxylate moieties interacting with iron (–COO-Fe bonds). Carboxylate groups are present on the surface because of the citrate ions, but they are also present in the tannic acid commercial compound, since it was previously reported to be an actual mixture of several galloyl subproducts including gallic acid [129]. DFT calculations also supported this assignment. In fact, the normal mode calculations made in this thesis supports that there is a mode at 576 cm^{-1}, which can be assigned to COO-Fe bonds in the GA-Fe complex where this carboxylate-iron interaction was studied [115].

Likewise, when the above two bands are more intense, there are two band at 290 and 228 cm^{-1} that also undergo a clear enhancement. These bands are attributed to the citrate adsorbed on the surface and corresponds to Ag^{+}-COO^{-} bonds. In order to demonstrate this assignment, we have registered the spectra of citrate in the AgC nanoparticles at different pH (**Figure 54**). At pH 5 the Ag-O region shows the existence of two bands at 285 and 222 cm^{-1} that correspond to the interaction of citrate with silver. When lowering the pH to 3, a unique band is observed at 225 cm^{-1} that is assigned to the Ag-O in the carboxylate groups.

In the case of the IGI prepared with a higher relative concentration of gum Arabic (**Figure 52**c and d), i.e. the IGI3 and IGI1, all the carboxylate related bands are weakened in the presence of gum Arabic. Conversely, the IGI2 and IGI4 inks for which a lower gum concentration was used (**Figure 52**e and f), the 530/425 cm^{-1} and the band at 290 cm^{-1} bands are enhanced. The intensification of the carboxylate bands in IGI2 and IGI4 is associated with a stronger interaction of the TA-Fe complex with the silver surface. The effect of gum on the Fe-O and Ag-O regions demonstrate the protective effect attributed to the gum Arabic on the stability of the complex, as also reported previously by M.G. Zamorano [15]. Other differences between the IGI1 and IGI2 inks are the existence of a doublet in the ν_2 mode region (1345/1322 cm^{-1}) and the intensification of the weak band at 1230 cm^{-1}, pointing out the influence of the –OH groups in the establishment of H-bond with the –OH phenol groups in the polyphenols.

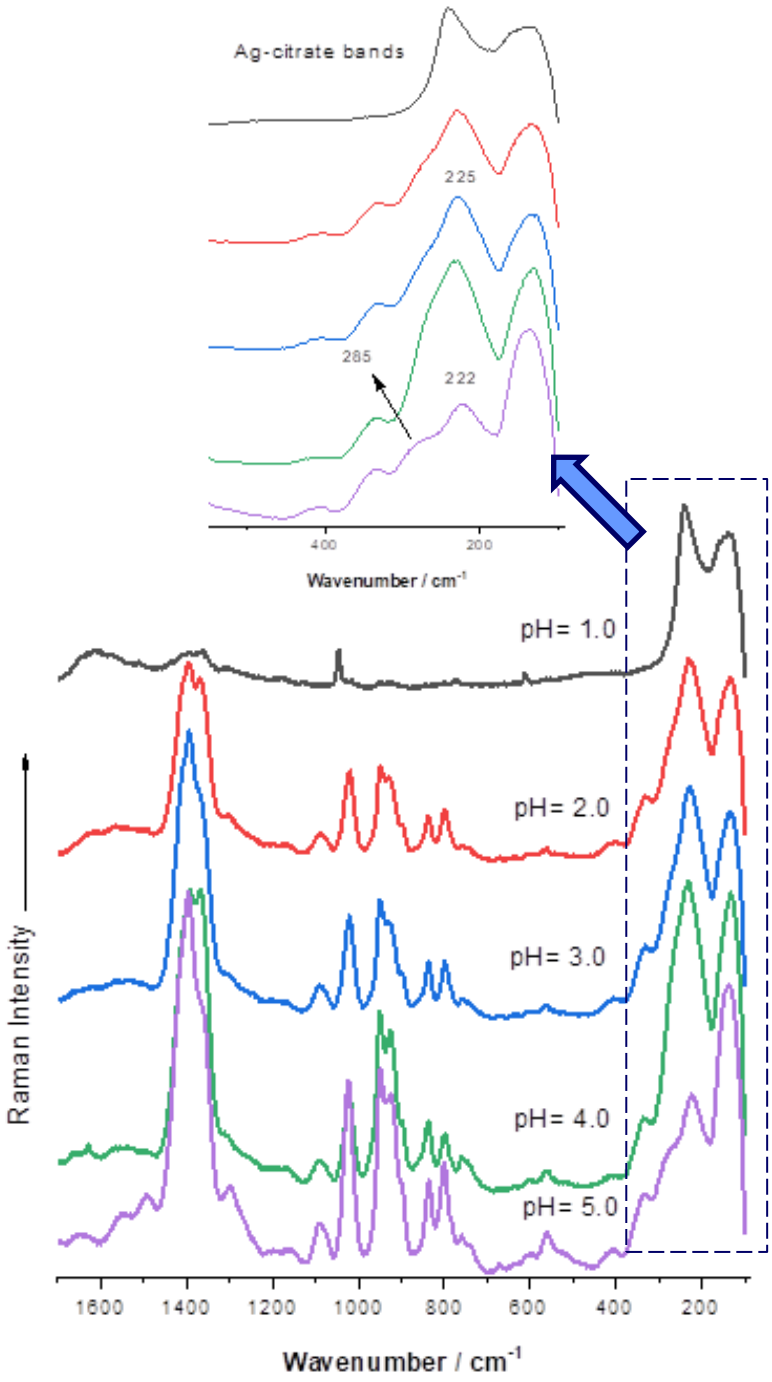

Figure 54. *SERS spectra of citrate at pH 1-5 and detail of the Ag-citrate bands (top).*

iv) SERS on different silver colloids

SERS spectra of the IGI4 ink sample were obtained in different metal substrates, gold and silver, prepared by different methods in order to investigate the efficiency of the different nanofabrication methods on the enhancement of IGIs SERS (**Figure 55**). As can be seen, SERS spectra can be divided in four different regions to better analyze them: *(i)* the region corresponding to the Ag-O interactions, related to the interaction of all species present in the interface (citrate and TA species) with the silver atoms

of nanoparticles; *(ii)* the region corresponding to all the Fe-O interactions involving the different oxygenated functional groups existing in all the species (carboxylates, hydroxyl, phenols, ester groups); *(iii)* the region corresponding to the specific TA molecular vibrations; and *(iv)* a high wavenumber region where overtone bands can appear. The presence of overtones indicates the strong influence of intensification via Raman resonance.

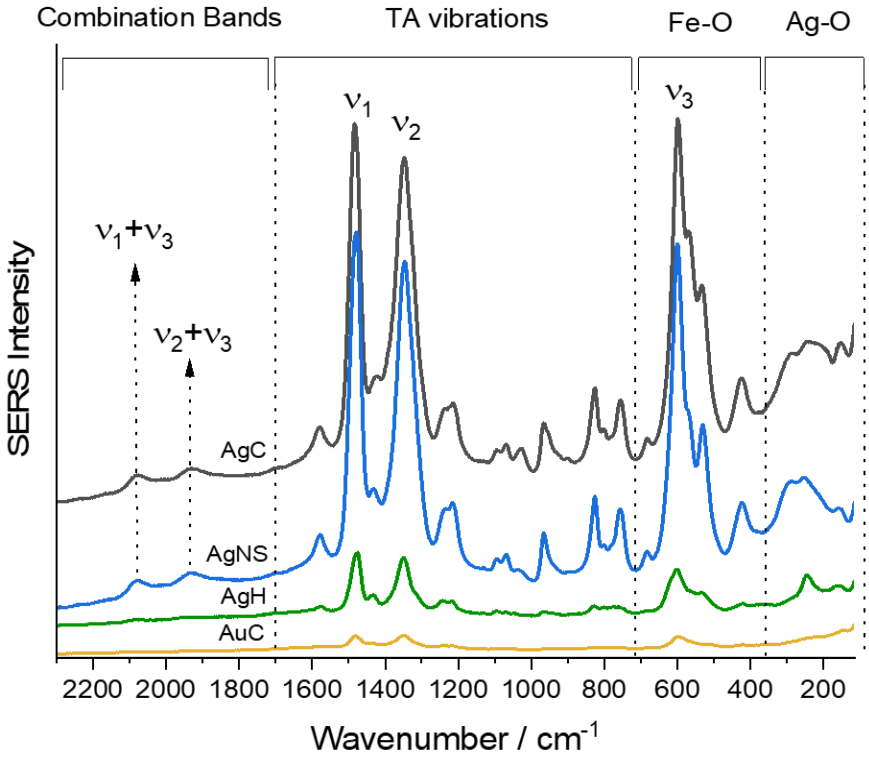

Figure 55. *SERS spectra of the IGI4 ink recorded on different Ag and Au NPs.*

In terms of intensity, the four SERS spectra indicates a strong enhancement in those metal nanoparticles where citrate exists (**Figure 56**). The exception is AuC, but in this case we presume that the affinity of TA-Fe for this metal is lower, and also the gold can induce a catalysis of the citrate species adsorbed onto the Au surface as already reported in previous works [156], [152]. The enhancement of the Raman spectrum in the presence of citrate is related to the higher affinity of the TA-Fe complex on citrate-capped nanoparticles. We suggest that citrate and its oxidation products, can favor the adsorption of the TA-Fe complex by stablishing interfacial complexes of the way indicated in **Figure 57**.

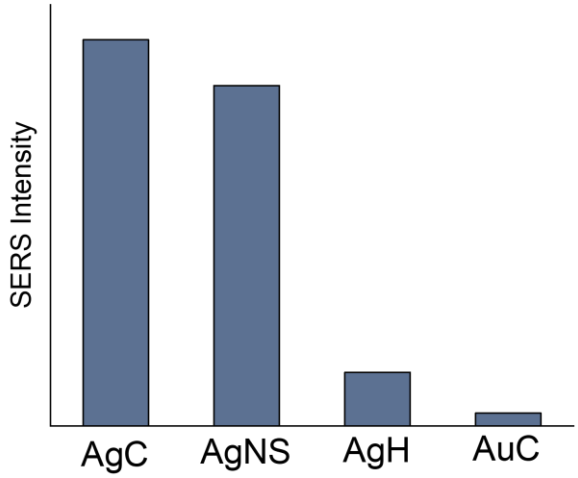

Figure 56. *Block diagram of the intensity of the ν_3 band of the IGI4 ink diplayed as a function of different metal nanoparticles.*

v) Interaction of TA-Fe complexes with the silver surface: adsorption models

Ag nanoparticles capped with citrate ions leads to new complexation possibilities for the iron sphere of coordination mediated by the citrate that do not exist in other nanoparticles. The adsorption of citrate on Ag surfaces seems to take place through the formation of bidentate complexes on the surface, while on Au the adsorption pattern is monodentate [156], [92], [80]. As it was shown above, the TA-Fe complex seems to be strongly adsorbed on the AgNPs surface as deduced from the high intensification of the SERS spectra. This is something possible only when a large amount of complexes is able to migrate from the bulk towards the interface. On the other hand, the binding point of the TA-Fe complex seems to be the iron Fe^{3+} ion, which acts as driving force to induce the adsorption. This interaction leads to an extra enhancement of the ν_3 mode assigned to the Fe-O stretching motions in the iron coordination sphere, which is placed close to the interface. In the case of AgH, where no citrate ions are present, a lower SERS intensity is observed, although the still high intensity of the ν_3 mode is probably due to other kind of interactions with the surface, such as the direct interaction of free –OH groups with the Ag atoms on the surface, or an interaction of Fe^{3+} ions with the Cl^- ions adsorbed on the silver surface.

Figure 57 shows the adsorption models proposed in the present work on the adsorption of TA on the surface through the interaction with the Ag@citrate@Fe^{3+} linking site under monodentate bridged (**Figure 57**a), completely bridged (**Figure 57**b) and bidentate configurations (**Figure 57**d). A direct interaction of TA or GA is possible by interaction of phenol –OH groups with Ag atoms on the surface (**Figure 57**c).

At this point, it is interesting the analysis of the role of gum on the ink adsorption. The presence of gum in the medium alters the interaction of the TA-Fe complex with the surface, since the citrate mediated bands are weaker for those IGI inks where the gum concentration is higher. We suggest that the polysaccharide also participates in the coordination with iron leading to TA-Fe-gum mixed complexes, but this occurs in the bulk, although these ternary complexes could afterwards be adsorbed through direct interaction of then through the pyrogallic moiety. It seems that the formation of these TA-Fe-gum mixed complexes represents a chemical protection against the chemical degradation induced by the metal. This effect indeed opens an interesting discussion regarding the role of this ancestral ink component, the gum Arabic, in relation with the stability of the resulting inks. In fact, a similar protective effect could have been exerted when these inks are impregnating the paper, since iron can also interact with the cellulose inducing a chemical degradation of the paper by the natural oxidation on the cellulose of the paper. This degradative process could be avoided in the presence of gum, which can compete with cellulose when the ink is applied to the paper in historic manuscripts.

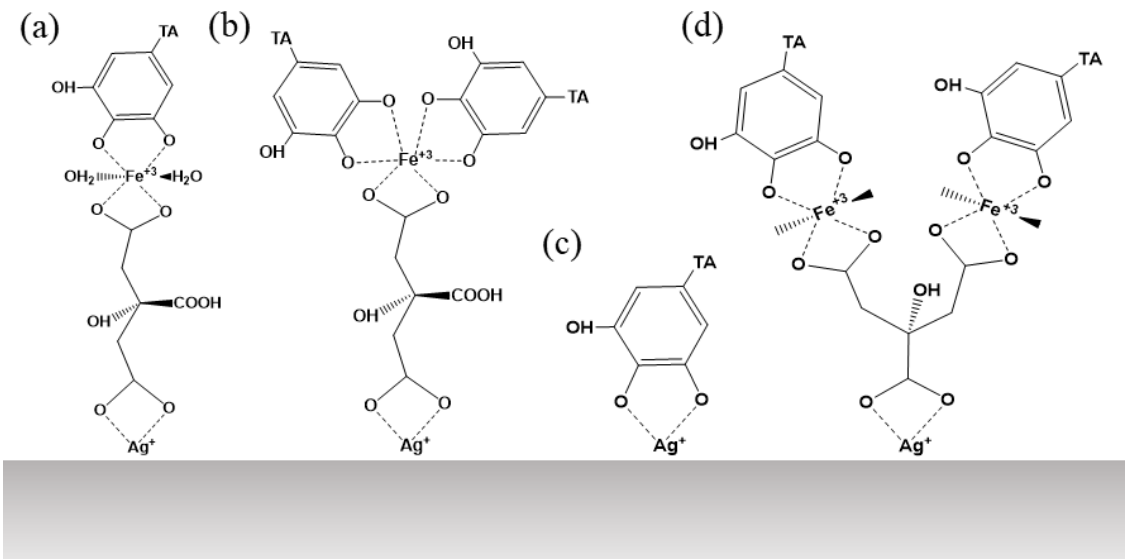

Figure 57. *Adsorption models for TA-Fe complexes on the Ag surface: (a) monodentate adsorption through the citrate linker and bridged TA-Fe with still incomplete iron coordination sphere; (b) monodentate adsorption through the citrate linker and bridged TA-Fe with complete iron coordination sphere; (c) direct interaction with the silver surface through pyrogallic terminal groups; and (d) bidentate adsorption of TA-Fe through two different carboxylic groups of citrate.*

vi) SERS of GAFE *vs* TAFE complex

The SERS of the GA-Fe complex (**Figure 58**) shows stronger 530/425 cm^{-1} bands indicating the prevalence of interactions with the nanoparticle surface through the pyrogallol moiety through the Ag@citrate@Fe^{3+} linking groups. In addition, a more intense band at 298 cm^{-1} is seen, thus demonstrating the existence of direct interactions of GA molecules with the surface as well.

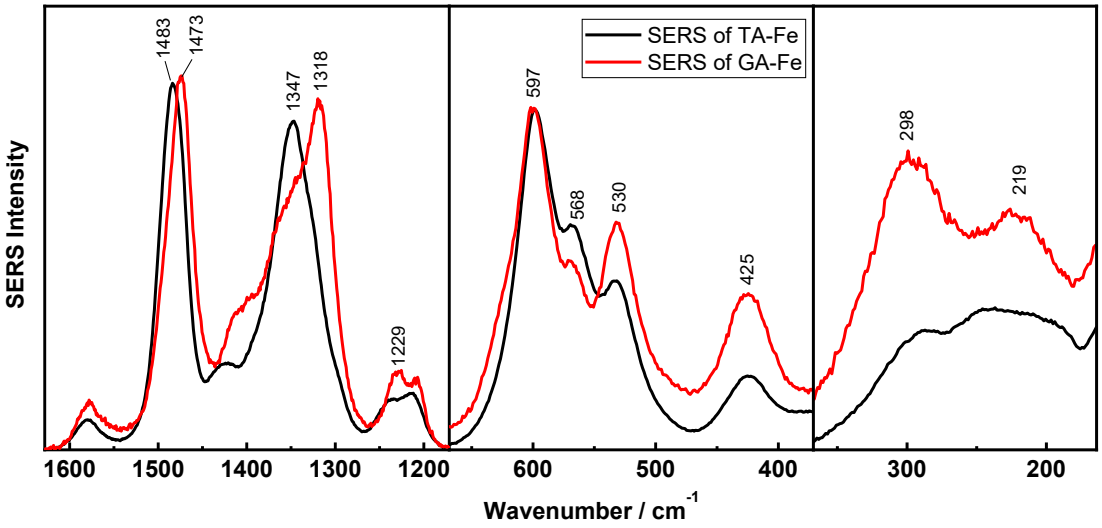

Figure 58. *SERS spectra of TA-Fe and GA-Fe complexes in the different important regions.*

As mentioned above, the commercial TA is actually a mixture of different compounds with the presence of a certain amount of free gallic acid [129]. Therefore, the SERS spectrum of TA could have a large contribution from free GA molecules existing in the mixture, although it is clear that other galloyl derivatives are detected in the SERS, as demonstrates the spectral differences between TA and GA spectra: a) the position of the ν_1 mode (1483 cm^{-1} in TA and 1473 cm^{-1} in GA); b) the inversion of the ν_2 mode to the lower component at 1318 cm^{-1}; c) the intensification of the band at 1229 cm^{-1}; and d) the lower intensity of the 568 cm^{-1} band. The similarity of the SERS spectra of TA-Fe and GA-Fe demonstrate that GA exists in the TA commercial compound, although the differences found between them indicates that other related compounds are present.

In order to get more insight on the role of iron regarding the TA-Fe adsorption on AgNPs, we have developed different experiments in which the TA-Fe compex was prepared in the presence of the silver nanoparticles under different orders: a) AgNPs/TA/Fe; b) TA/Fe/AgNPs; and c) AgNPs/Fe/TA. If the TA-Fe complex

is previously prepared and added to the AgNPs suspension the SERS spectrum is very similar to that of the experiment where the TA molecules were added on the silver and then the iron sulfate is added to the TA/AgNPs mixture (**Figure 59**a and b). However, a completely different situation is found when iron is first added to the AgNPs and then the TA molecules are added on the nanoparticles containing iron. In the latter case, stronger bands corresponding to the interaction of TA via carboxylate groups are observed pointing out the great importance of iron in the interaction of polyphenols on the Ag NPs.

The role of iron in the adsorption of polyphenolic compounds with Ag surface is further confirmed by using GA and a growing concentration of iron (**Figure 59**c and d). When an excess of iron is previously added to AgNPs, strong bands at 530, 425 and 225 cm^{-1} are seen. This demonstrates the gain the importance of the citrate/Fe linker in the adsorption of these polyphenols on the silver surface.

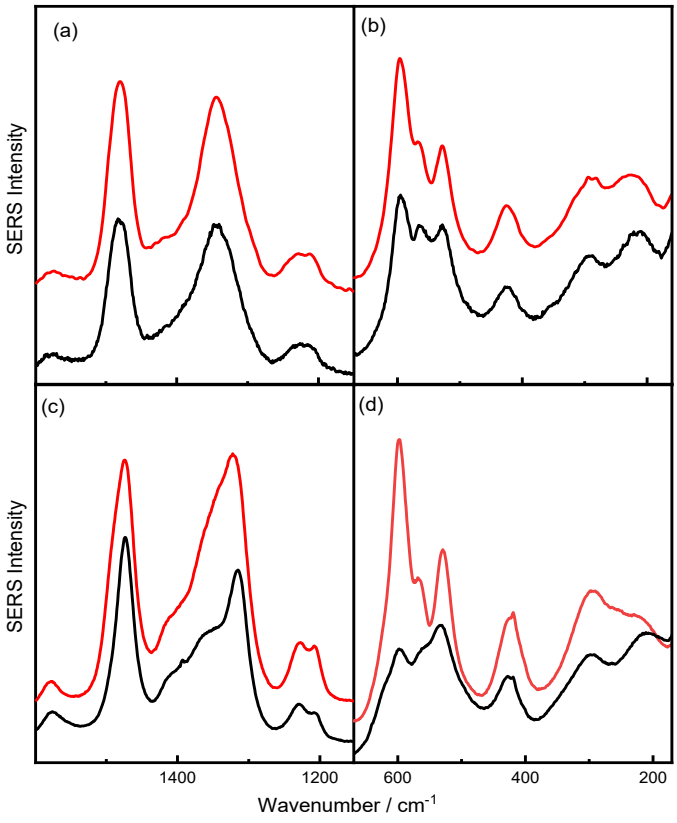

Figure 59. *Up: SERS spectra of TA-Fe complexes prepared ex-situ (a) and in-situ by adding first $FeSO_4$ in the AgNPs colloidal suspension and then the TA (b). Down: SERS spectra of the GA-Fe complexes prepared in-situ by adding $FeSO_4$ at relative concentrations 1:10 (c) and 1:100 (d) (GA/Fe M/M).*

vii) Effect of the pH on the SERS of the TA-Fe complex

Figure 60 shows the SERS spectra of the TA-Fe complex at different pH. Typical bands of TA-Fe complex are mainly seen with remarkable intensity in the 4.5-7.0 interval of pH. At pH 3.0, no TA-Fe bands are detected. Since the citric acid first pKa is 2.79, the absence of TA bands below 4.0 is attributed to the extensive protonation of the citrate anions to the completely protonated citric acid. The solubility of citric acid in solution is drastically reduced and, then, while its the affinity for the silver surface increases. In addition, the protonation of the exposed carboxylic acid groups to the bulk reduces the possibility of an interaction of TA-Fe complexes through the citrate. Because of all these reasons, the adsorption of TA-Fe complexes on the surface is hampered and the SERS bands are absent. In fact, the bands observed at 1415 and 895 cm^{-1} are assigned to the carboxylate symmetric bending and the C-COO^- coupled to CH_2 rocking motions. In the Ag-O region, a higher component at 215 cm^{-1} is seen, indicating the interaction of the carboxylate with the silver (Ag-COO^-).

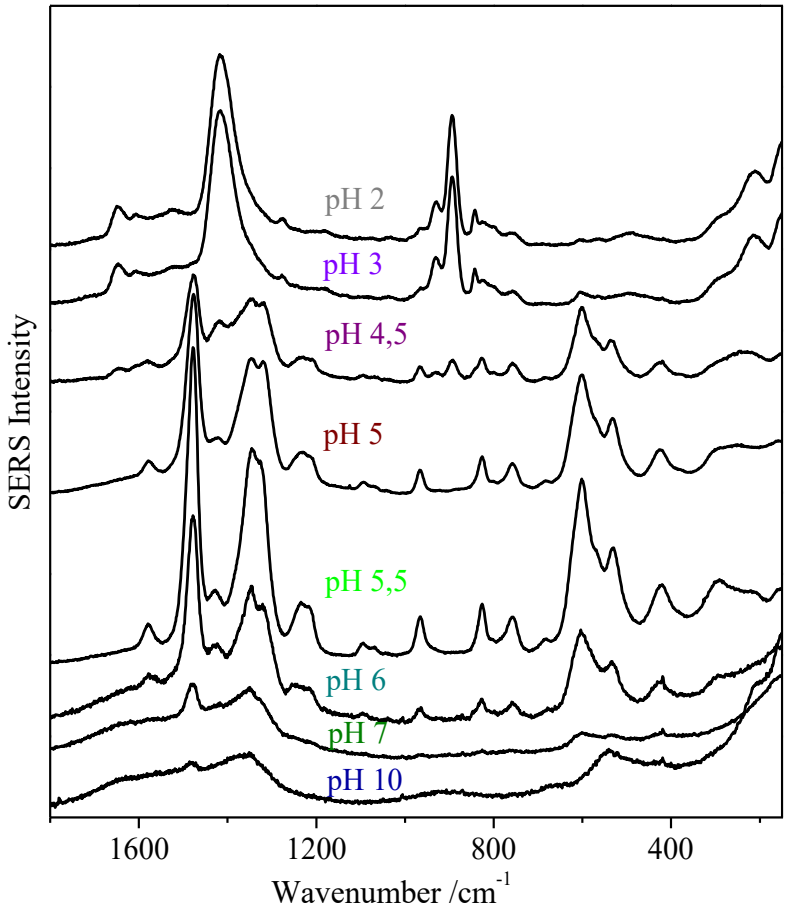

Figure 60. *SERS spectra of TA-Fe complex (10^{-5}/$2x10^{-5}$, TA/Fe M/M) at different pH.*

On the other hand, at pH above 7.0 the intensity of the SERS decreases because of the removal of the TA-Fe from the surface due to the predominant adsorption of OH^- ions. The interval of pH at which the SERS bands are more intense (4.0-7.0) indicates that the adsorption of TA-Fe is favored in the presence of the monoanionic ($CitH_2^-$) and the dianionic ($CitH^{2-}$) citrate ions. Under these forms, citrate is adsorbed on the surface and exhibits carboxylate groups to the bulk that may interact with the pyrogallol moieties of gallic and galloyl species via the Fe^{3+} ions as indicated in the **Figure 41**. The SERS intensity maximum is seen at pH 5.5, which is the optimal value to register the SERS spectra of these compounds. At the latter pH, an intense Ag-O band at 290 cm^{-1} is seen, thus indicating the existence of TA-Fe complexes interacting directly with the surface through the pyrogallic moieties.

viii) Effect of time on the SERS of TAFE and GAFE complexes

Raman spectroscopy was also employed to test the effect of time on TA-Fe and GA-Fe complexes. The normal Raman spectra of TAFE complexes show slight differences when studied in a period of time ranging from 1 h and 44 months (**Figure 61**).

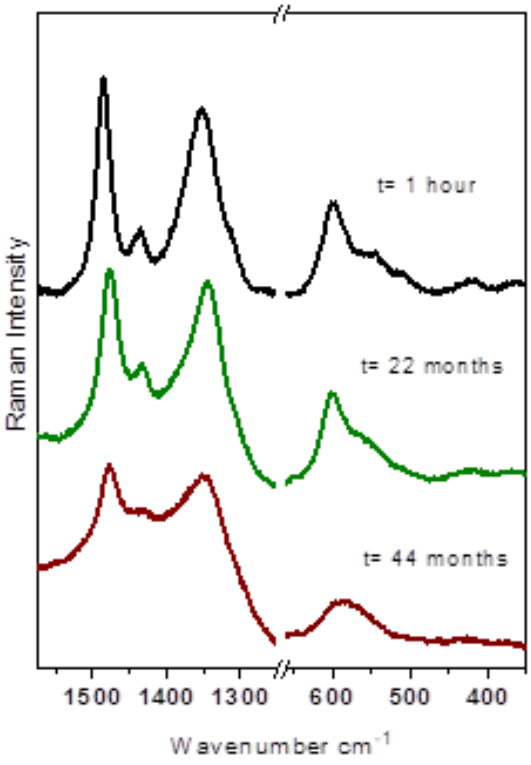

Figure 61. *Normal Raman spectra of TA-Fe complexes measured after 1h (black); 22 month (green) and 44 months (brown).*

In general, a progressive diminution of the intensity is seen and some slight changes are observed in the spectra. All these changes are associated with a progressive aggregation of the complex which is evident when time passes. When the TAFE samples which undergo the effect of time were analyzed with SERS the slight differences observed in the normal Raman are clearly enhanced (**Figure 62**). The most evident effect of time on the TA-Fe SERS spectra is the modification of the ν_2 mode, which undergoes a weakening accompanied by the appearance of a multimode structure of bands appearing at 1390, 1333 and 1302 cm^{-1} after 44 months. A similar effect was observed in the case of GA-Fe complexes (**Figure 62**b), although a lower 1333 cm^{-1} band was seen. The citrate-Fe-TA bands at 530/425 cm^{-1} almost disappear after 44 months.

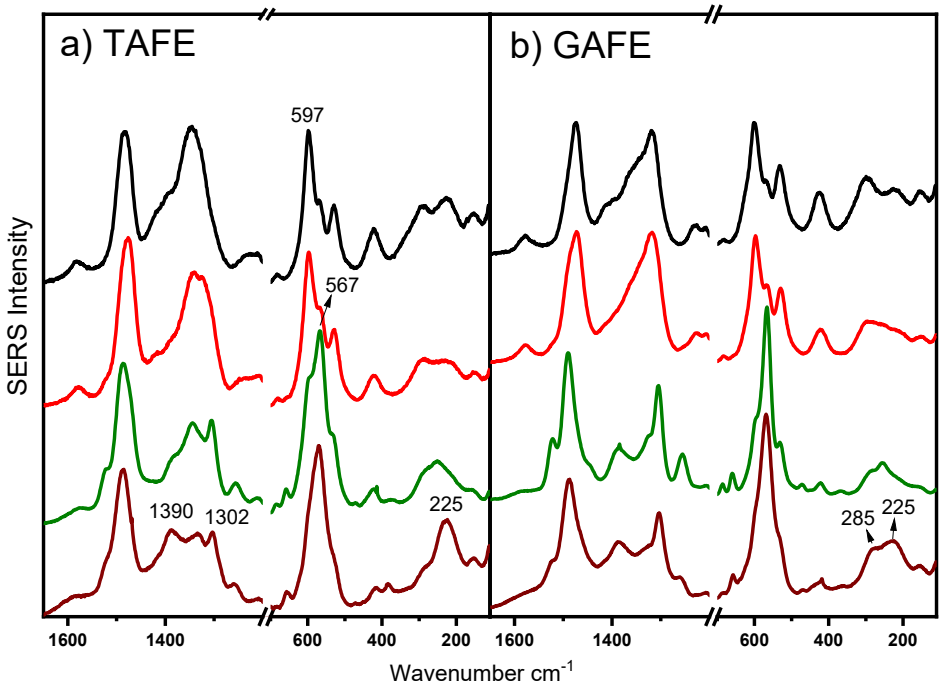

Figure 62. *SERS spectra of TA-Fe (a) and GA-Fe (b) complexes measured after 1h (black); 1 month (red); 32 months (green) and 44 months (brown).*

The ν_3 mode underwent an inversion between the most intense band in the fresh complex at 597 cm^{-1} and the 568 cm^{-1} one, being the latter one the unique band seen after 44 months. Similar behavior was also observed in GAFE.

Finally, the Ag-O region also underwent clear changes indicating a different adsorption pattern of the polyphenolic species existing in the mixture. In the TAFE complex, the final result is a unique band at 225 cm^{-1} (**Figure 62**a) pointing out a prevalent interaction of TAFE complexes through the Ag-citrate-Fe-TA adsorption

mechanism. Conversely, the final situation of the GAFE complex in this region is the existence of a 285/225 cm^{-1} doublet indicating that the indirect and direct interaction of this complex on silver is still taking place.

The changes observed in the Fe-O region affords important hints to understand the chemical modifications underwent by these important complexes with the time. The inversion of the 598/568 cm^{-1} doublet bands demonstrates that a change in the complexation pattern of TA-Fe from predominant terminal complexes to bridged complexes. This suggests that the initial complexes formed in the mixture are still incomplete regarding the iron sphere of complexation. The evolution in time leads to a progressive cross-linking of tannic species via the iron centers with the formation of bridged final complexes. This induces a structural change in the C-O bonds, which are the basis of the ν_2 mode, and in the Fe-O spectral pattern. The creation of final cross-linked structures with a higher size accounts for the aggregation observed in the suspension, as well as the predominance of the 225 cm^{-1} Ag-O band related with the indirect adsorption complexes. However, in the case of the gallic acid there still exists a high amount of free GA molecules and smaller GA-Fe that can interact directly with the silver surface.

4.4 Analysis of Historical Manuscripts

The analysis of historical manuscripts by Raman is a highly difficult task that implied the knowledge of the formation of metal complexes with the different materials employed in the fabrication of metallogallic complexes, the effect of these different components on the stability of the final ink and the effect of the time on inks.

Since the complex of polyphenolic compounds with iron and copper is the main process that is involved in the fabrication of metallogallic inks, we have previously studied these complexes in the above sections. SERS provided a helpful technique, not only to analyze very tiny amounts of the material, but also to induce an artificial aging on the ink. In fact, the SERS results provided important information about the possible protective effect of the gum Arabic. In this section the results obtained from the application of Raman spectroscopy on real historical manuscripts is presented in order to evaluate the effect of the aging on the original metallic complexes contained

in IGI inks. The changes on the key Raman features imposed by the pass of the time could afford important hints to evaluate and to date the analyzed manuscript.

i) *In-situ* Raman spectroscopy analysis of manuscripts from Spain

Figure 63 shows Raman spectra of the manuscripts belonging to the group of works originated in Spain (**Table 4**, 3.4 Historical Manuscripts). Among all the analysed manuscripts, only a clear Raman spectrum bearing an IGI profile was observed in the S012 and S015 samples by using a laser excitation at 785 nm. The works that did not provided any intense signal at 785nm (S009, S010, S011, S013, S014) were analyzed at 532 nm. At the later conditions very weak ν_1 and ν_2 could be seen. A common characteristic of these samples is the presence of two broad bands centered at ca. 1360 and 1550 cm^{-1} that point out the presence of carbon-based black pigments in these inks. Therefore, we have concluded that the ink of these manuscripts was prepared by mixing IGI with carbon in different proportions.

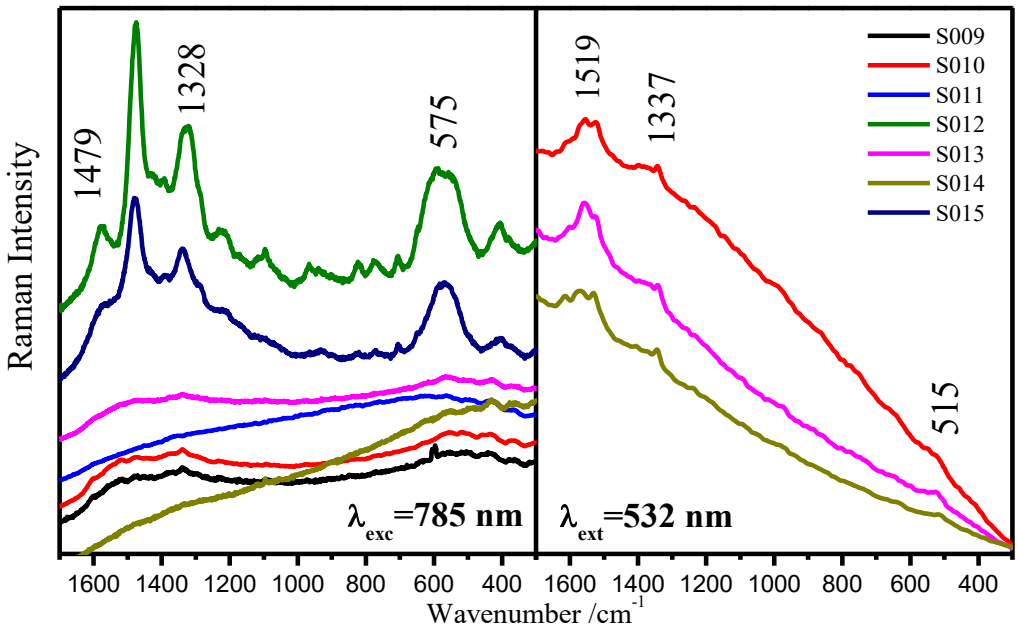

Figure 63. *Raman spectra of above mentioned manucripts analyzed at λ_{exc} = 785nm (measurement paramenters: power 0.1 to 1% (mW), exposure time of 30 seconds, 1 accumulations) (a), and λ_{exc} = 532nm (measurement paramenters: power 0.1 to 0.5% (mW), exposure time of 10 seconds, 1 accumulations) (b). The presented data represent the averaged Raman spectra recorded for 3 different points on the ink.*

Figure 64 displays the Raman spectra recorded on the manuscripts dated from the year 1703 (S015) to 1835 (S012) and they are compared to the IGI3 ink (freshly

prepared in the lab, i.e. now). As can be seen, all the samples present ν_1, ν_2 and ν_3 spectral features. However, they exhibit clear differences between them that can be summarized as follows:

- The relative intensity of the ν_2 mode decreases with the time and undergoes a shift.
- The ν_3 mode is enhanced and is shifted to lower wavenumbers. In some cases, it appears as a doublet (598/549 cm^{-1}; S012).
- There appears a medium band at 410 cm^{-1} with the time.
- Other medium bands at 1710, 1430 and 1243 cm^{-1} are weakened with the time.
- The *8a* aromatic band of benzene at 1610 cm^{-1} is shifted to 1578 cm^{-1}.

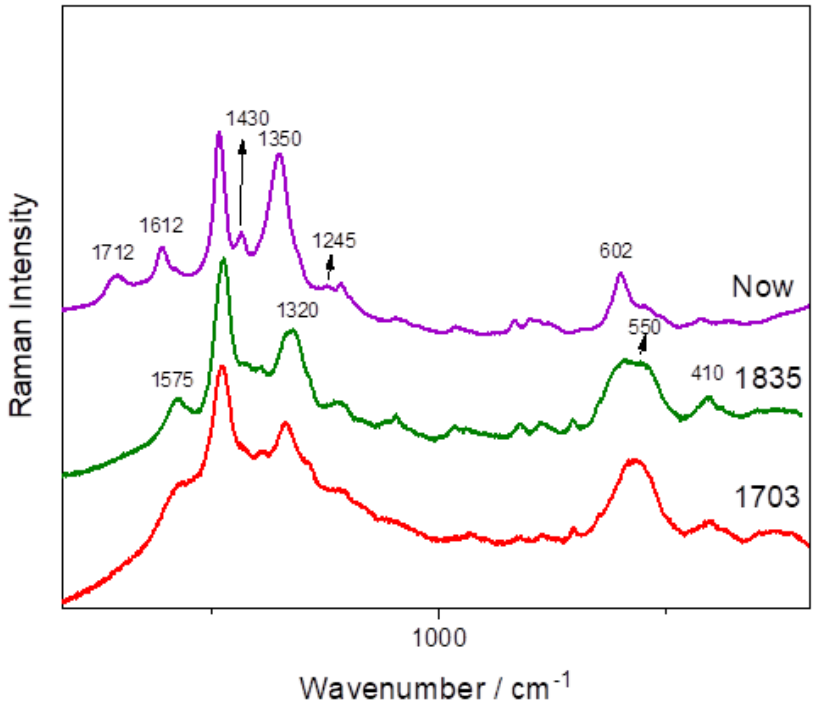

Figure 64. *Normal Raman spectra of the IGI3 ink (Now) as compared to the IGI in manuscripts no.S012, corresponding to the year 1835 and no. S015 dated from the 1703 year.*

These changes can be attributed to the progressive degradation of the IGI ink. For instance, the decrease of the ν_2 mode can be related to the oxidation of the polyphenol, that implies the disappearance of –OH groups and the appearance of other oxygen-containing functions like ketonic ones. The hydrolysis of polyphenols at the level of the ester groups is considered the responsible for the weakening of the 1710, 1430 and 1243 cm^{-1} bands. Finally, the clear changes in the Fe-O region are related to the formation of new Fe-O bonds after the degradation process of the original organic compounds. This process leads to the reorganization of the iron complexes and the formation of new metal coordination spheres. The effect of aging observed

in this thesis was similar to those observed in other previously reported studies of historical IGI manuscripts.

However, no explanation about the chemical processes involved in the ink degradation was proposed up to know. Therefore, a possible dating of historical documents made with IGI is proposed for the first time in this thesis based on the above spectral changes involving the Raman marker bands.

ii) Raman spectra of manuscripts from similar period of time collected from Slovakia

An interesting aspect in the effect of time on the metallogallic inks is the analysis of manuscripts dated from a similar age in order to observe possible effects on the ink structure that can be independent from the aging effect. **Figure 65** displays the Raman spectra registered from manuscripts with Slovak origin (Archives from Kežmarok) dating from the 1854-1858 period of time. In all these documents we observed similar effects of the time as described above, but between them it was observed a disparity in the aging effects. The analysis of the Fe-O spectral region could more be helpful in the comparative study.

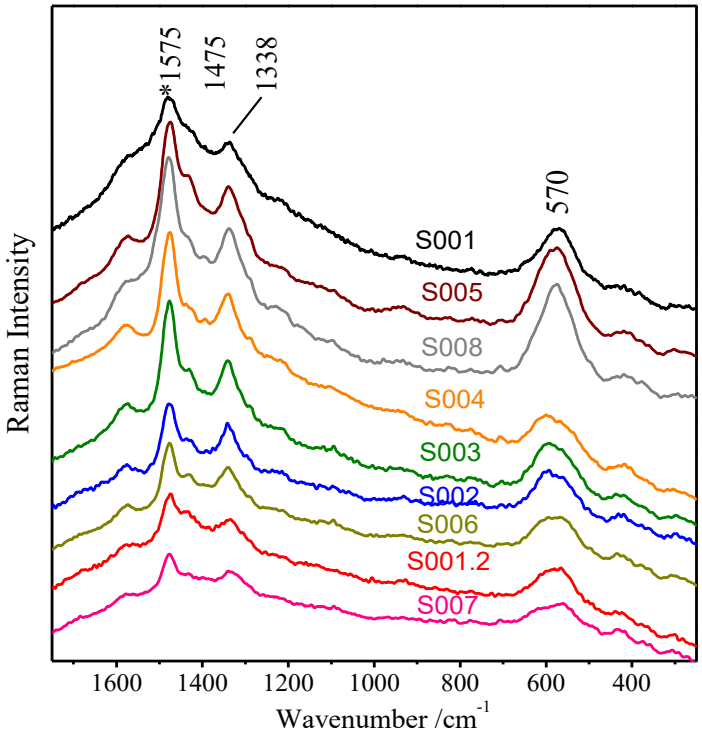

Figure 65. *Raman spectra of the manuscripts no. S001 to S008 registered after in-situ analysis of the manuscripts in selected areas. (λ_{exc} = 785 nm, spectra were normalized to the band at 1575 cm^{-1} and measurement parameters were: 0.1 to 1% (mW), exposure time of 30 seconds, 1 accumulation.)*

Figure 66 shows in more detail the 800-200 cm^{-1} region. Although the predominant band in the Fe-O region is usually centered at 570 cm^{-1}, with observation of a unique band (samples S001, S005 and S008), in some other cases a doublet can be observed (samples S002, S003, S004 and S006). When this doublet is balanced to the lower components such as in the case of the sample S007, where this mode appears at 560 cm^{-1}) the degradation of the ink seems to be stronger as deduced from the higher fluorescence background and the more intense degradation evidences (lower ν_2 mode and weaker 1430 and 1243 cm^{-1} bands).

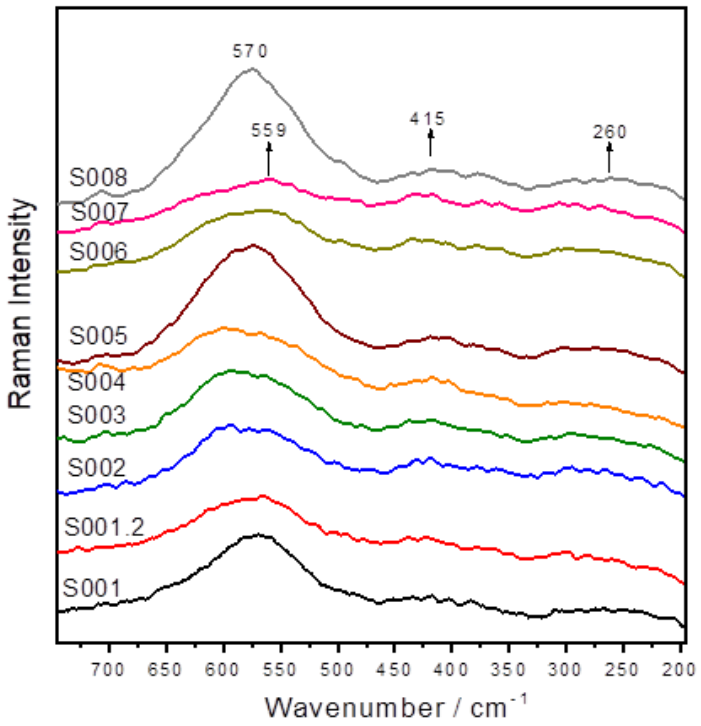

Figure 66. *Spectra of the Figure 65 amplified in the 800-200 cm^{-1} region.*

Therefore, it can de deduced that the ν_3 mode, corresponding to the Fe-O vibrations, is very sensitive to the degradation and corrosion of metallogallic inks undergone by these materials with the time, and this marker band can be employed in aging studies related to the inks. In any case, a deeper analysis based on higher statistics has to be performed to find a more precise correlation.

Necertheless, the shift downward of the Fe-O ν_3 mode to 550 cm^{-1} together with the appearance of a medium band at ca. 400 cm^{-1} and the broad feature in the 200-300 cm^{-1} interval in historical manuscripts is clear in the Raman spectra registered from the Slovak manuscripts dating from the 1854-1858 period, is indeed related

to the degradation of these manuscripts. These new bands observed in aged manuscripts can be associated with the appearance of oxalate in inks. The formation of oxalate has been also reported by other authors in recent analysis of historical manuscripts revealed by FTIR and Mössbauer spectroscopies [157]. The above bands could be associated to the formation of oxalate-iron complexes as also reported by Conde-Morales [158] in Raman spectra of iron oxalates after Fenton reaction of other biomolecules. This is a similar process that could also occur in the complex environment of manuscripts, where many different biomolecules (polyphenols, carbohydrates) coexist in the same medium. Lerf et al. reported that the oxalate could be produced after degradation of carbohydrates (cellulose and gum Arabic) by the oxidative action of Fe^{3+}. In addition, the formation of oxalic acid could contribute to a further decrease of pH that is summed to the final degradation of the paper in manuscripts.

iii) pH of manuscripts

The pH of the analysed manuscripts measured according to the drop method (3.5 Measurement of the pH on historical manuscripts) are shown in the **Figure 67**.

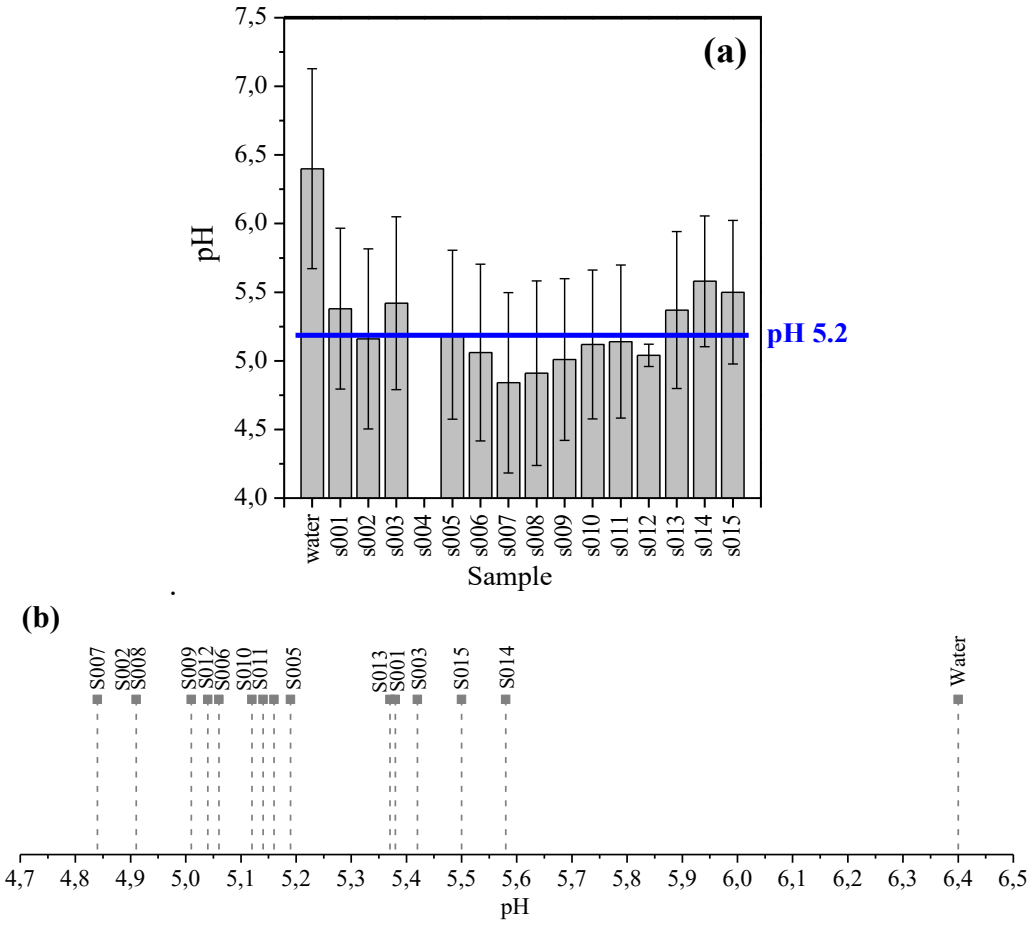

Figure 67. *(In the previous page) (a) pH data obtained from the samples of the Figure 65 and the reference sample, water. The presented data are the results of three independent measurements. (b) Linear representation of the estimated pH values data for the analyzed samples.*

The estimated pH values of the analyzed samples are really close each to other. In detail, the biggest difference between the pH of the most acidic manuscript and the pH of the most alkaline manuscript was found to be just 0.74 of pH unit. Besides, all inks in the manuscripts decreased their pH above the pH of the water (pH ~ 6.4). Moreover, there are two specific cases demonstrating even stronger pH decrease, i.e. sample no. S007 and S008. In the first case, it can be correlated to the high chemical degradation as deduced from the recorded Raman spectra. Therefore, a correlation between Raman data and the pH of the IGI found in the manuscript can be assumed.

iv) Analysis of the Letters from Cuba

The analysis of the ink found in letters originated in Cuba (samples no. S009, S010 and S011) gives rise to rather complex spectra when exciting at 785 nm (**Figure 68**). In principle, the recorded spectral features correspond to a mixture of pigments where three different components can be identified: a) black carbon, with broad bands at 1360/1580 cm^{-1}; b) iron gall ink, with features seen at 1478 and 1338 cm^{-1}; and c) other bands which do not correspond to any of the black pigments analyzed before, such as that at 1518 cm^{-1}.

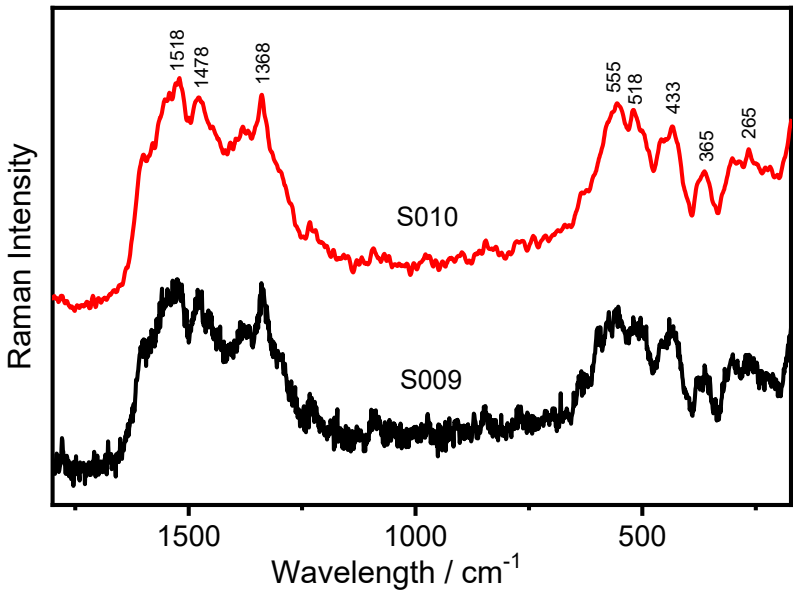

Figure 68. *Raman spectra of the ink samples no. S009 and S010 analyzed in the letters sent from Cuba in the year 1930.*

In these samples, many bands are appearing in the Fe-O region, at 555, 518, 433, 365, 298 and 265 cm^{-1}. Thus, one can suggest the presence of many different components in these inks what makes them very difficult to be analysed by Raman spectroscopy. In particular, the bands at 1518, 518 and 365 cm^{-1} suggest the presence of modern synthetic pigments in these inks dating from the beginning of the XX century, a period of time where the addition of these kind of colorants to inks was already a habitude.

v) The Castelar letters from the National Archaeological Museum (MAN) of Madrid

The analysis of the Emilio Castelar letters is interesting from the point of view of localization since these letters came from different parts of Spain, but we can classify them into the same time period. These documents dated from the end of the XIX century (around 1895). Therefore, the ink found in these letters could contain valuable information about the ink composition related to the same time period, but characterized by different geographical origins (different Spanish regions). We had to use to study these documents a portable Raman instrument Delta Nu (**Figure 69**). It was necessary to use it since in this case it was not allowed to move the Castelar letters from the MAN to our laboratory. A total of 35 samples of the ink's tracks corresponding to different signatures found in the analyzed documents and classified by the museum in provinces were analyzed.

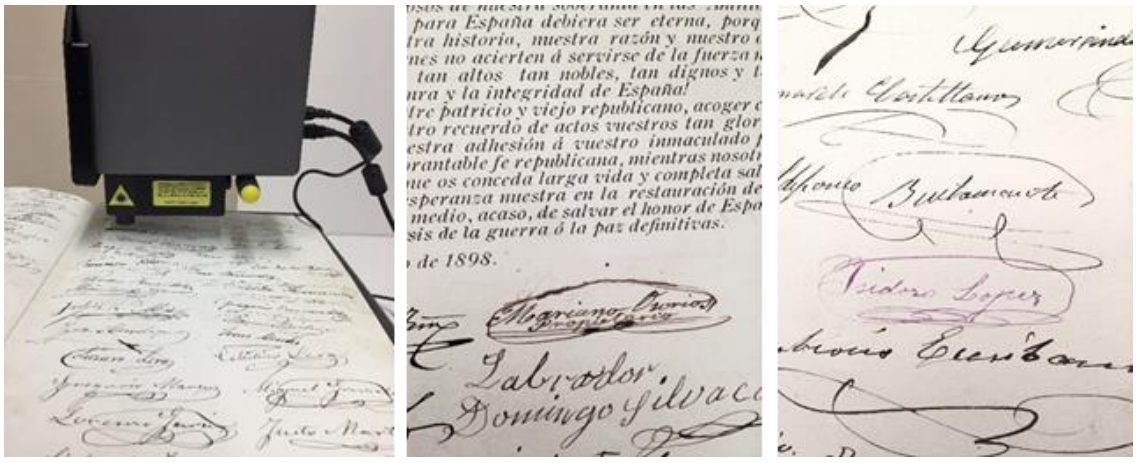

Figure 69. *Pictures are showing the in-situ measurements of Raman spectra on the Castelar letters made predominantely on the ink's tracks corresponding to different signatures found in the analyzed documents.*

Different measurements were done on several points of the letters corresponding to the inks employed by different persons who stamped their own signatures on the document. Therefore, this study provided the spectral evidence from diverse sources of inks in these documents. The Raman spectra corresponding to the punctual measurements from the different analyzed documents originated from Lugo, Leon, Castilla la Nueva and Guadalajara Spanish regions are displayed in **Figure 70**.

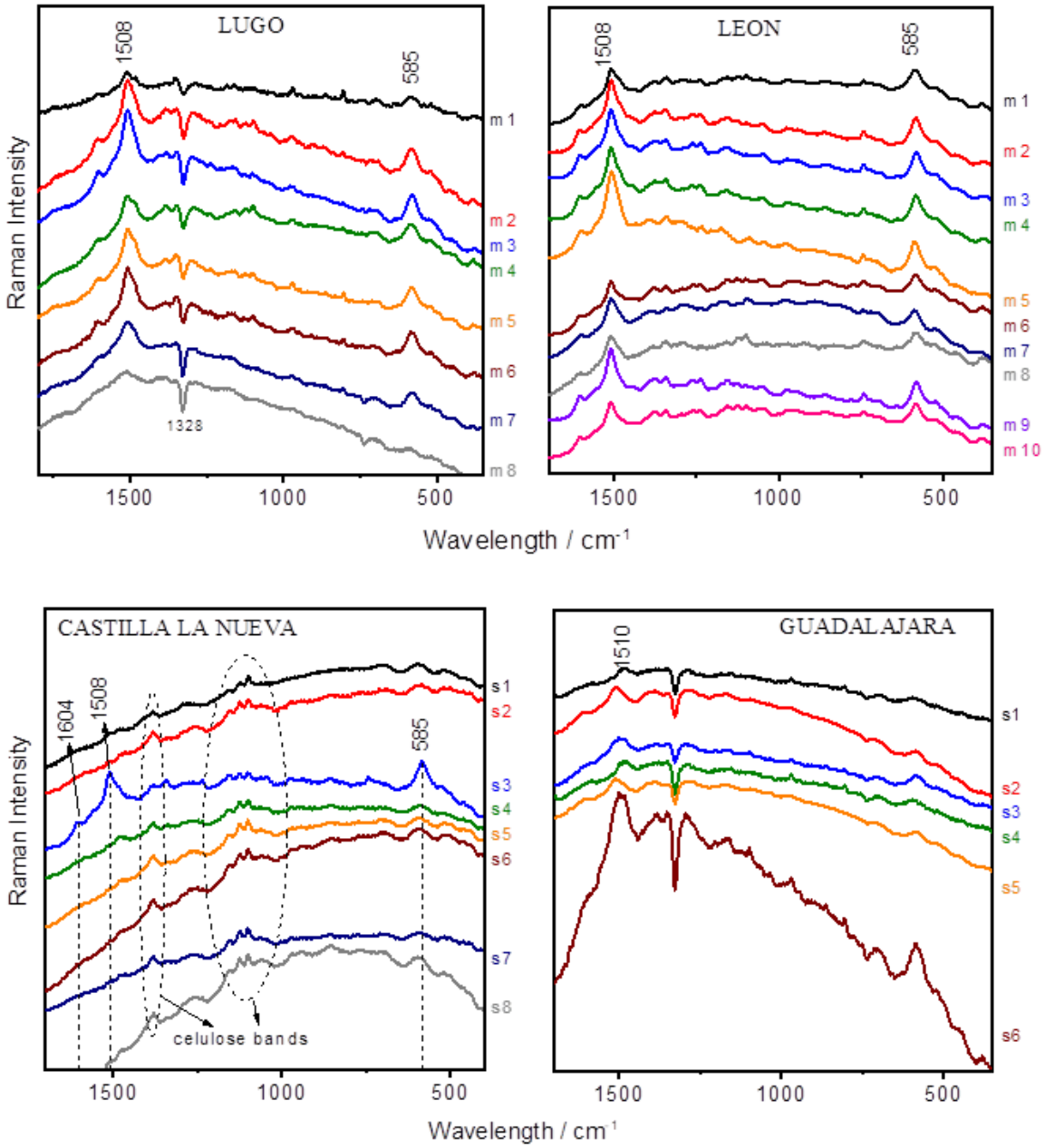

Figure 70. *Raman spectra measured on different points of the Castelar letters analyzed in the Museo Arqueológico Nacional de Madrid (MAN).*

Two main spectra were identified in punctual analysis applied on these letters that are shown in the **Figure 71**. The spectrum of the **Figure71**a shows intense bands at 1510 and 577 cm^{-1}. These bands cannot be assigned to the iron gall inks, although they could have been assigned in principle to the IGI ν_1, ν_2 and ν_3 modes. They can be rather attributed to some other synthetic colorant employed in the time where these letters were written.

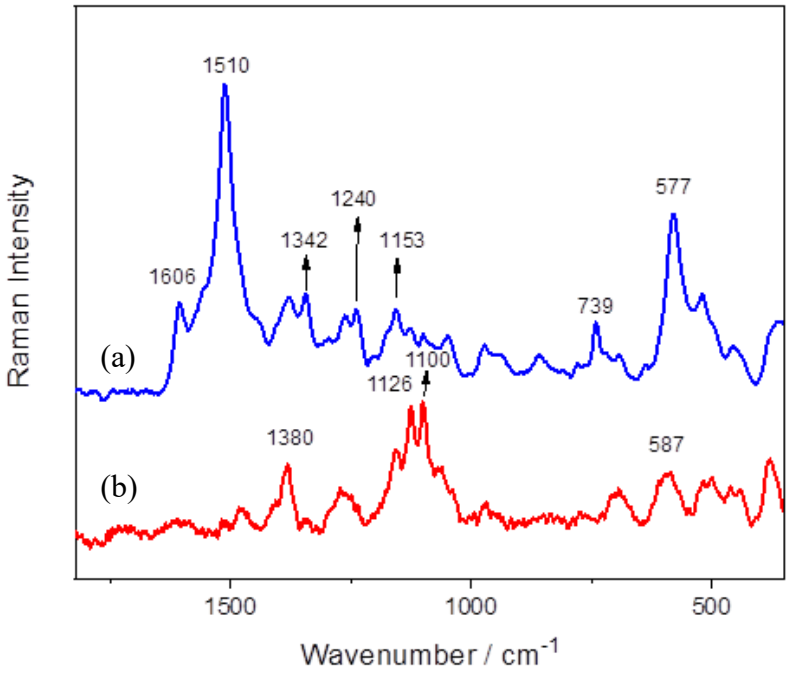

Figure 71. *Two main Raman spectra obtained from the Castelar letters analyzed in the Museo Arqueológico Nacional de Madrid (MAN).*

Several authors have reported that aniline colorant could have been added to the ink prepared at the end of the XIX century [159], in order to enhance the intensity of the ink and induce new and attractive hues in the ink. These colorants were introduced from the 1860 year following the synthesis done by Perkin of the aniline mauve. The use of aniline colorants was also generalized in the ink printing and stamps [160]. Therefore, the Raman spectrum of the **Figure71**a can be assigned to some aniline colorant, the most probably to aniline blue, employed at the end of the XIX century, the time at which the Castelar letters were written. Unfortunately, there is no published work dealing with the Raman analysis on aniline blue in the literature.

C.A. Smiths reported in 1944 an article entitled "The Chemistry of Inks" [160], which could be a good reference, due to the close proximity in time with the writing

habitudes of the end of the XIX and the beginning of the XX centuries. He reported the existence of a Black-permanent ink which writes black, become blacker by age, and that was good for V-mail letters. Likewise, he reported that it could be fabricated by two main methods: a) by mixturing gallotannate with a mixture of 3-4 aniline colorants, and b) by oxidizing logwood extract (hematoxylin) with chromate of soda, producing hematin, giving rise to a purple-black color. Therefore, it seems that there could be different versions of the pen inks rendering blue-black and purple-black colors in the resulting commercial inks. This is precisely what we have observed in the Castelar letters, where these two versions of colors were identified in the documents together with other brown colors (**Figure 71**).

A similar colorant, the aniline mauve or mauveine, was recently analyzed by Raman [160]. This dye shows intense features at 1637, 1566, 615 and 562 cm^{-1}. Although these bands are not exactly identified in the spectra of the MAN documents. Nevertheless, it should be also considered the possible effect of the metal complexation and the effect of the time to account for the aging of the structure of these colorants. This is something that is also missing in the literature and could be an interesting work for the future.

The other predominant Raman spectrum measured in the Castelar letters (**Figure71**b) is assigned to cellulose, which is evident in some points where the intensity of the ink colorants is weaker. In some cases, a negative band was registered at 1328 cm^{-1} that correspond to the background produced by the light emission of the ambient light of the museum.

The synthetic colorant seems to have been added on the IGI ink to enhance the color intensity. The fact that no IGI characteristic band was observed in the recorded spectra is likely due to the predominance of the synthetic colorant spectrum, that could overlap the Raman spectrum from the IGI ink. However, in some cases, like those corresponding to the m4 sample of the Lugo series (**Figure 70**), the presence of weak IGI bands is more evident at 1480 and 1348 cm^{-1}, that can be attribute to the IGI ν_1 and ν_2 modes, while the ν_3 may be overlapped by the modern colorant band at 577 cm^{-1}. Furthermore, the synthetic colorant identified in the Castelar letters displays similar bands to those observed in the Cuban letters (**Figure 68**), what indicates the generalized use of aniline colorants as ingredients in the original IGI inks from the year 1860.

The bands at 1510 and 577 cm^{-1} are very intense in the letters coming from two particular Spanish provinces: Lugo and León. These regions are geographically close and are localized in the Northwest part of Spain. Therefore, the presence of these bands in geographically related regions suggests that the modern ingredients could be originated from similar provider.

Conversely, the later bands are weaker in letters coming from the letters originated from Castilla la Nueva and Guadalajara, two regions that are currently forming part of the same Spanish region: Castilla La Mancha, localized in the center part of Spain. The presence of the 1605/1510/577 cm^{-1} group of bands in these letters is only evident in certain points like in the s3 sample. In addition, these bands are even weaker in the letters from Guadalajara. In fact, the main part of analyzed points give rise to a predominant spectrum corresponding to the cellulose, thus indicating the lower concentration of the colorant in the latter samples.

5. CONCLUSIONS/CONCLUSIONES

Conclusions

1. The Optical spectroscopy techniques used in the frame of this PhD thesis (UV-vis absorption spectroscopy, IR and Raman spectroscopies, SERS spectroscopy) offer an efficient tool to describe both qualitatively and quantitatively composition and structure of the IGIs prepared in the laboratory and those analyzed in historical manuscripts.
2. The vibrational and UV-vis absorption spectra clearly differ between the individual polyphenol molecule and its metal complexes. In particular, Raman spectroscopy demonstrated to be very useful in the analysis of iron interactions with phenolic compounds.
    a. The observed spectral changes can be associated with the complex formation, i.e. with the interaction of polyphenols with metal ions.
    b. UV-vis absorption spectra demonstrate appearance of a new band at higher wavelengths in the case of complex formation associated to ligand-to-metal charge transfer.
3. Tannic acid and gallic acid show very similar behavior in all studies. These molecules present the strongest interaction with metals among the molecules studied, while the syringic acid exhibits the weaker interaction with metals.
4. Three main Raman bands appeared at 1450-1490 cm^{-1} (ν_1), 1320-1345 cm^{-1} (ν_2), and 400-650 cm^{-1} (ν_3), that are characteristic of the metal complexes, and whose positions and intensities can be used to characterize the complex in function of the original structure of the polyphenol, and the changes undergone with pH, aging time and complex stoichiometry.
5. The difference between the position of ν_1 and ν_2 bands and the intensity ratio ν_1/ν_2 are connected with the structure of polyphenols, since these bands are related to the degree of electronic delocalization of the aromatic system. These two parameters depend on the ionization state of the molecule, which increases with the pH and can be employed to test the structure and chemical conditions of manuscripts.

6. An alkaline pH induces the polyphenol polymerization as well as formation of new polyphenolic species that strongly increases the fluorescence emission. This high fluorescence is quenched upon the formation of the iron complex.
7. The interaction with iron produces side effects such as the pH lowering. This is a negative effect in the case of the use of IGIs, as it induces a progressive degradation of the paper. In addition, it was demonstrated that the pH decreases even more with time after the deposition of the complex on the paper.
8. The formation of the complex leads to the fluorescence quenching, and this is a positive effect for the study of these complexes by Raman, as polyphenols show a strong fluorescence emission that overlap the Raman signal.
9. The presence of gum Arabic in IGI inks seems primordial to induce a protection of the polyphenol, preventing the oxidation and acidification because of the formation of H-bonds between hydroxyl groups of the polyphenol and the polysaccharide.
10. The SERS spectroscopy provided a useful structural information about the complexes and induced a large intensification of the Raman emission, mainly on the citrate reduced Ag NPs.
11. The presence of metal nanoparticles leads to a structural change with the formation of H-bonds between the citrate adsorbed onto the metal and the complex. The citrate acts as a linker attracting polyphenols and changing the coordination sphere of iron.
12. The adsorption of polyphenol/iron complexes on plasmonic nanoparticles induces a quick structural modification of the complex similar to the aging effect observed in historical manuscripts of different centuries, consisting in a weakening of the ν_2 mode and the large change of the FeO vibrations.
13. The analysis of historical manuscripts by Raman revealed the keys for the interpretation of the aging effect of iron gall inks, which consists in the oxidation and hydrolysis of polyphenols, along with a change in the coordination pattern of iron.
14. The pH deduced from the analysis of historical manuscripts points out that a further acidification occurs on manuscripts as time passes.

15. The analysis of manuscripts dating from the end of the XIX century and the beginning of the XX one revealed the presence of modern synthetized colorants that were added to IGI inks.

Conclusiones

1. Las técnicas de espectroscopia óptica utilizadas en el marco de esta tesis doctoral (espectroscopia de absorción UV-vis, espectroscopia IR y Raman, espectroscopia SERS) ofrecen una herramienta eficaz para describir cualitativa y cuantitativamente la composición y estructura de los IGI preparados en el laboratorio y los analizados en manuscritos históricos.
2. Los espectros de absorción de vibración y UV-vis difieren claramente entre la molécula de polifenol individual y sus complejos metálicos. En particular, la espectroscopia Raman demostró ser muy útil en el análisis de las interacciones del hierro con los compuestos fenólicos.
    a. Los cambios espectrales observados pueden asociarse con la formación de complejos, es decir, con la interacción de polifenoles con iones metálicos.
    b. Los espectros de absorción UV-vis demuestran la aparición de una nueva banda a longitudes de onda más altas en el caso de la formación de complejos asociados con la transferencia de carga de ligando a metal.
3. El ácido tánico y el ácido gálico muestran un comportamiento muy similar en todos los estudios. Estas moléculas presentan la interacción más fuerte con los metales entre las moléculas estudiadas, mientras que el ácido siríngico exhibe la interacción más débil con los metales.
4. Se observaron tres bandas Raman principales a 1450-1490 cm^{-1} (ν_1), 1320-1345 cm^{-1} (ν_2) y 400-650 cm^{-1} (ν_3), que son características de los complejos metálicos, y cuyas posiciones e intensidades pueden utilizarse para caracterizar el complejo en función de la estructura original del polifenol, y de los cambios sufridos con el pH, el tiempo de envejecimiento y la estequiometría del complejo.
5. La diferencia entre la posición de las bandas ν_1 y ν_2 y la relación de intensidad ν_1/ν_2 están relacionadas con la estructura de los polifenoles, ya que estas bandas están relacionadas con el grado de deslocalización electrónica del sistema aromático. Estos dos parámetros dependen del estado de ionización

de la molécula, que aumenta con el pH y pueden emplearse para probar la estructura y las condiciones químicas de los manuscritos.

6. Un pH alcalino induce la polimerización de polifenoles así como la formación de nuevas especies polifenólicas que aumentan fuertemente la emisión de fluorescencia. Esta alta fluorescencia se apaga con la formación del complejo de hierro.
7. La interacción con el hierro produce efectos secundarios como la disminución del pH. Este es un efecto negativo en el caso del uso de IGIs, ya que induce una degradación progresiva del papel. Además, se demostró que el pH disminuye aún más con el tiempo después de la deposición del complejo sobre el papel.
8. La formación del complejo conduce a la extinción de la fluorescencia, y esto es un efecto positivo para el estudio de estos complejos por Raman, ya que los polifenoles muestran una fuerte emisión de fluorescencia que se superpone a la señal Raman.
9. La presencia de goma arábiga en las tintas IGI parece primordial para inducir una protección del polifenol, previniendo la oxidación y acidificación debido a la formación de enlaces H entre los grupos hidroxilo del polifenol y el polisacárido.
10. La espectroscopia SERS proporcionó información estructural útil sobre los complejos e indujo una gran intensificación de la emisión Raman, principalmente en las NP de Ag reducidas en citrato.
11. La presencia de nanopartículas metálicas provoca un cambio estructural con la formación de enlaces H entre el citrato adsorbido en el metal y el complejo. El citrato actúa como ensamblador atrayendo polifenoles y cambiando la esfera de coordinación del hierro.
12. La adsorción de complejos de polifenol/hierro sobre nanopartículas plasmónicas induce una rápida modificación estructural del complejo similar al efecto de envejecimiento observado en manuscritos históricos de diferentes siglos, consistente en un debilitamiento del modo ν_2 y el gran cambio de las vibraciones de FeO.

13. El análisis de manuscritos históricos por parte de Raman reveló las claves para la interpretación del efecto de envejecimiento de las tintas con hiel de hierro, que consiste en la oxidación e hidrólisis de los polifenoles, junto con un cambio en el patrón de coordinación del hierro.

14. El pH deducido del análisis de los manuscritos históricos indica que se produce una mayor acidificación de los manuscritos a medida que pasa el tiempo.

15. El análisis de manuscritos de finales del siglo XIX y principios del XX reveló la presencia de colorantes sintéticos modernos que se añadían a las tintas IGI durante ese periodo.

6. REFERENCES

References

[1] R. Halleux, “Papyrus de Leyden, papyrus de Stockholm, fragments de recettes.,” in *Les alchimistes grecs*, Paris, 1981.

[2] D. M. Goltz, “A Review of Instrumental Approaches for Studying Historical Inks,” *Anal. Lett.*, vol. 45, no. 4, pp. 314–329, Mar. 2012.

[3] É. Delange, M. Grange, B. Kusko, and E. Menei, “Apparition de l’encre métallogallique en Egypte à partir de la collection de papyrus du Louvre,” *Rev. Egyptol.*, vol. 41, no. 0, pp. 213–217, Jan. 1990.

[4] A. S. Lee, P. J. Mahon, and D. C. Creagh, “Raman analysis of iron gall inks on parchment,” *Vib. Spectrosc.*, vol. 41, no. 2, pp. 170–175, Aug. 2006.

[5] “Archives and libraries,” in *The South China Sea: A Crucible of Regional Cooperation or Conflict-making Sovereignty Claims?*, Cambridge University Press, 2016, pp. 335–357.

[6] L. Gál, M. Ciglanská, M. Čeppan, B. Havl\’\inová, V. Jančovičová, and M. Reháková, “Chemické aspekty degradácie historick{\`y}ch dokumentov so železogalov{\`y}mi atramentami,” *Chem. List.*, vol. 108, no. 3, pp. 191–197, 2014.

[7] J. Kolar *et al.*, “Historical iron gall ink containing documents—properties affecting their condition,” *Anal. Chim. Acta*, vol. 555, no. 1, pp. 167–174, 2006.

[8] W. Kiefer, A. P. Mazzolini, and P. R. Stoddart, “Recent Advances in linear and nonlinear Raman spectroscopy I,” *J. Raman Spectrosc.*, vol. 38, no. April, pp. 1538–1553, 2007.

[9] M. Ursescu, T. Măluţan, and S. Ciovică, “Iron gall inks influence on papers’ thermal degradation FTIR spectroscopy applications,” *Eur. J. Sci. Theol.*, vol. 5, no. 3, pp. 71–84, 2009.

[10] H. Wilson, “Analysis of the current research into the chemistry of Iron Gall Ink and its implications for Paper Conservation,” *Honour Sch. Chem. Chem. part II. St. Anne’s Coll. Conserv. by Des. Timecare Work.*, vol. 5, 2007.

[11] M. Rashad, M. Rüsing, G. Berth, K. Lischka, and A. Pawlis, “CuO and Co3O4 nanoparticles: Synthesis, characterizations, and raman spectroscopy,” *J. Nanomater.*, vol. 2013, 2013.

[12] M. C. Alvarez-Ros, S. Sánchez-Cortés, O. Francioso, and J. V. García-Ramos, “Catalytic modification of gallic acid on a silver surface studied by surface-enhanced Raman spectroscopy,” *J. Raman Spectrosc.*, vol. 32, no. 2, pp. 143–145, Feb. 2001.

[13] C. Remazeilles, V. Rouchon-Quillet, and J. Bernard, “Influence of gum Arabic on iron gall ink corrosion. Part I: A laboratory samples study,” 2004.

[14] V. Jančovičová, M. Čeppan, B. Havl\’\inová, M. Reháková, and Z. Jakub\’\iková, “Interactions in iron gall inks,” *Chem. Pap.*, vol. 61, no. 5, pp. 391–397, 2007.

[15] G. M. C. Zamorano, “La tinta de escritura en los manuscritos de archivo valencianos, 1250-1600. Análisis, identificación de componentes y valoración de su estado de conservación,” Universitat de València, 2015.

[16] J. H. I. Martínez, “No Title,” in *ESTRUCTURA MOLECULAR Y APLICACIONES DE POLIFENOLES VEGETALES.*, 2005.

[17] J. Wisniak, “Nicolas-Jean-Baptiste-Gaston Guibourt.,” *Educ. química*, vol. 27, no. 2, pp. 163–171, 2016.

[18] C. A. Mitchell, “The colorimetric estimation of pyrogallol, gallotannin and gallic acid.,” *Analyst*, vol. 48, no. 562, pp. 2-15., 1923.

[19] S. K. Kroustallis, *Diccionario de Materias y Técnicas II. Secretaría general.* 2008.

[20] T. de de Paris, “morale et d’économie domestique composé vers 1393, par un bourgois Parisien,” *Paris Impr. Crapelet*, 1846.

[21] G. L. Greco and C. M. Rose, *The Good Wife’s Guide (Le Ménagier de Paris): Le ménagier de Paris: a medieval household book*. Cornell University Press, 2012.

[22] M. P. Merrifield, *Original Treatises: Dating from the XIIth to XVIIIth Centuries on the Arts of Painting, in Oil, Miniature, Mosaic, and on Glass; of Gilding, Dyeing, and the Preparation of Colours and Artificial Gems; Preceded by a General Introduction; with Translations,* vol. 2. J. Murray, 1849.

[23] H. Sauer, “The Transmission and Structure of Archbishop Wulfstan’s ‘Commonplace Book,’” in *Old English Prose*, Routledge, 2021, pp. 339–393.

[24] M. Zerdoun-Bat-Yehouda, “Les Encres Noires Au Moyen Âge,” *Ed. du CNRS Paris*, 1983.

[25] K. Nassau, *The physics and chemistry of color: the fifteen causes of color*. 2001.

[26] R. Christie, *Colour chemistry*. Royal society of chemistry, 2014.

[27] E. N. Abrahart, “Dyes and their intermediates,” 1977.

[28] A. Byrne and D. R. Hilbert, “Readings on Color: The Science of Color. vol. 2.” MIT Press, 1997.

[29] G. B. Z. C. Wunderlich, R. Weber, “No Title,” *iron Gall. ink. Allg. Chemie*, pp. 371–376, 1991.

[30] A. Ponce *et al.*, “Elucidation of the Fe (III) gallate structure in historical iron gall ink,” *Anal. Chem.*, vol. 88, no. 10, pp. 5152–5158, 2016.

[31] M. Budnar *et al.*, “In-air PIXE set-up for automatic analysis of historical document inks,” *Nucl. Instruments Methods Phys. Res. Sect. B Beam Interact. with Mater. Atoms*, vol. 219, pp. 41–47, 2004.

[32] I. G. I. Meeting and N. University, *The Iron Gall Ink Meeting: 4th & 5th September 2000, The University of Northumbria, Newcastle upon Tyne; postprints;[First Triannial Conservation Conference]*. Conservation of Fine Art, School of Humanities, The University of Northumbria.

[33] C. Remazeilles, V. Quillet, T. Calligaro, J. C. Dran, L. Pichon, and J. Salomon, “PIXE elemental mapping on original manuscripts with an external microbeam. Application to manuscripts damaged by iron-gall ink corrosion,” *Nucl. Instruments Methods Phys. Res. Sect. B Beam Interact. with Mater. Atoms*, vol. 181, no. 1–

4, pp. 681–687, 2001.
[34] B. Wagner, E. Bulska, A. Hulanicki, M. Heck, and H. M. Ortner, “Topochemical investigation of ancient manuscripts,” *Fresenius. J. Anal. Chem.*, vol. 369, no. 7, pp. 674–679, 2001.
[35] J. Burandt, “An investigation toward the identification of traditional drawing inks,” *B. Pap. Gr.*, vol. 13, 1994.
[36] O. Hahn, W. Malzer, B. Kanngießer, B. Beckhoff, and U. Waldschläger, “Characterization of iron gall inks in historical manuscripts using micro X-ray fluorescence spectrometry,” in *Proceedings of the European Conference on Energy Dispersive X-Ray Spectrometry*, 2002, p. 83.
[37] B. Wagner, E. Bulska, T. Meisel, and W. Wegscheider, “Use of atomic spectrometry for the investigation of ancient manuscripts,” *J. Anal. At. Spectrom.*, vol. 16, no. 4, pp. 417–420, 2001.
[38] R. Van Grieken, “7th International conference on non-destructive testing and microanalysis for the diagnostics and conservation of the cultural and environmental heritage: 2-6 June 2002... Antwerp, Belgium: proceedings,” 2002.
[39] C. Burgaud, V. Rouchon, P. Refait, and A. Wattiaux, “Mössbauer spectrometry applied to the study of laboratory samples made of iron gall ink,” *Appl. Phys. A Mater. Sci. Process.*, vol. 92, no. 1, pp. 257–262, Jul. 2008.
[40] M. Proost, K., Janssens, K., Wagner, B., Bulska, E. & Schreiner, “Determination of localized Fe2+/Fe3+ ratios in inks of historic documents by means of μ-XANES. Nucl. Instruments Methods Phys. Res. Sect. B Beam Interact. with Mater.,” *Atoms 213*, pp. 723–728, 2004.
[41] Arpino, P. et al., “‘Gas chromatographic-mass spectrometric analysis of tannin hydrolysates from the ink of ancient manuscripts (XIth to XVIth century).,’” *J. Chromatogr. A 134.2*, pp. 433-439., 1977.
[42] J. Senvaitiene, A. Beganskiene, and A. Kareiva, “Spectroscopic evaluation and characterization of different historical writing inks,” *Vib. Spectrosc.*, vol. 37, no. 1, pp. 61–67, 2005.
[43] X. Zhang, R. Boytner, J. L. Cabrera, and R. Laursen, “Identification of yellow dye types in pre-Columbian Andean textiles,” *Anal. Chem.*, vol. 79, no. 4, pp. 1575–1582, 2007.
[44] E. de Rijke *et al.*, “Analytical separation and detection methods for flavonoids,” *J. Chromatogr. A*, vol. 1112, no. 1–2, pp. 31–63, 2006.
[45] P. J. G. Bell, Ian M., Robin JH Clark, “‘Raman spectroscopic library of natural and synthetic pigments (pre-≈ 1850 AD).,’” *Spectrochim. Acta Part A Mol. Biomol. Spectrosc. 53.12*, pp. 2159–2179, 1997.
[46] P. Vandenabeele et al., “‘Comparative study of mobile Raman instrumentation for art analysis.,’” *Anal. Chim. Acta 588.1*, pp. 108–116, 2007.
[47] R. P. V. D. Casadio, Francesca, “‘Molecular analysis for art, archaeometry and conservation.,’” *Anal. 138.24*, pp. 7276-7278., 2013.
[48] P. Vandenabeele, H. G. M. Edwards, and L. Moens, “A Decade of Raman Spectroscopy in Art and Archaeology,” *Chem. Rev.*, vol. 107, no. 3, pp. 675–686, Mar. 2007.
[49] G. Piantanida, E. Menart, M. Bicchieri, and M. Strlič, “Classification of iron-based inks by means of micro-Raman spectroscopy and multivariate data analysis,” *J. Raman Spectrosc.*, vol. 44, no. 9, pp. 1299–1305, 2013.
[50] R. J. Clark, “‘Raman microscopy: application to the identification of pigments on medieval manuscripts.,’” *Chem. Soc. Rev. 24.3*, pp. 187-196., 1995.
[51] R. J. C. Burgio, Lucia, Dan A. Ciomartan, “‘Raman microscopy study of the pigments on three illuminated mediaeval Latin manuscripts.,’” *J. Raman Spectrosc. 28.2-3*, pp. 79-83., 1997.
[52] P. J. G. Clark, Robin JH, “‘Analysis of 16th century Qazwını manuscripts by Raman microscopy and remote laser Raman microscopy.,’” *J. Archaeol. Sci. 25.7*, pp. 621-629., 1998.
[53] P. Vandenabeele et al., “‘Pigment investigation of a late-medieval manuscript with total reflection X-ray fluorescence and micro-Raman spectroscopy.,’” *Anal. 124.2*, pp. 169-172., 1999.
[54] R. J. C. Smith, Gregory D., “‘Raman microscopy in art history and conservation science.,’” *Stud. Conserv. 46.sup1*, pp. 92-106., 2001.
[55] R. J. C. Brown, Katherine L., “‘Analysis of key Anglo-Saxon manuscripts (8–11th centuries) in the British Library: pigment identification by Raman microscopy.,’” *J. Raman Spectrosc. 35.3*, pp. 181-189., 2004.
[56] H. G. Pagès-Camagna, Sandrine, Alain Duval, “‘Study of Gustave Moreau’s black drawings: identification of the graphic materials by Raman microspectrometry and PIXE.,’” *J. Raman Spectrosc. 35.8-9*, pp. 628-632., 2004.
[57] El Bakkali, Ahmed et al., “‘Non-invasive micro Raman, SERS and visible reflectance analyses of coloring materials in ancient Moroccan Islamic manuscripts.,’” *J. Raman Spectrosc. 44.1*, pp. 114–120, 2013.
[58] D. Kurouski, S. Zaleski, F. Casadio, R. P. Van Duyne, and N. C. Shah, “Tip-Enhanced Raman Spectroscopy (TERS) for in Situ Identi fi cation of Indigo and Iron Gall Ink on Paper,” 2014.
[59] Kneipp, Katrin, “‘Single molecule detection using surface-enhanced Raman scattering (SERS).,’” *Phys. Rev. Lett. 78.9*, p. 1667., 1997.
[60] S. R. E. Nie, Shuming, “‘Probing single molecules and single nanoparticles by surface-enhanced Raman scattering.,’” *Sci. 275.5303*, pp. 1102-1106., 1997.
[61] D. P. Benedetti, et al., “‘In situ microanalysis of organic colorants by inkjet colloid deposition surface-enhanced Raman scattering.,’” *J. Raman Spectrosc. 45.1*, pp. 123-127., 2014.
[62] S. Sánchez-Cortés, O. Francioso, J. . García-Ramos, C. Ciavatta, and C. Gessa, “Catechol polymerization in the presence of silver surface,” *Colloids Surfaces A Physicochem. Eng. Asp.*, vol. 176, no. 2–3, pp. 177–184, Jan. 2001.
[63] S. Sánchez-Cortés and J. V. García-Ramos, “Adsorption and Chemical Modification of Phenols on a Silver Surface,” *J. Colloid Interface Sci.*, vol. 231, no. 1, pp. 98–106, Nov. 2000.

[64] Nastova, Irena, "'Micro-Raman spectroscopic analysis of inks and pigments in illuminated medieval old-Slavonic manuscripts.,'" *J. Raman Spectrosc. 43.11*, pp. 1729-1736., 2012.
[65] S. A. Centeno, "Identification of artistic materials in paintings and drawings by Raman spectroscopy: Some challenges and future outlook," *J. Raman Spectrosc.*, vol. 47, no. 1, pp. 9–15, Jan. 2016.
[66] M. T. Domenech-Carbo, "'Novel analytical methods for characterising binding media and protective coatings in artworks.,'" *Anal. Chim. Acta 621.2*, pp. 109-139., 2008.
[67] J. V. García Ramos, *Las moléculas: Cuando la luz te ayuda a vibrar.* 2014.
[68] P. Larkin, "Infrared and Raman spectroscopy: principles and spectral interpretation.," 2017.
[69] J. L. Snively, C. M., & Koenig, "Polymer applications of IR and Raman Spectroscopy.," 1999.
[70] E. C. Le Ru and P. G. Etchegoin, *Principles of Surface enhanced Raman spectroscopy (and related plasmonic effects)*. Amsterdam, the Netherlands: Elsevier, 2009.
[71] I. Izquierdo-Lorenzo, I. Alda, S. Sanchez-Cortes, and J. V Garcia-Ramos, "Adsorption and detection of sport doping drugs on metallic plasmonic nanoparticles of different morphology," *Langmuir*, 2012.
[72] R. Aroca, M. Campos-Vallette, J. V. Garc\'\ia-Ramos, S. Sánchez-Cortés, J. A. Sánchez-Gil, and P. Sevilla, *Amplificación plasmónica de espectros Raman y de fluorescencia: SERS y SEF sobre nanoestructuras metálicas.* Consejo Superior de Investigaciones Cient{\'\i}ficas (España), 2014.
[73] B. A. Leopold, N.; Lendl, "New Method for Fast Preparation of Highly Surface-Enhanced Raman Scattering (SERS) Active Silver Colloids at Room Temperature by Reduction of Silver Nitrate with Hydroxylamine Hydrochloride.," *J. Phys. Chem . B*, vol. 107, pp. 5723–5727, 2003.
[74] S. Garcia-Leis, A.; Garcia-Ramos, J.V.; Sanchez-Cortes, "Silver Nanostars with High SERS Performance.," *J. Phys. Chem. C*, vol. 117, pp. 7791–7795, 2013.
[75] G. C. Frens, "Nucleation for the Regulation of the Particle Size in Monodisperse Gold Suspensions.," *Nat. Phys. Sci.*, vol. 241, no. 20–22, 1973.
[76] M. Ciglanská, V. Jančovičová, B. Havlínová, Z. Machatová, and V. Brezová, "The influence of pollutants on accelerated ageing of parchment with iron gall inks," *J. Cult. Herit.*, vol. 15, no. 4, pp. 373–381, 2014.
[77] A. García Leis, "'Espectroscopía Raman intensificada por superficie de biomoléculas a través de nanopartículas plasmónicas ultrasensibles.,'" 2015.
[78] and J. V. G.-R. Sánchez-Cortés, S., "'Adsorption and chemical modification of phenols on a silver surface.,'" *J. colloid interface Sci. 231.1*, pp. 98-106., 2000.
[79] S. Sánchéz-Cortés and J. V. García-Ramos, "FT Surface-Enhanced Raman Evidence of the Oxidative Condensation Reactions of Caffeic Acid in Solution and on Silver Surface," *Appl. Spectrosc.*, vol. 54, no. 2, pp. 230–238, Feb. 2000.
[80] S. Canamares, M. V., Garcia-Ramos, J. V., Gomez-Varga, J. D., Domingo, C., & Sanchez-Cortes, "Comparative study of the morphology, aggregation, adherence to glass, and surface-enhanced Raman scattering activity of silver nanoparticles prepared by chemical reduction of Ag+ using citrate and hydroxylamine.," *Langmuir*, vol. 21(18), pp. 8546-8553., 2005.
[81] J. D. Sutherland, W. S., & Winefordner, "Colloid filtration: a novel substrate preparation method for surface-enhanced Raman spectroscopy.," *J. Colloid Interface Sci.*, vol. 148(1), pp. 129–141, 1992.
[82] A. Espina, S. Sanchez-Cortes, and Z. Jurašeková, "Vibrational Study (Raman, SERS, and IR) of Plant Gallnut Polyphenols Related to the Fabrication of Iron Gall Inks," *Mol. 2022, Vol. 27, Page 279*, vol. 27, no. 1, p. 279, Jan. 2022.
[83] M.-B. P., "Review of SERS substrates for chemical sensing.," *Nanomaterials*, vol. 7, no. 6, p. 142, 2017.
[84] S. Y. Zhang, P. X., Fang, Y., Wang, W. N., Ni, D. H., & Fu, "Influence of addition of potassium chloride to silver colloids.," *J. Raman Spectrosc.*, vol. 21, no. 2, pp. 127–131, 1990.
[85] Chris Stavroudis, "Measuring pH and Conductivity with Horiba Meters," 2018. .
[86] A. Vega-Bosch, V. Santamarina-Campos, A. Colomina-Subiela, and M.-Á. Carabal-Montagud, "Cryogenics as an Advanced Method of Cleaning Cultural Heritage Challenges and Solutions," *Sustainability*, vol. 14, no. 3, p. 1052, 2022.
[87] D. J. F. M.J. Frisch, G.W. Trucks, H.B. Schlegel, G.E. Scuseria, M.A. Robb, J.R. Cheeseman, G. Scalmani, V. Barone, B. Mennucci, G.A. Petersson, H. Nakatsuji, M. Caricato, X. Li, H.P. Hratchian, A.F. Izmaylov, J. Bloino, G. Zheng, J.L. Sonnenberg, M. Hada, M. Ehar, "Gaussian 09, Revision A.01." Gaussian, Inc., Wallingford CT, 2009.
[88] S. Espina, A., Cañamares, M. V., Jurašeková, Z., & Sanchez-Cortes, "Analysis of Iron Complexes of Tannic Acid and Other Related Polyphenols as Revealed by Spectroscopic Techniques: Implications in the Identification and Characterization of Iron Gall Inks in Historical Manuscripts.," *ACS omega.*, 2022.
[89] A. Ponce *et al.*, "Elucidation of the Fe(III) Gallate Structure in Historical Iron Gall Ink," *Anal. Chem.*, vol. 88, no. 10, pp. 5152–5158, May 2016.
[90] L. Öhrström and I. Michaud-Soret, "Fe−Catecholate and Fe−Oxalate Vibrations and Isotopic Substitution Shifts from DFT Quantum Chemistry," *J. Phys. Chem. A*, vol. 103, no. 2, pp. 256–264, 1999.
[91] D. Yapo-Kicho, P. Lagant, and G. Vergoten, "The SPASIBA force field for studying iron-tannins interactions: Application to Fe 3+/Fe 2+ catechol complexes," *Int. J. Mol. Sci.*, vol. 8, no. 3, pp. 259–272, Mar. 2007.
[92] P. J. Hay and W. R. Wadt, "Ab initio effective core potentials for molecular calculations. Potentials for K to Au including the outermost core orbitals," *J. Chem. Phys.*, vol. 82, no. 1, p. 299, Aug. 1998.
[93] M. J. Martelo-Vidal and M. Vázquez, "Determination of polyphenolic compounds of red wines by UV-VIS-NIR spectroscopy and chemometrics tools," *Food Chem.*, vol. 158, pp. 28–34, Sep. 2014.
[94] V. Jančovičová, M. Čeppan, B. Havlínová, M. Reháková, and Z. Jakubíková, "Interactions in iron gall inks," *Chem. Pap.*, vol. 61, no. 5, pp. 391–397, Oct. 2007.

[95] E. Bulska, B. Wagner, and M. G. Sawicki, “Investigation of Complexation and Solid–liquid Extraction of Ironfrom Paper by UV/VIS and Atomic Absorption Spectrometry,” *Microchim. Acta 2001 1361*, vol. 136, no. 1, pp. 61–66, 2001.
[96] J. M. Antosiewicz and D. Shugar, “UV–Vis spectroscopy of tyrosine side-groups in studies of protein structure. Part 1: basic principles and properties of tyrosine chromophore,” *Biophys. Rev.*, vol. 8, no. 2, p. 151, Jun. 2016.
[97] J. C. D. W. F. Forbes, “LIGHT ABSORPTION STUDIES PART XIV. THE ULTRAVIOLET ABSORPTION SPECTRA OF PHENOLS1,” *Can. J. Chem.*, vol. 37, p. 1294, 1959.
[98] S. Selvaraj, P. Rajkumar, K. Thirunavukkarasu, S. Gunasekaran, and S. Kumaresan, “Vibrational (FT-IR and FT-Raman), electronic (UV–vis) and quantum chemical investigations on pyrogallol: A study on benzenetriol dimers,” *Vib. Spectrosc.*, vol. 95, pp. 16–22, Mar. 2018.
[99] L. Falcão and M. E. M. Araújo, “Tannins characterization in historic leathers by complementary analytical techniques ATR-FTIR, UV-Vis and chemical tests,” *J. Cult. Herit.*, vol. 14, no. 6, pp. 499–508, 2013.
[100] M. Andjelković *et al.*, “Iron-chelation properties of phenolic acids bearing catechol and galloyl groups,” *Food Chem.*, vol. 98, no. 1, pp. 23–31, Jan. 2006.
[101] J. I. Ballesteros, H. J. R. Caleja-Ballesteros, and M. C. Villena, “Digital image-based method for iron detection using green tea (Camellia sinensis) extract as natural colorimetric reagent,” *Microchem. J.*, vol. 160, p. 105652, Jan. 2021.
[102] M. Elhabiri, C. Carrër, F. Marmolle, and H. Traboulsi, “Complexation of iron(III) by catecholate-type polyphenols,” *Inorganica Chim. Acta*, vol. 360, no. 1, pp. 353–359, Jan. 2007.
[103] R.H. Janssen, et al., “‘Iron-polyphenol complexes cause blackening upon grinding Hermetia illucens (black soldier fly) larvae.,’” *Sci. reports 9.1*, pp. 1-11., 2019.
[104] A. Torreggiani, Z. Jurasekova, S. Sanchez-Cortes, and M. Tamba, “Spectroscopic and pulse radiolysis studies of the antioxidant properties of (+)catechin: metal chelation and oxidizing radical scavenging,” *J. Raman Spectrosc.*, vol. 39, no. 2, pp. 265–275, Feb. 2008.
[105] C. Chikere, N. Faisal, P. Kong Thoo Lin, and C. Fernandez, “Interaction between Amorphous Zirconia Nanoparticles and Graphite: Electrochemical Applications for Gallic Acid Sensing Using Carbon Paste Electrodes in Wine,” 2020.
[106] T. B. Karpishin, M. S. Gebhard, E. I. Solomon, and K. N. Raymond, “Spectroscopic studies of the electronic structure of iron(III) tris(catecholates),” *J. Am. Chem. Soc.*, vol. 113, no. 8, pp. 2977–2984, 2002.
[107] P. Flowers, K. H. Theopold, R. Langley, and W. R. Robinson, *Chemistry 2e*. OpenStax, 2019.
[108] J. Huguenin, S. O. S. Hamady, and P. Bourson, “Monitoring deprotonation of gallic acid by Raman spectroscopy,” *J. Raman Spectrosc.*, vol. 46, no. 11, pp. 1062–1066, Nov. 2015.
[109] D. R. Pompeu, Y. Larondelle, H. Rogez, O. Abbas, J. A. F. Pierna, and V. Baeten, “Characterization and discrimination of phenolic compounds using Fourier transform Raman spectroscopy and chemometric tools,” *Biotechnol. Agron. Société Environ.*, vol. 22, no. 1, pp. 13–28, 2018.
[110] S. Nam *et al.*, “A reinforced thermal barrier coat of a Na–tannic acid complex from the view of thermal kinetics,” *RSC Adv.*, vol. 9, no. 19, pp. 10914–10926, Apr. 2019.
[111] Å. Henrik-Klemens, F. Bengtsson, and C. G. Björdal, “Raman Spectroscopic Investigation of Iron-Tannin Precipitates in Waterlogged Archaeological Oak,” *Stud. Conserv.*, 2021.
[112] I. Mohammed-Ziegler and F. Billes, “Vibrational spectroscopic calculations on pyrogallol and gallic acid,” *J. Mol. Struct. THEOCHEM*, vol. 3, no. 618, pp. 259–265, 2002.
[113] R. E. Clavijo, D. J. Ross, and R. F. Aroca, “Surface enhanced Raman scattering of trans-p-coumaric and syringic acids,” *J. Raman Spectrosc.*, vol. 40, no. 12, pp. 1984–1988, Dec. 2009.
[114] R. Ramasamy, “Vibrational Assignments of FT-IR and FT-Raman Spectra of Pyrogallol,” *Int. J. Eng. Res. Appl.*, vol. 6, pp. 64–68, 2016.
[115] C. Garrido, G. Diaz-Fleming, and M. M. Campos-Vallette, “SERS spectrum of gallic acid obtained from a modified silver colloid,” *Spectrochim. Acta. A. Mol. Biomol. Spectrosc.*, vol. 163, pp. 68–72, Jun. 2016.
[116] E. Clavijo, J. R. Menéndez, and R. Aroca, “Vibrational and surface-enhanced Raman spectra of vanillic acid,” *J. Raman Spectrosc.*, vol. 39, no. 9, pp. 1178–1182, Sep. 2008.
[117] A. Ricci, K. J. Olejar, G. P. Parpinello, P. A. Kilmartin, and A. Versari, “Application of Fourier transform infrared (FTIR) spectroscopy in the characterization of tannins,” *Appl. Spectrosc. Rev.*, vol. 50, no. 5, pp. 407–442, May 2015.
[118] F. Billes, I. Mohammed-Ziegler, and P. Bombicz, “Vibrational spectroscopic study on the quantum chemical model and the X-ray structure of gallic acid, solvent effect on the structure and spectra,” *Vib. Spectrosc.*, vol. 1, no. 43, pp. 193–202, Jan. 2007.
[119] G. Socrates, *Infrared and Raman Characteristic Group Frequencies: Tables and Charts*. John Wiley & Sons, 2004.
[120] Z. Xia, A. Singh, W. Kiratitanavit, R. Mosurkal, J. Kumar, and R. Nagarajan, “Unraveling the mechanism of thermal and thermo-oxidative degradation of tannic acid,” *Thermochim. Acta*, vol. 605, pp. 77–85, Apr. 2015.
[121] M. Bicchieri, M. Monti, G. Piantanida, and A. Sodo, “Non-destructive spectroscopic investigation on historic Yemenite scriptorial fragments: Evidence of different degradation and recipes for iron tannic inks,” *Anal. Bioanal. Chem.*, vol. 405, no. 8, pp. 2713–2721, Mar. 2013.
[122] T. G. Gardner, A. M., & Wright, “Consistent assignment of the vibrations of monosubstituted benzenes.,” *J. Chem. physics, 135(11)*, p. 114305., 2011.
[123] G. Varsányi, *Vibrational spectra of benzene derivatives*. Elsevier, 2012.
[124] S. Salama, J. D. Stong, T. G. Spiro, and J. B. Neilands, “Electronic and Resonance Raman Spectra of Iron(III)

Complexes of Enterobactin, Catechol, and N-Methyl-2,3-dihydroxybenzamide," *Biochemistry*, vol. 17, no. 18, pp. 3781–3785, 1978.
[125] R. Wrzalik, K. Merkel, and A. Kocot, "Ab initio study of phenyl benzoate: Structure, conformational analysis, dipole moment, IR and Raman vibrational spectra," *J. Mol. Model.*, vol. 9, no. 4, pp. 248–258, 2003.
[126] M. Bagheri, S. M. Jafari, and M. H. Eikani, "Development of ternary nanoadsorbent composites of graphene oxide, activated carbon, and zero-valent iron nanoparticles for food applications," *Food Sci. Nutr.*, vol. 7, no. 9, pp. 2827–2835, Sep. 2019.
[127] M. A. Rahim *et al.*, "Surface-Confined Amorphous Films from Metal-Coordinated Simple Phenolic Ligands," *Chem. Mater.*, vol. 27, no. 16, pp. 5825–5832, Aug. 2015.
[128] N. R. Perron and J. L. Brumaghim, "A Review of the Antioxidant Mechanisms of Polyphenol Compounds Related to Iron Binding," *Cell Biochem. Biophys. 2009 532*, vol. 53, no. 2, pp. 75–100, Jan. 2009.
[129] R. J. Díaz Hidalgo *et al.*, "New insights into iron-gall inks through the use of historically accurate reconstructions," *Herit. Sci.*, vol. 6, no. 1, Dec. 2018.
[130] C. Krekel, "NCJRS Abstract - National Criminal Justice Reference Service," *Int. J. Forensic Doc. Exam.*, vol. 5, pp. 54–58, 1999.
[131] J. C. Danilewicz, P. Tunbridge, and P. A. Kilmartin, "Wine Reduction Potentials: Are These Measured Values Really Reduction Potentials?," *J. Agric. Food Chem.*, vol. 67, no. 15, pp. 4145–4153, Apr. 2019.
[132] H. Elhabiri, M.; Carrër, C.; Marmolle, F.; Traboulsi, "Complexation of Iron(III) by Catecholate-Type Polyphenols.," *Inorganica Chim. Acta 2007, 360*, pp. 353–359.
[133] M. Bronzato, A. Zoleo, B. Biondi, and S. A. Centeno, "An insight into the metal coordination and spectroscopic properties of artistic Fe and Fe/Cu logwood inks," *Spectrochim. Acta - Part A Mol. Biomol. Spectrosc.*, vol. 153, pp. 522–529, 2016.
[134] R. J. Elias and A. L. Waterhouse, "Controlling the Fenton Reaction in Wine," *J. Agric. Food Chem.*, vol. 58, no. 3, pp. 1699–1707, Feb. 2010.
[135] J. A. Jaén, L. González, A. Vargas, and G. Olave, "Gallic Acid, Ellagic Acid and Pyrogallol Reaction with Metallic Iron," in *Hyperfine Interactions*, 2003, vol. 148–149, no. 1–4, pp. 227–235.
[136] J. C. Danilewicz, "Role of tartaric and malic acids in wine oxidation," *J. Agric. Food Chem.*, vol. 62, no. 22, pp. 5149–5155, Jun. 2014.
[137] R. K. Feller and A. K. Cheetham, "Fe(III), Mn(II), Co(II), and Ni(II) 3,4,5-trihydroxybenzoate (gallate) dihydrates; a new family of hybrid framework materials," *Solid State Sci.*, vol. 8, no. 9, pp. 1121–1125, Sep. 2006.
[138] G. Venkatesham, M., Ayodhya, D., Madhusudhan, A., & Veerabhadram, "Synthesis of stable silver nanoparticles using gum acacia as reducing and stabilizing agent and study of its microbial properties: A novel green approach.," *Int. J. green nanotechnology, 4(3)*, 2012.
[139] A. Maher, T., Kabbashi, N. A., Mirghani, M. E., Alam, M. Z., Daddiouaissa, D., Abdulhafiz, F., ... & Mohammed, "Optimization of Ultrasound-Assisted Extraction of Bioactive Compounds from Acacia Seyal Gum Using Response Surface Methodology and Their Chemical Content Identification by Raman, FTIR, and GC-TOFMS.," *Antioxidants, 10(10)*, p. 1612., 2021.
[140] B. Kostadinova, M., Jakovlevska-Spirovska, Z., & Minčeva-Šukarova, "Spectroscopic study of inks from rare old slavic munuscript: Liturgical proceedings with chronicle, scripture, etc.," 2013.
[141] D.ChiriuP.C.RicciG.Cappellini, "Raman characterization of XIV–XVI centuries Sardinian documents: Inks, papers and parchments," *Elsevier*, vol. 90, pp. 70–81, 2017.
[142] et al. Piantanida, Giovanna, "'Classification of iron-based inks by means of micro-Raman spectroscopy and multivariate data analysis.,'" *J. Raman Spectrosc. 44.9*, pp. 1299-1305., 2013.
[143] D. Kurouski, S. Zaleski, F. Casadio, R. P. Van Duyne, and N. C. Shah, "Tip-enhanced raman spectroscopy (TERS) for in situ identification of indigo and iron gall ink on paper," *J. Am. Chem. Soc.*, vol. 136, no. 24, pp. 8677–8684, Jun. 2014.
[144] J. Hanus and E. Hanusová, "ARCHIVES AND LIBRARIES-POSSIBILITIES AND NECESSITY FOR PROFESSIONAL COOPERATION."
[145] Z. Jurasekova, C. Domingo, J. V. Garcia-Ramos, and S. Sanchez-Cortes, "Adsorption and catalysis of flavonoid quercetin on different plasmonic metal nanoparticles monitored by SERS," *J. Raman Spectrosc.*, vol. 43, no. 12, pp. 1913–1919, Dec. 2012.
[146] J. Łojewska, T. Miśkowiec Paweland Łojewski, and L. M. Proniewicz, "Cellulose oxidative and hydrolytic degradation: In situ FTIR approach," *Polym. Degrad. Stab.*, vol. 88, no. 3, pp. 512–520, 2005.
[147] Y. Liu, I. K. Cigić, and M. Strlič, "Kinetics of accelerated degradation of historic iron gall ink-containing paper," *Polym. Degrad. Stab.*, vol. 142, pp. 255–262, 2017.
[148] A. Potthast, U. Henniges, and G. Banik, "Iron gall ink-induced corrosion of cellulose: aging, degradation and stabilization. Part 1: model paper studies," *Cellulose*, vol. 15, no. 6, pp. 849–859, 2008.
[149] J. Malešič, M. Šala, V. S. Šelih, and D. Kočar, "Evaluation of a method for treatment of iron gall ink corrosion on paper," *Cellulose*, vol. 21, no. 4, pp. 2925–2936, 2014.
[150] G. Varsányi, *Vibrational spectra of benzene derivatives*. New York: Academic Press, 1969.
[151] E. A. Carter, F. R. Perez, J. M. Garcia, and H. G. M. Edwards, "Raman spectroscopic analysis of an important Visigothic historiated manuscript," *Philos. Trans. R. Soc. A Math. Phys. Eng. Sci.*, vol. 374, no. 2082, Dec. 2016.
[152] H. Monti, S., Barcaro, G., Sementa, L., Carravetta, V., & Ågren, "Characterization of the adsorption dynamics of trisodium citrate on gold in water solution.," *RSC Adv.*, vol. 7, no. 78, pp. 49655–49663, 2017.
[153] N. S. Gonçolves, A. Horn, M. Lanznaster, L. K. Noda, and A. Neves, "Resonance Raman spectroscopy of

FeIIFeIII and Fe IIIFeIII model complexes containing an unsymmetrical dinucleating ligand: A biomimetic redox pair for uteroferrin," in *Journal of the Brazilian Chemical Society*, 2006, vol. 17, no. 8, pp. 1658–1663.
[154] A. Raza and B. Saha, "Silver nanoparticles doped agarose disk: Highly sensitive surface-enhanced Raman scattering substrate for in situ analysis of ink dyes," *Forensic Sci. Int.*, vol. 233, no. 1–3, pp. 21–27, 2013.
[155] R. H. Janssen *et al.*, "Iron-polyphenol complexes cause blackening upon grinding Hermetia illucens (black soldier fly) larvae."
[156] J. Kunze, J., Burgess, I., Nichols, R., Buess-Herman, C., & Lipkowski, "Electrochemical evaluation of citrate adsorption on Au (1 1 1) and the stability of citrate-reduced gold colloids.," *J. Electroanal. Chem.*, vol. 599, no. 2, pp. 147–159, 2007.
[157] A. Lerf, F. E. Wagner, M. Dreher, T. Espejo, and J. L. Pérez-Rodríguez, "Mössbauer study of iron gall inks on historical documents," *Herit. Sci.*, vol. 9, no. 1, pp. 1–14, Dec. 2021.
[158] M. Conde-Morales, I.I.; Hinojosa-Reyes, L.; Guzmán-Mar, J.L.; Hernández-Ramírez, A.; Sáenz-Tavera, I. del C.; Villanueva-Rodríguez, "Different Iron Oxalate Sources as Catalysts on Pyrazinamide Degradation by the Photo-Fenton Process at Different pH Values. Water. Air. Soil Pollut.," vol. 231, pp. 1–15, 2020.
[159] C. A. Smiths, "The Chemistry of Writing Inks. Journal of Chemical Education," 1944.
[160] A. S. Reinhardt, C., & Travis, "The introduction of aniline dyes to paper printing and Queen Victoria's postage stamps.," *Ambix*, vol. 44(1), pp. 11-18., 1997.

7. FUNDING AND DIFFUSION

7.1 Funding

This work is supported by the research grant provided by the Grant Agency of the Ministry of the Education, Science, Research, and Sport of Slovak Republic (VEGA-1/0929/16), by the grant of the Faculty of Science, P. J. Šafárik University in Košice (VVGS-PF-2020-1432), and by the project OPENMED (ITMS+:313011V455) from the EU Structural funds. This work has also been financially supported by Ministerio de Ciencia e Innovación/FEDER funds (Projects FIS2017-84318-R and PID2020-113900RB-I00).

7.2 Diffusion

Publications

- **Espina, A.**; Cañamares, M. V.; Jurašeková, Z.; Sanchez-Cortes, S. Analysis of iron complexes of tannic acid and other related polyphenols as revealed by spectroscopic techniques: implications in the identification and characterization of iron gall inks in historical manuscripts. *ACS Omega* 2022, 7(32), 27937–27949, ISSN 2470-1343, doi: 10.1021/acsomega. 2c01679.
- **Espina, A.**; Sanchez-Cortes, S.; Jurašeková, Z. Vibrational Study (Raman, SERS, and IR) of Plant Gallnut Polyphenols Related to the Fabrication of Iron Gall Inks. *Molecules* 2022, 27(1), 279, ISSN 1420-3049, doi:10.3390/molecules27010 279.
- Bonacini, I.; Gallazzi, F.; **Espina, A.**; Cañamares, M. V.; Prati, S.; Mazzeo, R.; Sanchez-Cortes, S. Sensitive 'on the fiber' detection of synthetic organic dyes by laser photoinduced plasmonic Ag nanoparticles. *Journal of Raman Spectroscopy* 2017, 48(7), 925-934, ISSN 03770486, doi:10.1002/jrs.5164.

Conference participation

- **Espina, A.**; Sanchez-Cortes, S.; Cañamares, M. V.; Jurašeková, Z. Structural in-depth analysis of iron complexes of plant gall polyphenols by optical spectroscopic techniques and DFT calculations. *RBC 2022, Regional Biophysics Conference*, Pécs, Hungary, August 22 – 26, 2022 (***poster presentation***).
- **Espina, A.**; Sanchez-Cortes, S.; Cañamares, M. V.; Jurašeková, Z. Structural in-depth analysis of iron complexes of plant gall polyphenols

by spectroscopic techniques: Implications in the analysis of historical manuscripts. *XXVII RNE - XI CIE, XXVII Reunión Nacional de Espectroscopía - XI Congreso Ibérico de Espectroscopía*, Book of Abstracts, pp. 64-64 (P8), Málaga, Spain, July 5 – 8, 2022 (***poster presentation***).

- **Espina, A.**; Cañamares, M. V.; Jurašeková, Z.; Sanchez-Cortes, S. Structural in-depth analysis of iron complexes of tannic acid and other related polyphenols as revealed by spectroscopic techniques. *SKBS 2022, X. Slovak Biophysical Symposium*, Book of contributions, pp. 75-76 (PO3), ISBN: 978-80-973719-4-4, Smolenice, Slovak Republic, May 3 – 5, 2022 (***poster presentation***).
- **Espina, A.**; Sánchez-Cortés, S.; Jurašeková, Z. Polyphenols and metal (iron, copper) ion complexation characterized by optical (UV-Vis and Raman) spectroscopy. *SKBS 2020, IX. Slovak Biophysical Symposium*, Book of Abstracts, pp. 58-59 (PO08), ISBN: 978-80-973719-0-6, Trnava, Slovak Republic, September 16 – 18, 2020 (***poster presentation***).
- Jurašeková, Z.; **Espina, A.**; Miškovský, P.; Sánchez Cortés, S. Spectroscopic study of Iron Gall Inks: New insights into the ink black colour. *ALMA 2019, 7th Interdisciplinary Alma Conference, The Colour Theme*, Book of Abstracts, pp. 69-70, ISBN: 978-80-8208-021-9, Bratislava, Slovak Republic, October 16 – 18, 2019 (***poster presentation***).
- **Espina, A.** Raman and SERS characterization of Iron Gall Inks. *5th edition of IOSA scientific seminars*, IOSA Student Chapter CSIC, https://sites.google.com/view/iosa-student-chapter-csic/activities/2018, Madrid, Spain, December 12, 2018 (***oral presentation***).
- **Espina, A.**; Miškovský, P.; Sánchez-Cortés, S.; Jurašeková, Z. Raman and SERS characterization of Iron gall inks: preliminary results. *SKBS 2018, VIII. Slovak Biophysical Symposium*, Book of Abstracts, pp. 57-58 (PO6), ISBN: 978-80-973086-7-4, Košice, Slovak Republic, May 30 – June 1, 2018 (***poster presentation***).
- Sanchez-Cortes, S.; **Espina, A.**; Jurasekova, Z. Raman and Surface-Enhanced Raman Scattering Analysis of Iron Gallic Inks in Ancient Manuscripts from Spain and Slovak Republic, *ISA 2018, 42nd International*

Symposium on Archaeometry, Conference Programme and Abstract Book, Abs. 116, Merida, Yucatan, Mexico, May 20 – 26, 2018 Merida, (***oral presentation***).

- **Espina, A.**; Miškovský, P.; Sánchez-Cortés, S.; Jurašeková, Z. Raman and SERS characterization of Iron Gall Inks. *RBC 2018, 8th Regional Biophysics Conference*, Book of Abstracts, pg. 134-134 (PS-58), ISBN: 978-96-190942-4-2, Zreče, Slovenia, May 16 – 20, 2018 (***poster presentation***).
- **Espina García, A.**; Miškovský, P.; Jurašeková, Z. Štúdium stability a rozkladu železogalových atramentov pomocou Ramanovej a SERS spektroskopie. *CSTI 2018, Conservation Science, Technology and Industry, Premosťovanie disciplín a druhov dedičstva – efektívna ochrana dedičstva v 21. storočí*, Book of Proceedings, pp. 85-102, ISBN: 978-80-8060-435-6, Bratislava, Slovak Republic, March 7 – 9, 2018 (***poster presentation***).
- **Espina, A.** Non-invasive micro-Raman and SERS analysis of coloring materials in paper-based artifacts of cultural and historical interest. *1st Annual meeting of PhD students in Biophysics and Biochemistry*, Herl'any, Slovakia, October 18 – 19, 2017 (***oral presentation***).
- **Espina García, A.**; Miškovský, P.; Jurašeková, Z. Raman and SERS *in-situ* detection and characterization of black inks: iron gall inks. *ALMA 2017, 6th Interdisciplinary ALMA Conference and 2nd CrysAC Workshop: Painting as a Story*, Book of Abstracts, pp. 56 (PI03), Brno, Czech Republic, May 31 – June 3, 2017 (***poster presentation***).

Madrid 2022